



KIT SCIENTIFIC REPORTS 7656

Final Workshop Proceedings of the Collaborative Project “Crystalline ROCK Retention Processes”

(7th EC FP CP CROCK)

Thomas Rabung, David García,
Vanessa Montoya, Jorge Molinero (Eds.)

Thomas Rabung, David García, Vanessa Montoya, Jorge Molinero (Eds.)

**Final Workshop Proceedings of the Collaborative Project
“Crystalline ROCK Retention Processes”**

(7th EC FP CP CROCK)

Bildnachweis Umschlag

<http://commons.wikimedia.org/wiki/File%3AKarlsruhe-Schloss-meph666-2005-Apr-22.jpg>

photo taken by Meph666

GFDL (<http://www.gnu.org/copyleft/fdl.html>), CC-BY-SA-3.0 (<http://creativecommons.org/licenses/by-sa/3.0/>) or CC-BY-SA-2.5-2.0-1.0 (<http://creativecommons.org/licenses/by-sa/2.5-2.0-1.0/>), via Wikimedia Commons

Karlsruhe Institute of Technology
KIT SCIENTIFIC REPORTS 7656

Final Workshop Proceedings of the Collaborative Project “Crystalline ROCK Retention Processes”

(7th EC FP CP CROCK)

by

Thomas Rabung, David García, Vanessa Montoya, Jorge Molinero
(Eds.)

Report-Nr. KIT-SR 7656

The report is printed without colours. The report with the original colours in different photos, tables, figures and logos, can be downloaded from the KIT Scientific Publishing homepage.

Karlsruher Institut für Technologie (KIT)
Institut für Nukleare Entsorgung
Hermann-von-Helmholtz-Platz 1
76344 Eggenstein-Leopoldshafen
Germany

Amphos 21 Consulting S.L.
Passeig de Garcia i Faria, 49-51, 1^o-1^a
E08019 Barcelona
SPAIN

Impressum



Karlsruher Institut für Technologie (KIT)
KIT Scientific Publishing
Straße am Forum 2
D-76131 Karlsruhe

KIT Scientific Publishing is a registered trademark of Karlsruhe Institute of Technology. Reprint using the book cover is not allowed.

www.ksp.kit.edu



This document – excluding the cover – is licensed under the Creative Commons Attribution-Share Alike 3.0 DE License (CC BY-SA 3.0 DE): <http://creativecommons.org/licenses/by-sa/3.0/de/>



The cover page is licensed under the Creative Commons Attribution-No Derivatives 3.0 DE License (CC BY-ND 3.0 DE): <http://creativecommons.org/licenses/by-nd/3.0/de/>

Print on Demand 2014

ISSN 1869-9669

ISBN 978-3-7315-0145-9

FOREWORD

The present document is the proceedings of the Final Workshop of the EURATOM FP7 Collaborative Project CROCK (Crystalline Rock Retention Processes). The electronic version of these proceedings is also available on the webpage of the project (www.crockproject.eu) and on the KIT Scientific Publishing homepage. The Workshop was hosted by KIT-INE and held in Karlsruhe (Germany) 14th – 16th May 2013. The project started January 2011 and has two and a half years duration. It is composed by 10 beneficiaries including 5 research organizations, 2 universities and 3 Small and Medium Enterprises (SME's).

The key purpose of the proceedings is to document and make available to the broad scientific community the outcome of the CROCK project. For this reason, a considerable part of the project activity reporting is done through the proceedings, together with the outcome of a large number of scientific-technical contributions and Topical Sessions on different topics, which could be important for the development of the project. In the Final CP CROCK Workshop this topic focused on In situ URL experiments. Additional purposes of the proceedings are to ensure ongoing documentation of the project outcome, promote systematic scientific-technical development throughout the project, and to allow thorough review of the project progress.

All Scientific and Technical papers submitted for the proceedings have been reviewed by the EUG (End-User-Group). The EUG is a group specifically set up within the project in order to represent the interests of the end users to the project and its desired outcome. To this aim, the composition of the EUG includes organizations representing national waste management (SKB, POSIVA, SURAO) and national regulators (SSM, STUK).

Thanks to all those who submitted Scientific and Technical contributions for review and, especially, the Workpackage leaders who provided the summary of the different workpackages for publication in these proceedings. We also want to give a special thanks to the reviewers, members of the EUG, whose effort and hard work reflect their commitment and dedication to the project.



TABLE OF CONTENTS

THE PROJECT	1
THE FINAL WORKSHOP	3
<i>Objectives</i>	3
<i>RTD sessions</i>	3
<i>Poster presentations</i>	4
<i>Topical session</i>	5
<i>Structure of the proceedings</i>	6
SUMMARY OF WP ACTIVITIES	7
WORKPACKAGE 1	9
Introduction	9
Description of the work performed.....	9
References	12
WORKPACKAGE 2	13
Introduction	13
Description of the work performed.....	14
References	26
WORKPACKAGE 3	27
Introduction	27
Description of the work performed.....	27
References	28
WORKPACKAGE 4	29
Introduction	29
Description of the work performed.....	30
References	32
WORKPACKAGE 5	35
Introduction	35
Description of the work performed.....	35
References	43
TOPICAL SESSION SUMMARY	45
S + T CONTRIBUTIONS	53
POSTERS	269

THE PROJECT

The EURATOM 7th EC Framework Program Collaborative Project Crystalline ROCK retention processes (CROCK) started in January 2011 and extends over 2 and a half years. The key driver for initiation the CP CROCK, identified by national Waste Management Organizations, is the undesired high uncertainty and the associated conservatism with respect to the radionuclide transport in the crystalline host-rock far-field around geological disposal of high-level radioactive wastes. In response to this, the CROCK project has been established with the overall objective to develop a methodology for decreasing the uncertainty in the long-term prediction of the radionuclide migration in the crystalline rock repository far-field and to show how the outcome of the project can be used in the Safety Assessment and in the forthcoming site investigations programs. From a more scientific point of view, the CROCK project is increasing the process understanding in the transport simulations used to support Performance Assessment (PA) exercises with the purpose of increasing confidence in the safety of nuclear waste disposal.

The project is implemented by a consortium of 10 beneficiaries consisting on 5 large European Research Institutions, 2 Universities and 3 small and medium enterprises from six different countries with dedicated crystalline host-rock disposal programs and particular competence in this field. The Coordination Team is based on two organizations, namely the Coordinator (KIT) and the Coordination Secretariat (AMPHOS). National Waste Management organizations and Regulators also participate in the project contributing with co-funding to beneficiaries, infrastructures, knowledge and information. The scientific-technical work program of the project is structured along six RTD (Research and Technological Development) workpackages (WP1-6). Workpackage 1 started at the very beginning of the project providing new drill core fracture samples and characterizing the experimental materials. Workpackage 2 focuses on radionuclide transport and sorption studies. Workpackage 3 deals with matrix diffusion and natural chemical homologue analysis. The general objective of workpackage 4 is to conceptualize and model radionuclide transport processes on systems at different scales. In workpackage 5 is described how the outcome of the other WPs can contribute to decrease the uncertainty in PA related with transport treatment. Workpackage 6 is a cornerstone of the project, since its first objective is to establish a state-of-the-art of the current knowledge on retention processes in crystalline rocks, then to continuously collect the results obtained in the other workpackages, and finally to deliver a report summarizing the major advances which will have been accomplished at the end of the project. There is also one workpackage on knowledge management, dissemination and training (WP7). The last workpackage is on administrative and financial project management (WP8).

The present proceedings document the outcome of the Final Project Workshop and give an overview of the outcome of the 2nd project reporting.

THE FINAL WORKSHOP

The Final Project Workshop was held in Karlsruhe (Germany) 14th – 16th May 2013. The Workshop was hosted by KIT-INE. There were 34 attendees at the workshop, representing all the beneficiaries, the End-User Group, and five project external organizations (NAGRA, FZ Jülich, Helsinki University, Bfs and Fortum). The workshop was organized in two and a half days organized in oral presentations on results obtained within the project, a poster session, and a topical session on “In situ URL experiments”.

Objectives

The Workshop combines different activities and meetings with the following objectives:

- Informing about the scientific progress. For this purpose, plenary sessions and the poster session are used for communicating results from the different technical workpackages.
- Informing about the administrative status.
- Informing/agreeing upon forthcoming final reporting.
- Discussing various topics of interest for the consortium.

Emphasis was on scientific-technical topics with administrative issues kept to the minimum necessary.

RTD sessions

The workshop included plenary sessions where the results from the different workpackages were presented. Next to an overview of the achievements within the respective WP, scientific highlights were explained. The following presentations were given within the project.

WP1 session:

- S. Holgersson. Characterisation of rock samples from Äspö
- V.G. Petrov, I.E. Vlasova, N.V. Kuzmenkova, V.A. Petrov, V.V. Poluektov and S.N. Kalmykov. Characterization of rock samples from areas of the proposed Russian HLW and SNF repository (Nizhnekansky massive).

WP2 session:

- S. Holgersson. Cs, Ra and U Sorption on rock samples from Äspö.
- Y. Totskiy, Th. Schäfer, F. Huber, D. Schild, H. Geckeis and S. Kalmykov. Tc(VII) sorption on natural granitic rocks and synthetic magnetite.
- K. Schmeide, S. Gürtler, F. Bok and V. Brendler. Interaction of Uranium(VI) and Neptunium(V) with Äspö diorite under anoxic conditions.
- T. Missana. CIEMAT activity in the project (WP2).
- V.G. Petrov, I.E. Vlasova, N.V. Kuzmenkova, V.A. Petrov, V.V. Poluektov and S. N. Kalmykov. U, Cs and Eu sorption onto rock samples from areas of the proposed Russian HLW and SNF repository (Nizhnekansky massive).
- V. Havlová, K. Videnska, J. Vejsadú and P. Večerník. UJV experimental studies on Äspö derived material.

- K. Videnska, V. Havlová, J. Vejsadú, M.G. Vašínová and P. Sajdl. Study of selenium sorption on Äspö diorite.

WP3 session

- J. Molinero J. Bruno, P. Trinchero and L.M. de Vries. On the relevance of matrix diffusion for understanding hydrogeological behaviour in crystalline rocks.

WP4 session

- J. Crawford. Approaches to modelling surface complexation sorption on complex geological materials with limited data.
- D. García, M. Pękala and C. Domènech. Decreasing Kd uncertainty through the application of mechanistic retention models.
- A. Itälä, E. Puhakka, M. Olin, and M. Tanhua-Tyrkkö. Biotite sorption by molecular level and surface complexation modelling.
- F. Huber, P. Trinchero, J. Molinero and Th. Schäfer. Radionuclide migration in a single fracture from Äspö, Sweden: Experiments and reactive transport modelling.

WP5 session

- P. Trinchero, J. Molinero and L.M. de Vries. Modelling radionuclide migration in crystalline media: From effective Kd distributions to reactive transport.
- V.-M. Pulkkanen, A. Seppälä and M. Olin. Reactive transport modelling support to PA analysis in fractured bedrock.
- J. Crawford. A simplified approach for reactive transport modelling involving strongly non-linear sorption and remobilisation.

WP6 session

- A. Idiart, M. Pękala and D. García. Documentation - State of the art.

Poster presentations

The following posters were presented during the Final Workshop:

- J. Crawford. A simplified PA model for reactive transport featuring non-linear sorption processes.
- J. Crawford. What might Kd ratios be able to tell us about surface complexation sorption mechanism?
- V. Havlová and P. Večerník. Diffusion of species through Äspö diorite.
- S. Holgersson. CROCK at Chalmers - Experimental program and results.
- F. Huber, S. Heck and Th. Schäfer. RN sorption experiments using Äspö diorite, fined granite and Äspö granite

- K. Schmeide, S. Gürtler, K. Müller, R. Steudtner, C. Joseph, F. Bok and V. Brendler. Interaction of uranium(VI) and neptunium(V) with Äspö diorite under anoxic conditions.
- L.M. de Vries, P. Trincherro and J. Molinero. MCPHREEQC: Automatic stochastic simulations for geochemical modelling.

Topical session

The Topical Sessions aim at covering the key areas of knowledge along with the project. The Topical Session of the Final CP CROCK Workshop was organized by Th. Schäfer (KIT-INE) and focuses on “In situ URL experiments”.

Presentations within this topic were:

- A. Winberg. The history of RN migration studies at the Äspö HRL: Experiences of the TRUE sites
- B. Kienzler. The CHEMLAB 2 experimental program at Äspö: Results of the actinide migration experiments.
- E. Krawczyk-Bärsch. Microbial experiments at URL sites: Influence on radionuclide,
- A. Martin and I. Blechschmidt. Almost 30 years of tracer testing @ Grimsel Test Site.
- V. Havlová, A. Martin, J. Rueedi, M. Siitari-Kauppi, J. Ikonen, P. Soler and Y. Tachi. LTD Phase I and II experiments: Study of radionuclide diffusion into crystalline rock matrix.
- M. Bouby, S. Büchner, J. Brendlé, G. Darbha, H. Geckeis, T. Kupcik, R. Götz, W. Hauser, S. Heck, F. Huber, P. Höss, M. Lagos and Th. Schäfer. The CRR & CFM project: Colloid enhanced radionuclide migration.
- L. Koskinen. URL migration studies within the Finnish nuclear Waste repository Research program.
- V. Petrov. URL research within the Russian Nuclear Waste repository Research program.

Structure of the proceedings

The proceedings are divided into the following sections:

- WP activity overviews, with summaries of the Research, Technology and Development Components
- A topical session summary compiling the whole set of information presented by the different authors
- Individual Scientific and Technical Contributions, containing reviewed scientific and technical manuscripts
- A compilation of posters presented at the Final Workshop

All the Scientific-technical contributions submitted were reviewed by the EUG members (End-User Group).

SUMMARY OF WP ACTIVITIES



WORKPACKAGE 1

EXPERIMENTAL MATERIAL AND CHARACTERIZATION

Thomas Rabung^{1*}

¹Institute of Nuclear Waste Disposal, Karlsruhe Institute of Technology,
Hermann-von-Helmholtz-Platz 1, 76344 Eggenstein-Leopoldshafen

* Corresponding author: thomas.rabung@kit.edu

Introduction

The organization and detailed characterization of new crystalline rock samples from Äspö (fractured and intact drill cores), sampled and handled under anoxic conditions, as well as ensuring the access to experimental samples from previous studies, were the main objectives within this WorkPackage (WP). The usage – for the first time – of un-oxidized material in subsequent sorption studies is of special importance for redox-sensitive radionuclides and reflects the conditions in a repository after closure. Besides bore core sections also disks and crushed material of different size fractions have been provided to the beneficiaries. All the handling and storage of the sampled material was done under argon atmosphere (glove boxes) to keep the material as much unaltered as possible.

Five organizations are involved in this WP: KIT-INE (Germany), CIEMAT (Spain), HZDR (Germany), CTH (Sweden) and MSU (Russia).

In this workpackage two deliverables, namely D1.1 and D1.2 (available on the webpage www.crockproject.eu) have been generated containing very detailed information on sampling and characterization.

The experimental work of this workpackage started in January 2011 and was finished after 24 months. Most of the work was performed in the first part of the project (first 18 months) and the outcome is well documented in the 1st Workshop proceedings. In the following only the remaining achievements and results within the second reporting period are mentioned.

Description of the work performed

The remaining work of **KIT** within this workpackage covers the characterization of fractured drill cores. This includes their hydraulic properties as permeability, conductivity and porosity. Besides migration experiments with conservative tracers, especially the μ -computed tomography (μ -CT) is a very useful tool to obtain geometrical information on the fracture (Fig. 1). The data gathered by this technique can be used directly in numerical codes to carry out computational fluid dynamics (CFD) simulations, conservative solute transport as well as reactive transport calculations for radionuclide migration for comparison to experimentally measured data.

More detailed information is given in deliverable D1.2 and in the S&T contribution within the Final Workshop Proceedings: *Tc(VII) sorption on natural granitic rocks and synthetic magnetite* by Y. Totksiy et al.

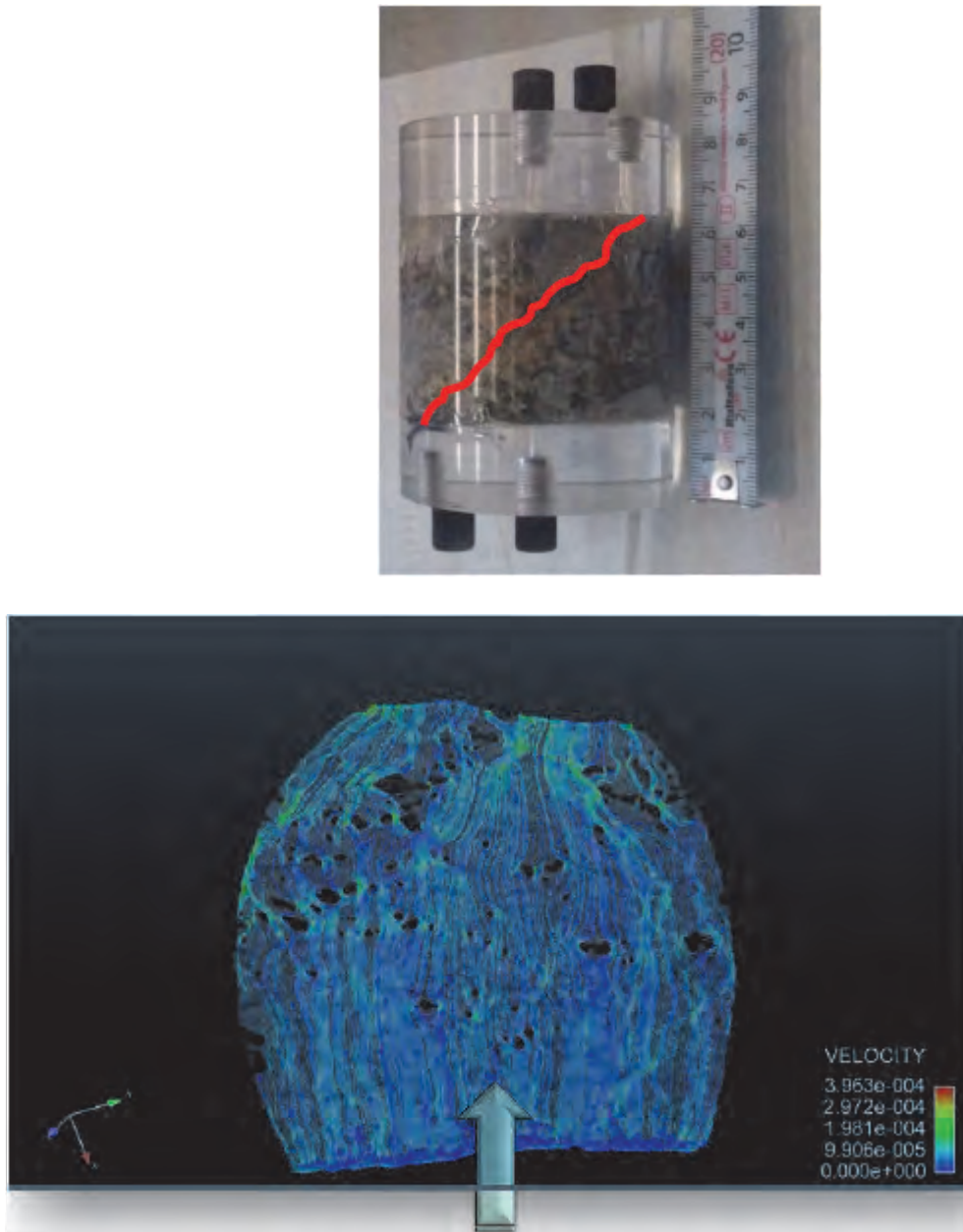


Figure 1: Fractured Äspö diorite core (above) and corresponding μ -CT of the fracture (below).

An update of sorption data for three different tracers (HTO, ^{36}Cl , $^{137}\text{Cs}^+$) on “block-scale” material was obtained by **CIEMAT** within this WP. The evolution of the activity of the conservative Cl and HTO has been periodically measured in 11 different boreholes placed in granite at different distances from the source. The experimental data are available for modellers in [García-Gutiérrez, in preparation].

In addition a comparison of sorption properties of granites from different origin (Spain, Switzerland, Finland and Sweden) was performed and the documentation of the characterization is summarized in the S&T contribution: *Analysis of sorption onto granites and granite minerals: the case of caesium* by T. Missana and M. García-Gutiérrez.

The objective of **HZDR** for the second reporting period of WP 1 was related to sampling and characterization of site-specific biofilms from Äspö HRL (Fig. 2) for subsequent U(VI) and Np(V) sorption studies. The characterization covers the analysis of the ultrastructure and elemental composition of the organic matter by EF-TEM (Energy-filtered Transmission Electron Microscopy), electron energy loss spectroscopy (EELS) as well as ICP-MS (Inductively coupled plasma mass spectrometry) and Powder X-ray diffraction of the cryo-dried BIOS (bacteriogenic iron oxides) biofilms. Mössbauer investigations have also been performed to study the bacterial ferrihydrite in BIOS biofilms. Details are given in the S&T contribution: *Retention of U(VI) and Np(V) in Bacteriogenic iron oxide-producing biofilms from Äspö HRL (Sweden)* by E. Krawczyk-Bärsch et al.



Figure 2: Rusty orange to brown *Gallionella ferruginea* dominated biofilms, attached to the fractured bedrock of the Äspö HRL tunnel.

The work of **CTH** in WP1 for the second reporting period covers the BET surface area determination of crushed material of different size fractions as well as the specific pore volume determination of crushed material and intact disks. The measured porosity of the intact material is found to be much larger than predicted by a model. This is interpreted as a macroporosity which contributes very much to the porosity of the intact samples but contributes very little to their BET areas. Details can be found in the S&T contribution: *Characterization of rock samples from Äspö using gas adsorption* by S. Holgersson.

Providing and characterizing sample material from disposal sites in Russia, including rock samples from the proposed international repository of spent nuclear fuel in Nizhnekansky rock massive is the objective of **MSU** in WP1.

Core materials from two of the supposed areas (area Kamenny, drilling depth down to 700 m, and area Itatsky, drilling depth down to 500 m) have been studied in terms of petrographic and mineralogical characterization; definition of filtration, elastic, petro-physical and strength properties; estimation of hydrothermal-metasomatic transformation of rocks. It was established that the most part of the core material from the area Kamenny is presented by granites and leucogranites, while the core material from the area Itatsky is mostly diorites and quartz diorites (Fig.3). More details are given by Kuzmenkova et al. in the S&T contribution included in the

Final Annual Workshop Proceedings: *Uranium (VI) sorption onto rock samples from areas of the proposed HLW and SNF repository in Russia (Nizhnekansky massive).*

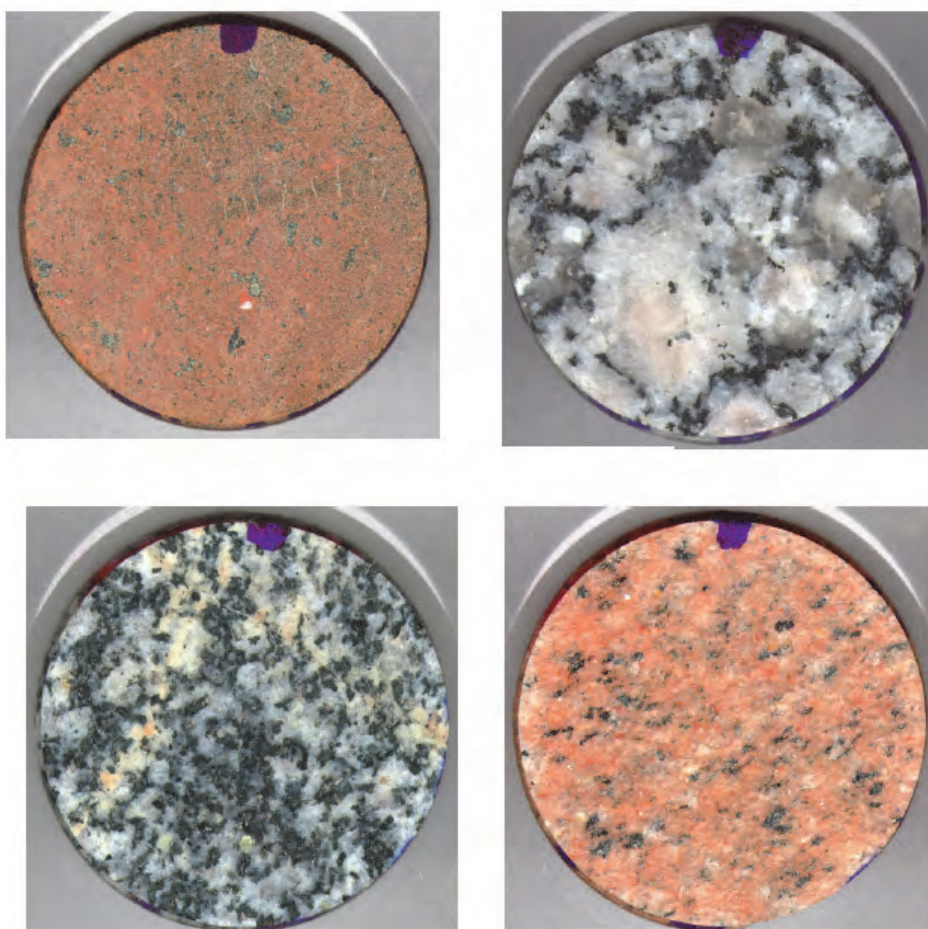


Figure 3: Rock samples from Kamenny area (above) and from Itatsky area (below).

References

García-Gutiérrez, M., Mingarro, M., Missana, M. (in preparation). Experimental results from the block-scale diffusion test at CIEMAT. CIEMAT Technical Report.

WORKPACKAGE 2

RADIONUCLIDE TRANSPORT AND SORPTION STUDIES

Tiziana Missana^{1*}

¹CIEMAT (ES), Avenida Complutense 40, 28040 Madrid

*Corresponding author e-mail: tiziana.missana@ciemat.es

Introduction

The main objective of the work carried out in Work Package 2 (Radionuclide Transport and Sorption Studies) of the CROCK Project was to decrease the uncertainties related to radionuclide retention in the performance assessment of geologic disposals of high-level radioactive waste in crystalline rocks and to understand from where the main uncertainties come from. This is fundamental for the prediction of radionuclide migration in the host rock at a long-term.

Retention data obtained from different literature sources showed large discrepancies, not always easily explicable. It is recognized that some conceptual aspects, that are not completely understood, still exist. To cite some of them: crystalline rock heterogeneity, kinetic aspects, sorption versus retention triggered by reduction, up-scaling effects and dependence of retention parameters on the hydrodynamic conditions of the system. All these may affect the determination of retention parameters. On the other hand, other problems related to experimental measurements might be relevant too. Retention parameters obtained under conditions not completely representative of the repository environment, or the use of not well preserved rock and aqueous samples might lead to a biased prediction of radionuclide behaviour.

Amongst the main aspects analysed in this WP we can find: the analysis of the effects on retention caused by the not correct preservation of the rock samples, especially on redox-sensitive elements; the importance of reduction processes on radionuclide retention; the procedures to derive realistic parameters, applicable to *in-situ* conditions starting from batch experiments; the importance of specific surface area determination; the relevance of measurements of retention parameters in conditions as similar as possible to the real ones over different spatial scale; the need of reproducible experimental procedures, and the use of complementary techniques.

The studies were focused on these radionuclides: an ion-exchangeable dominated (Cs), a strongly sorbing surface complexation dominated (Eu), redox sensitive elements (U, Tc, Se) and conservative non-sorbing tracers (HTO, Cl), as agreed by all the partners at the CROCK kick-off meeting.

Radionuclide sorption was studied in different crystalline rocks from Äspö (Sweden) diorite to Grimsel (Switzerland) granodiorite or Nizhnekansky (Russia) granite. Some groups studied sorption on different rocks using the same experimental methodology and chemical conditions, to analyse the variability of distribution coefficients; different groups determined sorption parameters for different radionuclides on the same material (Äspö diorite, ÄD), to establish the possible range of experimental uncertainties.

Crystalline rock material was delivered to the interested participants from CROCK drilling site of Äspö HRL (Sweden). Details on the sampling procedure and material characterization were presented as S&T contribution in the First Annual Meeting (Schäfer et al., 2012). Preparation and handling of Äspö rock samples was also described in a previous contribution (Totskiy et al., 2012).

The sampling was carried out providing that the contact with atmospheric O₂ was as short as possible, to prevent as much as possible the material from oxidation. The samples were moved at KIT-INE, in an anaerobic glove box, where they were crushed and sieved into two fractions with different grain size: 0.5 – 1 mm and 1 – 2 mm. The material was then distributed to each project partner for sorption tests. For all the experiments with ÄD, a synthetic Äspö groundwater (ÄGW) was produced following the indications obtained by KIT-INE (Heck and Schäfer, 2012).

The comparative sorption results obtained with uranium, selenium, technetium and caesium by the different partners with ÄD in ÄGW will be summarized at the end of this paper.

The studies performed in the CROCK project, also pointed out that the mechanistic understanding of retention processes needs a precise determination of the chemical and mineralogical properties of the system and a validation of models on the widest possible range of experimental conditions. Additionally, the specific surface area is identified as a key parameter to obtain surface area normalized K_a (m), to allow comparison of data from different materials and different experimental sources and for extrapolating the results from laboratory experiments to the field-scale.

The following organizations participated to WP 2: **KIT-INE** and **HZDR** (Germany); **CIEMAT** (Spain); **CTH** (Sweden); **UJV-Rez** (Czech Republic); **MSU** (Russia).

Description of the work performed

KIT-INE

KIT-INE analysed Tc(VII) adsorption onto natural granitic rock and also onto Fe-bearing minerals, to understand the role of Fe on its retention. The results are detailed in the Final Workshop proceedings (Totskiy et al., 2013). One of the objectives of KIT-INE was to compare sorption data obtained with well-preserved rock samples, with those obtained with oxidized samples. Previous to sorption experiments, the solid phases were characterized by different techniques.

Sorption experiments were carried out with crystalline rock materials from the Äspö Hard Rock Laboratory (Sweden), from Nizhnekansky massif (Russia) and with the mineral magnetite.

The aqueous phase used for sorption experiments with ÄD, was the synthetic Äspö groundwater (ÄGW), which composition was provided by (Schäfer et al., 2012) at the beginning of the project. Water representative of Nizhnekansky site was used for the tests with the Russian granite (Petrov et al., 2012). Background electrolyte for the Tc sorption on magnetite was 0.2 M NaCl.

KIT-INE also performed migration experiments with unoxidized Äspö diorite core #2.2 (0.53-0.97 m, borehole KA2370A-01) with a natural fracture and previously characterized by 3D computer tomography (μ CT). Transport experiments were carried out with HTO, Cl (as conservative tracers) and Tc(VII).

For batch sorption experiment, ^{99}Tc at different initial concentrations, was used; for XPS surface analysis diorite slices were used and $[\text{Tc(VII)}]$ was $1 \cdot 10^{-5}$ M. Results showed that significant differences in Tc retention between oxidized and well preserved samples exist. Oxidised materials were shown to adsorb Tc(VII) very weakly, whereas relatively high sorption could be observed under anaerobic conditions and unoxidized materials.

The high Tc(VII) immobilization was explained considering its reduction to insoluble Tc(IV): XPS measurements showed that only Tc(IV) is found on the rock surface, probably being Tc(VII) absent or under the detection limit. Furthermore, it was mainly located on dark Fe(II) minerals.

Therefore, the concentration of Fe(II) in the solids, higher in the well preserved samples, might be the main responsible of Tc retention. The quantity of Fe(II) in the Russian granite ($0.1 - 1 \mu\text{g}$ of Fe(II) per g) is lower than that observed in ÄD ($1 - 3 \mu\text{g/g}$ for oxidized Äspö diorite), thus Russian granite has a lower overall redox buffer capacity and less retention capability.

According this experimental work, Tc sorption behaviour on both ÄD and Nizhnekansky oxidized materials was quite similar, but it was dramatically different from that of non-oxidized Äspö samples.

In ÄD, distribution coefficients, K_d , values of 103 mL/g were observed for $[\text{Tc}] = 1 \cdot 10^{-9}$ M and $[\text{Tc}] = 1 \cdot 10^{-8}$ M; whereas only 3 mg/L were measured for $[\text{Tc}] = 1 \cdot 10^{-5}$ M, in agreement with literature data.

The limited redox capacity of the granitic rock is most probably the reason why Tc sorption seems to be not linear. The lowest the Tc(VII) concentration, the higher of the importance of Fe(II) on Tc reduction and thus on its retention. Due to low Fe(II) concentration found in granite materials, reduction process is much slower and less effective than in case of sorption on synthetic magnetite that was investigated in parallel. Sorption on this iron oxide was in fact, very high and rapid. Upon sorption, at the magnetite surface only Tc(IV) was found. To strengthen the hypothesis on the role of Fe(II) on Tc(VII) retention, new experiments were also planned with maghemite.

Desorption experiments under reducing conditions showed that desorption was almost negligible and independent of contact time, whereas after atmospheric oxidation Tc desorption significantly increased.

HZDR

HZDR performed batch sorption experiments to determine the sorption capacity of Äspö diorite, respect to neptunium (V) and uranium (VI). Preliminary results were presented at the First Annual CROCK workshop (Schmeide et al., 2012) and new tests are summarised in Schmeide et al., 2013, in this volume.

In the second part of the Project, HZDR carried out batch sorption experiments with U(VI) and Np(V) onto ÄD, under anoxic conditions (N_2 atmosphere). Sorption kinetic experiments (5 to 108 d) and isotherms were carried out. Kinetic tests were performed with a concentration of actinides of $1 \cdot 10^{-6}$ M and sorption isotherms with a concentration from $3 \cdot 10^{-9}$ to $2 \cdot 10^{-5}$ M.

Previous to sorption experiments, the solid was conditioned to the Äspö synthetic water (pH 7.8). The $1 - 2$ mm grain size fraction of diorite was used for new sorption experiments and the solid-to-liquid ratio was always 200 g/L. ATR FT-IR spectroscopy was used for the characterization of the adsorbed species. For redox speciation of actinides in sample solution or desorbed from the diorite, solvent extraction has been applied.

Previous experiments showed that U(VI) sorption onto diorite was strongly influenced by the groundwater composition and, in agreement with the speciation calculation, $\text{Ca}_2\text{UO}_2(\text{CO}_3)_3(\text{aq})$ was found to be the dominating species in Äspö groundwater at pH 7.8 (Schmeide et al., 2012). Then, U(VI) is stabilized in solution in this redox state and it did not show very high sorption onto the diorite. Kinetic experiments showed that U(VI) sorption equilibrium is reached within few weeks (10-20 days) and an average K_d value of 1.4 ± 0.2 (L/Kg) is measured (1 – 2 mm fraction).

The sorption isotherm for U(VI) sorption showed linear adsorption with a K_d value, determined from the Freundlich isotherm, amounts to 3.8 ± 0.6 L/kg, confirming the weak U(VI) sorption under Äspö conditions. Desorption tests showed that adsorbed uranium can be easily removed: 45 to 50% of the sorbed uranium can be desorbed with Äspö groundwater. Desorbed uranium is mainly in the form of U(VI), confirming that under Äspö conditions uranium is stabilized against reduction.

On the other hand, in ÄGW, the speciation of Np is dominated by NpO_2^+ (Schmeide et al., 2012). Sorption kinetic experiments showed that Np needs longer sorption time to reach the equilibrium (40 days) than U(VI) and stronger sorption is observed. This different behaviour can be induced by the reduction of Np(V) to Np(IV) induced by the presence of Fe(II) at the diorite surface (2.5 %).

Desorption experiments showed that only 5 to 6% of the sorbed neptunium can be desorbed with ÄGW. The small amount of neptunium, that can be desorbed, was identified as Np(V) by TTA solvent extraction. The part of neptunium, that cannot be desorbed under these conditions but remains immobilized, is probably Np(IV).

Due to the different speciation (aqueous and at the diorite surface) sorption and mobility of the two actinides under Äspö conditions are not comparable. The retention capacity of anoxic diorite towards Np is much higher than towards U.

CIEMAT

The objectives of the work proposed by CIEMAT were to provide a better insight on retention processes in crystalline rocks, gathering a very large set of data under the widest as possible range of experimental conditions and to describe them by quasi-mechanistic models.

Possible experimental (and conceptual) uncertainties were evaluated by the comparison of data in different materials (granite and granite minerals) under similar chemical conditions.

Amongst the rock properties it is very interesting to analyse the different mineral content, the BET surface area and competitive ions in solution.

Radionuclide sorption was analysed by means of different techniques in crushed/entire granite obtaining complementing information. The largest set of experimental data was obtained for Cs, whose sorption was studied on different granites from Sweden, Switzerland and Spain and various minerals (biotite, K-feldspar, muscovite, quartz) interpreted by simple thermodynamic sorption models (Missana and García-Gutiérrez 2012a, 2012b; Missana and García-Gutiérrez, 2013). All the materials investigated by CIEMAT are included in Table 1.

Batch sorption studies with U(VI) and Eu in different granites and granite minerals were also carried out; adsorption of Tc(VII) and Se(IV) was studied only on ÄD. In the case of ÄD, a synthetic groundwater (ÄGW) was used. For all the material two simplified waters were used (low and high saline water, LSW and HSW).

Kinetic tests, tests as a function of the pH, salinity of the water, radionuclide concentrations were carried out.

Apart from batch sorption experiments, CIEMAT made the analysis of U and Se sorption on not crushed ÄD, comparing aerobic and anaerobic conditions, complementing sorption studies by microanalysis with particle induced X-ray emission (PIXE).

Sorption of Cs, showed a kinetic dependent on the grain size of the material. In the finest fractions, sorption was rapid (hours) whereas the larger the fraction, the longer the time needed to reach sorption equilibrium. Spread in experimental data also tended to increase. However, similar Kd values than those obtained in the powdered material, were obtained also on intact rocks after 1.5 years.

Caesium showed in all granite and minerals non-linear sorption; sorption was independent of pH and dependent on water salinity suggesting ionic exchange as the main sorption mechanism. Comparing Cs adsorption in all the analysed granites, it could be observed that, at a fixed Cs concentration, the BET normalized distribution coefficients, were comparable within one order of magnitude. The largest source of variability for Kd values was Cs concentration (non-linear sorption): depending on Cs concentration, distribution coefficients could vary within up to 3 orders of magnitude. The non-linearity of Cs sorption indicated the existence of multiple adsorption sites. One sorption site with very low capacity but high affinity for Cs, other possible site(s) show lower affinity. Analysing the water in contact with the different solids, it was observed that the concentration of potassium is very relevant on Cs sorption, especially at low Cs loadings and low salinity.

Analysing Cs adsorption in minerals, it could be observed that, again, normalized Kd values showed a similar quantitative behaviour, with main differences observed at low Cs loading related to the presence of potassium. At medium-high loadings the normalized sorption values were similar for all the solids, with slightly higher values for those containing potassium feldspar. Additionally, the density of the high affinity sites seems to be slightly higher in the presence of this mineral.

U(VI) sorption equilibrium was reached within 10-30 days, in all the granites and the BET normalized distribution coefficients were within one order of magnitude larger differences were observed when adsorbing in minerals (lowest adsorption observed in potassic feldspar). Significant variations in Kd are observed with pH, as expected, and the main experimental difficulty encountered was to maintain the desired pH.

In ÄGW U(VI) sorption isotherms were carried out, sorption was lineal (up to saturation of sorption sites) and the determined Kd was approximately 6 ± 2 mg/L.

The analyses by PIXE of U(VI) sorption onto ÄD, under anaerobic conditions, showed that U is not homogeneously distributed: the highest surface distribution coefficient, Ka, was measured on biotite, titanite and zircon; an average Ka of $4.4 \cdot 10^{-4}$ m was estimated. Under oxic conditions, the measured value was lower ($3.5 \cdot 10^{-5}$ m). The recalculated Kd, considering the BET area, were comparable with those obtained by batch experiments.

Europium sorption was very rapid in all the crushed materials, with significant adsorption in most cases, especially in low saline water, LSW. The main experimental uncertainty is related to its almost quantitative sorption that increases the error in Kd determinations. In ÄD, Eu sorption was found to be relatively high too, in

spite of the salinity of the water, probably due to the high biotite content of this rock. Biotite was in fact shown to be the mineral that most adsorbs Eu under saline conditions.

The adsorption of Se(IV) in ÄGW was analysed by PIXE, both under anaerobic and aerobic conditions. PIXE analyses shows that selenium was not heterogeneously distributed over the surface with maximum K_a of $7 \cdot 10^{-5}$ m onto Fe bearing mineral and null in other minerals like quartz. K_d values recalculated from K_a comparable to those obtained in batch experiments.

Table 1. Solids used by CIEMAT for sorption experiments

Sample	Description	Size fraction (mm)	BET (m ² /g)
GFEB	FEBEX Granite, fraction 1, F1	< 0.5	0.089±0.02
b-GMIG	MIGRATION Granite (black)	<0.064	4.097 ±0.005
GMIG	MIGRATION Granite	<0.064	2.871±0.005
RAT	RATONES Granite	< 1	0.488±0.005
BER	BERROCAL Granite	<0.5	2.780±0.005
Äspö G	Äspö gross	1<x<2	0.079±0.005
Äspö F	Äspö fine	0.5<x<1	0.094±0.005
Äspö VF	Äspö very fine	<0.5	1.28±0.01
Sample Name	Description	Size fraction (mm)	BET (m ² /g)
Biotite (RAT)	RATONES Biotite	<1	1.148±0.005
Biotite 3h	Biotite from BER granite	0.125<x<0.250	3.261±0.005
Biotite 2c	Biotite from BER granite	0.064<x<0.125	4.813±0.005
Biotite 3F	Biotite from BER granite	<0.064	5.548±0.005
Biotite (Geost)	Standard	ND	ND
Muscovite (B)	Muscovite from BER granite	<0.5	0.402±0.005
Muscovite F	Muscovite from BER granite	0.125<x<0.250	0.730±0.005
Muscovite 2b	Muscovite from BER granite	<0.064	3.977±0.005
Muscovite 3c		0.064<x<0.125	2.867±0.005
FdK	Potassium feldspar	0.125<x<0.250	8.001±0.005
Q2	Quartz+plagioclase	0.125<x<0.250	1.290±0.005
Q3	Quartz+plagioclase+FdK	0.125<x<0.250	1.089±0.005

Finally, Tc(VII) sorption was studied in Äspö diorite, using well-preserved and oxidized material. Under oxidized conditions or using oxidized materials, K_d values were null. With well-preserved ÄD, under anoxic conditions, sorption isotherms were carried out. Tc sorption was not linear and the maximum K_d (25 ml/g) was obtained at the lowest Tc concentration used ($6 \cdot 10^{-7}$ m), reduction processes at the surface are most probably the responsible of the retention.

In conclusion, results showed that data normalisation by BET is the first step needed for comparison of K_d data from different sources. This procedure however, does not take into account the sorption kinetic, longer for larger fractions. This point can be of importance above all when different experimental methodologies are used. This first comparison, helps evaluating the role of other factors, like mineralogy of the solid or competing ion in solution. Therefore, a procedure for batch tests should be defined, to help comparing data from different sources.

The rocks that presented the highest sorption capacity for Cs, U and Eu were GFEB (Table 1) and Äspö diorite. The use of “well-preserved” materials increased K_d values of redox-sensitive elements, most probably due to reduction at the surface.

CTH

CTH studied radionuclide diffusion and sorption by batch experiments. A preliminary characterization of the crystalline rocks in terms of surface area and porosity is necessary to: 1) normalize the sorption data obtained from batch sorption tests in crushed and sieved material 2) normalize and interpret sorption and diffusion data obtained from diffusion experiments. CTH presented the characterization of rock samples from Äspö (BET and porosity). Four different fractions were analysed using the BET method: 0.125-0.063mm; 0.25-0.125mm; 0.5-0.25mm and 1-0.5mm and the respective average BET surface areas were: 0.3105 ± 0.0468 , 0.2029 ± 0.0280 , 0.1368 ± 0.0158 , 0.0874 ± 0.0107 (m^2/g). Surface area measurements were carried out also on intact section of the material and the average BET value was: 0.0066 ± 0.0013 m^2/g .

Results for specific pore volume (SPV) measurements of crushed and sieved fractions of Äspö diorite, utilizing about 90 points N_2 gas adsorption isotherm were: $1.20 \pm 0.19 \cdot 10^{-3}$, $7.89 \pm 0.82 \cdot 10^{-4}$, $5.63 \pm 0.76 \cdot 10^{-4}$, $5.49 \pm 1.43 \cdot 10^{-4}$ mL/g , for the four previously mentioned fractions. The porosity for intact material was not measurable with gas adsorption, dry/wet weighing method instead gave $2.54 \pm 0.47 \cdot 10^{-3}$ mL/g for the intact material (see S&T contribution Holgersson, S.: Characterization of rock samples from Äspö using gas adsorption).

The specific surface area (SSA) increases from the intact sections to the finest fraction in accordance with the expected effect of crushing the material. The crushing creates new surfaces and may also give access to previously closed porosity. The specific pore volume (SPV) was found to also increase with decreasing particle size of the crushed fractions, apparently in a linear dependency of SSA. The measured SPV for intact sections ($\text{SPV} = 2.54 \pm 0.47 \cdot 10^{-3} \text{mL/g}$) is about 10 times larger than what can be expected from an extrapolation of the size series of crushed material ($\text{SPV} = 1.20 \pm 0.19 \cdot 10^{-3} \text{mL/g}$ for the 0.063-0.125mm fraction to $\text{SPV} = 5.49 \pm 1.43 \cdot 10^{-4} \text{mL/g}$ for the 0.5-1.0mm fraction), and using measured average SSA for intact sections. This may be explained by that intact rock contains macro-porosity, with pore size above the upper detection limit ($>0.5 \mu\text{m}$) of the gas adsorption method. It is possible that this macro-porosity disappear upon crushing. This macroporosity in intact material will contribute to a relatively fast diffusion through rock, compared to the slow diffusion in individual pure minerals. However, due to the very small surface area, the contribution from the macroporosity to sorption capacity will be low. Instead the mesoporosity will likely dominate sorption. The presence of two diffusion paths in drill core sections of granitic rock from Äspö has previously been shown (Johansson et al., 1998).

CTH also made sorption and diffusion experiments on the Äspö rocks (HTO, Cs, Ra and U). Sorption experiments were carried out in the four fractions (0.125-0.063 mm, 0.25-0.125 mm, 0.5-0.25mm, and 1-0.5mm), under N_2 atmosphere, using synthetic Äspö groundwater, and lasted up to 3 months. Radionuclide used were ^{134}Cs , ^{226}Ra and ^{233}U , with a concentration of: $1 \cdot 10^{-7}\text{M}$, $1 \cdot 10^{-8}\text{M}$ and $1 \cdot 10^{-9}\text{M}$, respectively.

The main sorption distribution coefficients obtained after 1 month sorption (in the four different fractions, average values for 8 samples, expressed in m^3/Kg) are: Cs) 0.0894 ± 0.0108 , 0.0478 ± 0.0079 , 0.0257 ± 0.0026 , 0.0157 ± 0.0024 ; Ra) 0.034 ± 0.0084 , 0.0213 ± 0.0085 , 0.0112 ± 0.0055 , 0.0054 ± 0.0019 . For U only preliminary results for one sample are available: 0.0050 ± 0.0010 , 0.0031 ± 0.0015 , 0.0019 ± 0.0008 , 0.00096 ± 0.00052 . Diffusion experiments with HTO, Cs and Ra were made in intact drill-core samples, sampled perpendicular to a fracture, to analyse the difference of R_d and effective diffusivity D_e depending on the distance from the fracture

surface and a detailed description of the samples collected for Chalmers has been reported (Holgersson, 2013). The average D_e of HTO for 8 samples was $1.28 \pm 0.26 \cdot 10^{-13} \text{ m}^2/\text{s}$ and the average SPV was measured to $7.54 \pm 2.21 \cdot 10^{-4} \text{ mL/g}$. The average D_e of Cs for 8 samples was $1.98 \pm 0.85 \cdot 10^{-12} \text{ m}^2/\text{s}$ and average K_d was $1.16 \pm 0.62 \cdot 10^{-3} \text{ m}^3/\text{kg}$. The average D_e of Ra for 8 samples was $1.05 \pm 0.27 \cdot 10^{-12} \text{ m}^2/\text{s}$ and average K_d was $1.82 \pm 0.28 \cdot 10^{-3} \text{ m}^3/\text{kg}$. The relative errors of 10-30% in these average values show that any significant or systematic effect of the distance of the material from the fracture surfaces is probably not measured, at least not with the method used here. (see S&T contribution Holgersson, S.: HTO, Cs and Ra sorption on and diffusion in rock samples from Äspö).

UJV

UJV-REZ studied selenium sorption behaviour onto ÄD, combining batch sorption experiments and spectroscopic techniques (Electron Spectroscopy for Chemical Analysis, ESCA, and Laser Ablation Inductively Coupled Plasma Mass Spectrometry, LA-ICP-MS) to obtain information on the selenium sorption and distribution on rock surface. The results obtained by of UJV-Rez, in the second reporting period, are summarized in Videnská et al., 2013a and Videnská et al., 2013b.

Batch sorption experiments on crushed rock were performed under aerobic and anaerobic conditions, focusing the attention on the potential role of iron on Se retention. They used the material provided by KIT-INE at the start of the project; part of the material was maintained under anoxic conditions, another fraction was exposed to air. Batch sorption experiments were carried out in triplicate with both the “well preserved” and oxidized diorite in two size fractions.

The experiments under aerobic conditions lasted 112 days. K_d -values showed similar behaviour of selenite for both studied fractions, therefore clear influence of grain size on sorption was not observed. Results showed only very limited selenite sorption: after 112 days, K_d reached 1.3 mL/g in case of finer fraction and 1.6 mL/g in case of the larger one. Only 12-14 % of selenite was sorbed on diorite. Results of sorption experiments with selenate indicate K_d values approaching zero. pH and Eh values were measured throughout the experiment and slightly increasing trend in pH values was observed in case of both selenite and selenate. After 112 days of experiment the pH values increased from 7.2 to 7.4.

The experiments under anaerobic conditions led to K_d values only slightly higher than those performed under aerobic conditions. After 112 days of experiment the pH values decreased from 8.4 to 8.

The analysis of the surface with spectroscopic techniques (ESCA and LA-ICM-MS) was focused to iron as potential reducing agent, therefore in the analysis of iron bearing minerals like biotite, epidote, titanite and magnetite. These experiments were performed using rock cubes (dimension $1 \times 1 \times 0.2 \text{ cm}$) that were immersed into 10 mL ÄGW with $2 \cdot 10^{-3} \text{ mol/L}$ selenium, during 7 days.

Results partially confirmed the initial assumption that Se retention was in correlation to the presence of Fe minerals. However, the methods did not confirm presence of reduced Se species. The possibility of selenium complexation with other elements, e.g. with Ca, was discussed as possible cause of Se surface retention.

MSU

MSU studied sorption of U(VI) onto rock samples from areas of the proposed HLW and SNF repository in Russia (Nizhnekansky massive), accompanied by various spectroscopic investigations with micro- to nano-resolution and bulk scale.

A summary of the results obtained in the second period of the project can be found in Kuzmenkova et al., 2013. Rock samples were previously analysed to determine their mineralogical composition; they were crushed and sieved with size 1-2 mm.

Batch sorption experiments, as a function of time and pH, were performed in glove box with inert atmosphere (N₂) to exclude possible influence of carbonate complexes formation of U(VI). Sodium perchlorate was used as a background electrolyte (0.01 M). Initial concentration of uranium was $1 \cdot 10^{-7}$ mol/L and isotope ²³³U ($T_{1/2} = 1.59 \cdot 10^5$ years) was used for liquid-scintillation counting. The solid to liquid ratio was 1:4. Rock samples were crushed and sieved with size 1-2 mm.

Sorption equilibrium for U(VI) was obtained in 10-15 days, similar for all the all the samples.

Sorption increased with time in the whole investigated pH range. Shape of the observed sorption pH-dependence is typical for U(VI): increase of sorption from acidic to near neutral pH region (pH >4), plateau from pH ~5 to ~8, further decrease of sorption due to hydrolysis of uranyl-cation. The average pH value of pore water for used rock samples is about 8 which is close to the decreasing edge of U(VI) sorption pH-dependence.

Comparison of distribution coefficients obtained on Äspö diorite by different beneficiaries

In the next Tables, the comparison between the experimental sorption data obtained for uranium (VI) (Table 2), selenium (Table 3) technetium (Table 5) and caesium (Table 4), will be shown. The tables summarize some experimental details, and the distribution coefficients, as determined by the participant. The Tables provide also the sorption values normalized to the BET area of the material (measured by each participant, when specifically indicated). In the case that the BET area was not measured the values used were the following: for the 0.5⁻¹mm fraction 0.0912 m²/g (provided by CTH); for the 1-2 fraction 0.125 m²/g (provided by HZDR) and for not crushed materials 0.0066±0.0013 m²/g (provided by CTH).

Table 2. Summary of U(VI) sorption results obtained in Äspö diorite and synthetic Äspö groundwater by different groups.

	HZDR	HZDR	CIEMAT	CIEMAT	CIEMAT	KIT-INE	KIT-INE	KIT-INE	CTH
Radionuclide	²³³ U	²³³ U	²³³ U	²³³ U	²³³ U	²³³ U	²³³ U	²³³ U	²³³ U
Oxidation state	U(VI)	U(VI)	U(VI)	U(VI)	U(VI)	U(VI)	U(VI)	U(VI)	U(VI)
Solid fraction (mm)	1-2	1-2	0.5-1	1-2	1-2	1-2	1-2	1-2	0.5-1
BET (if measured) (m²/g)	0.125	0.125	0.094	0.079	0.0066(*)	0.1389	0.1389	0.1389	0.091
Oxidised/not oxidized material	Not Ox.	Not Ox.	Not Ox.	Not Ox.	Not Ox.	Not Ox.	Oxidized	Oxidized	Not Ox.
Solid:Liquid ratio (g/L)	200	200	10	10	300-400	250	250	250	20
pH	8.02±0.09	8.03±0.02	7.70±0.15	7.60±0.15	5	8	8	8	7.47±0.32
Atmosphere	Anoxic (N ₂) Centr: 2280 x g, 15 min + filtration (450 mm)	Anoxic (N ₂) Centr: 2280 x g, 15 min + filtration (450 mm)	Anoxic (N ₂) Centr: 20000 x g, 30 min	Anoxic (N ₂) Centr: 20000 x g, 30 min	Anoxic (N ₂) Centr: 20000 x g, 30 min	Anoxic (Ar) Ultracentrifugation tested: (694,000 × g, 1 hour): no clear influence	Anoxic (Ar) Ultracentrifugation tested: (694,000 × g, 1 hour): no clear influence	Anoxic (Ar) Ultracentrifugation tested: (694,000 × g, 1 hour): no clear influence	Anoxic(N ₂) Centr: 1000xg 15 min
Separation									
Type of experiment, contact time	Kd deter., 3 months	Isotherm, 60 days	Isotherm, 14 days	Isotherm, 14 days	Ka determ., 1 week	Kd deter., 63 days	Kd deter., 63 days	Kd deter., 63 days	Kd deter. 1 month
RN Concentration	1 × 10 ⁻⁶ M	3 × 10 ⁻⁹ - 6 × 10 ⁻⁵ M	4.5 × 10 ⁻⁷ - 1 × 10 ⁻³ M	4.5 × 10 ⁻⁷ - 1 × 10 ⁻³ M	1 · 10 ⁻³ M	1.0 × 10 ⁻⁷ & 4.7 × 10 ⁻⁸ M	1.0 × 10 ⁻⁷ & 4.7 × 10 ⁻⁸ M	1.0 × 10 ⁻⁷ & 4.7 × 10 ⁻⁸ M	1.0 × 10 ⁻⁹ M
Kd value (L/Kg)	1.4 ± 0.2	Linear sorption Mean K _d = 3.8 ± 0.6	Linear sorption: Precipit [U] > 1 · 10 ⁻⁴ Mean K _d = 5.3 ± 1.0	Linear sorption Precipit. [U] > 1 · 10 ⁻⁴ Mean K _d = 4.0 ± 2.0	Recalculated from Ka Kd(anoxic)*=2.90 Kd(oxic)*=0.23	3.16-5.62	3.16-5.62	3.16-5.62	0.99±0.52
Log(Kd)	0.146	0.580	0.728	0.600	0.762	0.500-0.750	0.500-0.750	0.500-0.750	-0.043
Normalized Kd (m)	1.1 · 10 ⁻⁵	3.0 · 10 ⁻⁵	5.6 · 10 ⁻⁵	5.1 · 10 ⁻⁵	---	2.3 - 4.1 · 10 ⁻⁵	2.3 - 4.1 · 10 ⁻⁵	2.3 - 4.1 · 10 ⁻⁵	1.1 · 10 ⁻⁵
Valence of sorbed RN	Predominantly U(VI)	---	ND	ND	ND	ND	ND	ND	ND
Kinetics // (t)	YES, 5-108 days	---	NO	NO	NO	Yes, 1-63 days	Yes, 1-63 days	Yes, 1-63 days	YES, 1w-3 months
Equilibrium time	10-20 days	---	---	---	---	not reached	not reached	not reached	7 days
Complementing techniques	TRLIF, ATRFT-IR	---	---	---	PIXE	ND	ND	ND	---
Other experimental parameters	---	---	---	---	Ka(anoxic)=4.4 · 10 ⁻⁴ (m)	---	---	---	---
					Ka(oxic)=3.5 · 10 ⁻⁵ (m)				

Table 3. Summary of Se sorption results obtained in Äspö diorite and synthetic Äspö groundwater by different groups.

	UJV-NRI	UJV-NRI	UJV-NRI	UJV-NRI	CIEMAT
Radionuclide	Se	Se	Se	Se	Se
Oxidation state	Se(IV)/Se(VI)	Se(IV)/Se(VI)	Se(IV)/Se(VI)	Se(IV)/Se(VI)	Se(IV)
Solid fraction (mm)	0.5-1	0.5-1	1-2	1-2	Not Crushed
BET (if measured) (m²/g)	0.091 (*)	0.091 (*)	0.125(*)	0.125(*)	0.0066(*)
Oxidised/not oxidized material	Oxidised	Not Oxidised	Oxidised	Not Oxidised	Oxidised/Not Oxidised
Solid:Liquid ratio (g/L)	100	100	100	100	300-400
pH	7.2-7.4	8.4-8.1	7.2-7.4	8.7-8.2	7.9
Atmosphere	Air	Anoxic (N ₂)	Air	Anoxic (N ₂)	Anoxic(N ₂)/Air
Separation	Centr.:12000 rpm, 10 min	Centr.:12000 rpm, 10 min	Centr.:12000 rpm, 10 min	Centr.:12000 rpm, 10 min	Not crushed
Type of experiment, contact time	Kd determ., 112 days	Kd determ., 112 days	Kd determ., 112 days	Kd determ., 112 days	Ka determ., 1 week
RN Concentration	2·10 ⁻⁵ M	2·10 ⁻⁵ M	2·10 ⁻⁵ M	2·10 ⁻⁵ M	1·10 ⁻³ M
Kd value (L/Kg)	1.3±0.1 / 0	2.2±0.1 / 0.3±0.1	1.6±0.1 / 0	2.1±0.1/0.2	Recalculated from Ka* Kd(anoxic)*=0.6 Kd(oxic)*=0.3 0.903/0.301
Log(Kd)	0.114 / --	0.342/ -0.52	0.204 / --	0.322 / -0.698	
Normalised Kd (m)	1.4·10 ⁻⁵ / 0	2.4·10 ⁻⁵ / 3.2·10 ⁻⁶	1.3·10 ⁻⁵ / 0	1.7·10 ⁻⁵ / 1.6·10 ⁻⁶	
Valence of sorbed RN	---	---	---	---	---
Kinetics // (t)	YES, 1-112 d	YES, 1-112 d	YES, 1-112 d	YES, 1-112 d	NO
Equilibrium time	30-60 d	30 d	30-60 d	30 d	---
Complementing techniques	ESCA, LA-ICP-MS	---	ESCA, LA-ICP-MS	---	PIXE
Other experimental parameters	---	---	---	---	Ka(anoxic)=9·10 ⁻⁵ (m) Ka(oxic)=4.5·10 ⁻⁵ (m)

Table 4. Summary of Cs sorption results obtained in Äspö diorite and synthetic Äspö groundwater by different groups.

	KIT-INE	KIT-INE	CTH	CIEMAT	CIEMAT	CIEMAT
Radionuclide	¹³⁷ Cs	¹³⁷ Cs	¹³⁷ Cs	¹³⁷ Cs	¹³⁷ Cs	¹³⁷ Cs
Oxidation state	Cs(I)	Cs(I)	Cs(I)	Cs(I)	Cs(I)	Cs(I)
Solid fraction (mm)	1-2	1-2	0.5-1	0.5-1	1-2	1-2
BET (if measured) (m²/g)	0.1389	0.1389	0.091	0.094	0.079	0.079
Oxidised/not oxidized material	Oxidised	Not Oxidised	Not Ox.	Not Ox.	Not Ox.	Not Ox.
Solid:Liquid ratio (g/L)	250	250	20	10	10	10
pH	8	8	7.47±0.32	7.2±0.2	7.2±0.2	7.2±0.2
Atmosphere	Anoxic (Ar)	Anoxic (Ar)	Anoxic (N ₂)			
Separation	Ultracentrifugation tested;(694,000 × g, 1 hour); no clear influence	Ultracentrifugation tested;(694,000 × g, 1 hour); no clear influence	Centr: 1000xg 15 min	Centr: 20000 x g, 30 min	Centr: 20000 x g, 30 min	Centr: 20000 x g, 30 min
Type of experiment, contact time	Kd determ., 63days	Kd determ., 63days	Kd deter. 1 month	Kd deter., 57 days	Kd deter., 57 days	Isotherm. 14 days
RN Concentration	9.89·10 ⁻¹⁰ M	9.89·10 ⁻¹⁰ M	1·10 ⁻⁷ M	5.4·10 ⁻⁹ M	5.4·10 ⁻⁹ M	1·10 ⁻⁹ – 1·10 ⁻³ M
Kd value (L/Kg)	31.6	44.7	15.7	75±10	93±10	Non linear sorption Max: 104 ([Cs] ₈)<1·10 ⁴ Min: 4 ([Cs] ₈)>1·10 ⁴
Log(Kd)	1.50	1.65	1.20	1.875	1.968	2.017 / 0.602
Normalized Kd (m)	2.3·10 ⁻⁴	3.2·10 ⁻⁴	1.8·10 ⁻⁴	7.9·10 ⁻⁴	1.2·10 ⁻³	1.3·10 ⁻³ /5.0·10 ⁻⁵
Valence of sorbed RN	---	---	---	---	---	---
Kinetics // (t)	Yes, 1-63 days ~ 7days	Yes, 1-63 days ~ 7days	YES, 1w-3 m 7 days	YES, 1d – 2 months 1d	YES, 1d – 2 months 1d	---
Equilibrium time	---	---	---	---	---	---
Complementing techniques	---	---	---	---	---	---
Other experimental parameters	---	---	---	---	---	---

Table 5. Summary of Tc sorption results obtained in Äspö diorite and synthetic Äspö groundwater by different groups.

	KIT-INE	KIT-INE	CIEMAT	CIEMAT
Radionuclide	⁹⁹ Tc	⁹⁹ Tc	⁹⁹ Tc	⁹⁹ Tc
Oxidation state	Tc(VII)	Tc(VII)	Tc(VII)	Tc(VII)
Solid fraction (mm)	1-2	1-2	0.5-1	1-2
BET (if measured) (m²/g)	0.1389	0.1389	0.094	0.079
Oxidised/not oxidized material	Not Oxidised	Oxidised	Not Ox.	Not Ox.
Solid:Liquid ratio (g/L)	250	250	10	10
pH	8	8	7.9±0.1	7.7±0.2
Atmosphere	Anoxic(Ar)	Anoxic (Ar)	Anoxic (N ₂)	Anoxic (N ₂)
Separation	Centr: 694,000 × g, 1 hour	Centr: 694,000 × g, 1 hour	Centr: 20000 x g, 30 min	Centr: 20000 x g, 30 min
Type of experiment, contact time	sorption kinetics, 1 hour-6 months	sorption kinetics, 1 hour-6 months	Isotherm, 14 days	Isotherm, 14 days
RN Concentration	1·10 ⁻⁵ /1·10 ⁻⁸ /1·10 ⁻⁹ M	1·10 ⁻⁵ /1·10 ⁻⁸ /1·10 ⁻⁹ M	5.9·10 ⁻⁷ - 5.3·10 ⁻⁵ M	5.9·10 ⁻⁷ - 5.3·10 ⁻⁵ M
Kd value (L/Kg)	1.2/500/1000	0.5/3/3	Non-linear sorption Max: 5.59 ([Tc]=6·10 ⁻⁷) Min: 0 ([Tc]=5·10 ⁻⁵)	Non-linear sorption Max: 5.59 ([Tc]=6·10 ⁻⁷) Min: 0 ([Tc]=5·10 ⁻⁵)
Log(Kd)	0.08/2.699/3	-0.301/0.477/0.477	1.46/--	0.75/--
Normalised Kd (m)	8.6/3600/7200 · 10 ⁻⁶	3.6//21.6/21.6 · 10 ⁻⁶	Max: 3.1·10 ⁻⁴	Max: 7.1·10 ⁻⁵
Valence of sorbed RN	Tc(IV)	Tc(IV)	--	--
Kinetics // (t)	---	---	--	--
Equilibrium time	---	---	---	---
Complementing techniques	XPS	XPS	---	---
Other experimental parameters	---	---	---	---

References

- Heck, S. and Schäfer T. (2012) “Short Note: CP Crock groundwater sample characterization”. Note distributed to all project participants.
- Holgersson, S. and Albinsson, Y.: Diffusion of HTO and cement pore fluids through host rock. *Radiochimica Acta* 90, 99-108 (2002).
- Johansson, H., Siitari-Kauppi, M., Skålberg, M. and Tullborg, E.L.: Diffusion pathways in crystalline rock-examples from Äspö-diorite and fine-grained granite. *Journal of Contaminant Hydrology* 35, 41-53 (1998).
- Kuzmenkova N., Petrov V., Vlasova I., Petrov V., Poluektov V., Kalmykov S. “ U(VI) sorption onto rock samples from areas of the proposed HLW and SNF repository in Russia (Nizhnokansky massive)”. Final CROCK Workshop (May 14-16, 2013, Karlsruhe, Germany). Paper & Oral Communication;
- Missana T. and García-Gutiérrez M. (2012 a) “Analysis of the caesium sorption behaviour on biotites of different origin”- 1st CROCK Workshop (May 22-24, 2012, Stockholm, Sweden) Paper & Poster;
- Missana T. and García-Gutiérrez M. (2012 b) “Comparison of the caesium adsorption on different crystalline rocks” – 1st CROCK Workshop (May 22-24, 2012, Stockholm, Sweden) Paper & Oral Communication;
- Missana T. and García-Gutiérrez M. (2013) “Analysis of sorption onto granites and granite minerals: the case of Cs”. Final CROCK Workshop (May 14-16, 2013, Karlsruhe, Germany). Paper;
- Petrov V.G., Vlasova I.E., Kuzmenkova N.V., Petrov V.A., Poluektov V.V., Grivot A., Kalmykov S.N. (2012) “Characterisation of rock samples from areas of the proposed Russian HLW and SNF repositories (Nizhnokansky massive) and first sorption studies - 1st CROCK Workshop (May 22-24, 2012, Stockholm, Sweden). Paper;
- Petrov, V.G. et al. (2012) Characterisation of rock samples from areas of the proposed. Russian HLW and SNF repository (Nizhnokansky massive) and first sorption studies. 1st Workshop Proceedings of the Collaborative Project „Crystalline Rock Retention Processes“ (7th EC FP CP CROCK): 37-42.
- Schäfer, T., Stage, E., Büchner, S., Huber, F., Drake, H. (2012) Characterization of new crystalline material for investigations within CP CROCK. 1st CROCK Workshop Proceedings.
- Schmeide, K., Gürtler, S., Müller, K., Steudtner, R., Joseph, C., Bok, F., Brendler, V. (2012): Sorption of U(VI) and Np(V) onto diorite from Äspö HRL” – 1st CROCK Workshop (May 22-24, 2012, Stockholm, Sweden). Paper & Oral Communication
- Totskiy Y., Schäfer T., Huber F., Schild D., Geckeis H., Kalmykov S. (2013) Tc(VII) sorption on natural granitic rocks and synthetic magnetite). Final CROCK Workshop (May 14-16, 2013, Karlsruhe, Germany). Paper;
- Totskiy, Y., Geckeis, H., Schäfer, T. (2012) Sorption of Tc(VII) on Äspö Diorite (ÄD). 1st Workshop Proceedings of the Collaborative Project „Crystalline Rock Retention Processes“ (7th EC FP CP CROCK): 97-105.
- Videnská K., Havlová V., Vašinová M., Sajdl P. (2013) “Study of Selenium sorption on Äspö diorite surface using spectroscopic methods”. Final CROCK Workshop (May 14-16, 2013, Karlsruhe, Germany). Paper & Oral Communication;
- Videnská K., Havlová V., Vejsadů J. (2013) “Study of selenium sorption on Äspö DIORITE” Final CROCK Workshop (May 14-16, 2013, Karlsruhe, Germany). Paper & Oral Communication

WORKPACKAGE 3

REAL SYSTEM ANALYSIS

John Smellie^{1*}

¹ Conterra AB (Sweden)

* Corresponding author: john.smellie@conterra.se

Introduction

Real systems analysis is used specifically for identification of matrix diffusion on real time and spatial scales. The matrix diffusion process is identified by real system analysis making use of findings from the past Swedish site selection programme.

WP3 overall objectives were twofold:

- to use WP3 data in order to obtain insight into matrix diffusion processes based on natural conservative tracers determined in real system samples selected from profiles extending from water conducting fracture surfaces out into the adjacent low transmissive rock matrix. Furthermore, using data generated from these natural chemical homologues, the effect of matrix diffusion on the far field behaviour of radionuclides in fractured crystalline rock in Sweden may be evaluated;
- to use WP3 data, (i.e. natural conservative tracers determined in real system samples from Sweden selected from profiles extending from water conducting fracture surfaces out into the adjacent low transmissive rock matrix), to produce estimates of the geometric formation factor for solute diffusion with corrections for surface conduction bias.

It was hoped that this calibration process could provide reliable effective parameters (e.g. effective diffusion coefficient, capacity ratio, retardation factors etc.) to be used in the framework of the benchmark exercise for WP5.

Description of the work performed

CONTERRA AB

The main objective for Conterra in Workpackage 3 has been to supply the beneficiaries Kemakta and Amphos all relevant background sources of the analytical and field porewater data, together with interpretations, from the recent Swedish site characterisation programme with a focus on matrix diffusion. All data are from the Forsmark and Laxemar sites with the majority collected from the period 2003-2008 and some additional data from Forsmark taken more recently in 2011 (Smellie, 2011; 2012a; 2012b).

AMPHOS 21

In Workpackage 3 an improved method for correcting the measurement data to remove the theoretical bias introduced by surface conduction has been demonstrated (Molinero and Trinchero, 2012). The method is based on the use of an empirical power law relation describing how surface conduction varies as a function of the true geometric formation factor as ascertained in independent laboratory experiments made using core samples saturated with water of differing ionic strengths. Then, the corrected formation factors have been used to derive upscaled values of diffusion length, porosity and diffusion coefficients, which are key parameters required for the quantitative models of Workpackage 5.

KEMAKTA

As part of the Geophysical programme in the recently completed SKB site investigations at Forsmark (Crawford, 2012a), a large number of measurements were made of in-situ formation factors using a downhole electrical resistivity probe technique. The formation factor is obtained as the ratio of the electrical conductivity of the rock divided by that of the pore water in the rock matrix. The accuracy of the method is strongly determined by, among other things, the accuracy with which the porewater conductivity can be estimated and the bias introduced by the effect of charge conduction in the electrical double layer in the constrictive pores of the rock matrix. Since the porewater ionic strength is uncertain and frequently too low to be able to discount this effect, a significant bias can be introduced which may result in an overestimation of the formation factor when interpreting data obtained using the in-situ geophysical technique. In Workpackage 3 Kemakta have demonstrated an improved method for correcting the measurement data to remove the theoretical bias introduced by surface conduction (Crawford, 2012b). The method is based on the use of an empirical power law relation describing how surface conduction varies as a function of the true geometric formation factor as ascertained in independent laboratory experiments made using core samples saturated with water of differing ionic strengths.

References

- Crawford, J. (2012a). Diffusive retention processes. Estimation of in-situ formation factors by electrical resistivity measurements - 1st CROCK Workshop (May 22-24, 2012, Stockholm, Sweden), Oral communication.
- Crawford, J. (2012b). Decreasing uncertainty of radionuclide migration predictions in safety assessment modelling - 1st CROCK Workshop (May 22-24, 2012, Stockholm, Sweden), Paper.
- Molinero, J. and Trinchero, P. (2012). On the relevance of matrix diffusion for the hydrogeochemical stability of the Deep Geological Repository - 1st CROCK Workshop (May 22-24, 2012, Stockholm, Sweden), Oral communication.
- Smellie, J. (2011). Real system analysis. Deliverables D3.1 and D3.2 published in the CP CROCK web homepage.
- Smellie, J. (2012a). Real system analysis: Update. Deliverables D3.1 and D3.2 published in the CP CROCK web homepage.
- Smellie, J. (2012b). Real system analysis - 1st CROCK Workshop (May 22-24, 2012, Stockholm, Sweden), Paper.

WORKPACKAGE 4

CONCEPTUALIZATION AND MODELLING

James Crawford^{1*}

¹ Kemakta konsult AB, Warfinges väg 33, S-112 93 Stockholm (SWE)

* Corresponding author: james@kemakta.se

Introduction

In the work package 4 (WP4) of the CROCK collaborative project, the main aim was the reduction of uncertainties in performance assessment (PA) modelling by developing and evaluating approaches for generating reliable data, improving the understanding of geochemical controls over radionuclide migration, and evaluating different modelling approaches spanning the continuum from microscopic and macroscopic laboratory investigations to field scale applications.

The lack of site-specific data for transport modelling was identified early on as an important area of uncertainty in PA. This was found to concern both the selection of relevant K_d values for use in PA models incorporating simplified descriptions of sorptive chemistry as well as for the direct integration of mechanistic modelling approaches within more sophisticated PA tools. Therefore, a significant effort was made to develop and evaluate methods for generating these kinds of data by each of the four beneficiaries.

One of the interesting outcomes of this work has been the diverse range of approaches adopted by the different modelling teams to attack these various issues. Amphos 21 approached the problem of K_d estimation in PA through the use of a semi-empirical spreadsheet tool based on a simplified representation of surface complexation and ion exchange. Kemakta, on the other hand, studied the K_d estimation problem by framing the issue in terms of generalised empirical relations describing binding constants in surface complexation models through the use of geochemical analogies. VTT looked at the problem on both a microscopic level using quantum chemistry computational approaches in parallel to more traditional approaches involving fitting of surface complexation binding constants to macroscopic sorption measurement data for biotite; a mineral thought to dominate sorption on site specific rocks within the Finnish national program for storage of spent nuclear fuel.

While the first three beneficiaries studied K_d selection issues in PA involving batch measurement data, the KIT-INE team instead studied the simultaneous flow and reactive transport of radionuclides in laboratory tracer migration experiments involving a confined fracture sample. By looking at the dynamics of the coupled transport processes, additional insights were obtained that would not have been apparent when considering only batch data in isolation. The following paragraphs detail the detailed work that has been performed by each of the beneficiaries in this challenging and relatively ambitious work package.

Description of the work performed

AMPHOS 21

The work by Amphos 21 documented in García et al. (2013) seeks to reduce uncertainty in conditional K_d estimates for PA using a spreadsheet based approach which incorporates features of surface complexation and cation exchange models in a simplified manner. Although the concept of K_d is generally regarded as having no particular mechanistic basis, a thermodynamically consistent K_d for a sorbing nuclide can be defined nonetheless as the ratio of the sum of contributions of various surface sorbed species (surface complexation and cation exchange) to the total dissolved concentration of that nuclide in solution. The basic idea pursued in this work was to substitute the appropriate thermodynamic mass action equations directly into the analytical K_d expression to give the concentrations of each individual surface species in terms of the independent variables sorbent mass, binding site density, pH, ionic strength and dissolved ligand concentrations in the aqueous phase.

In order to make a directly evaluable analytical expression, however, some simplifying assumptions were needed to be made. Chief among these was that the concentration of the sorbing nuclide was negligible relative to the concentration of binding sites. A further implicit assumption was that the sorption of the nuclide had negligible impact on the distribution of other chemical components in the aqueous phase. The second assumption in particular, allowed corrections for electrostatic effects to be simply accounted for since these could then be estimated as a function of ionic strength and pH without iterative calculation and thus incorporated directly into the analytical expression for the K_d .

Data were calculated for three systems that each involved one radionuclide and one mineral, with the aim of eventually using an additive approach for more complex systems. The K_d values calculated were generally found to be within one order of magnitude of experimental data from a number of studies, which themselves spanned up to five orders of magnitude. Evaluation of the estimated K_d values against more sophisticated numerical calculations made using PhreeqC (Parkhurst and Appelo, 1999) showed that the simplifications applied in the model introduced some additional data scatter, but the overall agreement was reasonable..

Kemakta Konsult AB

Kemakta's approach to reducing K_d uncertainty centred around the application of linear free energy relationships (LFER's) to overcome the scarcity of experimental data to constrain surface complexation models (Crawford, 2013). Customary methods for fitting surface complexation models to laboratory data are difficult to apply when dealing with mineralogically and microstructurally complex materials such as granite. It is generally not feasible, for example, to obtain detailed sorption edge measurements for granular materials with diffusive equilibration times which may extend many months, or perhaps years (a *sorption edge* is a detailed set of measurements correlating K_d or percentage sorbed versus pH). With this in mind, the aim of the work was therefore to develop more reliable methods for fitting surface complexation models to sparse, non-ideal data sets for the purpose of extrapolating K_d values to conditions for which there are no experimental data.

The existence of an LFER posits a systematic analogy between a general class of surface complexation reaction and hydrolysis reactions in solution involving the same nuclide. Typically this reveals itself as an empirical linear relation between the thermodynamic binding constants for sorption of dissolved nuclides to a mineral phase and the analogous hydrolysis reaction constants when plotted on a log-log scale. Each mineral has its own LFER with a characteristic intercept and slope. Theoretical analysis suggests that the slope of the LFER has overwhelming importance for describing the relative variation of sorption with pH, whereas the intercept can be treated as a normalizable parameter in a similar fashion to binding site density or mineral surface area. On the

basis of this observation a method referred to as the “*bootstrapped component additivity approach (BCA)*” was developed (see Crawford, 2013).

The approach was evaluated using site-specific data for Am, Eu and Ni sorption to Forsmark metagranite in saline and fresh groundwater. Parameter fitting was used to identify empirical weighting factors incorporating both the uncertain intercept of the LFER and availability of sites for a few assumed key minerals that would give the best match to the measurement data for saline groundwater. The slopes (only) of the LFER's for the various minerals were specified using data reported in the literature. Since LFER intercepts are sensitive to small differences in surface site density and mode of preparation or preconditioning of single phase minerals typically used in laboratory experiments reported in the literature, the implicit optimization of LFER intercepts to match the surface reactive properties of the actual target material therefore affords potential improvements in model performance over using literature binding constants directly as in the conventional “*component additivity (CA)*” modelling approach.

The calculations were made in an iterative fashion using PhreeqC (Parkhurst and Appelo, 1999) and a simplified non-electrostatic model of surface complexation. The weighting factors were then applied to predict sorption of the radionuclide species calculated to be present in the fresh Forsmark groundwater also using PhreeqC and assuming linear additivity of contributions from the different mineral surfaces. The model appears to make a skilful prediction of sorption in contact with Fresh groundwater without any further adjustment of parameters. This suggests that the approach might be useful for reducing uncertainty in effectively blind K_d predictions for specific groundwater conditions based on surface complexation modelling where little or no measurement data exists.

VTT

The work carried out by VTT-Finland attempts to link the description of sorption processes over different spatial scales ranging from molecular- to laboratory- and finally the field-scale. The aim of this work is to provide a mechanistically based means of partially validating the much simplified models used in PA modelling using detailed mechanistic information gathered from lower hierarchies of detailed model abstraction. To this end the work has focused both on *ab initio* molecular modelling of sorption processes and macroscopic surface complexation modelling of experimental data obtained within the Finnish programme. Since the accessory mineral biotite is considered to be an important reactive mineral phase at the Finnish Olkiluoto repository site, this mineral was the focus of two studies conducted in parallel by VTT (Puhakka and Olin, 2013; Itälä et al. 2013).

In the work detailed in Puhakka and Olin (2013) a quantum chemistry approach was used to calculate the molecular interactions of water and hydrated Ni^{2+} sorption to annite, the Fe-end member of the biotite series. The study identified two distinct surface environments: basal surfaces, with a reactivity controlled by surface bound K^+ ions; and terminal surfaces, which react readily with water to give a hydroxylated surface structure. On the basal sites, sorption of $Ni(H_2O)^{2+}$ involved ion exchange with surface bound K^+ , while on the terminal sites, $Ni(H_2O)^{2+}$ formed a surface complex with the water molecule layer. Therefore, when the ratio of the two sites is known, each reaction can be calculated for the relevant proportion of the total surface.

In the second work phase detailed in Itälä et al. (2013), three surface complexation models (non electrostatic, diffuse layer and constant capacitance) were tested for their ability to fit macroscopic Ni and Eu sorption data to 3 biotite and 2 rock samples (Ni only) over a pH range of 2-10. Titration curves were available for one biotite sample (Luumäki), and these were fitted to generate stability constants for protonation/deprotonation reactions

at the surface sites and sorption site density data. Although this data was used in the surface complexation modelling of Ni and Eu to Luumäki biotite, it did not improve the model fits to the other data sets. It was therefore found that each material needed to be parameterised independently. In general, the non-electrostatic model gave better fits to the data than the diffuse layer or constant capacitance models, and it was able to model Ni better than Eu, due to the very high Eu sorption observed at high pH.

KIT-INE

In the work carried out by KIT-INE (in collaboration with Amphos 21) and documented in Huber et al. (2013), a PA modelling approach was used to simulate laboratory scale migration experiments involving a sampled natural fracture in a confined Äspö diorite drill core. The FASTREACT modelling tool (Trincherio et al. 2011) was used to simulate the migration of tritiated water (Hto) as well as the redox sensitive ^{237}Np nuclide. The streamtube modelling approach in FASTREACT assumes steady state flow with no mass exchange between adjacent streamlines in the fracture flow field. Owing to difficulties in fully specifying the experimental boundary conditions it was found to be difficult to reproduce the breakthrough of the conservative solute (Hto) using the computed flow field directly and an alternative approach based on computing an empirical residence time distribution probability density function was used to characterise the solute travel time. Sorption of the reactive tracer ^{237}Np was modelled using a number of different sorption modelling techniques ranging from simple K_d based sorption models (first order reversible sorption/desorption kinetics) to more complex, mechanistically based surface complexation models involving up to three separate mineral sorbing phases (hydrous ferric oxide, biotite, and kaolinite).

Assuming that sorption occurs primarily on the flow exposed fracture surface, the retardation factor for ^{237}Np transport could be estimated directly as the ratio of the central moments of the ^{237}Np and Hto tracer breakthrough curves. From the 3D model of the flow space obtained by tomographic techniques, the specific surface area (i.e. flow wetted surface to flow volume ratio) could also be computed and the surface area normalised sorption partitioning coefficient, K_a calculated directly given the previously estimated retardation factor. Using this approach it was not possible to obtain a satisfactory match to the measured breakthrough curves for ^{237}Np using either the empirical K_d based approach or the PhreeqC based approach using surface complexation modelling, suggesting that the flow-wetted surface area estimated from the 3D model might not be representative of the true reactive surface area.

In further studies, the specific reactive surface area was treated as a fitting parameter using the FASTREACT model together with the PEST parameter optimization program (Gallagher and Doherty, 2007). Using this procedure, the model was able to better match the breakthrough time of the ^{237}Np elution, although not the peak concentration or the pronounced tailing in the breakthrough curve. It was proposed that this might be addressed in future work by coupling the model to a code that can describe kinetically controlled surface complexation reactions.

References

Crawford J, (2013) Approaches to modelling surface complexation sorption on complex geological materials with limited data. Scientific and Technical Summary paper. Final CP CROCK Workshop, Karlsruhe, Germany, 14-16th May 2013.

Gallagher M, Doherty J, (2007). Parameter estimation and uncertainty analysis for a watershed model. *Environmental Modelling & Software*, 22(7): 1000-1020.

García D, Pękal M, Domènech C, (2013). Decreasing K_d uncertainties through the application of mechanistic retention models. Scientific and Technical summary paper. Final CP CROCK Workshop, Karlsruhe, Germany, 14-16th May 2013.

Huber F, Trincherio P, Molinero J, Schäfer T, (2013) Application of the numerical framework fastreact for reactive transport modelling of Np(V) migration in a single fracture from Äspö, Sweden. Scientific and Technical summary paper. Final CP CROCK Workshop, Karlsruhe, Germany, 14-16th May 2013.

Itälä A, Tanhua-Tyrkkö M, Olin M, (2013) Surface complexation modelling of biotite – nickel and europium models. Scientific and Technical summary paper. Final CP CROCK Workshop, Karlsruhe, Germany, 14-16th May 2013.

Parkhurst D L, Appelo C A J, (1999). User's guide to PHREEQC (version 2): a computer program for speciation, batch-reaction, on-dimensional transport, and inverse geochemical calculations. Water Resources Investigations Report 99 4259, U.S. Geological Survey, Denver CO, USA.

Puhakka E, Olin M, (2013) Ab initio studies on cation exchange and surface complexation reactions on biotite surface. Scientific and Technical summary paper. Final CP CROCK Workshop, Karlsruhe, Germany, 14-16th May 2013.

Trincherio P, Molinero J, Roman-Ross G, (2011). FASTREACT - Final Report - Streamline Approach for the Solution of Multicomponent Reactive Transport Problems Svensk Kärnbränslehantering AB (SKB).

WORKPACKAGE 5

APPLICATION TO THE SAFETY CASE

Jorge Molinero^{1*}

¹Amphos 21 Passeig de Garcia i Fària, 49-51, 1-1, 08019 Barcelona

* Corresponding author: jorge.molinero@amphos21.com

Introduction

The objective of this WP was to apply the outcome of other WPs to the application in the Safety Assessment, thereby decreasing the PA uncertainty and providing improvements for future site characterizations. Also, a benchmark exercise has been set-up in order to demonstrate the entire sequence from basic chemical and physical information from the nm scale, through to application to PA and demonstration that the outcome leads to decrease in PA conservatism. The different beneficiaries of this WP have used different approaches for the solution of the benchmark exercise and the results have been compared and thoroughly analysed.

Description of the work performed

Here, we provide a brief description of the work performed by each partner in the framework of WP5 of the CROCK project. For a detailed account of the modelling results as well as the underlying conceptual models the reader is referred to the related S&T contributions (Crawford, 2013; Puhakka and Olin, 2013; Trincherro et al., 2013b).

Amphos 21

In the framework of WP5 of the CROCK project, AMPHOS 21 has developed a tool, denoted as MCPhreeqc, for the stochastic simulation of geochemical problems. The software has been used to infer effective K_d values related to caesium sorption in a typical Fennoscandian crystalline medium. The results are treated in terms of probability distributions functions (PDFs) in order to account for the uncertainties arising from the heterogeneity of the medium and the intrinsic nonlinearities of the underlying processes.

The results of this stochastic analysis have been used to set up a benchmark exercise whose aim was to demonstrate the entire “upscaling procedure”: from basic chemical and physical information from the lab scale to applications to PA studies. In order to circumvent the limitations of K_d-based models, mechanistic reactive transport simulations were carried out using the FASTREACT methodology (Trincherro et al., 2013a). These simulations, which mimic the potential release of a set of radionuclides at repository depth and the related migration along a network of fractures, are used to infer the resulting K_a value of caesium and two other radionuclides (i.e. strontium and uranium).

Summary of the results

Monte Carlo simulations were used to evaluate the uncertainty related to the caesium distribution coefficient. To this end, 50,000 equiprobable batch models are carried out using the software MPhreeqc (see Figure 1), which is used to sample the two probability distributions described in the previous section (i.e. CES and aqueous concentration of caesium, Cs) and to run the Phreeqc batch simulations. The resulting bivariate histogram of the random input parameters is shown in Figure 2.

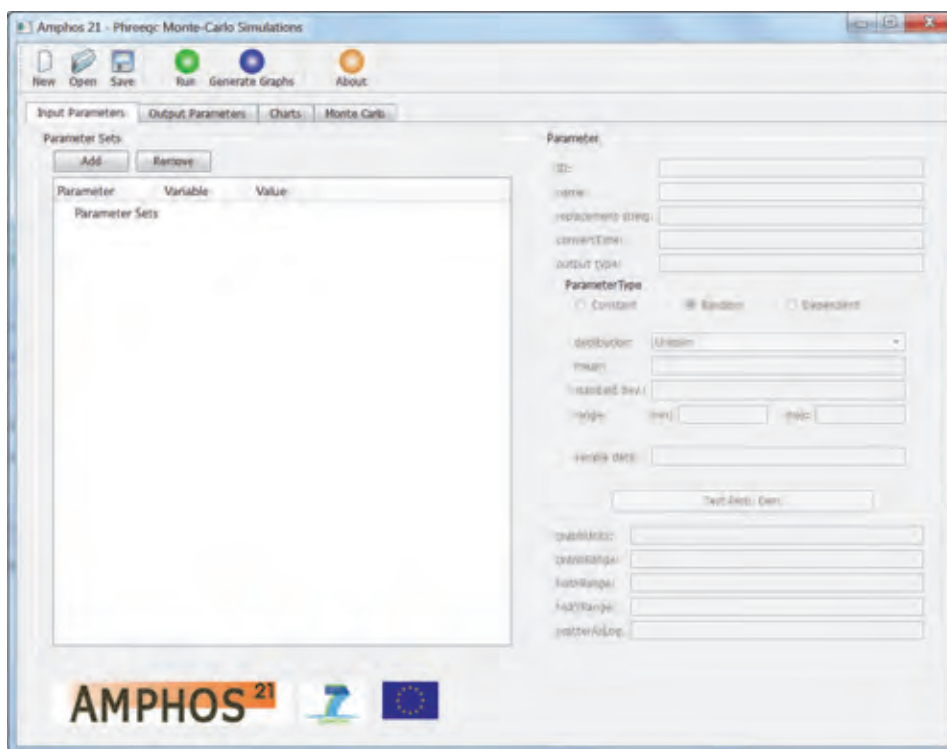


Figure 1. Screenshot of MPhreeqc graphical user interface.

Figure 3 shows the distribution of K_d values as a function of Cs aqueous concentration and the CES. It is worth noting that the uncertainties related to the heterogeneous mineralogy of the medium along with nonlinearities arising from competition and depletion of sorption sites result in a large variation of the computed K_d values, which span more than seven orders of magnitudes.

Using the results of the Monte Carlo simulations, three sorption isotherms are computed for three different values of the CES: the 2th, the 50th and the 98th percentile of the log-normal distribution (Figure 4, left). From the figure once can notice that at low concentrations, K_d values are constant (i.e. linear behaviour). Nonlinearities appear at concentrations around 10^{-8} mol/L as a consequence of the progressive depletion of sorption sites. Interestingly, the “most probable isotherm” (i.e. the one computes using the 50th percentile from the CES distribution) agrees well with recent laboratory experiments focused on caesium sorption on biotite (Missana and García-Gutierrez, 2010; see Figure 4, right).

As explained before, the results of the Monte Carlo simulation are treated in a probabilistic fashion in order to provide a parametric distribution function that may be used as input in subsequent radionuclide transport modelling. The resulting cumulative distribution function (CDF) of caesium K_d is shown in Figure 5. Again,

once can notice that the distribution function spans several orders of magnitude, with mean and standard deviation of the logarithm equal to 3.0 and 1.1 mL/g respectively. These results further suggest that, when modelling radionuclide transport with constant K_d approximations, uncertainties and nonlinearities should be explicitly recognized and properly accounted for (e.g. by using companion mechanistic geochemical models and updating the K_d values according to the geochemical changes of the system).

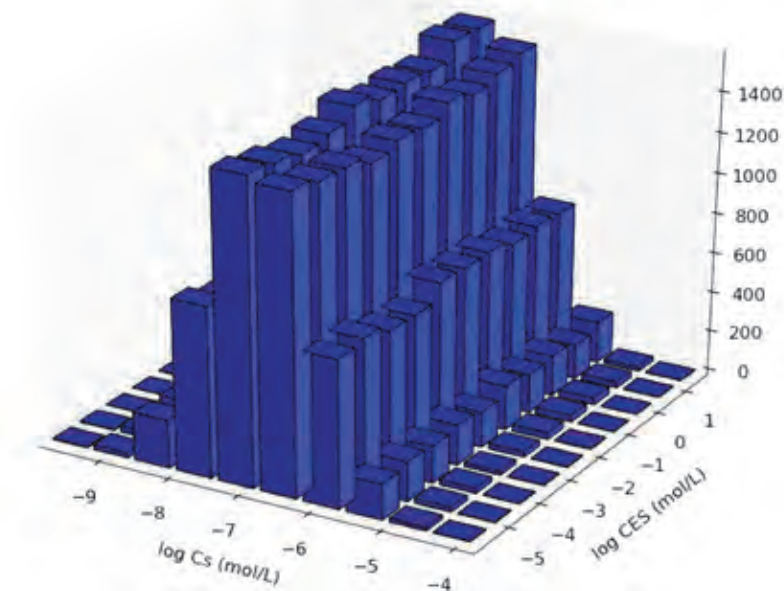


Figure 2. Bivariate histogram of the outcomes (i.e. logarithm of Caesium concentration and CES) of the Monte Carlo simulation (50000 realizations).

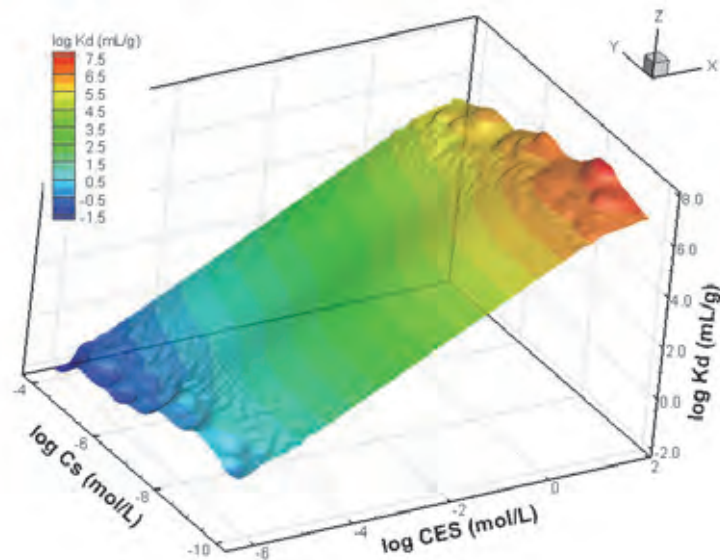


Figure 3. Results of the Monte Carlo simulation: caesium distribution coefficient (K_d) as a function of the aqueous concentration of caesium and the number of exchange sites (CES).

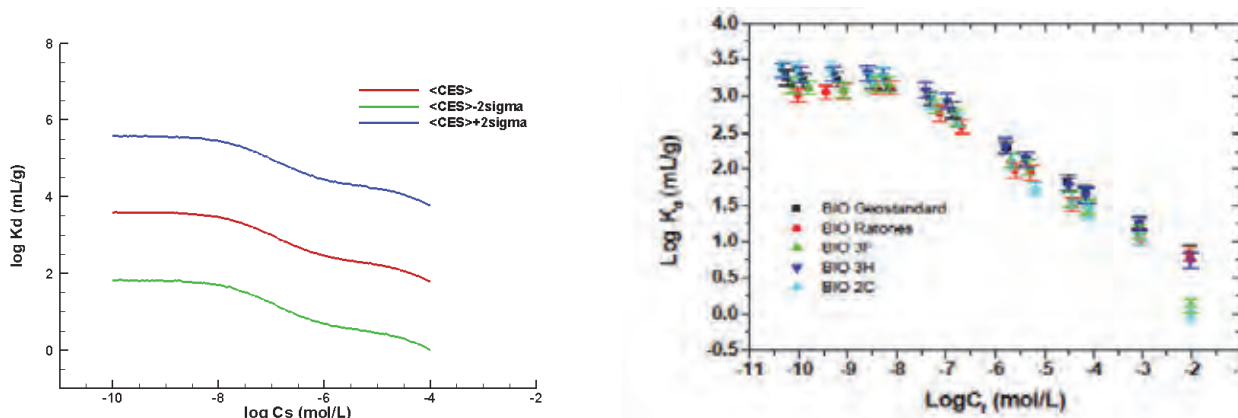


Figure 4. (left) sorption isotherms for caesium computed using different values of CES (i.e. the 2th, the 50th and the 98th percentile of the log-normal distribution) and (right) sorption isotherms obtained from experiments of caesium sorption on biotite (Missana and García-Gutiérrez, 2010).

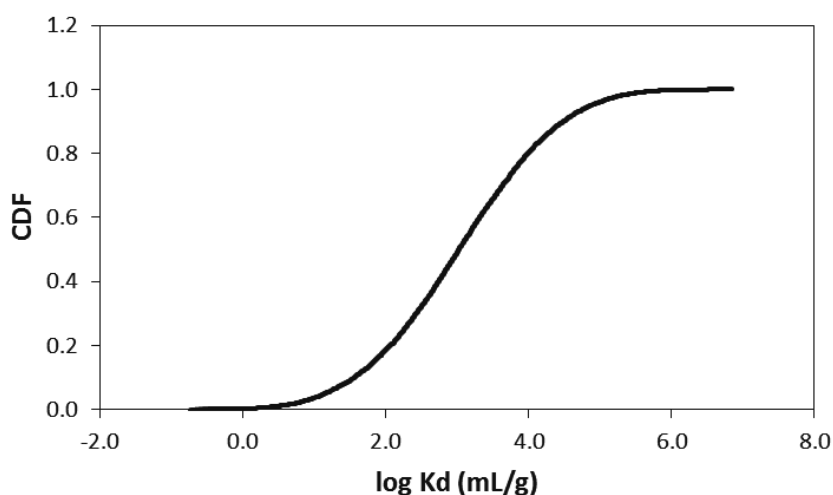


Figure 5. Cumulative distribution function (CDF) of caesium Kd obtained from the Monte Carlo simulation.

KEMAKTA

In order to test the non-linear impact of evolving groundwater composition, a simple scenario is modelled involving the intrusion of alternating pulses of Saline and Fresh groundwater end-members into a fracture system initially equilibrated with Saline groundwater. Table 1 summarises the material property data, hydrodynamic boundary conditions and other parameters used in the simulations. The hydrodynamic boundary conditions are fully specified by the F-factor (y/m) and advective travel time (y). The transport half-aperture is equal to the quotient of advective travel time and F-factor. In the present set of case studies this corresponds to a transport aperture of 0.2 mm. In the simulations, the hydrodynamic conditions are assumed to be temporally constant and only the chemical composition of the infiltrating groundwater is variable.

It should be noted by the reader that although Forsmark site-specific data for groundwater composition and material properties have been employed in this simulation exercise, the modelling scenario itself (i.e. alternating pulses of Saline and Fresh groundwater compositions and the low hydrodynamic transport resistance) should not in any way be taken to imply a case study of transport properties relevant for a hypothetical repository at the actual Forsmark site. The selected boundary conditions have been chosen to provoke clearly non-linear

behaviour in order to test underlying assumptions inherent in the adopted modelling approach and are not necessarily considered to be realistic for the performance assessment of an actual repository.

Table 1. Material property data, hydrodynamic boundary conditions, and other simulation parameters for the reactive transport case studies.

Parameter	Value (units)	Description
F-factor	10^4 y/m	hydrodynamic transport resistance
t_w	1 y	advective travel time
D_e	10^{-14} m ² /s	effective diffusivity of solute in rock matrix
ε_p	0.001	matrix storage porosity
A_0	0.018 m ² /g	BET surface area of rock matrix
CEC	1.0 mol/kg	cation exchange capacity
δ_m	1.0 m	matrix depth
K_d^{\min}	0.0036 m ³ /kg	K_d value for Ra ²⁺ , Saline end-member
K_d^{\max}	0.36 m ³ /kg	K_d value for Ra ²⁺ , Fresh end-member

Simulation results obtained using PATHTRAC are shown in Figure 6 together with corresponding results obtained using the fully coupled code CrunchFlow. It should be noted that the timing schedule of the Saline/Fresh groundwater pulses is also slightly different to the previously presented results in (Crawford, 2012). The simulation results demonstrate the main non-linearity associated with rapid turnover of groundwater salinity where solute accumulated near the surface of the rock matrix during the Fresh time domain is promptly remobilised when conditions become more saline.

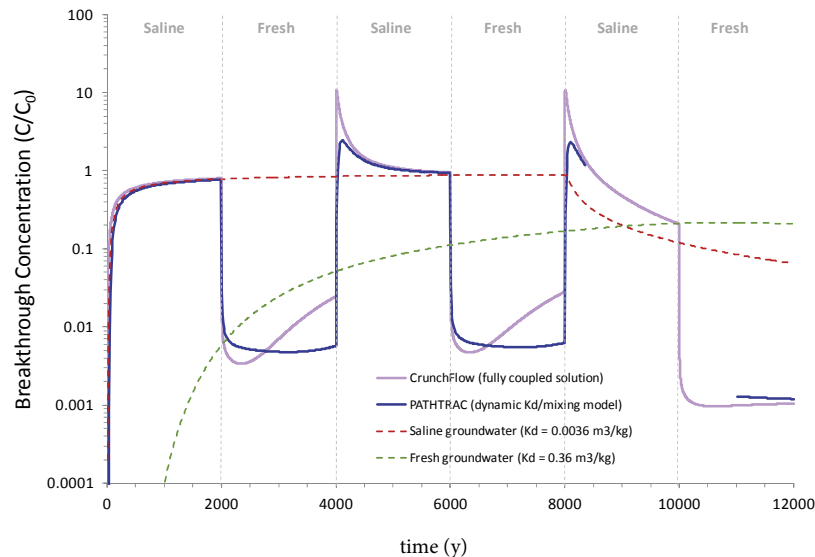


Figure 6. Comparison of breakthrough curves for Ra²⁺ migration simulated using PATHTRAC and a fully coupled reactive transport simulation using CrunchFlow for the temporally variable boundary conditions (as indicated by the fresh/saline labelled intervals in the figure). Breakthrough data are normalised relative to the constant inlet concentration boundary condition (10^{-12} mol/kgw).

VTT

Biotite has a sheet-like structure, where the sheets are connected to each other by potassium cation layer (Accelrys (2011)). According to the density functional calculations, the optimized lattice parameters of the energetically stable biotite structure are $a = 528.4$ pm, $b = 916.2$ pm, $c = 2077.3$ pm and $c/a = 3.931$ (Figure 7a). Construction of surface models to molecular modelling studies revealed that the smallest meaningful models are very atomic-rich, which causes long calculation times. In order to simplify model structures, it can be used end-members of biotite: annite and phlogopite. In this study, annite (Accelrys (2011)), where all magnesium ions are substituted by iron ions, was utilized. The unit cell of annite is about half of that of biotite. The optimized lattice parameters are $a = 513.1$ pm, $b = 893.3$ pm, $c = 1037.3$ pm, and $c/a = 2.022$ (Figure 7b), and the Si:Al ratio is 3:1.

In WP5, VTT has carried out molecular modelling to deepen understanding the chemical properties of biotite and corresponding minerals. Therefore, the molecular modelling was used to investigate formation of water molecular layer onto annite surfaces, and reaction of Ni^{2+} species on cation exchange and surface complexation sites. It was supposed that the cation exchange sites are basal surfaces like the (001) surface, and surface complexation sites are terminal surfaces like the (110) surface.

First, formation of water molecular layer was considered including both the adsorption and possible dissociation of water on the basal (001) and terminal (110) surfaces. On the basal surface, the reactivity of the surface depends on the existence of potassium ions on the surface. Otherwise, the surface structure is rather stable. On the terminal surface, there are no empty vacancies in the coordination sphere of aluminium and/or silicon atoms. However, this oxide surface can be very reactive with water forming hydroxylated surface structure. In the water adsorption studies, water molecules were adsorbed onto the surface one by one, and water molecules were allowed to find their energetically favourable positions on the surface. Also, dissociation of water molecules was allowed on the surfaces. As a result, the formation of the first water molecular layer was described.

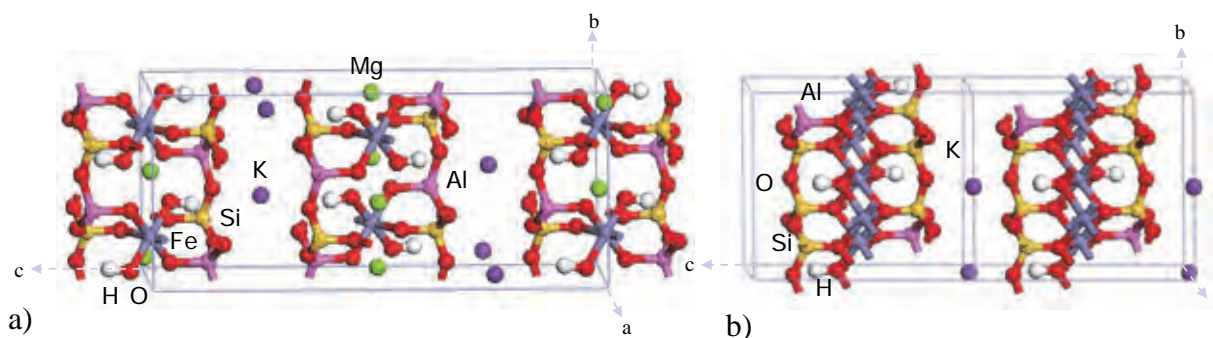


Figure 7. Optimized unit cells for a) biotite, and b) annite.

On the ideal basal (001) surface, there are no hydroxyl groups originated from the crystal structure of annite, and there are 4.4 K^+ ions/ nm^2 and 11 bridged O atoms/ nm^2 . On this surface, water forms a molecular layer, and no water dissociation happens. The water molecular layer consists of $11 \text{ H}_2\text{O}$ molecules/ nm^2 (Figure 8a).

On the ideal terminal (110) surface, there are 1.9 K^+ ions/ nm^2 and 6.6 H^+ sites/ nm^2 . Based on the calculations, every sixth water molecule dissociates forming surface hydroxyl groups in the adsorption of water onto the surface. On the first water molecular layer, there are $10 \text{ H}_2\text{O}$ molecules/ nm^2 (Figure 8b).

After the structure of water molecular layer was defined, then reaction of $\text{Ni}(\text{H}_2\text{O})_2^{2+}$ species on cation exchange and surface complexation sites was considered. The aim was to define, if a difference between the sites can be detected. It was calculated step-by-step mechanism for the reaction path which consists of a) sorption of $\text{Ni}(\text{H}_2\text{O})_2^{2+}$ above the first water molecule layer, b) desorption of water molecules from the surface, so that $\text{Ni}(\text{H}_2\text{O})_2^{2+}$ can adsorb onto the surface, and c) re-formation of the water molecule layer.

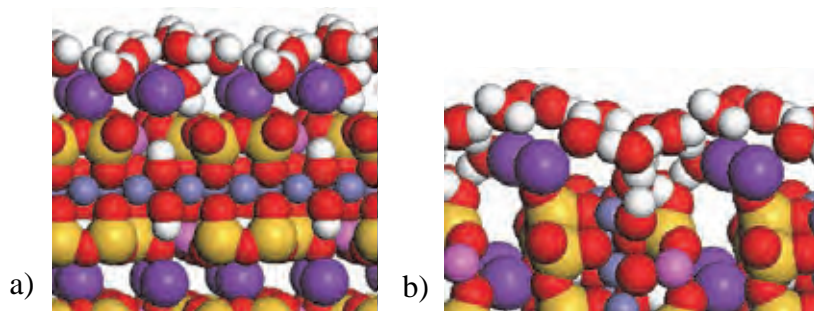
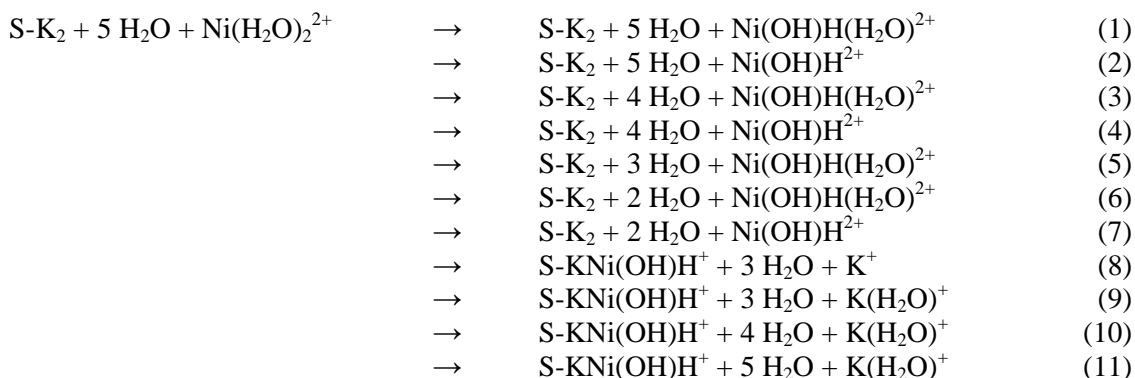


Figure 8. The first water molecular layer on the annite surfaces: a) (001) and b) (110).

On the basal (001) surface, the reaction proceeds according to Scheme 1, where S represents $\text{K}_2\text{Fe}_{12}\text{Si}_{12}\text{Al}_4\text{O}_{40}(\text{OH})_8$ surface structure:



First, $\text{Ni}(\text{H}_2\text{O})_2^{2+}$ species adsorbs onto the water covered surface (Figure 9a). After that about half of the water molecules desorb from the surface (Reactions 1-5), and $\text{Ni}(\text{H}_2\text{O})_2^{2+}$ species gets closer to the mineral surface. Re-arrangement of Ni^{2+} and K^+ ions starts during Reaction 6, and cation exchange reaction achieves the final state during Reaction 8 (Figure 9b). After that re-formation of the water molecular layer happens (Fig. 4c). The cation exchange reaction (including also re-formation of the water layer) is spontaneous reaction, which releases energy -0.29 eV. Based on this, the cation exchange reaction between Ni^{2+} and K^+ ions takes place on the basal (001) surface of annite.

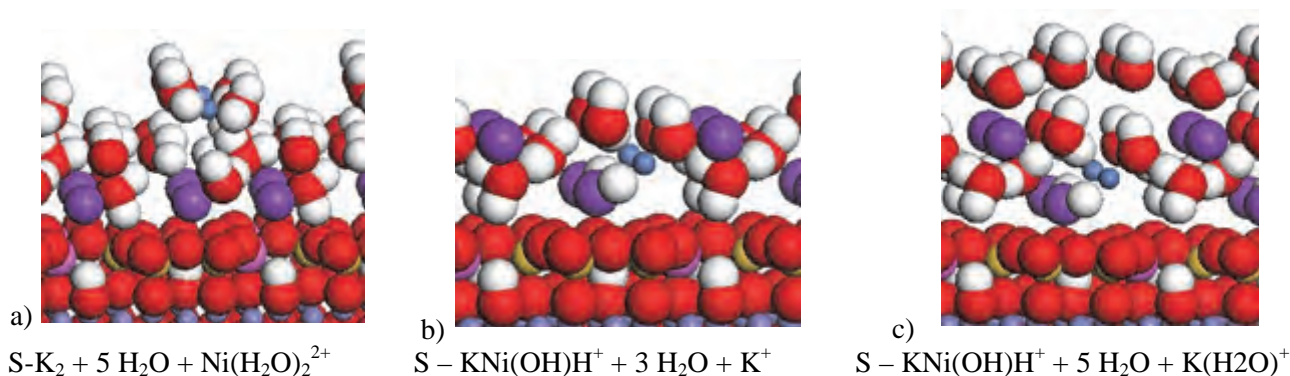
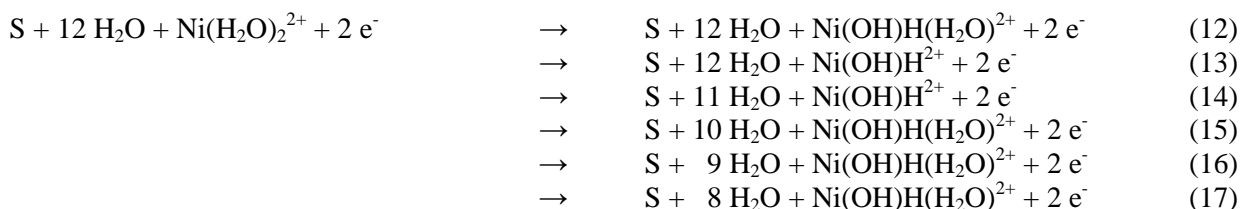


Figure 9. The annite (001) surface: a) $Ni(H_2O)_2^{2+}$ above the first water molecule layer, b) Ni^{2+} ion has replaced K^+ ion (cation exchange), and c) the re-formed water molecule layer.

Possibility for the cation exchange reaction was also investigated on the terminal (110) surface. There the reaction proceeds according to Scheme 2, where S represents $K_6Fe_{12}Si_{12}Al_4O_{42}(OH)_8$ surface structure:



On this surface, $Ni(H_2O)_2^{2+}$ species forms a surface complex with the water molecule layer (**Figure 10a**). This complex does not dissociate and move to other position on the surface, though desorption of water molecules reduces steric hindrance on the surface (Fig. 5b). Therefore, steric shielding around the K^+ ions reduces, and K^+ ions are susceptible for other reactions. Energy needed for this surface re-arrangement reaction is 1.57 eV.

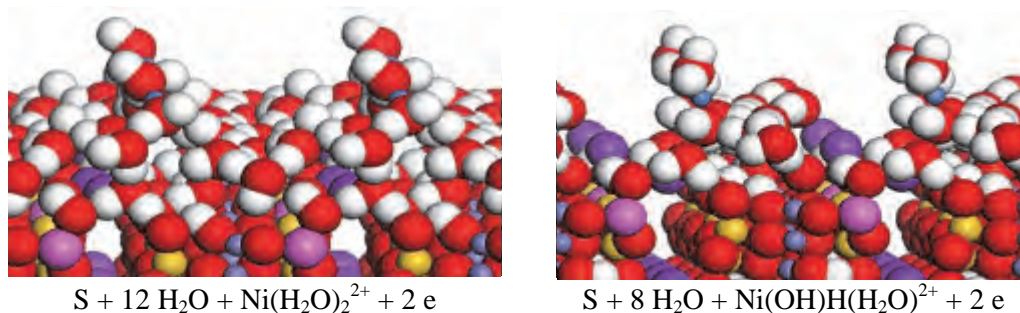


Figure 10. The annite (110) surface: a) $Ni(H_2O)_2^{2+}$ above the first water molecule layer, and b) surface complexed $Ni(H_2O)_2^{2+}$.

Based on the calculated results, surface reactions are different on the basal and terminal surfaces on biotite and its end-member (annite). Cation exchange reactions between K^+ and Ni^{2+} ions take place on the basal surfaces, and surface complexation reactions on the terminal surfaces. If the ratio between the basal and terminal surfaces can be determined, then reactions needed in the surface complexation modelling can be restricted only essential reactions.

References

Accelrys (2011). *MS Modeling*, Release 6.0. San Diego: Accelrys Software Inc.

Crawford J, 2012. Decreasing uncertainty of radionuclide migration predictions in safety assessment modelling. In: 1st Workshop Proceedings of the Collaborative Project “Crystalline Rock Retention Processes” (7th EC CP CROCK). Eds. Rabung T, Molinero J, Garcia D, Montoya V. KIT Scientific Reports 7629, Karlsruhe Institute of Technology, Germany.

Crawford, J. (2013) A simplified approach for reactive transport modelling involving strongly non-linear sorption and solute remobilization; S&T contribution to the Crock final workshop (Karlsruhe, Germany, 14-16 May 2013)

de Vries, L. M., Trincherro, P., & Molinero, J. (2012). MPhreeqc: Extending geochemical modelling with automatic stochastic simulations. In EGU General Assembly Conference Abstracts (Vol. 14, p. 6355).

Missana, T. & Garcia-Gutierrez, M. (2012) Comparison of the caesium adsorption on different crystalline rocks. Proceedings of the 1st CP CROCK Workshop, Stockholm, Sweden.

Puhakka, E. & Olin, M. (2013) Ab-initio studies on cation exchange and surface complexation reactions on biotite surface; S&T contribution to the Crock final workshop (Karlsruhe, Germany, 14-16 May 2013)

Trincherro, P., Molinero, J &, Román-Ross, G. (2013a) A streamline approach for the solution of multicomponent reactive transport problems, SKB R-10-45

Trincherro, P., Molinero, J. & de Vries, M., (2013b) radionuclide migration in crystalline media: from effective K_d distributions to reactive transport modelling, S&T contribution to the Crock final workshop (Karlsruhe, Germany, 14-16 May 2013)

TOPICAL SESSION SUMMARY

SUMMARY OF THE TOPICAL SESSION “IN SITU URL EXPERIMENTS”

Thorsten Schäfer^{1*}

¹ Karlsruhe Institute of Technology (KIT), Institute for Nuclear Waste Disposal (INE) (DE)

* Corresponding author: thorsten.schaefer@kit.edu

The motivation to organize a topical session based on underground research laboratory (URL) investigations was to give an overview on radionuclide migration studies in URLs as a methodology for up-scaling and decreasing the uncertainty in the long-term prediction of the radionuclide mobility.

The abbreviation “URL” stands for Underground Research Laboratory or Underground Rock Laboratory, and has become the accepted generic term for underground facilities in which activities are carried out in support of repository development programs (NEA 2001, <http://www.ha.nea.fr/html/rwm/docs/2001/index.html>).

In the past thirty years different terms have been used as “1st generation URLs”, “rock characterisation facilities – RCFs”, “off-site URLs”, “2nd-generation URLs”, “site-specific URLs”, “on-site URLs” or “performance confirmation facilities”. The most accepted definitions currently used are “Generic URLs” and “Site-specific URLs”.

Generic URLs (equivalent to “off-site URLs” or “1st generation URLs”) are (Blechs Schmidt & Vomvoris, 2010):

Independent of final disposal sites

Facilities that are developed for research and testing purposes at a site that will not be used for waste disposal.

They provide, however, information that may support the disposal of radioactive waste elsewhere.

Both non-destructive as well as destructive experiments are performed (experiments often culminate with a post-mortem phase) and a flexible approach, in which modifications are possible.

The role of generic URLs is *inter alia* the

Development of methodology (preparations for in situ testing (surface/ underground) and testing of the transferability of data obtained in the laboratory to in situ tests; e.g. sorption processes, rock mechanics)

Collection of information (host rock – barrier properties, engineering feasibility, interactions between host rock and engineered barriers, work process, empirical observations, data for direct use, e.g. by use of transfer factors, modelling, etc.)

Concept testing and demonstration (e.g. engineered barriers – emplacement, evolution, retrieval)

Platform for international interaction (professional community – different organisations, different disciplines; broad public)

Site-specific URLs (on-site URLs, 2nd-generation URLs or rock characterization facilities) as the name suggests, are (Blechs Schmidt & Vomvoris, 2010):

Located in the host rock in an area that is considered as a potential future repository.

They include facilities that are developed for specific investigations at the given site and may, indeed, be a forerunner to the development of a repository at the site.

Because they may become part of a future repository, activities performed as well as the URL itself should not unduly affect the potential future repository; e.g., negative impact on the rock performance.

Planning and execution is part of the development of the specific repository project with more formal requirements.

A special case is the ‘performance confirmation facility’ designed for confirming key phenomena of importance during and after waste emplacement in an existing repository, e.g. provide input to the decision-making for the final closure of the repository.

URL in situ experiments are concerning the dimension and duration (observation period) intermediate between *laboratory experiments* (well-defined boundary conditions; time span: days to years; lateral scale: nm to cm) and *natural analogues* (boundary conditions less well defined, realistic environment, time span: up to millions of years, lateral scale: 100m to 1km). URL studies provide therefore information under defined but complex boundary conditions, giving the chance to observe processes in a realistic environment over several years to decades under a cm to m scale.

Twenty-six URLs in ten countries have been operated between 1965 and 2006, located in different geological formations as argillaceous sedimentary rocks, magmatic rocks, evaporites, or volcanic tuff. Some of these laboratories have been installed in existing facilities; others have been built on purpose. The URLs in crystalline formations include the following:

Whiteshell Underground Research Laboratory (URL) 1984–2003, Canada AECL Granite 240–420m; Purpose built; generic Shaft sealing on-going.

Olkiluoto Research Tunnel 1992– present, Finland Posiva Granite (tonalite) 60–100m; Purpose built; parallel to repository facilities.

Fanay-Augères 1980–1990, Granite, Uranium mine, Pre-existing tunnels

Kamaishi 1988–1998, Granite, Fe mine, Pre-existing tunnels

Mizunami Underground Research Laboratory (MIU) 2004– (shaft sinking initiation) Granite 1000m (shaft) Purpose built; generic Surface investigations since 1996

KURT– Korean Underground Research Tunnel 2006– present, South Korea KAERI Granite 90m, Purpose built

Stripa Mine 1976–1992, Sweden SKB Granite, Fe mine, 360–410m, Pre-existing tunnels

Äspö Hard Rock Laboratory (HRL) 1995– present Granite 200–460m (ramp/ spiral), Purpose built; generic

Grimsel Test Site (GTS) 1984– present Switzerland Nagra Granite, 450m, Purpose built; parallel to existing tunnels

Climax, Nevada 1978–1983 USA US-DOE Granite, mine, 420m, Pre-existing tunnels

The presentations of the topical session focused mainly on results over the past decades in the Olkiluoto Research Tunnel, the Äspö HRL and the Grimsel Test Site (GTS) as indicated by bold script. Presentations within this topical session included:

Anders Winberg (CONTERRA), “*The history of RN migration studies at the Äspö HRL: Experiences of the TRUE site*”

Bernhard Kienzler (KIT-INE) “*The CHEMLAB experimental program at Äspö: results*”

Evelyn Krawczyk-Bärsch (HZDR) “*Microbial experiments at URL sites: Influence on RN uptake*”

Andrew Martin (NAGRA) “*The history of radionuclide migration studies at the GTS*”

Vaclava Havlová (UJV Rez) “*LTD Phase I and II experiments: Study of radionuclide diffusion into crystalline rock matrix*”

Thorsten Schäfer (KIT-INE) “*The CRR & CFM project: Colloid enhanced radionuclide migration*”

Lasse Koskinen (POSIVA) “*URL migration studies within the Finnish Nuclear Waste repository Research program*”

Vladimir Petrov (MSU) “*URL research within the Russian Nuclear Waste repository Research program*”

Anders Winberg (CONTERRA) presented the TRUE experiments at Äspö HRL which have provided (repeated) demonstration of in situ retention at different localities. The TRUE data and parameterizations have not been used explicitly in the Swedish safety analysis SR-Site given their Äspö association, but the TRUE concepts and models have however been indirectly used in SR-Site, while TRUE-1/TRUE BS constituted the foundation for the transport site description models (SDMs), that in turn formed the basis for SR-Site (incl. abstraction of process models to safety assessment level).

The take home messages presented by Anders Winberg included (a) the need to establish the rationale and objectives of in situ tracer tests in relation to available knowledge and the geological system considered, (b) a careful site characterisation being pre-requisite to establish the necessary hydro-structural context, thereby establishing the basis for successful performance and interpretation, (c) the interpretation of in situ tracer tests requires a supporting laboratory programme to ensure relevant conceptual micro-structural models and their parameterisation, (d) Multiple modelling approaches (and modelling groups) provide a stimulating and creative environment for planning and evaluating tracer tests and finally although quantitative extrapolations to safety assessment (SA) flow geometry and time scales are not possible, tracer tests are important for understanding mechanisms of field scale retention processes.

Similar conclusions were drawn by Bernhard Kienzler (KIT-INE) for the CHEMLAB experiments on actinide migration at the Äspö HRL. Again the interpretation of in situ tracer tests requires a supporting laboratory programme to ensure relevant conceptual micro-structural models and detailed radionuclide speciation via *state-*

of-the art spectro-microscopic techniques to proof reactive transport modelling approaches. Data on actinide retention has been observed to be strongly dependent on flow rate/residence time showing the potential impact of kinetics for Am, Pu U, Np and Tc sorption/sorptive reduction in natural fractures.

Evelyn Krawczyk-Bärsch (HZDR) presented microbial experiments at Äspö HRL and ONKALO (Olkiluoto) URL and its effect on U/Np uptake. It could be shown that the subsurface biofilms generated at the URL tunnel surface have a significant effect on the adsorption capacity of host rock formation by forming a “barrier” between the rock surface and the groundwater decreasing the rock adsorption capacity or acting as a sink by precipitation of secondary phases. For a quantitative assessment of the relevance of microbial processes in water conducting features of crystalline host rocks, the in situ biofilm coverage (sources of electron donors and acceptors for biofilm production and their kinetics) and the in situ microbial consortia leading to changes in mineral – radionuclide interaction have to be characterized.

Andrew Martin (NAGRA) gave an in detail overview of almost thirty year activities at the Grimsel Test Site (GTS) concerning radionuclide migration studies, namely the Migration experiments (MI), the Excavation Project (EP), and the Hyperalkaline Plume in Fractured Rocks (HPF). Details on the Long-term diffusion test (LTD) were given by *Vaclava Havlová* (UJV Rez) focusing on the answering the key question of possible over-estimation of matrix diffusion due to sample preparation or stress release for laboratory experiments in comparison with real conditions under natural rock pressure. The Colloid Retention and Retardation (CRR) and Colloid Formation and Migration (CFM) projects were presented by *Thorsten Schäfer* (KIT-INE) to evaluate the influence of colloidal phases on radionuclide migration. The construction of a megapacker system has allowed controlling the hydraulic system giving a chance to decrease the gradients and consequently increase the travel time to the post-closure situation: 1% gradient and $\sim 10^{-5}$ m/s while maintaining high radionuclide recovery. The in situ colloid/homologue tracer tests demonstrate a radionuclide/homologue colloid associated transport over increasing residence time detectable in the MI shearzone, whereas the radionuclide recovery is lower for trivalent actinides compared to tetravalent actinides and the reversibility kinetics as well as redox reactions faster than observed in laboratory studies.

The common motivation to all these projects is (a) the upscaling from lab to field, (b) identification of radionuclide sorption sites (minerals)/ retention process understanding and (c) transferability to other parts of a host rock formation (host rock variability). Lessons learned throughout the years of field experiments at GTS are that in order to gain process understanding there should not be too many processes occurring at the same time within one experiment and that large scale experiments require and foster international cooperation and constant innovation.

Lasse Koskinen (POSIVA) presented the current programme for repository host rock characterisation in the ONKALO mentioning the (a) SURE (Sulphate reduction under deep bedrock conditions), (b) HYDCO (Hydrogeological properties in the near field), (c) POSE (Rock spalling experiment), (d) EDZ (Excavation damaged zone) projects and mainly focusing in his presentation on the REPRO (Experiments to investigate rock matrix retention properties) project. Matrix diffusion and sorption are the main retention processes in geosphere in the performance assessment conditions and retention takes place mainly in the vicinity of the deposition holes for most of the sorbing tracers. Therefore experiments to investigate rock matrix retention properties at the repository depth by characterizing porosity and diffusivity and demonstrate that assumptions applied in the safety case are in line with the site evidence are of paramount importance. The approach used in the REPRO project is similar to e.g. LTD at the GTS using a combination of laboratory experiments on REPRO-site drill core (total porosities, pore structures characterised by ^{14}C -PMMA autoradiography, gas-, through- diffusion and electro-migration experiments) and field through diffusion experiments.

Finally, *Vladimir Petrov* (MSU) gave an overview on the current activities of URL research within the Russian Nuclear Waste repository Research program. Based on the DOI (Declaration of Intent, 2008) the final isolation of long-lived high level waste and intermediate level waste as well as conditioned waste from future reprocessing of SNF is planned in a crystalline deep geological formation. The purpose of the DOI is the construction of a repository in the Eniseysky area (near Krasnoyarsk/ Zheleznogorsk) as main investigation site including an underground laboratory. The development for an innovative technology of SNF reprocessing is also planned in the Krasnoyarsk area. The current status of the project is that in August 2012 a public debate was held in Zheleznogorsk resulting in a public agreement on the planning and VNIPIpromtehnologii had been chosen as a main company responsible for construction of the facilities end 2012. Current activities focus on preliminary work.

References

Blechsmidt, I.; Vomvoris, S. (2010) Underground research facilities and rock laboratories for the development of geological disposal concepts and repository systems. In Geological repository systems for safe disposal of spent nuclear fuels and radioactive waste, J., A.; Apted, M. J., Eds. Woodhead Publishing Limited, Vol. 9, pp 82-118.

S + T CONTRIBUTIONS



List of contributions

Decreasing K_d uncertainties through the application of mechanistic retention models.....	57
Retention of U(VI) and Np(V) in bacteriogenic iron oxide-producing biofilms from Äspö HRL (Sweden)	69
A simplified approach for reactive transport modelling involving strongly non-linear sorption and solute remobilisation	77
Approaches to modelling surface complexation sorption on complex geological materials with limited data.....	83
Documentation, evaluation of treatment of radionuclide transport and retention phenomena in recent performance assessments	89
Radionuclide migration in crystalline media: from effective K_D distributions to reactive transport modelling	95
<i>AB INITIO</i> studies on cation exchange and surface complexation reactions on biotite surface.....	113
Reactive transport modelling of nickel in fractured bedrock.....	121
Surface complexation modelling of biotite: nickel and europium.....	127
Possible causes of uncertainty in the sorption data for pa studies	135
Study of selenium sorption on Äspö diorite.....	141
Application of electromigration method on long rock samples: Determination of migration parameters (F_F , D_E).....	151
Uranium (VI) sorption onto rock samples from areas of the proposed HLW and SNF repository in Russia (Nizhnekansky massive).....	163
Analysis of sorption onto granites and granite minerals: the case of caesium	167
RN migration in a single fracture from Äspö, Sweden: experiments and reactive transport modelling	175
Study of selenium sorption on Äspö diorite surface using spectroscopic methods	185
Tc(VII) sorption on natural granitic rocks and synthetic magnetite	197
Interaction of uranium(VI) and neptunium(V) with Äspö diorite under anoxic conditions.....	211
Real system analysis	225
Characterization of rock samples from Äspö using gas adsorption.....	229
HTO, Cs, Ra and U sorption on and diffusion in rock samples from Äspö	243

DECREASING K_d UNCERTAINTIES THROUGH THE APPLICATION OF MECHANISTIC RETENTION MODELS

David García^{1*}, Marek Pękala¹ and Cristina Domènech^{1,2}

¹Amphos 21, Barcelona (ES)

²Department of Crystallography, Mineralogy and Mineral Deposits, University of Barcelona, Barcelona (ES)

* Corresponding author: david.garcia@amphos21.com

Abstract

It is widely recognised that distribution coefficient (K_d) values generally have a narrow field of validity, and that the uncertainty of the K_d outside this field increases significantly. The work performed by Amphos 21 in the framework of WP4 of the CROCK project has focused on finding a reliable and easy approach to minimise the uncertainty of the K_d values commonly used in radionuclide transport modelling.

In this S&T contribution the possibility of deriving a simplified way of predicting K_d values under a variety of geochemical conditions is investigated. The proposed approach utilises surface complexation and cation-exchange models in combination with some simplifying assumptions to arrive at an analytical formulation that enables the estimation of K_d for a given radionuclide in a straightforward and traceable manner. As such, this approach can be easily implemented (e.g. in a computer spread-sheet programme) and used to provide first estimates on the K_d used in Performance Assessment (PA) of radioactive waste repository concepts. The derived analytical formulation has been tested using experimental data for three independent systems.

Introduction

Retention processes can strongly affect radionuclide mobility in the geosphere (RETROCK, 2005). K_d -based models are commonly used to represent radionuclide retention processes occurring in the natural and engineered barriers in the vicinity of a nuclear waste repository. Although mechanistic coupled geochemical models can in principle be used in Performance Assessment (PA) to represent radionuclide retention explicitly, the K_d -based approach is often still favoured as it facilitates rapid calculations required in probabilistic PA. For many radionuclides, the evaluated transfer functions depend critically on the K_d values used (Cronstrand, 2005). A K_d value represents the distribution of a radionuclide between the aqueous and solid phases, which depends on the physico-chemical conditions of a given system (e.g. pH, ionic strength, I , the presence of ligands, etc.), and which often cannot be extrapolated to different conditions without increasing the uncertainties in the K_d . For this reason, the traditional K_d values are “conditional” (i.e. valid under a narrow set of conditions only) and are typically derived from laboratory experiments carried out under geochemical conditions for which the parameter is planned to be used.

Alternatively, K_d values can be predicted by means of geochemical modelling if sufficient information about the dominant processes is available (e.g. Duro et al., 2001). This approach allows for the K_d values to be estimated under a variety of conditions. In this contribution we are investigating the possibility of using simplified analytic expressions for the K_d that could represent the dependence on geochemical conditions with sufficient accuracy,

thus avoiding the need to use geochemical codes (such as PhreeqC). This approach could provide an easy to use tool for PA scientists to obtain reliable estimates of the effect of varying geochemical conditions (e.g. water chemistry or system mineralogy) on the K_d .

Mathematical Formulation

The proposed model is based on the work by Duro et al. (2001) and develops it further to include electrostatics for surface complexation reactions as well as cation exchange. Sorption coefficient (K_d) for a Radionuclide (Rn) is defined in eq. 1, where $\{Rn\}_{ads}$ and $[Rn]_{aq}$ stand for the total concentration of the Rn retained in the solid and the Rn total aqueous concentration, respectively.

$$K_d = \frac{\{Rn\}_{ads}}{[Rn]_{aq}} \quad \text{eq. 1}$$

$[Rn]_{aq}$ is the sum of all aqueous species of the Rn (eq. 2). For simplicity, the example given below is for a monovalent radionuclide cation; however a similar derivation can easily be applied to radionuclides of any charge. The aqueous complexes are cast in terms of complexation constants associated with the equilibrium reactions of the different ligands (L, Q, etc., where L or Q may be the hydroxyl ion, chloride ion, etc.) present in the solution, which after substituting in eq. 2 leads to eq. 3.

$$[Rn]_{aq} = [Rn^+] + [RnL] + [RnL_2^-] + \dots + [RnQ^-] + \dots \quad \text{eq. 2}$$

$$[Rn]_{aq} = [Rn^+] \times \{1 + K_{L,1}[L^-] + K_{L,2}[L^-]^2 + \dots + K_{Q,1}[Q^{2-}] + \dots\} \quad \text{eq. 3}$$

Eq. 3 could be re-written in a more general form (eq. 4).

$$[Rn]_{aq} = [Rn^+] \times \left\{ 1 + \sum_{L,p} K_{L,p}[L^-]^p \right\} \quad \text{eq. 4}$$

Similarly, $\{Rn\}_{ads}$ is defined in terms of the sum of all surface complexes of the Rn, and hence depends on the solid surface properties (i.e. acidity and/or site density) and on the surface complexation or exchange equilibrium of Rn with the solid surface. Eq. 5 shows an example for a case where sorption occurs on a single site ($>SO^-$) and exchange occurs in two different types of sites ($>X^-$ and $>Y^-$).

$$\{Rn\}_{ads} = \{>SORn\} + \{>SORn(OH)^-\} + \dots + \{>XRn\} + \{>YRn\} + \dots \quad \text{eq. 5}$$

As in the case of the aqueous phase equilibrium description, one can re-arrange eq.5 in terms of the surface complexation constants or the exchange equilibrium constants.

For the sake of conciseness here we will show the mathematical development of eq. 5 assuming non-electrostatic surface complexation of a single Rn onto a solid surface (eq. 6).

$$\{Rn\}_{ads} = [Rn^+] \times \{ K_{S,1}\{>SO^-\} + K_{S,2}\{>SO^-\}^2 + \dots \} \quad \text{eq. 6}$$

Eq. 6 could be re-written in a general expression (eq. 7).

$$\{Rn\}_{ads} = [Rn^+] \times \left\{ \sum_{s,q} K_{S,q}\{>SO^-\}^q \right\} \quad \text{eq. 7}$$

Combining eq. 1, 4 and 7 a new expression for calculating the K_d is obtained (eq. 8), where $\{>SO^-\}$ and $[L^-]$ stand for the concentration of solid ligands ($\text{mol} \cdot \text{kg}^{-1}$) and the concentration of aqueous ligands ($\text{mol} \cdot \text{dm}^{-3}$), respectively.

$$K_d = \frac{\sum_{s,q} K_{S,q}\{>SO^-\}^q}{1 + \sum_{L,p} K_{L,p}[L^-]^p} \quad \text{eq. 8}$$

$\{>SO^-\}$ must be determined from the rock properties, the amount of mineral in the host rock and the number of coordination (or exchange) sites on the mineral surface. Combining this information with the surface equilibria of the proposed solid surface and re-arranging terms, one obtains eq. 9, where W_s is the amount of mineral ($\text{kg}_{\text{of mineral}} \cdot \text{kg}_{\text{host rock}}^{-1}$) and A_s is the number of coordination (or exchange) sites ($\text{mol}_{\text{sites}} \cdot \text{kg}_{\text{mineral}}^{-1}$).

$$K_d = \frac{\sum_{s,q} \left(K_{S,q} \frac{A_s W_s}{1 + \frac{[H^+]}{K_{S,a}}} \right)}{1 + \sum_{L,p} K_{L,p}[L^-]^p} \quad \text{eq. 9}$$

Eq. 9 is a function that allows the fast calculation of K_d values based on information regarding the expected aqueous and surface complexation, and based on properties (mineral composition, porosity, density) of the rock.

Additional terms need to be considered in the case of electrostatic models as well as in the case of exchange models (described below). In the following section the application of this model to some cases of interest is presented alongside a general discussion of the applicability of the model in more complex situations.

Major Model Assumptions

In the case of sorption, it was assumed that, if Rn is in trace concentrations and/or the number of available sites is high, the concentration of occupied sites is negligible in front of the concentration of un-complexed sites.

Moreover in the case of Rn exchange with illite (see Case 3 below) the simplified assumption is made that the equilibrium C_s concentration in solution is equal to the initial C_s concentration, however this assumption results in a proportional overestimation of both the C_s in solution and on the exchanger which cancels out in the K_d calculation.

Model Application

In this S&T contribution we have applied the previous approach to 3 different systems and we have tested its validity in front of experimental data and of values calculated following a mechanistic sorption or exchange model. The systems are: 1) *Eu sorption onto illite* 2) *Cs sorption onto iron-hydroxide phases* and 3) *Cs exchange within illite*.

As a first step, the geochemical simulator PhreeqC (Parkhurst and Appelo, 1999) was used to implement relevant retention processes for a given radionuclide onto a single mineral. The reactions and key parameters of each model are detailed in Table 1 at the end of this section. Each model was tested against available experimental data. As a second step, the developed K_d -function model was applied to the same experimental datasets. The results obtained using PhreeqC and the K_d -function models were compared with each other to understand the qualitative effect of the simplifying assumption made in the latter.

In the presented contribution, the developed K_d -functions are applied to simplified mineral systems. However, we expect that in a future step the additivity approach could be used to tackle more complicated mineral assemblages.

Case 1: Eu sorption onto illite

Bradbury and Baeyens (2002; 2004) studied the retention of Eu onto illite. The authors reported two mechanisms governing the behaviour of Eu in that system: sorption of Eu onto two types of illite sites (strong and weak), and Eu cation exchange with Na originally present in the illite exchange positions.

The model reported by Bradbury and Baeyens (2004) was chosen in this work for an overall representation of Eu retention onto illite. As reported by the authors, due to the hydrolysis of Eu, the exchange with Na positions is only relevant at pH values below 4.5, and given that the pH of the interest is ~7-8 (Schäfer et al., 2012), we have neglected this process.

The model of Bradbury and Baeyens (2004) was implemented in PhreeqC and thus calculated K_d values were compared with experimental ones obtained from several datasets (pH between 4.5-11.5 and I between 0.01-0.5M) on Eu sorption onto illite (Bradbury and Baeyens, 2004; Poinssot et al.; 1999, Schnurr et al., 2013) (Figure 1).

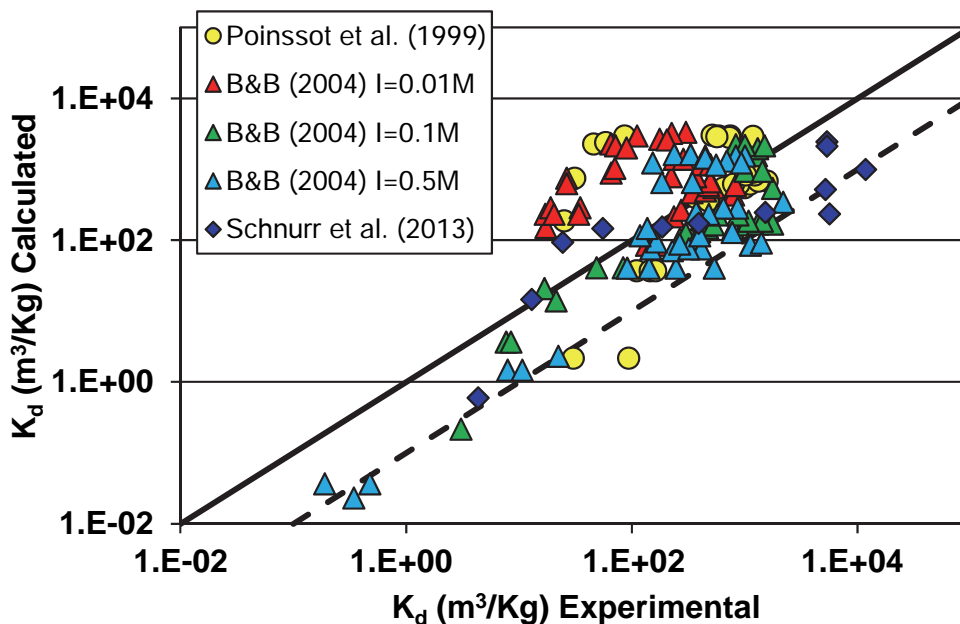


Figure 1: Comparison of K_d values for the Eu-illite system calculated using PhreeqC and obtained from experiments. Dashed lines indicate a K_d deviation of ± 1 log unit. Experimental error bars are within data point symbols. Experimental data from: Bradbury and Baeyens (2004); Poinssot et al. (1999); Schnurr et al. (2013).

Using the analytical K_d model presented in the section *Mathematical Formulation*, K_d values were calculated for the same experimental datasets. Figure 2 presents the comparison between the K_d calculated using the analytical approach and the experimental values.

It can be seen from Figure 2 that the analytical K_d model calculates K_d values which are relatively close to the measured (experimental) ones over a range of conditions. It is also observed that in this example the analytical model results in a small, but consistent, K_d overestimation. This is due to the simplifying assumption that the concentration of occupied sites is negligible compared to the concentration of uncomplexed sites.

Case 2: Cs sorption onto iron-hydroxide phases

The retention of Cs onto iron oxide phases (i.e. magnetite) has been previously studied by several authors (Catalette et al., 1998; Ebner et al., 2001; Granizo and Missana, 2006; Marmier et al., 1999; Rovira et al., 2004). Granizo and Missana (2006) described Cs sorption onto magnetite by deriving a surface complexation model (SCM) including electrostatic effects (Diffuse Layer Model, DLM).

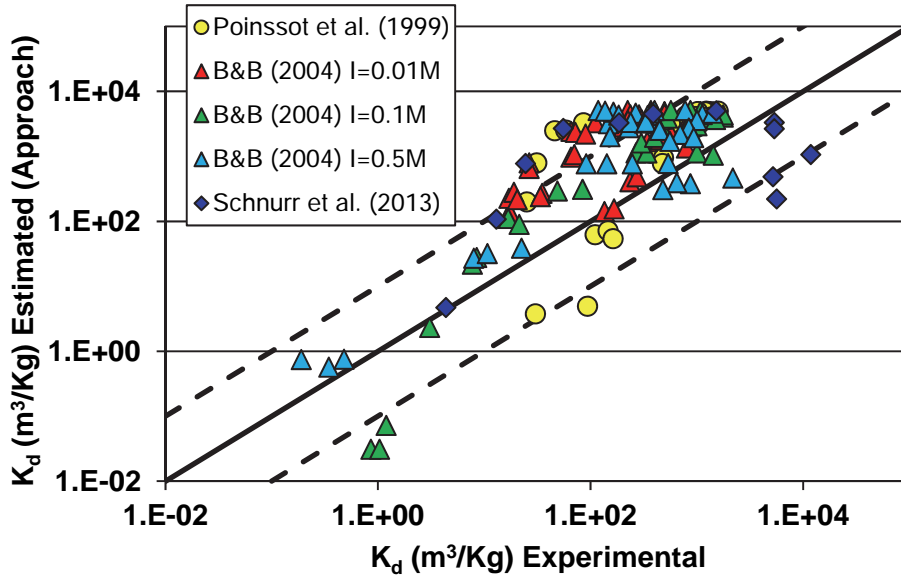


Figure 2: Comparison of K_d values for the Eu-illite system calculated using the analytical K_d model and obtained from experiments. See Figure caption 1 for experimental data details. Dashed lines indicate a K_d deviation of ± 1 log unit. Experimental error bars are within data point symbols.

Implementing the model of Granizo and Missana (2006), and additional parameters from the model of Rovira et al. (2004) in the PhreeqC code (for a detailed description of the input model see Table 1), we recalculated the experimental data obtained under different conditions (pH between 3 and 13.5, I between 0.001 and 0.1, S/L ratio between 0.8 and 40 g·L⁻¹) with a reasonable accuracy (Figure 3).

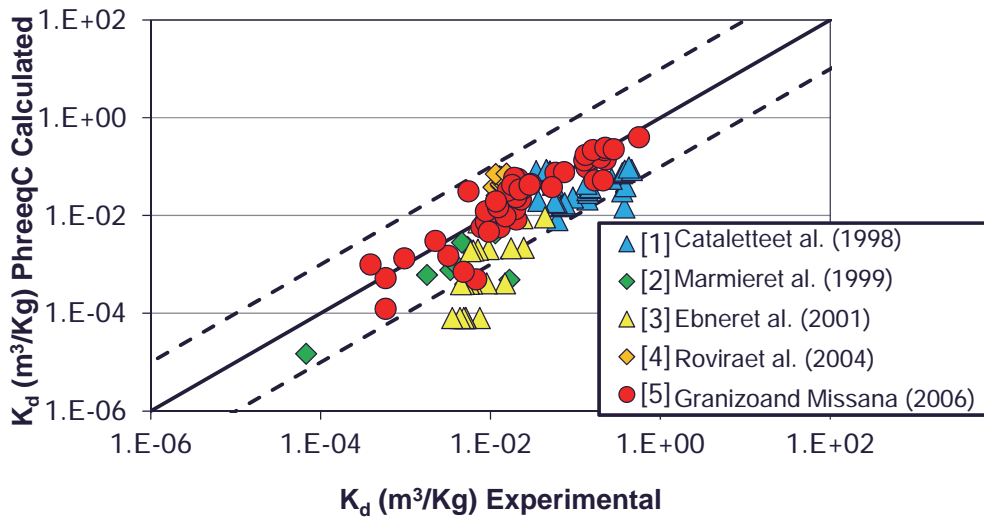


Figure 3: Experimental K_d values for the Cs-magnetite system vs values calculated with PhreeqC using the model of Granizo and Missana (2006). Experimental data from: Catalette et al. (1998); Ebner et al. (2001); Granizo and Missana (2006); Marmier et al. (1999); Rovira et al. (2004). Dotted lines stand for a K_d deviation of ± 1 log unit. The error bars of each value are within data point symbols.

Based on this SCM model, an analytical K_d -model was developed following the procedure explained above in the section *Mathematical Formulation*. In this specific case, electrostatic effects were considered in the mathematical formulation for K_d (eq. 10) by adding the Coulombic term, CT (compare eq. 9 and 10).

$$K_d = \frac{\sum_{s,q} K_{s,q} CT \frac{A_s W_s}{1 + \frac{[H^+]}{K_{s,q} CT}}}{1 + \sum_{L,p} K_{L,p} [L^-]^p} \quad \text{eq. 10}$$

The CT parameter, which depends on the system pH, I and surface charge, was estimated based on the results obtained with the PhreeqC code. Figure 4 shows the results calculated using eq.10.

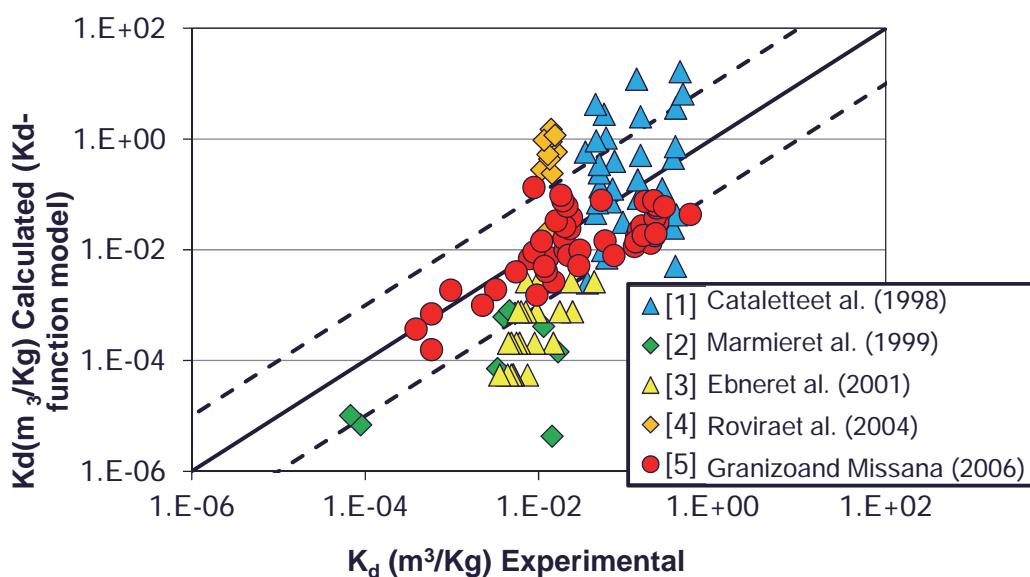


Figure 4: K_d calculated by using the analytical K_d model vs experimental K_d values for the Cs-magnetite system. See Figure 3 caption for experimental data details. Dotted lines indicate a K_d deviation of ± 1 log unit. The error bars of each value are within data point symbols.

As can be seen in Figure 4, the analytical K_d model (eq.10) can reproduce experimental K_d values with reasonable accuracy. Nevertheless, the scattering in the estimated K_d values is higher when using the analytical K_d model than when the calculation is made with PhreeqC. This is due to the simplified assumptions made in the mathematical formulation of the analytical K_d model.

Case 3: Cs exchange within illite

Cs retention on clay minerals is mainly due to cation exchange. Bradbury and Baeyens (2000) proposed a generalised sorption model for representing Cs retention onto illite. The authors reported a three-site cation exchange model that predicts the uptake of Cs at equilibrium concentrations below $\sim 10^{-3}$ M. This model was selected here for implementation in PhreeqC in order to calculate K_d values (Figure 5) corresponding to the experimental data obtained by several authors (Comans et al. 1991, Poinssot et al. 1999, and Staunton and Roubaud, 1997) in a variety of conditions (pH between 3 and 12, I between 0.01 and 0.1, S/L ratio between 0.01

and $1 \text{ g}\cdot\text{L}^{-1}$). The model applied in this case assumes Cs-K exchange to be the most important exchange reaction controlling Cs behaviour and sufficient to represent the overall system behaviour.

Based on this, a simplified analytical K_d model was developed following an approach similar to that used for Cs sorption onto magnetite discussed above. The model utilises the Gaines-Thomas convention, the convention also considered within PhreeqC calculations, to represent cation activity on the exchanger. Results obtained with the derived analytical K_d model are also shown in Figure 5. As can be seen the results calculated with the derived analytical K_d model are close to the values calculated with PhreeqC, and both agree fairly well with the experimental data.

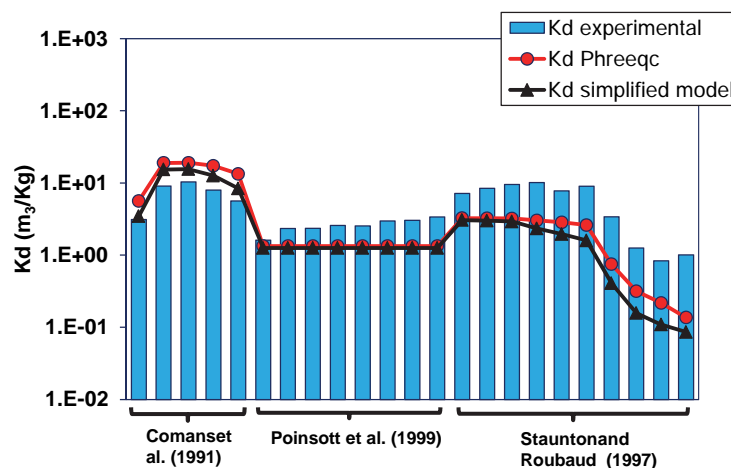


Figure 5: Comparison of Cs K_d values calculated with PhreeqC and using the analytical K_d model against experimental values for cation exchange in the Cs-K illite system. Experimental data from: Comans et al. (1991); Poinssot et al. (1999); Staunton and Roubaud (1997). The error bars of each value are within data point symbols.

Table 1: Equilibrium reaction input data used.

Eu - Illite			
Reaction	log K	Reference	
$>S^sOH + H^+ \rightarrow >S^sOH_2^+$	5.50	Bradbury and Baeyens (2004)	
$>S^sOH \rightarrow >S^sO^- + H^+$	-6.20	Bradbury and Baeyens (2004)	
$>S^wOH + H^+ \rightarrow >S^wOH_2^+$	5.50	Bradbury and Baeyens (2004)	
$>S^wOH \rightarrow >S^wO^- + H^+$	-6.20	Bradbury and Baeyens (2004)	
$Eu^{3+} + >S^sOH \rightarrow >S^sOEu^{2+} + H^+$	3.10	Bradbury and Baeyens (2004)	
$Eu^{3+} + >S^sOH + H_2O \rightarrow >S^sOEu(OH)^+ + 2H^+$	-4.40	Bradbury and Baeyens (2004)	
$Eu^{3+} + >S^sOH + 2H_2O \rightarrow >S^sOEu(OH)_2 + 3H^+$	-12.70	Bradbury and Baeyens (2004)	
$Eu^{3+} + >S^wOH \rightarrow >S^wOEu^{2+} + H^+$	0.30	Bradbury and Baeyens (2004)	
$Eu^{3+} + >S^wOH + H_2O \rightarrow >S^wOEu(OH)^+ + 2H^+$	-6.20	Bradbury and Baeyens (2004)	
S^s sites (mol·kg⁻¹ mineral)	2.0·10⁻³	S^w sites (mol·kg⁻¹ mineral)	4.5·10⁻²
Cs - Magnetite			
Reaction	log K	Reference	
$>SOH + H^+ \rightarrow >SOH_2^+$	5.10	Granizo and Missana (2006)	
$>SOH \rightarrow >SO^- + H^+$	-9.10	Granizo and Missana (2006)	
$>SOH + Cs^+ \rightarrow >SOHCs^+$	1.05	Granizo and Missana (2006)	
$>SOH + Cs^+ \rightarrow >SOCs + H^+$	-10.5	Granizo and Missana (2006)	
$>SOH + H_4SiO_4 + Cs^+ \rightarrow >SSiO_4H_3Cs^+ + H_2O$	6.09	Rovira et al. (2004)	
Surface	8.5 m²·g⁻¹	Sites·nm⁻²	3.54
Cs - Illite			
Reaction	log K	Reference	
$KX^* + Cs^+ \rightarrow CsX + K^+$	4.10-5.00	Bradbury and Baeyens (2000)	
$KY^* + Cs^+ \rightarrow CsY + K^+$	1.00-1.60	Bradbury and Baeyens (2000)	
$KZ^* + Cs^+ \rightarrow CsZ + K^+$	0.65	Bradbury and Baeyens (2000)	

*Illite site distribution according with B&B (2000): Frayed edge site (FES) represented as X is 0.25% of total CEC, Type II sites represented as Y is 79.75% of total CEC, and Planar sites represented as Z is 20% of total CEC.

Conclusions and Future work

In the three cases studied in this work, the K_d values estimated using the analytical K_d - model compare quite well with the experimental values and with the results obtained when calculating with PhreeqC. K_d values obtained with the K_d -function model produce some additional scattering (due to the simplifications made), whose magnitude depends on the particular experimental conditions of each dataset. Nevertheless we consider

the proposed approach to be a useful technique of obtaining K_d values estimations in an easy way with a reasonable accuracy. This could be useful in PA studies.

The application of these kinds of models to a complex rock system is envisaged through an additive model which is planned to be developed in the future.

Acknowledgement

The research leading to these results has received funding from the European Union's European Atomic Energy Community's (Euratom) Seventh Framework Programme FP7/2007-2011 under grant agreement n° 269658 (CROCK project).

References

- Bradbury, M.H. and Baeyens, B. (2000). A generalised sorption model for the concentration dependent uptake of caesium by argillaceous rocks. *Journal of Contaminant Hydrology*, 42, 141-163.
- Bradbury, M.H. and Baeyens, B. (2004). Experimental and modelling Investigations on Na-Illite: Acid-Base Behaviour and the Sorption of Strontium, nickel, Europium and Uranyl. Nagra Technical Report, NTB-04-02.
- Catalette, H., Dumonceau, J. and Ollar, P. (1998). Sorption of caesium, barium and europium on magnetite. *J. Contam. Hydrol.*, 35, 151-159.
- Comans, R.N.J., Haller, M. and De Preter, P. (1991). Sorption of Caesium on Illite: non-Equilibrium behaviour and reversibility. *Geochimica et Cosmochimica Acta*, 55, 433-440.
- Cronstrand, P. (2005). Assessment of uncertainty intervals for sorption coefficients. SFR-1 uppföljning av SAFE. SKB R-05-75.
- Duro, L., Bruno, J. and Honeyman, B. (2001). Proposal for the development of predictive surface complexation models (SCM) to be used as a supporting tool to K_d parameters in PA. In "Using thermodynamics sorption models for guiding radioelement distribution coefficient (K_d) investigations." OECD-NEA Report.
- Ebner, A.D., Ritter, J.A. and Navratil, J.D. (2001). Adsorption of Caesium, Strontium, and Cobalt Ions on Magnetite and a Magnetite-Silica Composite. *Ind. Eng. Chem. Res.*, 40, 1615-1623.
- Geckeis, H., Lützenkirchen, J., Polly, R., Rabung, Th. and Schmidt, M. (2013). Mineral-Water interface reactions of actinides. *Chemical Reviews*, 113, 1016-1062.
- Granizo, N. and Missana, T. (2006). Mechanisms of caesium sorption onto magnetite. *Radiochim. Acta*, 94, 671-677.
- Marmier, N., Delisée, A. and Fromage, F. (1999). Surface Complexation Modelling of Yb(III), Ni(II), and Cs(I) Sorption on Magnetite. *J. Colloid Interf. Sci.*, 211, 54-60.
- Parkhurst, D. and Appelo, T. (1999). User's guide to PhreeqC (Version 2). USGS Report 99-4259.

Poinsot, C., Baeyens, B. and Bradbury, M.H. (1999). Experimental and modelling studies of caesium sorption on illite. *Geochimica et Cosmochimica Acta*, 63, 3217-3227.

Poinsot, C., Baeyens, B., and Bradbury, M. H. (1999). Experimental studies of Cs, Sr, Ni, and Eu sorption on Na-illite and the modelling of Cs sorption. PSI Nr. 99-06.

Schnurr, A., Marsac, R., Rabung, Th., Lützenkirchen, J. and Geckeis, H. (2013). Investigations of actinide and lanthanide sorption on clay minerals under saline conditions. Proceedings of the ABC-Salt Workshop III, Santa Fe, USA.

RETROCK (2005). Treatment of radionuclide transport in geosphere within safety assessments. Final Report of the European Commission Project RETROCK (C.No.: FIKW-CT-2001-20201).

Rovira, M., de Pablo, J., Casas, I., Giménez, J. and Clarens, F. (2004). Sorption of Caesium on Commercial Magnetite with low Silica Content: Experimental and Modelling. *Mat. Res. Soc. Symp. Proc.*, 807, 677-682.

Schäfer, T., Stage, E., Büchner, S., Huber, F. and Drake, H. (2012). Characterization of new crystalline material for investigations within CP CROCK 7th EC FP - CROCK CP. Proceedings of the 1st CP CROCK Workshop, Stockholm, Sweden.

Staunton, S. and Roubaud, M. (1997). Adsorption of ¹³⁷Cs on montmorillonite and illite: Effect of charge compensating cation, ionic strength, concentration of Cs, K and fulvic acid. *Clays and Clay Minerals*, 45, 251-260.

RETENTION OF U(VI) AND Np(V) IN BACTERIOGENIC IRON OXIDE-PRODUCING BIOFILMS FROM ÄSPÖ HRL (SWEDEN)

Evelyn Krawczyk-Bärsch*, Katja Schmeide, Frank Bok

Helmholtz-Zentrum Dresden-Rossendorf e.V., Institute of Resource Ecology,
P.O. Box 510119, 01314 Dresden (D)

* Corresponding author: E.Krawczyk-Baersch@hzdr.de

Abstract

At the Äspö HRL (Sweden) *Gallionella ferruginea* dominated biofilms associated with bacteriogenic iron oxides (BIOS) and groundwater were sampled from an *in situ* continuous flow cell, which has been installed in a cavity of the main access tunnel at 2200 A site, 300 m below sea level (Anderson & Pedersen, 2003). In laboratory sorption experiments $\text{UO}_2(\text{ClO}_4)_2$ and $\text{NpO}_2(\text{ClO}_4)$ were added to the BIOS biofilms in groundwater under aerobic conditions adjusting a final U(VI) concentration of 1.9×10^{-5} M.U(VI) and 3.27×10^{-5} M Np(V). At the end of the experiments the groundwater/BIOS biofilm samples were ultra-centrifuged and the pH and E_h of the supernatants were defined to be 7.52 ± 0.1 and 355 ± 30 mV in the uranium contaminated samples and 7.02 ± 0.1 and 367 ± 30 mV in the neptunium contaminated samples. The analysis showed a substantial decrease of uranium and neptunium in the groundwater of approximately 85 % and 95 %, respectively. Thermodynamic calculation of the theoretical predominant field of uranium species was performed using the analytical data of the uranium-contaminated groundwater. Under the given pH and E_h the formation of the aqueous uranium carbonate species $\text{Ca}_2\text{UO}_2(\text{CO}_3)_3(\text{aq})$ is predicted due to the high concentration of carbonate in the groundwater. In the BIOS biofilm the ferrous iron-oxidizing and stalk-forming bacterium *Gallionella ferruginea* is dominating the sorption process. The stalk represents an organic surface upon which Fe oxyhydroxides can precipitate. Due to the high concentration of ferric iron in the BIOS biofilm the portion of iron oxyhydroxides (ferrihydrite) amounts approximately to 70 wt.%. Under the given pH conditions the uptake of U and Np depends predominantly on the high amount of ferrihydrite precipitated onto the stalks. Conclusively, the combination of this biological material and iron oxides creates an abundant surface area for adsorption of radionuclides.

Introduction

The dominant transport medium for radionuclides in nonporous crystalline rocks is groundwater, which is flowing through subsurface fracture zones. On the surface of these fractures processes are occurring like mineral dissolution, formation of precipitates, metal adsorption and ion exchange. Since the groundwater containing microorganisms is seeping through the fractures biological growth is supported on the aquifer fracture surfaces. The microbial cells appear not only as individual, unattached cells but also in multicellular, attached communities called biofilms (Jägevall et al., 2011). They are embedded in extracellular polymeric substances (EPS), for example, polysaccharides, proteins, lipoproteins, and glycoproteins (Flemming, 1991). Specific interactions between microorganisms and radionuclides are known and can be distinguished as biosorption, bioaccumulation, biotransformation, biomineralization, and bioreduction (Lloyd and Macaskie, 2002) with

potential for the substantial retention of radionuclides. Consequently, biofilms have to be considered along with minerals as an important factor influencing the transport of radionuclides in the environment.

At the Äspö HRL biofilms are commonly found on the tunnel wall, where fractures are present (Figure 1). After Hallbeck & Pedersen (2005) the predominant biomass in these biofilms is *Gallionella ferruginea*, an autotrophic ferrous iron-oxidising bacterium. *Gallionella ferruginea* is known as a gram-negative, stalk-forming bacterium (Hallbeck et al., 1993). It requires Fe(II) as an electron donor and oxygen as an electron acceptor to yield cellular energy and growth at circumneutral pH. *Gallionella ferruginea* does not form a stalk at pH < 6 and at a redox potential < -40 mV (Konhauser et al., 2011). The stalk represents an organic surface upon which Fe oxyhydroxides can precipitate (Hallbeck & Pedersen, 1990). These bacteriogenic iron oxides (BIOS) are forming the rusty orange to brown sludge. At 2200 A site, 300 m below sea level, an *in situ* continuous flow cell has been installed in a cavity of the main access tunnel for experiments as described in Anderson & Pedersen (2003). Groundwater for the flow cell is sourced from borehole KA2198A that intersects a water-conducting fracture. In this flow cell *Gallionella* biofilms associated with BIOS are growing. They have been sampled for *in situ* and laboratory U(VI) and Np(V) sorption experiments during the CROCK project.



Figure 1: Rusty orange to brown *Gallionella ferruginea* dominated biofilms, attached to the fractured bedrock of the Äspö HRL tunnel.

Experimental

During the sampling campaign BIOS biofilms were removed from the flow cell located in a cavity of the main access tunnel at 2200 A site. The groundwater seeping over the biofilms was sampled in 2 × 250-mL boxes. The boxes were transported together with the biofilm to the laboratory for further studies. For analysis, samples were taken from the groundwater at the beginning and at the end of the experiments, each with a volume of 10 mL. The samples were acidified and analysed for cation determination by means of inductively coupled plasma mass

spectrometry (ICP-MS) using both an ELAN 9000 ICP-MS spectrometer (PerkinElmer, Überlingen, Germany) and an AXIOM ICP-MS spectrometer (VG Thermo Elemental, Winsford, UK). The initial and final Np concentration in solution was determined by liquid scintillation counting (Winspectral α/β , Wallac 1414, Perkin Elmer) using α/β discrimination. For this, 100 μL of the supernatant was mixed with 5 mL of an Ultima GoldTM scintillation cocktail (Perkin Elmer, USA). The anions were determined by means of ion chromatography (IC) using the 732/733 IC system (Metrohm, Filderstadt, Germany). In addition, the groundwater used in our experiments was analysed before and after the experiments. The pH and redox potential of the groundwater were measured using conventional electrodes (SenTix Mic, WTW and SenTix ORP, WTW). Since the oxidation reduction potential was measured, the redox potential values were corrected for the hydrogen electrode potential.

Laboratory sorption experiments were performed under aerobic conditions. Two 50 mL tubes were each filled with 20 mL groundwater, including BIOS biofilms (0.25 g dry mass). In the first tube $\text{UO}_2(\text{ClO}_4)_2$ was added to the groundwater and biofilm, adjusting a final U(VI) concentration of 1.9×10^{-5} M (4500 $\mu\text{g/L}$). The groundwater and biofilm of the second tube were exposed to $\text{NpO}_2(\text{ClO}_4)$ to adjust a final Np(V) concentration of 3.27×10^{-5} M (7680 $\mu\text{g/L}$). After 20 days the suspensions were centrifuged and the supernatant were used for analysis. The BIOS biofilms were cryodried, powdered and analysed. The analytical data of the groundwater samples after the experiments were used for the calculation of the predominance fields of different uranium species in the pH- E_h diagram at 25°C by using the geochemical speciation code “Geochemist’s Workbench” Version 9.0.5/ACT2.

Results and discussion

At the end of the experiments the groundwater/BIOS biofilm samples were ultra-centrifuged and the pH and E_h of the supernatants were defined to be 7.52 ± 0.1 and 355 ± 30 mV in the uranium contaminated samples and 7.02 ± 0.1 and 367 ± 30 mV in the neptunium contaminated samples, respectively. The analysis of the supernatants showed significant differences between the uranium and neptunium concentration at the beginning and at the end of the experiments. The initial concentration of 1.9×10^{-5} M (4500 $\mu\text{g/L}$) U(VI) has decreased during 20 days to 3×10^{-6} M (708 $\mu\text{g/L}$). Also, the initial Np(VI) concentration of 3.27×10^{-5} M (7680 $\mu\text{g/L}$) has decreased to 1.45×10^{-6} M (344 $\mu\text{g/L}$). The results show a substantial removal of uranium and neptunium from the groundwater of approximately 85 % and 95 %, respectively (Table 1). It can be considered that the uptake depends predominantly on the amount of iron oxyhydroxides precipitated onto the stalks of *Gallionella ferruginea*. However, the precipitation of iron oxide on the surface of bacteria is depending on the total supply of dissolved ferric iron and availability of reactive sorption sites (i.e. carboxyl or phosphoryl groups) on the individual cells (Konhauser, 1997). Anderson & Pedersen (2003) showed in their studies that up to 90 wt.% iron oxyhydroxides can be formed on the extracellular stalk material. Due to the amount of ferric iron in the BIOS biofilm of our study (Table 2) we assume that the portion of iron oxyhydroxides amounts approximately 71 wt.%. The residual mass must be derived mostly from bacterial organic matter. Results obtained by powder X-ray diffraction of the dried BIOS biofilm clearly indicate the presence of a two-line ferrihydrite. As known from several studies (i.e. Waite et al., 1994; Payne et al., 1998; His et al., 1985) the sorption of U(VI) onto ferrihydrite in neutral pH of 5.4 to 8.2 and in carbonate-free solution systems can reach 95-99 %. Similarly, in carbonate-free solution systems and in the pH range from 6.9 to 9.0 Np(V) is almost completely sorbed by ferrihydrite (Girvin et al., 1991). However, in the presence of carbonate and hydrocarbonate a uranyl carbonate complex will form and inhibit uranyl sorption onto ferrihydrite.

Table 1: Mean concentration of cations and anions in the groundwater and after the experiments with U(VI) and Np(V). The elemental activities are listed, which were obtained by geochemical modelling of the groundwater after adding U(VI).

Groundwater from the BIOS biofilm flow cell					
	after adding U(VI) [in µg/L]	elemental activity	after the experiment [in µg/L]	after adding Np(V) [in µg/L]	after the experiment [in µg/L]
Na	1,48E+06	4,99E-02	1,44E+06	Na	1,48E+06
Mg	1,47E+05	3,02E-03	1,41E+05	Mg	1,47E+05
Si	5,44E+03	1,96E-04	6,41E+03	Si	5,44E+03
Ca	1,62E+05	1,99E-03	1,72E+05	Ca	1,62E+05
K	4,34E+04	8,43E-04	1,27E+05	K	4,34E+04
Al	7,41E+00	2,21E-07	8,82E+00	Al	7,41E+00
Fe	1,36E+03	2,35E-05	3,57E+03	Fe	1,36E+03
Co	2,62E-01	3,31E-09	2,15E-01	Co	2,62E-01
Ni	5,66E+00	4,20E-08	4,24E+00	Ni	5,66E+00
Cu	1,47E+00	2,71E-08	2,40E+00	Cu	1,47E+00
As	<10		<10	As	<10
Br	8,82E+03	8,37E-05	1,02E+04	Br	8,82E+03
Sr	2,44E+03	1,20E-05	2,98E+03	Sr	2,44E+03
U	4,50E+03	1,83E-05	7,08E+02	Np	7,68E+03
Cl ⁻	2,70E+06	5,74E-02	2,70E+06	Cl ⁻	2,70E+06
NO ₃ ⁻	<200		3,37E+04	NO ₃ ⁻	<200
PO ₄ ³⁻	<500		<500	PO ₄ ³⁻	<500
SO ₄ ²⁻	3,14E+05	1,67E-03	3,13E+05	SO ₄ ²⁻	3,14E+05
CO ₃ ²⁻	2,08E+05	2,75E-03	2,01E+05	CO ₃ ²⁻	1,50E+05

In a biological system, such as the studied BIOS biofilms, the situation is more complex. The BIOS biofilms are grown in a groundwater with a carbonate concentration of 4.5×10^{-3} M (Table 1). Nevertheless, U(VI) and Np(V) are probably sorbed on the BIOS biofilm components, i.e. ferrihydrite and organic stalk material. Analysis of the BIOS biofilm dry mass showed a U(VI) concentration of 499 µg/g, indicating that almost the initial U(VI) concentration was sorbed. We assume that the carbonate concentration of the bulk solution does not have a significant effect on the sorption behaviour of U(VI) and Np(V) in the BIOS biofilm since biofilms are microenvironments, which differ significantly from that of the bulk solution (Krawczyk-Bärsch et al., 2012).

Table 2: Mean concentration of cations in the BIOS/biofilm dry mass after the experiments with U(VI) (initial conc. = 1.9×10^{-5} M).

BIOS biofilm dry mass after the experiment with U(VI) [µg/g]	
Na	1,17E+04
Mg	4,10E+04
Al	9,45E+01
Si	1,01E+03
P	4,01E+03
K	7,71E+02
Ca	2,06E+04
Fe	3,76E+05
Co	2,29E-01
Ni	3,54E+00
Cu	2,34E+00
As	<5
Br	1,55E+02
Sr	6,19E+02
Sn	4,07E-01
Ba	5,74E+02
Pb	4,24E-01
U	5,00E+02

In contrast, the carbonate concentration of the groundwater is of great importance when considered without the biofilm. We used the analytical data of the uranium-contaminated groundwater for the calculation of the predominance fields of different uranium species in the pH- E_h diagram by using the geochemical speciation code "Geochemist's Workbench" Version 9.0.5/React/ACT2. The command "speciate over x-y" was used for every basis species within the calculation of the E_h -pH-diagram to consider the chemical speciation of every element during pH and E_h change. The database used was the thermo.dat accompanying the code, supplemented by the most recent NEA database for aqueous uranium species and mineral uranium phases (Guillaumont et al., 2003), and for the aqueous calcium uranyl carbonates species $\text{Ca}_2\text{UO}_2(\text{CO}_3)_3$ (Bernhard et al., 2001). As shown in Figure 2 the theoretical predominance fields of various solid and aqueous uranium species are defined under the ambient condition found in the uranium-contaminated groundwater. Several theoretical predominance fields of solid and aqueous uranium species can be defined. When plotting the measured pH and E_h values of the uranium-contaminated groundwater in the pH- E_h diagram, the formation of an aqueous uranium carbonate species is predicted (Figure 2). We assume that after the addition of uranium to the groundwater $\text{Ca}_2\text{UO}_2(\text{CO}_3)_3$ were formed using the large available amount of carbonate in the water. Probably, the presence of carbonate may affect sorption by the formation of $\text{NpO}_2\text{CO}_3^-$, too.

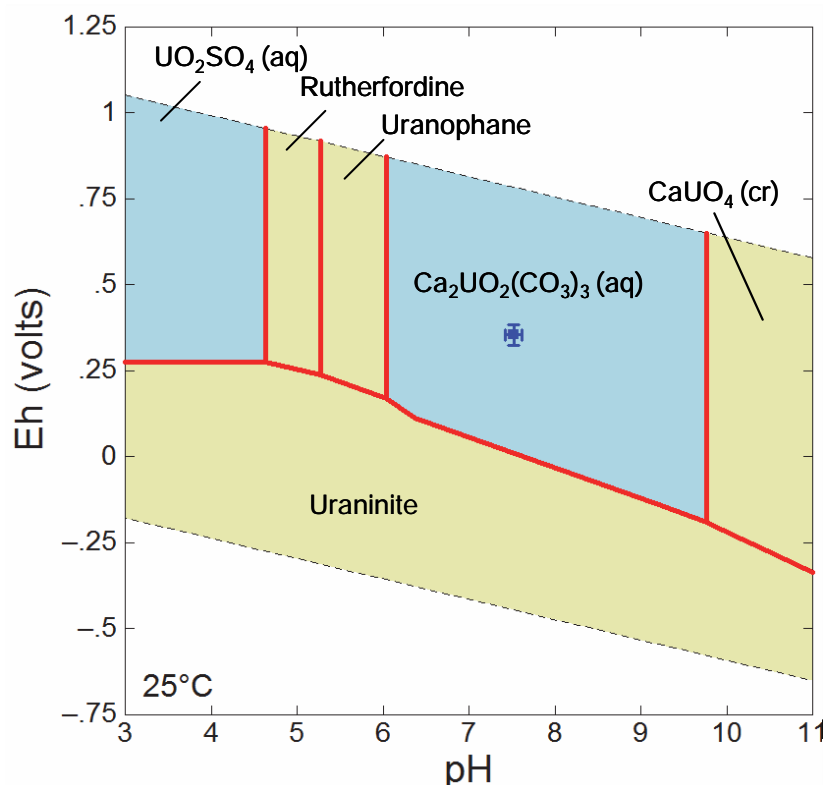


Figure 2: pH- E_h predominance diagram for the uranium-contaminated groundwater after thermodynamic calculation using the geochemical speciation code Geochemist's Workbench Version 9.0.5/Act2. The plotted E_h and pH data correspond to the measured values in the uranium-contaminated groundwater.

Conclusions

U and Np were removed from solution and immobilized exclusively in the BIOS biofilm whereas aqueous calcium carbonate species were formed in the groundwater and contribute to the migration of U and Np and consequently to environmental hazard. The presence of the bacteriogenic iron-producing microbial community in the fracture water results in a high rate of iron precipitation, which is 60 times faster than iron precipitation in an abiotic system (Søgaard et al, 2000). The combination of iron oxides and the biological material creates an abundant surface area for adsorption. Consequently, radionuclides which are not adsorbed by iron oxyhydroxides present in fractures, will be immobilized by BIOS biofilms.

Acknowledgement

The research leading to these results has received funding from the European Union's European Atomic Energy Community's (Euratom) Seventh Framework Programme FP7/2007-2011 under grant agreement n° 269658 (CROCK project). We thank SKB for their cooperation in biofilm and water sampling. We thank Aline Ritter and Carola Eckardt (HZDR Dresden) for analysis.

References

- Anderson, C.R. and Pedersen, K. (2003). *In situ* growth of *Gallionella* biofilms and partitioning of lanthanides and actinides between biological material and ferric oxyhydroxides. *Geobiology*, 1, 169–178.
- Bernhard, G., Geipel, G., Reich, T., Brendler, V., Amayri, S. and Nitsche H. (2001). Uranyl (VI) carbonate complex formation: Validation of the $\text{Ca}_2\text{UO}_2(\text{CO}_3)_3$ (aq.) species. *Radiochim. Acta*, 89, 511-518.
- Flemming, H.-C. (1991). Biofilme und Wassertechnologie. Teil 1: Entstehung, Aufbau, Zusammensetzung und Eigenschaften von Biofilmen. *Gewaesserschutz, Wasser, Abwasser*, 132(4), 197–207.
- Girvin, D.C., Ames, L.L., Schwab, A.P., McGarrah, J.E. (1991). Neptunium sorption on synthetic amorphous iron oxyhydroxide. *J. Colloid Interface Sci.*, 141, 67–78.
- Guillaumont, R., Fanghänel, T., Fuger, J., Grenthe, I., Neck, V., Palmer, D. A. and Rand, M. H. (2003) Update on the chemical thermodynamics of uranium, neptunium, plutonium, americium and technetium. *Chemical Thermodynamics*, vol. 5, ed. OECD Nuclear Energy Agency, Elsevier, Amsterdam.
- Hallbeck, L., Stahl, F. and Pedersen, K. (1993). Phylogeny and phenotypic characterization of the stalk-forming and ironoxidizing bacterium *Gallionella ferruginea*. *Journal of General Microbiology*, 139, 1531-1535.
- Hallbeck, L. and Pedersen, K. (1990). Culture parameters regulating stalk formation and growth rate of *Gallionella ferruginea*. *Journal of General Microbiology*, 136, 1675–1680.
- Hallbeck, L., and Pedersen, K., (1995). Benefits associated with the stalk of *Gallionella ferruginea*, evaluated by comparison of a stalk-forming and a non-stalk-forming strain and biofilm studies in situ. *Microbial Ecology*, 30, 257–268
- His, C.K.D. and Langmuir, D. (1985). Adsorption of uranyl onto ferric oxyhydroxides: application of the surface complexation site-binding model. *Geochim. Cosmochim Acta*, 49, 1931–1941.
- Jägevall, S., Rabe, L. and Pedersen, K. (2011). Abundance and diversity of biofilms in natural and artificial aquifers of the Äspö Hard Rock Laboratory, Sweden. *Microb. Ecol.*, 61, 410–422.
- Konhauser, K.O. (1997). Bacterial iron biomineralization in nature. *FEMS Microbiol. Rev.*, 20, 315-326.
- Konhauser, K.O., Kappler, A. and Roden, E.E. (2011). Iron in microbial metabolisms. *Elements*, 7, 89–93
- Krawczyk-Bärsch, E., Lünsdorf, H., Pedersen, K., Bok, F., Steudtner, R., Lehtinen, A. and Brendler, V. (2012). Immobilization of uranium in biofilm microorganisms exposed to groundwater seeps over granitic rock tunnel walls in Olkiluoto, Finland. *Geochimica et Cosmochimica Acta*, 96, 94–104.
- Lloyd, J. R. and Macaskie, L. E. (2002). Biochemical basis of microbe-radionuclide interactions. In *Interactions of microorganisms with radionuclides*. Ed. Miranda J. Keith-Roach and Francis R. Livens, Elsevier Sciences, Oxford, UK, 313-342.
- Payne, T.E., Lumpkin, G.R. and Waite, T.D. (1998). Uranium(VI) sorption on model minerals, in: E.A. Jenne (Ed.). *Sorption of Metals by Geomedia*, 75–97.

Søgaard, E.G., Medenwaldt, R. and Abraham, P.J.V. (2000). Conditions and rates of biotic and abiotic iron precipitation in selected Danish freshwater plants and microscopic analysis of precipitate morphology. *Water Research*, 34, 2675–2682.

Waite, T.D., Davis, J.A., Payne, T.E., Waychunas, G.A. and Xu, N. (1994). Uranium(VI) sorption to ferrihydrite: application of a surface complexation model. *Geochim. Cosmochim. Acta*, 58, 5465–5478.

A SIMPLIFIED APPROACH FOR REACTIVE TRANSPORT MODELLING INVOLVING STRONGLY NON-LINEAR SORPTION AND SOLUTE REMOBILISATION

James Crawford*

Kemakta Konsult AB (SWE)

* Corresponding author: james@kemakta.se

Abstract

This paper summarises the work that has been performed by the present beneficiary in the final reporting period for WP5 of the CROCK collaborative project. In this work package the focus has been on deployment of process based modelling approaches in safety assessment. We have previously presented (Crawford, 2012) a fast modelling algorithm based on a decoupled major ion chemistry approximation that allows one to simulate the transport of dilute radionuclides separately from the evolution of major components dominating groundwater chemistry. The modelling approach allows considerable savings in CPU time to be achieved in simulations involving advectively dominated flow along discrete flowpaths with matrix interactions. Demonstration simulations of the reactive transport of the cation exchanging solute Ra^{2+} have been made using the simplified technique in a case study involving alternating pulses of saline and fresh groundwater intended to provoke strongly non-linear migration behaviour. Here, we present additional reactive transport simulations made with the CrunchFlow simulation program (Steefel, 2009) to compare with the results obtained using the simplified modelling technique.

Introduction

In the previously presented work (Crawford, 2012), the modelling strategy and theory underpinning the decoupled major ion chemistry approximation implemented in the PATHTRAC simulation tool was outlined. In the modelling approach, the non-linear sorption of a trace solute is separated into an intrinsic non-linear accumulation term and a pseudo-reaction term under the assumption that the migrating trace solute itself exerts a negligible influence on bulk groundwater chemistry. The intrinsic accumulation term accounts for Langmuirian saturation of different site types, while the pseudo-reaction term accounts for non-linear influences of other groundwater components on the sorption of the trace solute. A parametric K_d model can then be used to calculate both terms in a numerical simulation of solute migration where the evolution of groundwater composition is established separately. The evolution of bulk groundwater composition can be determined either in an independent simulation using a fully coupled reactive transport code, or by means of a simplified process representation such as a mixing model.

The parametric K_d data are calculated in separate simulations made using a suitable geochemical modelling tool such as PhreeqC (Parkhurst and Appelo, 1999) or CrunchFlow (Steefel, 2009). The sorption mechanisms underlying the parametric model can be made arbitrarily complex provided they represent true adsorptive

processes such as surface complexation and ion-exchange where there is a 1:1 correspondence between sorbed and mobile solute concentrations.

Since preliminary simulations using the PATHTRAC simulation tool have been reported previously, much of the work in the present reporting period has been directed towards the development of a comparative simulation of reactive transport using a fully coupled code. For this purpose the CrunchFlow simulation program (Steeffel, 2009) has been selected, partly owing to its robust coupling of chemistry and transport using the global implicit method, and partly owing to its status as a well-established model in the scientific literature for reactive transport in porous media.

Estimation of the parametric K_d response function

The original sorption model for Ra^{2+} , Cs^+ , and Sr^{2+} was based on discrete mixing calculations performed in PhreeqC with a single site cation exchange model based on selectivity coefficients reported by (Byegård et al. 1998) for Äspö fine-grained granite. In this paper, we have switched to an alternative cation exchange model based on Finnsjön granite (Byegård et al. 1995) which we believe is more internally consistent for the reactive transport problem currently under consideration. To ensure consistency, relevant parts of the SKB thermodynamic database (Duro et al., 2006) were translated into a CrunchFlow compatible format for use in the calculations so that exactly the same thermodynamic data could be used in conjunction with both programs.

K_d values calculated using CrunchFlow and PhreeqC were found to differ by less than 10% when exactly the same thermodynamic data were used in batch equilibration calculations. In the test calculations, calcite equilibrium was assumed and the Cl^- concentration was adjusted to achieve charge balance at the specified pH of the groundwater type (temperature was assumed to be 25°C). The discrepancy between the programs appears to be related to minor differences in the activity models employed by both programs which are reflected in small deviations of the equilibrium concentrations of Ca^{2+} , HCO_3^- , and Cl^- and consequently also the ionic strength.

The parametric K_d was calculated using discrete batch mixing calculations in PhreeqC with the Fresh and Saline groundwater compositions as end-members. For a system with two groundwater end-members, the discrete mixing calculations performed in PhreeqC gives a smooth interpolation curve spanning the K_d values obtained for the pure end members. Although we attempt to correlate sorption of the trace components Sr^{2+} , Cs^+ , Ra^{2+} in terms of ionic strength (by way of the Fresh-Saline groundwater mixing fraction), this is not a correct representation since it does not properly account for changes in composition and K_d relating to the chromatographic separation of base cation reaction fronts.

In an accurate representation of multicomponent sorption, we would need to correlate K_d values over the entire envelope of variability of the major groundwater constituents (Na^+ , K^+ , Ca^{2+} , Mg^{2+}) since the sorption is effectively a multicomponent, competitive Langmuir isotherm. Figure 1 shows the parametric function describing relative variation in K_d (f_{chem}) calculated using the PhreeqC mixing model. The composition of the Saline and Fresh end-members is given in Table 1.

One of the important questions we attempt to answer in this work is to what extent it is necessary to simulate the full reactive transport problem in PA calculations, and whether it is permissible in certain situations to use a simplified mixing model to estimate groundwater compositional trends.

Table 1: Groundwater chemistry parameters for Fresh and Saline groundwater types. The Saline groundwater is a typical site specific groundwater (~650 m depth) representative of the Forsmark site investigation area, Sweden. The Fresh composition is a typical groundwater of altered meteoric character found in the upper 200 m of bedrock at the same site. Concentrations and ionic strength are given in units of mol/kg water.

	Fresh	Saline	Constraint
pH	8.58	7.55	specified activity
Ionic strength	6.5×10^{-3}	0.19	
Na ⁺	5.52×10^{-3}	7.35×10^{-2}	total concentration
K ⁺	5.52×10^{-2}	3.63×10^{-4}	total concentration
Ca ²⁺	7.91×10^{-5}	2.59×10^{-2}	calcite equilibrium
Mg ²⁺	5.88×10^{-5}	2.17×10^{-3}	total concentration
HCO ₃ ⁻	4.08×10^{-3}	3.59×10^{-4}	total concentration
Cl ⁻	1.51×10^{-3}	1.26×10^{-1}	charge balance
SO ₄ ²⁻	8.91×10^{-5}	2.03×10^{-3}	total concentration

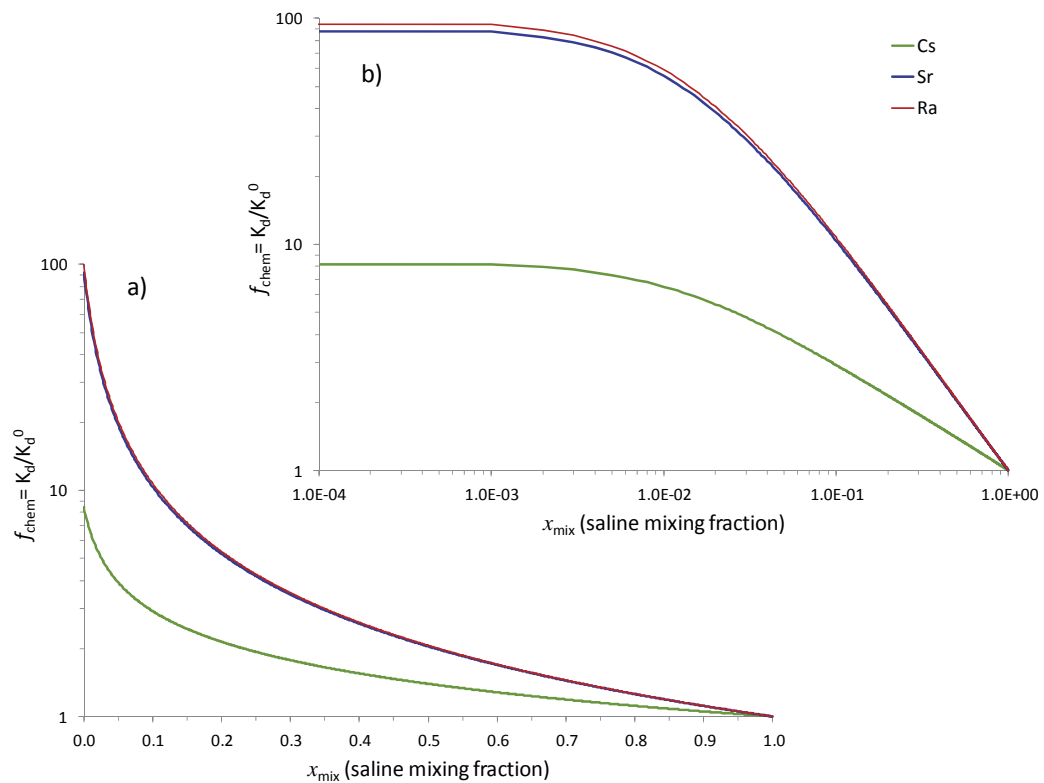


Figure 1: The parametric response function, f_{chem} calculated using PhreeqC where the pure Saline groundwater is the reference condition. Data are shown on a) log-linear axes and, b) log-log axes to highlight details.

Reactive transport simulations

In order to test the non-linear impact of evolving groundwater composition, a simple scenario is modelled involving the intrusion of alternating pulses of Saline and Fresh groundwater end-members into a fracture system initially equilibrated with Saline groundwater. Table 2 summarises the material property data, hydrodynamic boundary conditions and other parameters used in the simulations. The hydrodynamic boundary conditions are fully specified by the F-factor (y/m) and advective travel time (y). The transport half-aperture is equal to the quotient of advective travel time and F-factor. In the present set of case studies this corresponds to a transport aperture of 0.2 mm. In the simulations, the hydrodynamic conditions are assumed to be temporally constant and only the chemical composition of the infiltrating groundwater is variable.

It should be noted by the reader that although Forsmark site-specific data for groundwater composition and material properties have been employed in this simulation exercise, the modelling scenario itself (i.e. alternating pulses of Saline and Fresh groundwater compositions and the low hydrodynamic transport resistance) should not in any way be taken to imply a case study of transport properties relevant for a hypothetical repository at the actual Forsmark site. The selected boundary conditions have been chosen to provoke clearly non-linear behaviour in order to test underlying assumptions inherent in the adopted modelling approach and are not necessarily considered to be realistic for the performance assessment of an actual repository.

Table 2: Material property data, hydrodynamic boundary conditions, and other simulation parameters for the reactive transport case studies.

Parameter	Value (units)	Description
F-factor	10^4 y/m	hydrodynamic transport resistance
t_w	1 y	advective travel time
D_e	10^{-14} m ² /s	effective diffusivity of solute in rock matrix
ε_p	0.001	matrix storage porosity
A_0	0.018 m ² /g	BET surface area of rock matrix
CEC	1.0 mol/kg	cation exchange capacity
δ_m	1.0 m	matrix depth
K_d^{\min}	0.0036 m ³ /kg	K_d value for Ra ²⁺ , Saline end-member
K_d^{\max}	0.36 m ³ /kg	K_d value for Ra ²⁺ , Fresh end-member

Simulation results obtained using PATHTRAC are shown in Figure 2 together with corresponding results obtained using the fully coupled code CrunchFlow. It should be noted that the timing schedule of the Saline/Fresh groundwater pulses is also slightly different to the previously presented results in (Crawford, 2012). The simulation results demonstrate the main non-linearity associated with rapid turnover of groundwater salinity where solute accumulated near the surface of the rock matrix during the Fresh time domain is promptly remobilised when conditions become more saline.

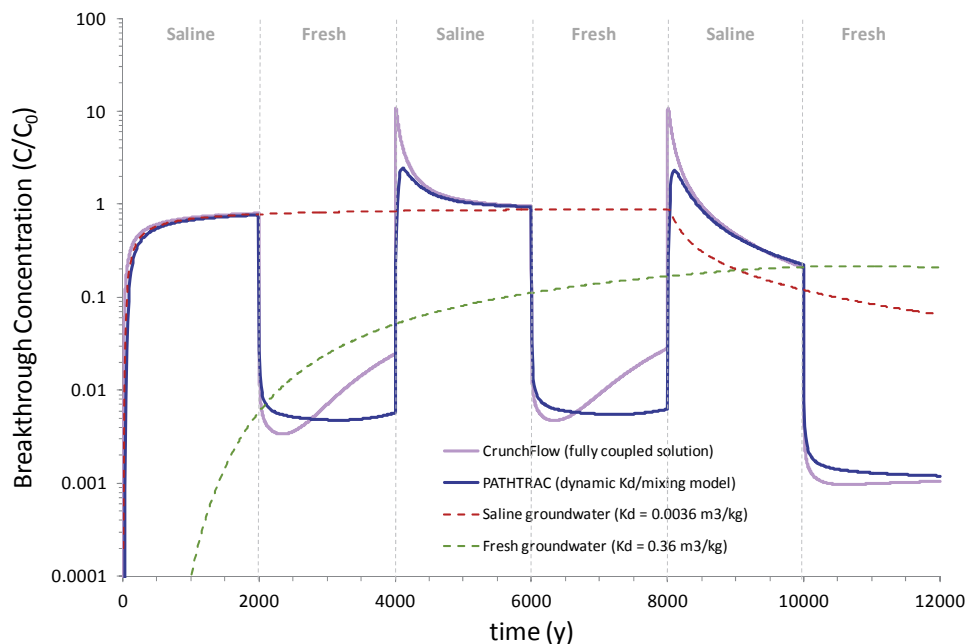


Figure 2: Comparison of breakthrough curves for Ra^{2+} migration simulated using PATHTRAC and a fully coupled reactive transport simulation using CrunchFlow for the temporally variable boundary conditions (as indicated by the fresh/saline labelled intervals in the figure). Breakthrough data are normalised relative to the constant inlet concentration boundary condition (10^{-12} mol/kgw).

Conclusions and Future work

The results indicate that the PATHTRAC simulations using a dynamic K_d correlated with a underlying mixing model approximately captures the broad features of the radionuclide remobilisation process although it significantly underestimates the peak concentration of the remobilised pulse and does not exactly match the transient concentrations obtained in the fully-coupled solution during the time domains dominated by Fresh groundwater. In spite of this, the simulation results demonstrate the utility of the PATHTRAC modelling approach for modelling highly non-linear scenarios of reactive transport involving temporally and spatially variable sorptivity that cannot be captured using a constant K_d modelling approach.

Deviations between the PATHTRAC simulated results and those obtained using the fully coupled CrunchFlow simulations relate to the underlying assumption of a simplified mixing model used to correlate temporal changes in K_d with ionic strength. The divergence arises due to the inability of a mixing model to adequately capture the chromatographic sequence of base cation reaction fronts in the heterovalent cation exchange process. This might be avoided if pre-existing hydrochemical simulation data from other PA analyses are imported into PATHTRAC for use with a more detailed multicomponent parametric K_d model.

The fully coupled solution takes roughly 6 days of CPU time to obtain breakthrough curves to a recovery time of 12 ka for this particular system. This is too slow to be of routine use in PA, particularly if multiple flowpaths featuring different (usually much larger) F-factors are to be simulated. The present version of the PATHTRAC code takes about 10 hours to achieve the same breakthrough time implying a factor 15 increase in speed over the fully coupled model, although it is not optimised for speed and could probably be improved.

Future work will focus on improving the process description for the underlying parametric K_d model with the aim of improving the match between simplified and fully coupled process descriptions as well as extending the analysis to surface complexing radionuclides. Since pH and carbonate concentration transients are not expected to be subject to chromatographic front separation in the same fashion as for base cations when considering cation exchange, it is expected that deviations between the fully-coupled and mixing based modelling approaches will be less in the case of radionuclides that sorb by way of a surface complexation mechanism. This, however, remains to be demonstrated in subsequent work.

Acknowledgement

The research leading to these results has received funding from the European Union's European Atomic Energy Community's (Euratom) Seventh Framework Programme FP7/2007-2011 under grant agreement n° 269658 (CROCK project). Additional funding from the Swedish Nuclear Fuel and Waste Management Co. (SKB) is also gratefully acknowledged.

References

Byegård, J., Skarnemark, G. and Skålberg, M. (1995). The use of some ion-exchange sorbing tracer cations in in-situ experiments in high saline groundwaters. In: Murakami, T., Ewing, R. C. (eds). Scientific basis for nuclear waste management XVIII: symposium held in Kyoto, Japan, 23–27 October 1994. Pittsburgh, PA: Materials Research Society. (Materials Research Society Symposium Proceedings 353), 1077–1084.

Crawford, J. (2012). Decreasing uncertainty of radionuclide migration predictions in safety assessment modelling. In: 1st Workshop Proceedings of the Collaborative Project “Crystalline Rock Retention Processes” (7th EC CP CROCK). Eds. Rabung, T., Molinero, J., Garcia, D., Montoya, V. KIT Scientific Reports 7629, Karlsruhe Institute of Technology, Germany.

Duro, L., Grivé, M., Cera, E., Domènech, C. and Bruno, J. (2006). Update of a thermodynamic database for radionuclides to assist solubility limits calculation for performance assessment. SKB TR-06-17, Swedish Nuclear Fuel & Waste Management Company, Stockholm, Sweden.

Parkhurst, D. L. and Appelo, C. A. J. (1999). User's guide to PHREEQC (version 2): a computer program for speciation, batch-reaction, on-dimensional transport, and inverse geochemical calculations. Water Resources Investigations Report 99-4259, U.S. Geological Survey, Denver CO, USA.

Steeffel, C. (2009). CrunchFlow. Software for modelling multicomponent reactive flow and transport. User's Manual, Lawrence Berkeley National Laboratory, CA, USA.

APPROACHES TO MODELLING SURFACE COMPLEXATION SORPTION ON COMPLEX GEOLOGICAL MATERIALS WITH LIMITED DATA

James Crawford*

Kemakta Konsult AB (SWE)

* Corresponding author: james@kemakta.se

Abstract

This paper together with the accompanying poster presentation (Crawford, 2012) summarises the main work that has been performed by the present beneficiary in the final reporting period for WP4 of the CROCK collaborative project. In this work package the focus has been on conceptualisation and modelling of transport retardation processes with particular emphasis on producing scalable mechanistic models for sorption in granitic rock that can be deployed in performance assessment (PA). Models of a top-down and bottom-up nature have been examined and some novel approaches developed to simplify surface complexation modelling on complex geological materials with limited data.

Introduction

In this work the focus is mainly on surface complexation modelling (SCM) involving the formation of covalent bonds between ionic charged species and reactive surface groups at liquid-solid interfaces. There are two distinct modelling strategies used for applying SCM to complex environmental substrates such as granitic rock. The first, *top down* (generalised composite, GC) modelling approach attempts to model the composite mineral system based on the assumption of a generic binding site type without consideration of the detailed properties of the mineral surfaces upon which sorption is occurring. The second *bottom-up* (component additivity, CA) approach involves careful consideration of the identity and proportion of total reactive surface area of individual minerals comprising the rock and combining separate SCM's for pure mineral phases from the literature under the assumption of linear additivity of resultant sorption.

It is difficult to apply customary methods for fitting a sorption model to laboratory data when dealing with mineralogically and microstructurally complex materials such as granite. It is generally not feasible, for example, to obtain detailed sorption edge measurements (i.e. K_d vs. pH) for granular materials with diffusive equilibration times which may extend many months, or perhaps years. At the same time, titration-based methods for ascertaining pH-dependent surface charging behaviour of reactive sites are usually neither feasible nor easily interpreted for composite materials as might be possible for fine particulate single mineral systems such as clays, oxides, and hydroxide minerals.

Much of the present work has centred on the conjectured existence of linear free energy relations (LFER) describing surface complexation binding reactions. LFER's are well-known empirical relations commonly applied in aquatic chemistry to establish correlations between paired data sets of closely related phenomena (see, e.g. Stumm and Morgan 1996). In the case of SCM, the binding reactions of solutes with surface hydroxyl groups share similarities with analogous aqueous phase hydrolysis reactions, the main difference being that a

surface hydroxyl group takes the place of one water molecule in the reaction stoichiometry. The LFER is formulated in terms of a slope (m) and intercept term (b) relating the log-transformed mass action constants for the reactions. These parameters are typically obtained by linear regression of previously fitted data sets although our work has indicated that there are ways in which they might also be directly inferred from the underlying data in certain cases (see Crawford, 2012).

Theoretical development

The distribution coefficient (K_d) for sorption of a given metal cation on the different mineral surfaces comprising granitic rock can be written in terms of the concentration sum of individual surface complexes formed by the solute on different binding site types. Since the true reactive surface area associated with each class of binding site is usually not possible to measure, it is customary to assume surface area as measured by the BET method as a proxy. The reactive surface area of each binding site is then taken to be equal to a weighted fraction of the bulk surface area where the weights are based on the measured volumetric fraction of component minerals and their BET surface areas reported in the literature. This implies a simple proportionality with volumetric fraction and literature data for pure mineral surface areas which is not necessarily a good assumption. The procedure of weighting contributions to macroscopic sorption using literature binding constants for individual minerals, volumetric mineral fractions, and BET surface area compounds uncertainties in several steps in an unsatisfactory fashion.

In this work we implicitly assume that there is an underlying LFER for each mineral comprising the granitic rock and that the surface reactions follow a simple monodentate template with reactions analogous to successive hydrolysis steps of the cation in the aqueous phase. It is relatively straight forward to demonstrate that the scaling factor implied by the numerical value of the LFER intercept affects each surface species identically for a given binding site type (Crawford, 2012). Based on this observation, we have found that it is possible to merge the surface area weighting fractions and the scaling factors corresponding to the LFER intercepts together and treat them as a single lumped parameter that can be fitted to measurement data.

It is still necessary to specify the slopes of the underlying LFER's for each mineral, although many of the remaining uncertainties are consolidated into the empirical weighting parameters described above. For a three mineral model, it is then only strictly necessary to fit three lumped weighting parameters (i.e. which combine LFER slopes and reactive surface areas) in a least squares sense, the numerical values of the underlying LFER intercepts and surface area fractions of the minerals then being essentially redundant variables. Since this technique is a hybrid of the top-down and bottom-up approaches, we refer to this procedure as the *boot-strapped component additivity (BCA)* approach.

For guidance in the surface complexation modelling, we have relied on the previous work by Bradbury and Baeyens (2005, 2009a,b) for illite and montmorillonite which we expect to share many similarities to the biotite mineral phase present in granite. In these studies, it was found that 4 surface complexes each were needed to fit Am and Eu sorption edges. The authors neglected the fourth hydrolysis steps in the aqueous phase for Am and Eu speciation on account of weak evidence for their existence, even though they were tacitly assumed for the surface speciation. For Ni, on the other hand, 3 surface complexes were required to fit the sorption edge even though there were 4 hydrolysis steps used in the aqueous phase speciation. Although these apparent irregularities are not necessarily physically inconsistent with the underlying principles of an LFER, they highlight the semi-empirical nature of the analogy and suggest that any extrapolation to different groundwater compositions should be treated with caution.

Modelling with PhreeqC (Parkhurst and Appelo, 1999) indicates that slope factors greater than about unity imply a diminished relative role for surface complexes corresponding to higher hydrolysis steps of a given cation and the associated uncertainty therefore appears to be largely an issue for minerals with low slope factors. Since the slope factor appears to be correlated with the pH of zero net proton charge (pH_{PZPC}) this would tend to imply minerals such as quartz, feldspar, and plagioclase. This might also explain why LFER's reported in the literature for hydrous ferric oxide ($m = 1.17$) and gibbsite ($m = 1.32$) are only correlated in terms of first hydrolysis constants (Dzombak and Morel, 1993; Karamalidis and Dzombak, 2010), whereas for illite ($m = 0.83$) and montmorillonite ($m = 0.90$) up to four hydrolysis constants are used (Bradbury and Baeyens, 2005; 2009a,b).

Application of the BCA method to Forsmark site-specific data

Since sorption measurements were not available for the Äspö materials characterized in WP2, we have elected to concentrate our efforts on understanding sorption data obtained during the site investigation carried out by SKB at Forsmark, Sweden (SKB, 2008). In particular, we have focused on measurement data obtained for the sorption of Am, Eu, and Ni on Forsmark metagranite (1-2 mm crushed size fraction and ≈ 168 days contact time). Although sorption edge data are not available, there are replicate sets of measurements for samples derived from several different borehole sections in contact with synthetic groundwaters including a Saline, Fresh, Marine, and a Brine type groundwater.

The procedure we have adopted is to use the measured K_d data set for Saline groundwater (ionic strength 0.19 M, $\text{pH } 8.4 \pm 0.3$) to establish a best fit SCM to the central estimate K_d values and then use the resultant model to make a prediction of what the corresponding K_d values should be for the same materials in contact with the Fresh groundwater type (ionic strength 6.5×10^{-3} M, $\text{pH } 9.7 \pm 0.3$). The match between the predicted K_d value for Fresh groundwater and the actually measured value then gives an idea of the skill of the model in extrapolating to different groundwater compositions.

The Forsmark metagranite contains, on average, 5% biotite, 35% quartz, 23% K-feldspar, and 34% plagioclase, with the remainder made up by minor accessory minerals. A small amount of hydrous ferric oxide or magnetite is also likely to be present, although this has not been quantified and is likely to be very small. Given their high specific surface area and strong sorptivity, however, the presence of Fe-oxides may influence the sorptivity in a disproportionate fashion. As a working hypothesis, a three-mineral mixture comprised of quartz, illite (assumed to be an approximate geochemical analogue for biotite), and hydrous ferric oxide sites was assumed as the basis for a simplified model. Since these three minerals also represent a broad range of LFER slope factors, it was thought that they might be sufficient to capture the most important sorptive trends even though the full mineralogy of the rock is not accounted for.

Using the BCA approach it was relatively straightforward to find a set of positive weights to give a simultaneous match to the sorption data for Am, Eu, and Ni using Matlab. The sorption calculations themselves were made with PhreeqC (Parkhurst and Appelo, 1999) using the SKB thermodynamic database (Duro et al., 2006) and assuming consistency with an underlying LFER for each component mineral either obtained from or derived from literature sources (Dzombak and Morel, 1993; Bradbury and Baeyens, 2009b; Schindler et al., 1976). Furthermore, a $2\text{-p}K_a$ surface charging model was assumed for each component mineral and electrostatics were neglected as a first approximation. Carbonate chemistry was also included, although since the actual headspace gas composition for the experiments was unknown, the CO_2 partial pressure was adjusted in the modelling to roughly 10^{-5} atm to give a match to the measured pH of the equilibrated groundwater

solutions. This was necessary since there was a pH drift of about 1-1.5 units in the experiments which we have good reason to suspect may be the result of partial re-equilibration of the contact solutions to a lower CO₂ partial pressure. Since the crushed rock samples were pre-equilibrated with the synthetic contact groundwater for a period of roughly 90 days (with 10 water changes during the first 36 days) prior to spiking with the radionuclide tracer it is thought that the pH drift most likely occurred prior to spiking, although this cannot be confirmed from the recorded data since only post mortem pH measurements were made.

Although the fit to the Saline groundwater is based on an extremely limited data set (1 central estimate data point for each metal ion), the extrapolation to Fresh groundwater appears to be remarkably accurate as can be seen in Figure 1. Not only does the model reasonably predict both Am and Eu sorption, the sorption of Ni is very slightly underestimated (slightly below the lower error bound of the measurement data) which is consistent with the presumed impact of cation exchange as an additional sorption mechanism for Ni at the much lower ionic strength of the Fresh groundwater. It is expected that the same general approach should also apply to 1-pK_a charging models and for models incorporating electrostatic corrections, although this has not been investigated at the present time.

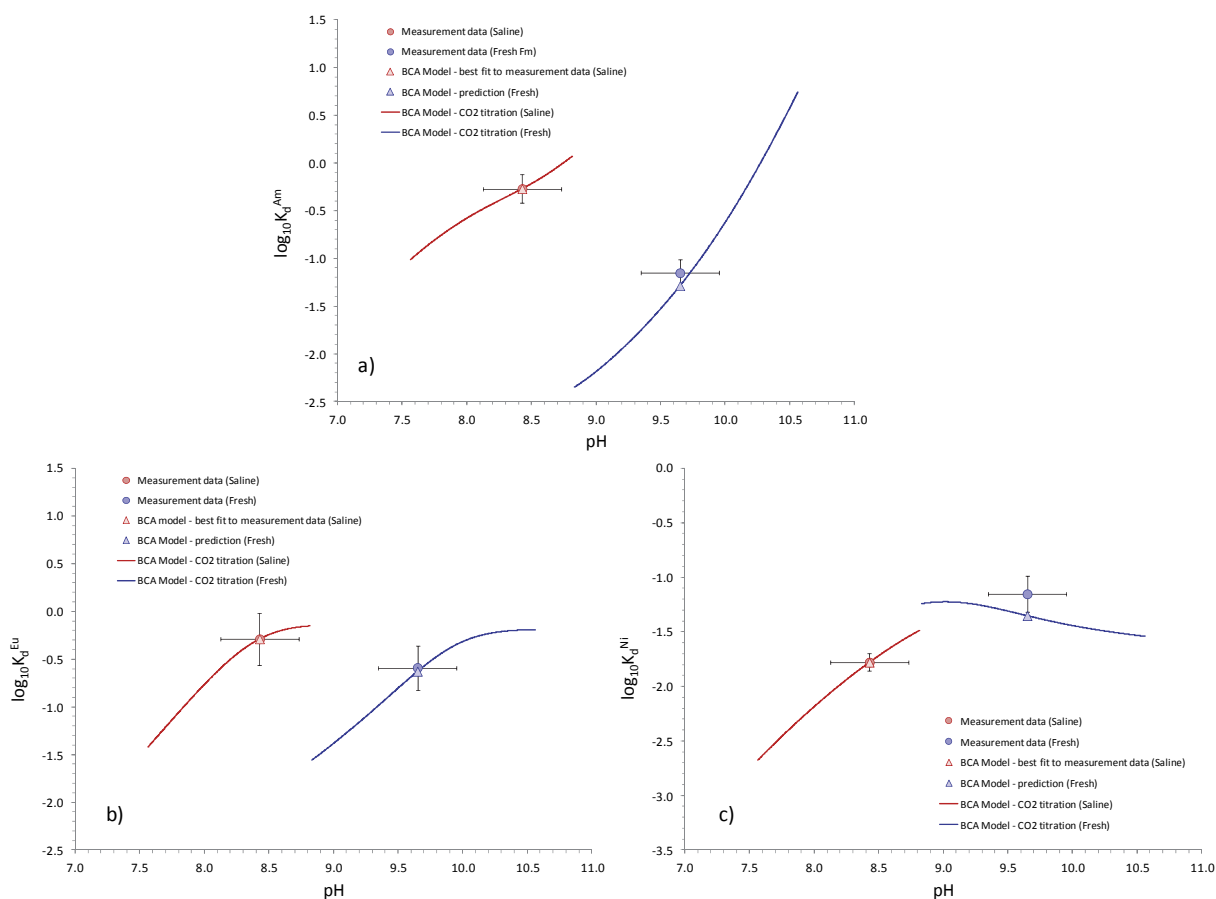


Figure 1: Boot-strapped component additivity model (BCA) predictions of K_d for a) Am, b) Eu, and c) Ni on Forsmark metagranite in contact with the Fresh groundwater (blue triangular markers) as compared with measured values (blue circular markers). The values for Saline groundwater (red markers) are calibrated to give an exact fit to the measured data. Solid lines indicate the simulated sorption edge for each groundwater where pH is adjusted by alteration of CO₂ partial pressure.

Conclusions and Future work

The hybrid bottom-up approach (*BCA, boot-strapped component additivity*) appears to be a promising method for fitting a mechanistically reasonable model to sorption data for complex materials comprised of several different mineral surfaces with dissimilar sorptive properties. Although the method is dependent on the existence of good quality data for the individual component minerals via the underlying LFER's, the analysis suggests that it is the slope of the LFER that is of overwhelming importance since the weights estimated for each mineral surface automatically accommodate uncertainty in the underlying LFER intercepts to give the boot-strapped fit to the data upon which the model is conditioned.

The model appears to make a skilful prediction of sorption in contact with Fresh groundwater suggesting that the approach might be useful for reducing uncertainty in surface complexation modelling of such systems, particularly when faced with limitations of incomplete or sparse measurement data. Although the extrapolation appears convincing, it is not clear yet whether this is a coincidence or whether the model is an accurate reflection of the actual sorption mechanisms.

At this time we have not investigated the impact of neglecting higher surface complexes of Am and Eu (i.e. $>SOAm(OH)_3^-$ and $>SOEu(OH)_3^-$), although this is likely to have some influence on the calculated weights given that the existence of the associated aqueous phase hydrolysis reactions is questionable. The role of diffusive kinetics must also be investigated further since there are some indications that 168 days of contact time is insufficient to guarantee a true equilibrium state for the mm-size crushed granite particles used in the laboratory investigations. Future work will also focus on extending the analysis to site specific data from Laxemar and the Äspö Hard Rock Laboratory to further evaluate the method including extending it to SCM sub-types incorporating electrostatic corrections.

Acknowledgement

The research leading to these results has received funding from the European Union's European Atomic Energy Community's (Euratom) Seventh Framework Programme FP7/2007-2011 under grant agreement n° 269658 (CROCK project). Additional funding from the Swedish Nuclear Fuel and Waste Management Co. (SKB) is also gratefully acknowledged.

References

- Bradbury, M. H. and Baeyens, B. (2005). Modelling the sorption of Mn(II), Co(II), Ni(II), Zn(II), Cd(II), Eu(III), Am(III), Sn(IV), Th(IV), Np(V) and U(VI) on montmorillonite: Linear free energy relationships and estimates of surface binding constants for some selected heavy metals and actinides. *Geochimica et Cosmochimica Acta*, 69(4), 875-892.
- Bradbury, M. H. and Baeyens, B. (2009a). Sorption modelling on illite Part I: Titration measurements and the sorption of Ni, Co, Eu and Sn. *Geochimica et Cosmochimica Acta*, 73(4), 990-1003.
- Bradbury, M. H. and Baeyens, B. (2009b). Sorption modelling on illite. Part II: Actinide sorption and linear free energy relationships. *Geochimica et Cosmochimica Acta*, 73(4), 1004-1013.

Crawford, J. (2012) What might K_d ratios be able to tell us about surface complexation sorption mechanisms? Poster presented at the CROCK Final Workshop in Karlsruhe, Germany, May 14-16, 2012.

Duro, L., Grivé, M., Cera, E., Domènech, C. and Bruno, J. (2006). Update of a thermodynamic database for radionuclides to assist solubility limits calculation for performance assessment. SKB TR-06-17, Swedish Nuclear Fuel & Waste Management Company, Stockholm, Sweden.

Dzombak, D. A. and Morel, F. M. M. (1990). Surface complexation modelling. Hydrous ferric oxide. Wiley, New York.

Karamalidis, A. K. and Dzombak, D. A. (2010). Surface complexation modelling. Gibbsite. Wiley, New York.

Parkhurst, D. L. and Appelo, C. A. J. (1999). User's guide to PHREEQC (version 2): a computer program for speciation, batch-reaction, on-dimensional transport, and inverse geochemical calculations. Water Resources Investigations Report 99-4259, U.S. Geological Survey, Denver CO, USA.

Schindler, P., Fuerst, B., Dick, R. and Wolf, P. (1976). Ligand properties of surface silanol groups. I. Surface complex formation with Fe^{3+} , Cu^{2+} , and Pb^{2+} . Journal of Colloid and Interface Science, 55, 469-475.

SKB (2008). Site description of Forsmark at completion of the site investigation phase. SDM-Site Forsmark. SKB Technical Report TR-08-05, Swedish Nuclear Fuel and Waste Management Company, Stockholm.

Stumm, W. and Morgan, J. (1996). Aquatic chemistry. Chemical equilibria and rates in natural waters. 3 ed. Wiley, New York.

DOCUMENTATION. EVALUATION OF TREATMENT OF RADIONUCLIDE TRANSPORT AND RETENTION PHENOMENA IN RECENT PERFORMANCE ASSESSMENTS

Andres Idiart*, Marek Pekala

Amphos 21 Consulting (Barcelona, Spain)

* Corresponding author: andres.idiart@amphos21.com

Abstract

Work Package 6 (WP-6) of the CROCK European collaborative project focus on the review of those processes which exert a major influence on the transport and retention of radionuclides in the far-field, as well as on the main conceptual models describing these processes available in the scientific literature. Based on the results of a questionnaire distributed among different international organisations, an analysis of how these retention processes are taken into account and modelled in the different Performance Assessments (PAs) currently being carried out by radioactive waste management organisations has been conducted. The focus is on the evaluation of the long-term safety of deep geological disposal facilities for radioactive waste in crystalline rocks. This contribution summarizes the main conclusions and knowledge gaps identified by the participants.

Introduction

The main objective of WP-6 of the CROCK project is to compile and document the state-of-the-art on retention processes in crystalline rock, focusing on recent advances in Performance Assessments exercises (PAs). A questionnaire was prepared and distributed among members of all organizations participating in the CROCK project, as well as some external contributors (Table 1). Responses were received from eight participating organizations. The responders have either been directly involved in a recent Performance Assessment work, or else have other relevant experience and knowledge of the methodologies and practices applied in this area at present. The questionnaire aimed to elicit expert opinion on the main assumptions and simplifications of radionuclide transport and retention in mathematical modelling as applied in the context of Performance Assessment. The questions were formulated so as to enquire about both the treatment of critical transport/retention processes such as groundwater flow, diffusion or sorption, and about the possible interplay between them. The responders were asked to provide their subjective ranking of the most relevant phenomena involved in radionuclide transport as well as their opinions on the main limitations of current Performance Assessment modelling. In addition the responders were given an opportunity to express their opinion on the most challenging issues that should be dealt with in order to help improve Performance Assessments modelling in the future. A sample of the questionnaire is provided in the Appendix.

In this contribution, a short summary of the information supplied by the different participants is given. Common views on various issues related to Performance Assessment as well as main discrepancies were analysed. It is stressed that the following paragraphs describe the different views of the participant organizations individually.

There is no consensus in the issues presented, and some of them may not be applicable to a given Performance Assessment.

Table 1: List of participants in the questionnaire exercise.

Host organization for a responder participating in the questionnaire	Performance Assessment activities in which the responder has been involved	Year
Kemakta Konsult AB	SR-Site (2011)	2011
Nuclear Research Institute Řež plc.	Initial safety report study (2010); C2 Long-term safety evaluation of GDR	2010
KIT-INE	First long-term Safety Assessment for a generic German SF repository in granite; KOLLORADO-1 (Colloid and nano-particle formation and mobility in the concept of a deep GDF)	
CIEMAT	Enresa 2000	2000
Lomonosov Moscow State University		
Technical Research Centre of Finland (VTT)	TILA-99	1999
Japan Atomic Energy Agency (JAEA)	H12 performance assessment	1999
Gesellschaft für Anlagen- und Reaktorsicherheit (GRS)		

Relative Importance of Processes Assumed to Have an Impact on Radionuclide Transport and Retention Phenomena

Generally, there is no distinct agreement between the experts on the relative importance (rank) of the different phenomena for radionuclide transport and retention. It appears however, that a majority of responders give priority to phenomena related to transport by groundwater flow (advection), such as:

- Groundwater flow velocity
- Transport pathway length
- Hydraulic connectivity of fracture system
- Mixing and dilution

All experts have emphasized the importance of chemical retardation processes, mainly radionuclide sorption onto mineral surfaces. In addition, a majority of responders mentioned the relatively high impact of matrix diffusion as a retention process.

Main Assumptions and Simplifications of Current Performance Assessment Models

As mentioned above, advective transport has been identified as one of the most important processes for radionuclide transport in the geosphere. The following assumptions and simplifications applied to advective transport in Performance Assessments have been highlighted by the experts as having potentially high impact on the modelling results:

- Flow of groundwater is assumed to be isothermal and laminar, and only steady-state conditions are generally considered
- Groundwater flow is assumed to be homogenous through the rock volume and channelling phenomena are not accounted for
- The frequency and conductivity of groundwater conducting fractures are estimated based on borehole data only
- The conductivity of groundwater conducting fractures is assumed to scale with the fracture aperture
- Dispersion coefficient is simplified as dependent on groundwater flow velocity only

With regard to radionuclide sorption onto mineral surfaces, the responders pointed out that a major simplification made is to represent the process using the constant distribution coefficient (K_d) approach, instead of applying the more realistic surface complexation models. Among the main drawbacks of this approach the experts mentioned that:

- The constant K_d approach is unlikely to adequately represent the variations in sorption along a flow path, and that it assumes complete reversibility and chemical equilibrium
- K_d values used in Performance Assessments are sometimes taken from generic literature sources, rather than being based on laboratory-derived data. However, even where efforts were made to derive laboratory-based K_d values that could represent in-situ conditions more closely, the in-situ groundwater conditions (e.g. the redox potential) could often not be reliably established. In such cases it is a common practice to select conservative conditions that cautiously underestimate radionuclide retention
- Where laboratory-derived K_d values are used, these are often obtained from batch experiments on crushed/dispersed rock samples. In applying these parameter values an assumption is made that the high liquid/solid ratio represents the in-situ Performance Assessment conditions sufficiently well.
- The simplified K_d approach is not capable of capturing coupled reactions in complex systems, where multiple interactions between radionuclides, colloids and the rock matrix occur

In addition, radionuclides are considered to sorb only onto the rock matrix within the rock pore-space, but not onto fracture surfaces or, especially, fracture infilling secondary minerals, which often are characterized by increased sorption properties.

All experts acknowledged matrix diffusion as an important retention process for radionuclide transport. The main simplifications applied to matrix diffusion in Performance Assessment models have been identified to be:

- The diffusion coefficient for all transported species is assumed to be the same (e.g. no detailed consideration is given to distribution of solutes among different cationic and anionic species)

- The diffusion coefficient is assumed to be spatially constant (constant porosity, tortuosity)
- Anion exclusion is approximated by reducing the diffusion coefficient for anions by an arbitrary safety factor (e.g. by assuming that a portion of the matrix porosity is not accessible to anions)
- It is assumed that the rock matrix is homogenous in time and space
- Only limited matrix thickness available to diffusion is considered
- Diffusion into fault gouge is not included

Among other geochemical aspects relevant to radionuclide transport and retention it was pointed out that:

- The formation of solid solutions, radionuclide (co-) precipitation and potential re-dissolution are often disregarded
- Colloid-mediated radionuclide transport may be important but is generally not included in Performance Assessments

Main Limitations of Current Performance Assessment Models

Most experts agree that the main challenges in modelling of radionuclide transport within Performance Assessment lie in the areas of:

- Sufficient conceptual understanding of relevant processes that control the transport and retention of radionuclides
- Adequate implementation of conceptual models into Performance Assessment codes
- Acquisition of reliable data for model parameterization

There is a general consensus among the responders that important gaps in understanding of relevant phenomena still exist. For example, it is known that large scale physical heterogeneities will be an important control for groundwater flow both in terms of flow path and volume. However, the exact interplay between channelling phenomena and mass transfer into effectively stagnant zones of the fracture network is not well understood at present.

As Performance Assessment simulations are carried out for very long times (typically up to 1 Ma), changes of groundwater flow patterns and chemistry are expected due to for example climate change or tectonic activity. Understanding and quantification of these effects are currently associated with very high uncertainties.

In terms of implementation of conceptual models into Performance Assessment codes, major difficulties identified are associated with coupling of transport and chemical reactions, which is typically not implemented. Moreover, transport and chemical processes may operate over significantly different temporal and spatial scales, and a major challenge is to represent these phenomena on the scale typical of Performance Assessment calculations. Three-dimensional Performance Assessment simulations are capable of capturing more adequately groundwater mixing and dispersion as well as represent the repository geometry in a more realistic way. However, one-dimensional simplified models are typically used instead.

There is a general agreement among the experts that computational power to perform large-scale, three-dimensional and fully-coupled simulations of radionuclide transport in the geosphere is currently not available. However, some responders argue that this is not a relevant limiting factor given that significant gaps in conceptual understanding of phenomena involved still exists. In addition, no verified and validated reactive transport codes suitable for use in Performance Assessment currently exist.

Reliability of Performance Assessment models is heavily dependent on the quality of field and laboratory data used to constrain parameter values applied in the codes. All experts highlighted the importance of applying reliable experimental methodologies and up-scaling techniques to acquire site-specific and accurate parameter values. In particular, the issue of parameter value up-scaling remains problematic, also for the most critical transport and retention parameters. A comparison of values obtained from laboratory and in-situ experiments constitutes one way in which the problem can be reduced. In addition, the process of up-scaling from laboratory- to field-scale introduces uncertainty, which needs to be adequately quantified and documented. Available techniques for multi-scale modelling have been suggested by some responders as a way forward, although the interfaces between models used in PAs would have to be improved.

Processes not Considered in Current Performance Assessment Modelling that Deserve Special Attention

Several processes were identified as currently not incorporated into Performance Assessment models, but having potentially high impact on radionuclide transport in the geosphere. These include:

- Bentonite erosion and formation of colloids as a result of intrusion of low-salinity waters into the near-field;
- Mixing and dilution during advective transport;
- Radionuclide re-mobilization. This could for example occur as a result of change in groundwater geochemistry or due to radioactive decay and the production of daughter-radionuclides with different chemical properties;
- The effect of degradation of cementitious materials due to interactions with groundwater: the formation of hyper-alkaline plume and its impact on physical and chemical properties of the affected rock;
- Microbial activity. In particular microbial-mediated remobilization processes that may be characterized by slow kinetics;
- Modelling of solute transport: PA exercises could be improved by considering more detailed transport models than the simple models currently used

Acknowledgement

The work presented here has received funding from the European Union's European Atomic Energy Community's (EURATOM) Seventh Framework Programme FP7 under grant agreement n° 269658. We are grateful with all the beneficiaries of the CROCK project for their participation in this Work Package and for filling the questionnaires. The external contributors to the questionnaires are also gratefully acknowledged.

Appendix – Sample of the Questionnaire

NAME:		AFFILIATION:
CROCK WP NUMBER:		DATE:
PA name:	PA year:	Reference:
What are the main assumptions and simplifications made with regard to the following processes:		
Matrix diffusion	e.g. no anion exclusion in the model, homogeneous matrix composition, etc.	
Groundwater flow	e.g. simplifications regarding how fracture wet surface is calculated, steady-state simulations, etc.	
Sorption onto mineral surfaces	e.g. use of K_d values instead of surface complexation models, etc.	
Other geochemical aspects (specify)	e.g. no chemical equilibrium calculations are considered in the PA, etc.	
Other relevant processes	e.g. the effect of colloids on RN transport is neglected, gas generation is not considered, etc.	
Rank in order of importance the most relevant processes considered to have an impact on safety (concerning PA aspects).		
e.g.: sorption onto mineral surfaces matrix diffusion, etc.		
In your opinion, are there other processes not considered in PA exercises that should deserve special attention?		
e.g.: effect of bentonite and other type of colloids on the transport of RN		
What are the main limitations of the current PA with regard to:		
Conceptual understanding of the different phenomena involved	e.g.: mitigation of RN transport due to dilution effects in the geosphere	
Modelling aspects	e.g.: limitations of the transport modelling due to a bad representation of the fractured rock in the geosphere	
Computational power	e.g.: lack of computational power to perform full-scale reactive transport modelling in the geosphere	
Data acquisition and quality	e.g. measurements and interpretation of rock matrix porewater	
Up-scaling of data	e.g. how to use sorption K_d values measured in lab experiments in the PA	
What do you think that are the 2 or 3 most challenging issues to be dealt with in future PAs that would help at improving the supporting calculations incorporated in PA exercises?		

RADIONUCLIDE MIGRATION IN CRYSTALLINE MEDIA: FROM EFFECTIVE K_d DISTRIBUTIONS TO REACTIVE TRANSPORT MODELLING

Paolo Trincherio*, Jorge Molinero, Luis Manuel de Vries

Amphos 21 Consulting S.L. (Spain)

* Corresponding author: paolo.trincherio@amphos21.com

Abstract

Radionuclide transport models are key numerical tools for safety assessment studies of repositories of nuclear waste. These models usually rely on lumped parameters (i.e. solid/liquid distribution coefficients) that provide aggregated information on sorption and other processes retarding radionuclide migration. An important limitation of the aforementioned modelling approaches is that the K_d values they rely on may change dramatically in space and time as a consequence of both the heterogeneity of the medium and the changing geochemical conditions of the site. In this paper, these two issues are addressed separately. In the first part of the manuscript, we apply an ad-hoc numerical tool, denoted as MPhreeqc (de Vries et al., 2012), to stochastically evaluate the effect of the heterogeneous composition of the fracture filling mineral on the resulting radionuclide K_d values. In the second part of the document, we use a novel methodology (FASTREACT) to solve a large scale benchmark exercise. Due to its numerical efficiency, FASTREACT allows radionuclide transport and major geochemistry to be represented in a single coupled framework that explicitly describes their mutual interdependence. The results of this case study demonstrate the potentiality of the proposed approach, which could be used as supporting tool of existing K_d -based simulators in order to improve the scientific soundness of their retention

models. Overall, the results presented here along with those obtained by the other participants in the benchmark exercise (Crawford, 2013; Olin et al., 2013) highlight that when modelling radionuclide transport, uncertainties and nonlinearities should be explicitly recognized and properly accounted for within a rigorous and efficient stochastic framework.

Introduction

Radionuclide fate and migration is a key scientific field in a safety assessment study for a repository for spent nuclear fuel. In these applications, solid/liquid distribution coefficients (K_d) are commonly used to describe the retention of contaminants, i.e., sorption and other processes that retard radionuclide transport (SKB, 2010 and references therein and references therein).

This approach, which is denoted as K_d -based transport modelling, is mathematically robust but it relies on an important assumption: the K_d value of each radionuclide is constant in time. This assumption could be critical when geochemical conditions are changing dramatically (e.g. in the transition from temperate to glacial conditions) or when the mineralogy of the geological medium is highly heterogeneous.

Moreover, the constant K_d approach (linear sorption) has a tendency to overestimate sorption at elevated solute concentrations, and is strictly valid only under the experimental conditions under which the K_d value was determined (Crawford, 2010).

A particular problem associated with the constant K_d approach is that it is unable to capture some kinds of geochemical non-linearities, for example those arising from competition for sorption sites (Skopp, 2009).

In this work, we apply different ad-hoc numeric tools (i.e. MChreeqc and FASTREACT) to show how geological heterogeneity and geochemical non-linearities affect radionuclide transport. The ultimate goal of these numerical exercises is to provide a robust methodological framework that, if applied in support of existing K_d -based simulators, may increase the scientific soundness of the retention models they rely on, thus reducing the uncertainty (and related conservatism) of safety assessment calculations.

Stochastic simulation of K_d values in heterogeneous systems

Methodological approach

When radionuclides escape from deep engineered barriers, these are transported with flowing water and interact with the surrounding rock resulting in retardation. In performance assessment calculations, these retention parameters are typically represented using a lumped value, the distribution coefficient (K_d) that relates the amount of radionuclide mass retained in the solid phase to its aqueous concentration (SKB, 2010 and references therein). As all lumped parameters, the distribution coefficient depends on a large number of processes and variables (e.g. the redox conditions, the amount of available sorption sites, the scale of the problem, etc.) and hence, the estimation of effective K_d values (i.e. “upscaled” K_d values representative of the “average” retention processes occurring at the PA scale) is subject to large uncertainty. Moreover, the constant K_d approach (linear sorption) has a tendency to overestimate sorption at elevated solute concentrations, and is strictly valid only under the experimental conditions under which the K_d value was determined. A particular problem associated with the constant K_d approach is that it is unable to represent the intrinsic heterogeneity of natural systems.

Thus, here we apply an ad-hoc methodological framework for the evaluation of probability functions of effective K_d s based on Monte Carlo simulations. This framework aims at integrating the information obtained at different scales (e.g. mineralogical information coming from field investigation campaigns, results of laboratory experiments carried out under controlled conditions, ...) in order to provide users with quantitative information about the epistemic uncertainty related to specific distribution coefficients and thus overcoming the conceptual limitations of “constant K_d approaches”.

Conceptual model

Within the Forsmark site investigation campaign, quantitative mapping of different fracture minerals was performed. This was done by studying fracture surfaces of drill core sections from many different boreholes at the Forsmark site (Eklund and Mattsson 2009). The drill core mapping was focused on the rock in the vicinity of flow anomalies detected by the Posiva Flow Log (PFL). The quantitative mapping was performed only on open fractures. The fracture minerals that were mapped are calcite, chlorite, clay minerals (as a group), hematite, and pyrite. In a subsequent study (Löfgren and Sidborn, 2010), data from the quantitative mineral mapping campaign were refined, sorted into different data subsets, and analysed by parametric and non-

parametric statistical methods. Here, we have used these parametric models (i.e. parametric probability density functions of the thickness of each mineral) as a proxy for the heterogeneous composition of a synthetic crystalline medium.

It is worth mentioning that in the study of Löfgren and Sidborn, 2010, the resulting PDFs referred to the amount of fractures where the given mineral was actually found whereas, for the sake of simplicity, in this exercise we assume a heterogeneous but continuous distribution of mineral. The simulations could be readily extended to account for a second statistical population of fractures where the considered mineral is absent.

The present work has focused on studying the retention processes of caesium. For this radionuclide, clay minerals are strong sinks and therefore, in the Monte Carlo simulations, the sorption of caesium onto clay minerals is the only retention process considered.

Bradbury and Baeyens (2000) proposed a model of cation exchange for illite, which is here considered as representative for all the clay minerals, considering three types of sites. The most abundant sites (~80% CEC) are the so-called “Planar sites”, which are considered of low affinity and can adsorb either divalent species or monovalent cations. The second and third type of sites, called “Type II” (~20% CEC) and “Frayed Edge Sites” (FES) (~0.25% CEC), are considered of high affinity and involve monovalent cations.

The total concentration of sites is kept constant during the reactive transport simulations since it is assumed that the clay minerals phase do not dissolve nor precipitate in the environmental conditions considered in the model. This concentration has been estimated based on the parametric probability density functions provided by Löfgren and Sidborn, (2010) (see Figure 1), assuming that only 30% of the total amount of clay minerals is reactive and considering an average porosity equal to $4 \cdot 10^{-3}$.

A cation exchange capacity (CEC) value of 225 meq/kg has been reported for illite (Baeyens and Bradbury, 2004). This along with the suggested log-normal distribution of clay mineral thickness (Löfgren and Sidborn, 2010) results in a distribution of Cation Exchange Sites (CES) that is log-normally distributed, with mean $\mu = 2.03 \text{ mol/L}$ and standard deviation $\sigma = 0.95 \text{ mol/L}$.

The thermodynamic database used for aqueous speciation is the SKB-TDB (Hummel et al. 2002) with substantial modifications as reported in Duro et al. (2006), Grivé et al. (2008) and Arcos and Piqué (2009).

The Monte Carlo analysis consists in a number of equiprobable batch simulations where a mildly reducing saline groundwater (see Table 1) with a random concentration of Caesium (i.e. uniform concentration, ranging from 10^{-10} to 10^{-4} mol/L) is equilibrated with the exchanger.

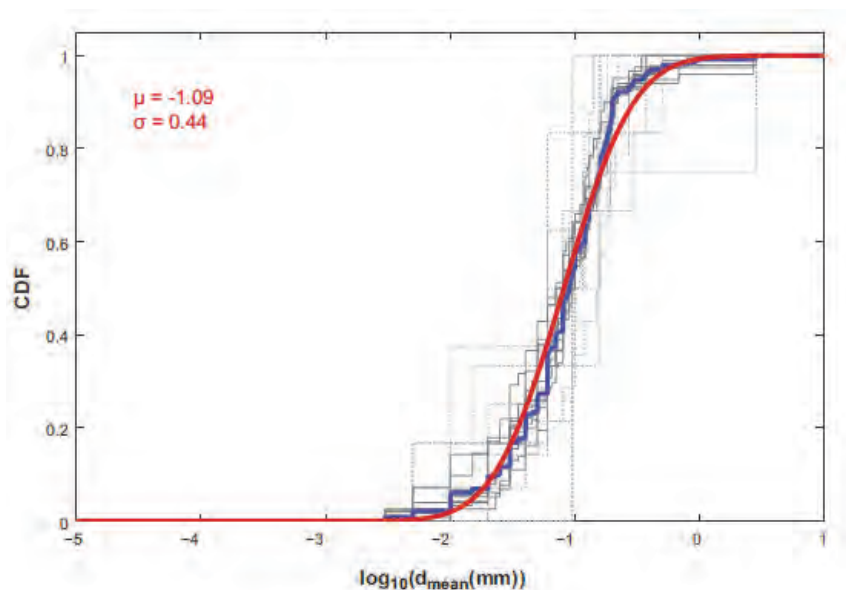


Figure 1: Cumulative distribution functions and suggested parameters (i.e. mean and standard deviation of the log-normal distribution) for the clay mineral thickness (figure taken from Lofgren and Sidborn, 2010)

Table 1: Geochemical composition of the groundwater used in the batch calculations (Concentrations in mol·L⁻¹).

Initial porewater	
pH	6.83
Eh (mV)	-2.63
[Cl] _{total}	1.01x10 ⁻¹
[S] _{total}	2.21x10 ⁻³
[Si] _{total}	5.63x10 ⁻⁴
[PO ₄ ³⁻] _{total}	6.46x10 ⁻⁸
[Na] _{total}	6.13x10 ⁻²
[K] _{total}	8.00x10 ⁻⁴
[Ca] _{total}	1.83x10 ⁻²
[Mg] _{total}	1.83x10 ⁻²
[Ba] _{total}	4.36x10 ⁻⁷
[C] _{total}	4.82x10 ⁻³
[Fe] _{total}	5.80x10 ⁻⁵
[NH ₄ ⁺] _{total}	7.28 x10 ⁻⁵

The tool

Geochemical processes can be modelled with many different types of software. These processes all have in common the uncertainty about the exact value of the used parameters. The classical approach is to do direct modelling combined with calibration to find the “correct” parameter values. A limited trial-and-error sensitivity analysis is often applied afterwards. In the framework of WP5 of the Crock project, we have developed a tool, called MCPHreeqc, to apply Monte Carlo simulations automatically to the PHREEQC geochemical models.

The software MPhreeqc provides a way to do Monte-Carlo simulations automatically. As input it uses a Phreeqc input file, a PDF for each of the uncertain parameters and the settings for the Monte Carlo simulation. It comes with a graphical user interface (see Figure 2) to enter the configuration of the simulations that need to be run. In addition it can automatically generate histograms and scatter plots from the results. Simulations can be run in parallel to benefit from all the processor cores in the machine. It is written in the programming language Python and is released under an open source license (LGPL).

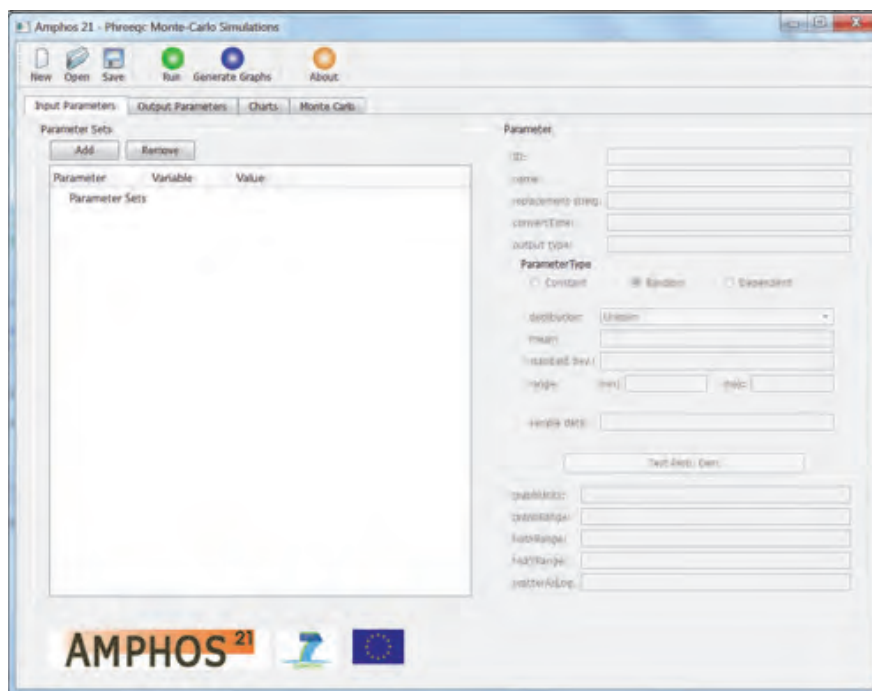


Figure 2: Screenshot of MPhreeqc graphical user interface.

Results

In this section Monte Carlo simulations are used to evaluate the uncertainty related to the caesium distribution coefficient. To this end, 50,000 equiprobable batch models are carried out using the software MPhreeqc, which is used to sample the two probability distributions described in the previous section (i.e. CES and aqueous concentration of caesium, Cs) and to run the Phreeqc batch simulations. The resulting bivariate histogram of the random input parameters is shown in Figure 3.

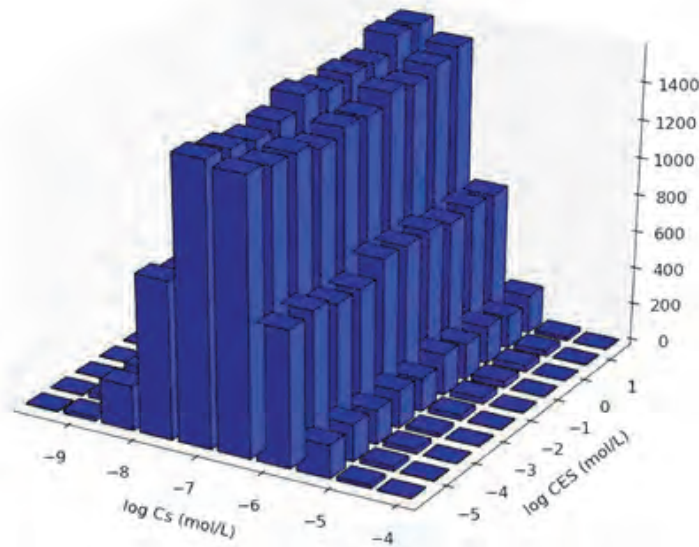


Figure 3: Bivariate histogram of the outcomes (i.e. logarithm of Caesium concentration and CES) of the Monte Carlo simulation (50000 realizations).

Figure 4 shows the distribution of K_d values as a function of Cs aqueous concentration and the CES. It is worth noting that the uncertainties related to the heterogeneous mineralogy of the medium along with nonlinearities arising from competition and depletion of sorption sites result in a large variation of the computed K_d values, which span more than seven orders of magnitudes.

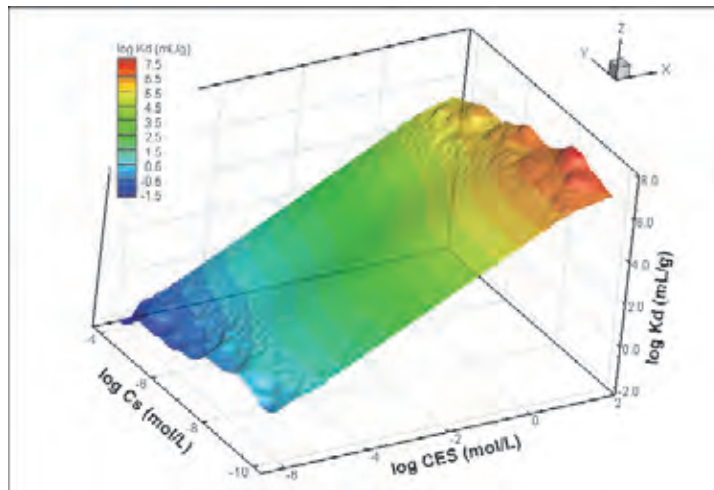


Figure 4: Results of the Monte Carlo simulation: caesium distribution coefficient (K_d) as a function of the aqueous concentration of caesium and the number of exchange sites (CES).

Using the results of the Monte Carlo simulations, three sorption isotherms are computed for three different values of the CES: the 2th, the 50th and the 98th percentile of the log-normal distribution (Figure 5, left). From the figure one can notice that at low concentrations, K_d values are constant (i.e. linear behaviour). Nonlinearities appear at concentrations around 10-8 mol/L as a consequence of the progressive depletion of sorption sites. Interestingly, the “most probable isotherm” (i.e. the one computes using the 50th percentile from the CES

distribution) agrees well with recent laboratory experiments focused on caesium sorption on biotite (Missana and García-Gutiérrez, 2010; see Figure 5, right)

As explained before, the results of the Monte Carlo simulation are treated in a probabilistic fashion in order to provide a parametric distribution function that may be used as input in subsequent radionuclide transport modelling. The resulting cumulative distribution function (CDF) of caesium K_d is shown in Figure 6. Again, one can notice that the distribution function spans several orders of magnitude, with mean and standard deviation of the logarithm equal to 3.0 and 1.1 mL/g respectively. These results further suggest that, when modelling radionuclide transport with constant K_d approximations, uncertainties and nonlinearities should be explicitly recognized and properly accounted for (e.g. by using companion mechanistic geochemical models and updating the K_d values according to the geochemical changes of the system).

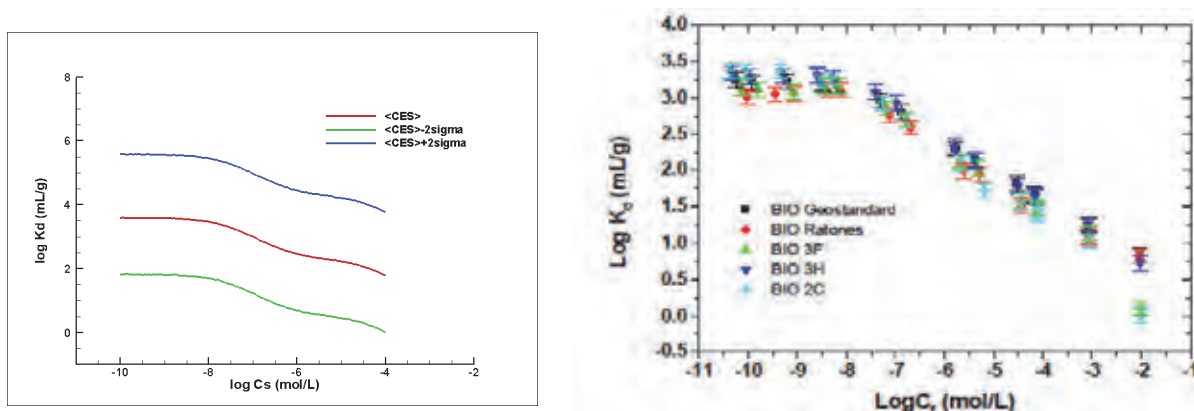


Figure 5: (left) sorption isotherms for caesium computed using different values of CES (i.e. the 2th, the 50th and the 98th percentile of the log-normal distribution) and (right) sorption isotherms obtained from experiments of caesium sorption on biotite (Missana and García-Gutiérrez, 2010).

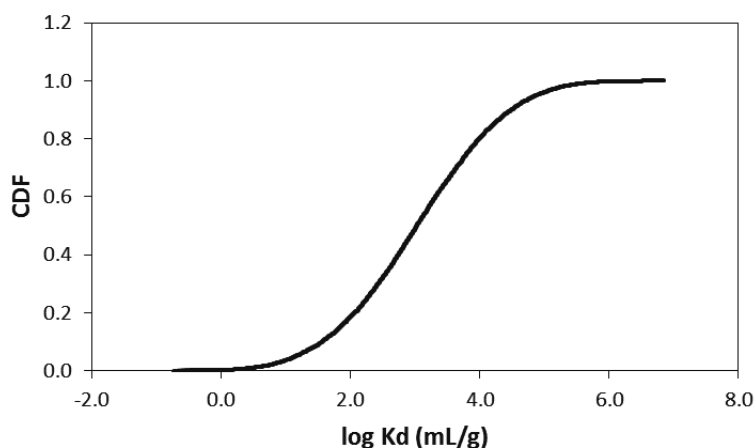


Figure 6: Cumulative distribution function (CDF) of caesium K_d obtained from the Monte Carlo simulation.

Mechanistic radionuclide transport simulations at the PA scale

Some of the efforts of WP5 of the Crock project were devoted to the simulation of a benchmark exercise whose aim was to demonstrate the entire “upscaling procedure”: from basic chemical and physical information from the lab scale to applications to PA studies.

In this section, we present some of the results of this benchmark exercise, giving special emphasis to the potential of the proposed methodology rather than the results themselves.

Conceptual model

The conceptual model assumes the release of the set of radionuclides from a number of deposition holes located in a deep geological repository.

First, a set of discharge streamlines (from the canister to the repository) has been delineated (Figure 7). The distribution of travel times for the 3960 streamlines is shown in Figure 7. The length of these recharge paths is very variable (it spans one order of magnitude, from about 200 m to more than 2000 m) as a result of the high heterogeneity of the underlying hydrogeological model (see Trincherio et al., 2013a for details on the particle tracking simulation used for the delineation of the flow paths).

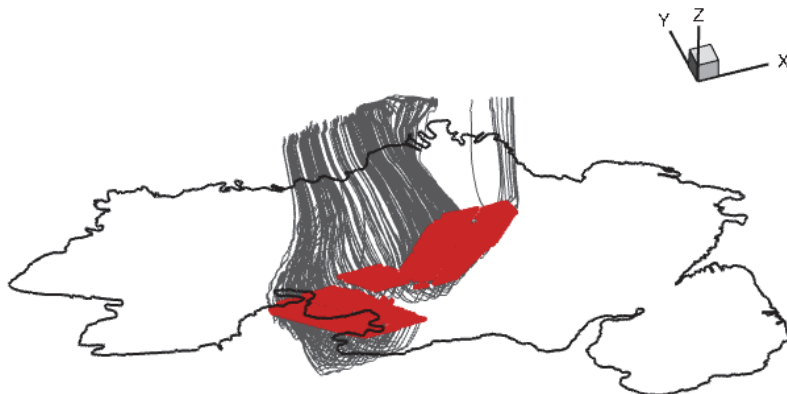


Figure 7: Set of 3960 particles that delineate streamlines from the repository to the surface.

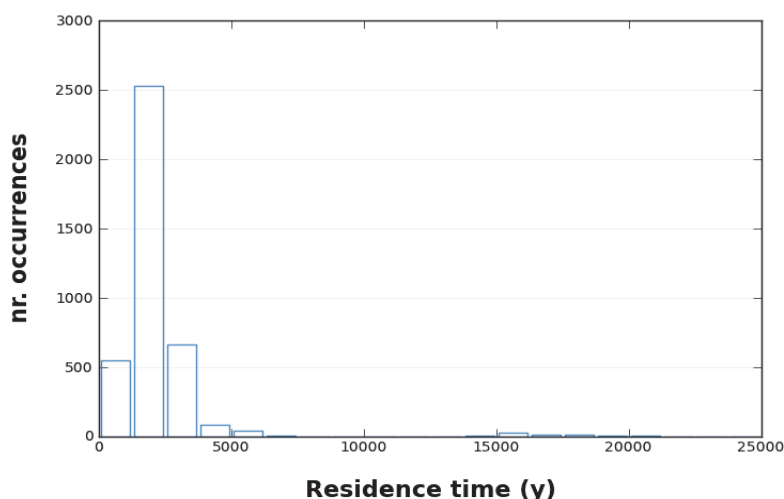


Figure 8: Histogram of travel times for the 3960 injected particles.

A representative groundwater composition has been chosen for both the initial and the boundary conditions of the model. This proposed groundwater is the same used for the Monte Carlo simulations (Table 1): a mildly reducing water representative of the average hydrochemical conditions that are found at repository depth in a typical Fennoscandian site.

A pulse-like release of caesium is assumed to occur at repository depth. Furthermore, to mimic the competition for sorption sites and the related nonlinearities, strontium and uranium are included in the model. The three radionuclides are injected with the following concentrations: $[Cs]=3.65 \cdot 10^{-9}$ mol/L, $[Sr]=6.95 \cdot 10^{-5}$ mol/L and $[U]=3.90 \cdot 10^{-9}$ mol/L.

It is assumed that the open fractures of this synthetic system are mainly populated by calcite, hematite and clay minerals. As for what concern clay minerals and the related CES, it has been used the average value of the statistical distribution presented before (i.e. $CES=4.4 \cdot 10^{-3}$ mol/L). It is worth stressing that in this conceptual model the sorption sites are assumed to be homogeneously distributed over the fracture surface. For this reason, in this section we will refer to K_a values rather than K_d values.

The average fracture aperture as well as the parameters related to matrix diffusion is summarized in Figure 9 and Table 2.

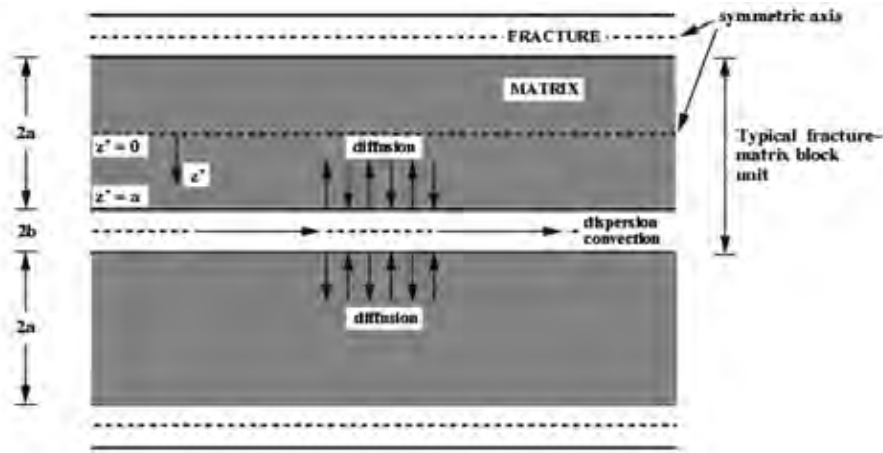


Figure 9: Parallel fracture model used to describe the fractured system (modified from Löfman et al., 2010).

Table 2: Parameters and values used for the DP model parameterization.

Symbol	Parameter	Value
a	Half matrix thickness	4.15 m
b	Half fracture aperture	$1.83 \cdot 10^{-4}$ m
D_0	Molecular diffusion coefficient in the water	$1.0 \cdot 10^{-9}$ m ² /s
ϕ_{im}	Matrix porosity	$1.0 \cdot 10^{-4}$ (-)

Methodological approach

As discussed in the previous section, radionuclide sorption processes are subject to large degrees of uncertainties. Furthermore, the underlying processes may be highly nonlinear and thus numerical modelling based on a constant Kd approach may result in bias. For this reason, the benchmark exercise has been solved using a mechanistic approach where all the geochemical processes (e.g. cation exchange, mineral dissolution/precipitation, etc.) are represented explicitly.

Yet, the large spatial and temporal scale of this exercise rendered the implementation of a fully coupled three-dimensional reactive transport model unfeasible. Thus, an alternative approach has been adopted where flow and reactions are coupled using a streamline-based methodology. This approach, known as FASTREACT (FrAmework for STochastic REActive Transport, Trincherio et al. 2013b), consists in coupling a set of 1D reactive transport simulations with one or multiple random-walk particle tracking realizations (Figure 10).

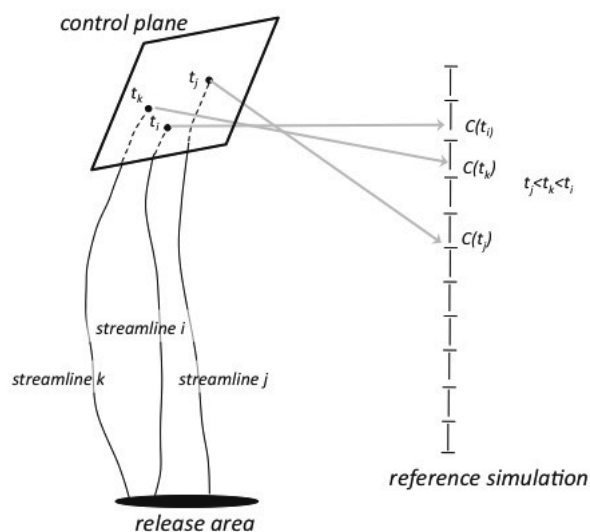


Figure 10: Illustrative sketch of the FASTREACT methodology.

Geochemical reactions

- **Strontium:** For the case of strontium, the two main processes considered as possible retention mechanisms are the co-precipitation of Sr with calcite, forming a solid solution, and the sorption of Sr onto clays. In the numerical modelling, the co-precipitation of strontium with calcite will take place as long as saturation is reached. Sr sorption onto clays is modelled using the thermodynamic constants reported for illite. In other words, illite has been selected as a proxy mineral phase to represent the behaviour of the clay minerals in the model.
- **Caesium:** Similarly to Strontium, clay minerals are strong sinks for caesium. Therefore, in the numerical model, the sorption of caesium onto illite is the only retention process considered. In this case too illite is selected as a mineral phase representing the behaviour of all clay minerals in the fractures.
- **Uranium:** In the reactive transport simulations, a set of minerals has been selected as possible solubility-limiting phases of aqueous uranium. For U(VI), a hydrated amorphous phase ($\text{UO}_2 \cdot 2\text{H}_2\text{O}$) has been used instead of a crystalline phase (e.g. uraninite). Also, schoepite and uranophane are allowed to precipitate if the solution becomes oversaturated with any of these phases.

The geochemical database and the model of cation exchange are the same used for the Monte Carlo simulations, whereas the number of available sites (CES) has been set equal to the median of the related probability distribution (i.e. the medium is assumed to be chemically homogeneous with a constant amount of fracture filling minerals). Table 3 shows the detail of the cation exchange reactions and related Gaines-Thomas selectivity coefficients.

Table 3: Cation exchange reactions and their corresponding Gaines-Thomas selectivity coefficients for illite.

Reaction	Log K (25°C)	Reference
Planar sites		
$X^- + Na^+ \leftrightarrow NaX$	0.0	(1)
$X^- + K^+ \leftrightarrow KX$	1.1	(1)
$X^- + Cs^+ \leftrightarrow CsX$	1.6	(1)
$2X^- + Sr^{2+} \leftrightarrow SrX_2$	1.13	(2)
$2X^- + Ca^{2+} \leftrightarrow CaX_2$	1.13	(2)
$2X^- + Ba^{2+} \leftrightarrow BaX_2$	1.13	(2)
$2X^- + Mg^{2+} \leftrightarrow MgX_2$	1.13 ^(a)	
$2X^- + Ra^{2+} \leftrightarrow RaX_2$	1.13 ^(a)	
$2X^- + UO_2^{2+} \leftrightarrow UO_2X_2$	0.65	(3)
Type II sites		
$X^{II-} + Na^+ \leftrightarrow NaX^{II}$	0.0	(1)
$X^{II-} + K^+ \leftrightarrow KX^{II}$	2.1	(1)
$X^{II-} + Cs^+ \leftrightarrow CsX^{II}$	3.6	(1)
FES		
$X^{FES-} + Na^+ \leftrightarrow NaX^{FES}$	0.0	(1)
$X^{FES-} + K^+ \leftrightarrow KX^{FES}$	2.4	(1)
$X^{FES-} + Cs^+ \leftrightarrow CsX^{FES}$	7	(1)
$X^{FES-} + NH_4^+ \leftrightarrow NH_4X^{FES}$	3.5	(1)
(1) /Bradbury and Baeyens 2000/. (2) /Brouwer et al. 1983/. (3) /Bradbury and Baeyens 2009/.		
(a) Value assumed, considering an equal sorption behaviour for all the alkaline earth elements.		

The calculations have been carried out using both a single and a dual porosity approach. In the former (denoted as Model A), transport and reactions occurs only in the fractures while in the latter (denoted as Model B) mass exchange occurs between the mobile domain (the fractures) and the matrix. The dual porosity approach has been implemented using a first-order exchange approximation (van Genuchten 1985) and the matrix has been considered as non-reactive.

Figure 11 shows the breakthrough curves, normalized by the total injected mass, of a conservative tracer for the two considered models. It is worthwhile noting that in model A the breakthrough curve reflects the distribution of the ensemble of trajectories (Figure 8), with a sharp arrival peak followed by a fast decrease of concentration. In model B, the effect of the matrix is evident as the breakthrough curve shows a lower peak value and a long tail.

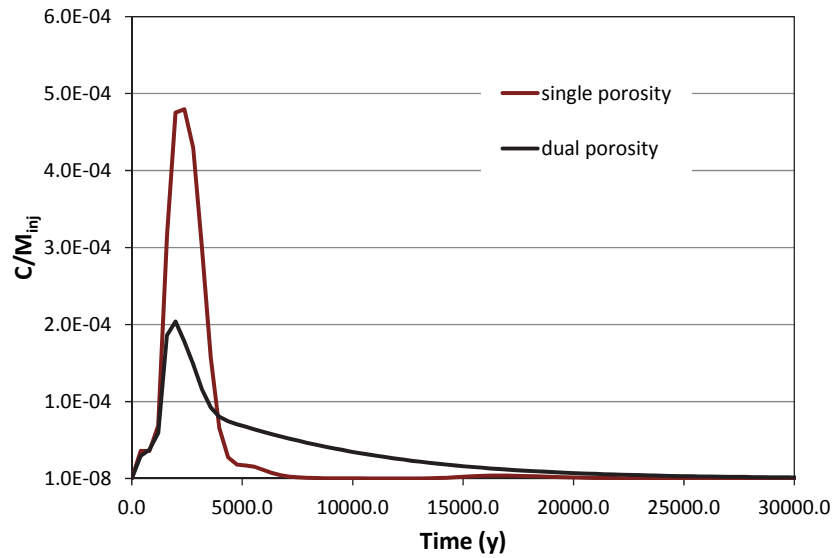


Figure 11: Breakthrough curve of the conservative tracer for the single porosity model (red line) and the dual porosity model (black line). The curves are normalized by the injected mass.

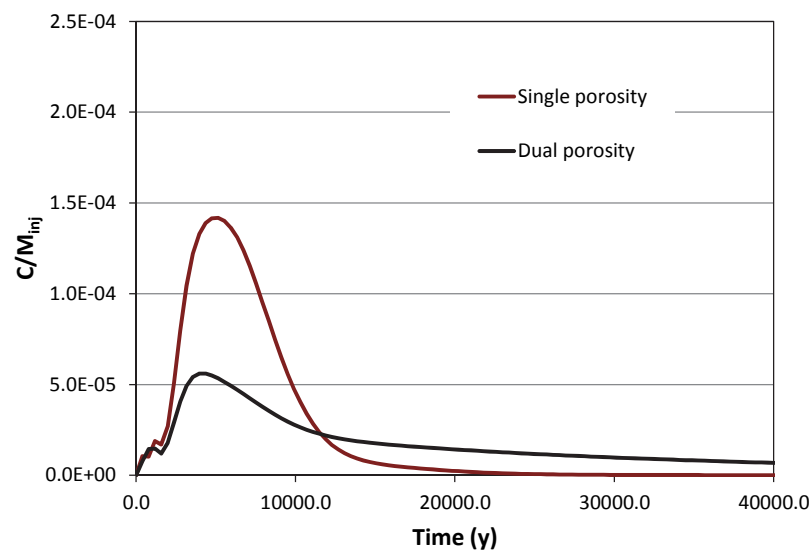


Figure 12: Breakthrough curve of uranium for the single porosity model (red line) and the dual porosity model (black line). The curves are normalized by the injection concentration.

Figure 12 and Figure 13 show the breakthrough curves of uranium and strontium respectively. Their qualitative shapes are similar to those of the conservative simulations although the different retention processes implemented in the model result in an average retardation factor, which is here calculated as the ratio between the time of arrival of the radionuclide to the time of arrival of the conservative solute, of 2.4 and 2.0 respectively.

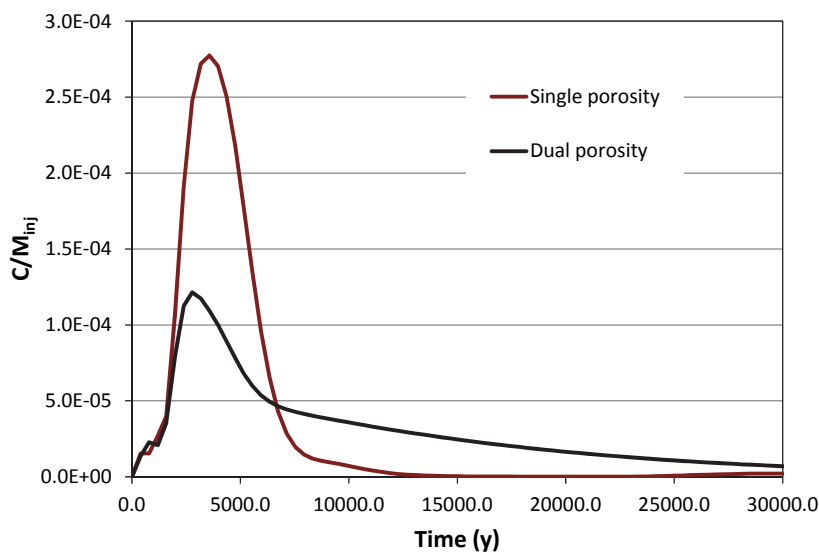


Figure 13: Breakthrough curve of Strontium for the single porosity model (red line) and the dual porosity model (black line). The curves are normalized by the injection concentration.

Figure 14 shows the breakthrough curve of caesium. It is evident that the isotope is strongly sorbed onto the available clay minerals (in particular, illite) and the rise of concentration is extremely slow during the considered time frame. The resulting retardation factor is 316, meaning that caesium is hundred times more retarded than the other two radionuclides.

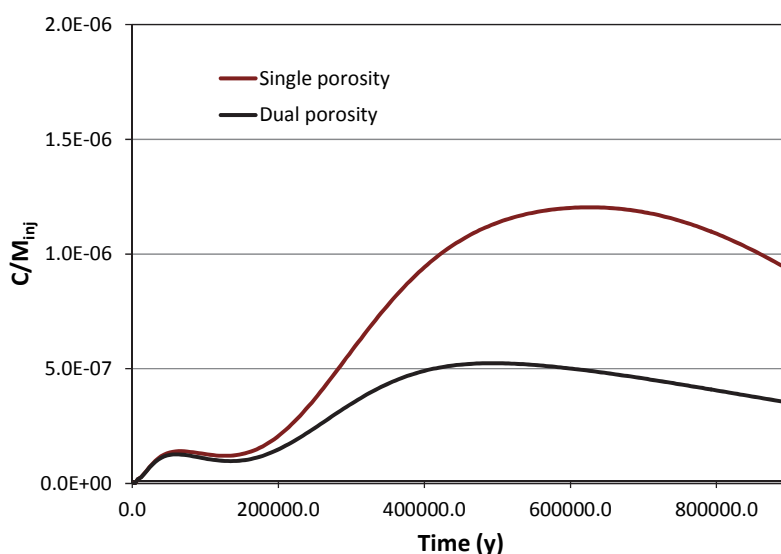


Figure 14: Breakthrough curve of caesium for the single porosity model. The curve is normalized by the injection concentration.

As explained in the introduction, the FASTREACT methodology could be seen as a robust supporting tool for existing K_d -based simulators. In fact, recently, an interface denoted as iFM (interface FASTREACT-MARFA; Amphos 21, 2013) has been developed to periodically update the K_d values used by MARFA (Painter and Mancillas, 2009) based on mechanistic radionuclide transport simulations. Here, we illustratively show how the results of the numerical exercise (Figures 11 to 14) can be used to evaluate K_a values. These values, which in

the case of changing geochemical conditions will vary in space and time, can be then used in subsequent K_d -based transport simulations.

As shown by Wels et al. (1996), the K_a value for a given radionuclide can be computed as:

$$K_a = (R_a - 1) / a_w$$

where R_a is the surface retardation factor and a_w is the specific surface area defined as $a_w = 1/b$. The related K_a values are summarized in Table 3.

Table 3: FASTREACT -Computed K_a values for the three selected radionuclides.

Radionuclide	K_a (m^3/m^2)
<i>Uranium</i>	1.83×10^{-4}
<i>Strontium</i>	7.21×10^{-5}
<i>Caesium</i>	5.67×10^{-2}

Discussion and conclusions

In this work, we have applied different ad-hoc numeric tools (i.e. MCPhreeqc and FASTREACT) to show how geological heterogeneity and geochemical non-linearities affect radionuclide transport. The ultimate goal of these numerical exercises was to provide a robust methodological framework that, if applied in support of existing K_d -based simulators, may increase the scientific soundness of the retention models they rely on, thus reducing the uncertainty (and related conservatism) of safety assessment calculations.

First, we have used the numerical tool MCPhreeqc to study the effect of geological heterogeneity on the resulting radionuclide K_d values. To this end, 50000 Monte Carlo simulations have been carried out assuming a variable distribution of fracture filling clay minerals (the related PDF has been borrowed from Löfgren and Sidborn, 2010) and a uniformly variable amount of radionuclides. The results show that:

- the uncertainties related to the heterogeneous mineralogy of the medium along with nonlinearities arising from competition and depletion of sorption sites result in a large variation of the computed K_d values, which span more than seven orders of magnitudes.
- the linear isotherm computed using the average amount of cation exchange sites agrees well with recent laboratory experiments (Missana and Garcia-Gutierrez, 2012) focused on caesium sorption on biotite (Figure 8).
- the resulting cumulative distribution function (CDF) of caesium K_d , which spans several orders of magnitude (Figure 9), with mean and standard deviation of the logarithm equal to 3.0 and 1.1 mL/g respectively, could be used in support of subsequent numerical studies

Second, we have applied the FASTREACT methodology to simulate radionuclide transport over a large scale problem. The same problem has been solved using alternative approaches by the other participants in WP5 of the Crock project (Crawford, 2013; Olin et al., 2013). Yet, in this paper we have focused more on the potential of the proposed methodology rather than on the results themselves. More specifically, the conclusions of the numerical exercise are as follows:

- Due to its numerical efficiency, FASTREACT allows radionuclide transport and major geochemistry to be represented in a single coupled framework that explicitly describes their mutual interdependency
- The results of the simulation can be used to compute K_d/K_a values that, given the previous bullet point, fully account for the variable geochemical conditions of the site.
- The resulting K_a/K_d values, which in the case of dramatic changes in the boundary conditions will vary in space and time, can be used to feedback existing K_d -based simulators, thus increasing the soundness of the retention models they rely on.

The overall conclusions of the study are that, when modelling radionuclide transport, uncertainties and nonlinearities should be explicitly recognized and properly accounted for within a rigorous and efficient stochastic framework.

Acknowledgement

The research leading to these results has received funding from the European Union's European Atomic Energy Community's (Euratom) Seventh Framework Programme FP7/2007-2011 under grant agreement n° 269658 (CROCK project).

References

- Amphos 21 (2013). Interface MARFA-FASTREACT v1.0 – user's guide.
- Arcos, D. and Piqué, À., (2009). Update of the thermodynamic database used in SKB TR-06-32 and SKB TR-06-17. Amphos 21 technical note to SKB.
- Baeyens, B. and Bradbury, M.H., (2004). Cation exchange capacity measurements on illite using the sodium and caesium isotope dilution technique: effects of the index cation, electrolyte concentration and competition: modelling. *Clays and Clay Minerals*, 52, 421–431.
- Bradbury, M.H., and Baeyens, B., (2000). A generalised sorption model for the concentration dependent uptake of caesium by argillaceous rocks. *Journal of Contaminant Hydrology*, 42, 141–163.
- Bradbury, M.H. and Baeyens, B. (2009). Sorption modelling on illite Part I: Titration measurements and the sorption of Ni, Co, Eu and Sn. *Geochimica et Cosmochimica Acta*, 73, 990–1003.
- Brouwer, E., Baeyens, B, Maes, A. and Cremers, A., (1983). Caesium and rubidium ion equilibria in illite clay. *J. Phys. Chem.*, 87, 1213-1219.

Crawford, J., (2010). Bedrock Kd data and uncertainty assessment for application in SR-Site geosphere transport Calculations SKB R-10-48.

Crawford, J., (2013). A simplified approach for reactive transport modelling involving strongly non-linear sorption and solute remobilization, S&T contribution of the CROCK project (to be published).

de Vries, L. M., Trincherro, P. and Molinero, J. (2012). MCPHreeqc: Extending geochemical modelling with automatic stochastic simulations. In EGU General Assembly Conference Abstracts (Vol. 14, p. 6355).

Duro, L., Grivé, M., Cera, E., Domènech, C. and Bruno, J., (2006). Update of a thermodynamic database for radionuclides to assist solubility limits calculation for performance assessment. SKB TR-06-17, Swedish Nuclear Fuel & Waste Management Company, Stockholm, Sweden.

Eklund, S. and Mattsson, K. J., (2009). Forsmark site investigation. Quantitative mapping of fracture minerals in Forsmark. SKB P-08-47, Svensk Kärnbränslehantering AB.

Grivé, M., Domènech, C., Montoya, V. and Duro, L., (2008). Update of the Thermodynamic Database of sulphur aqueous species and solids phases. Project S-TDB. Amphos 21 report.

Hummel, W., Berner, U., Curti, E., Pearson, F. J. and Thoenen, T. (2002). Nagra/PSI chemical thermodynamic data base 01/01. *Radiochimica Acta*, 90(9-11/2002), 805-813.

Löfgren, M. and Sidborn, M. (2010). Statistical analysis of results from the quantitative mapping of fracture minerals in Forsmark. Site descriptive modelling - complementary studies SKB R-09-30.

Missana, T. and Garcia-Gutierrez, M. (2012). Comparison of the caesium adsorption on different crystalline rocks. Proceedings of the 1st CP CROCK Workshop, Stockholm, Sweden.

Olin, M., Poteri, A., Pulkkanen, VM and Koskinen, L. (2013). Evaluation of sorption uncertainties in PA studies, S&T contribution of the CROCK project (to be published).

Painter S. and Mancillas, J. (2009). MARFA version 3.2.3 user's manual: migration analysis of radionuclides in the far field. SKB Report R-9-56. Svensk Kärnbränslehantering AB.

SKB (2010). Radionuclide transport report for the safety assessment SR-Site, SKB TR-10-50.

Skopp J, (2009). Derivation of the Freundlich adsorption isotherm from kinetics. *Journal of Chemical Education*, 86, 1341.

Sohlenius, G., Saetre, P., Norden, S., Grolander, S., and Sheppard, S. (2013). Inferences about radionuclide mobility in soils based on the solid/liquid partition coefficients and soil properties. *AMBIO*. doi:10.1007/s13280-013-0408-4.

Trincherro, P., Molinero, J., and Crawford, J. (2013a). Results of the benchmark exercise, deliverable 5.2 of the CROCK project.

Trincherro, P., Molinero, J. and Román-Ross, G. (2013b). A streamline approach for the solution of multicomponent reactive transport problems, SKB R-10-45.

van Genuchten, M. T. and Nielsen, D. R. (1985). On describing and predicting the hydraulic properties of unsaturated soils. *Ann. Geophys.*, 3, 615–628.

Wels, C., Smith, L. and Vandergraaf, T. T. (1996). Influence of specific surface area on transport of sorbing solutes in fractures: An experimental analysis. *Water Resources Research*, 32(7), 1943-1954.

AB INITIO STUDIES ON CATION EXCHANGE AND SURFACE COMPLEXATION REACTIONS ON BIOTITE SURFACE

Eini Puhakka*, Markus Olin

VTT Technical Research Centre of Finland (FI)

* Corresponding author: eini.puhakka@vtt.fi

Abstract

Molecular modelling was utilized to investigate surface properties of biotite. The present work was focused on formation of water molecular layer onto biotite surfaces and sorption of nickel onto basal and terminal surfaces of biotite. Based on the calculated results, surface reactions differ on the basal and terminal surfaces on biotite and its end-member (annite). Cation exchange reactions between K^+ and Ni^{2+} ions take place on the basal surface, but on the terminal surface, Ni^{2+} ion forms a stable surface complex.

Introduction

Molecular modelling approach was utilized to investigate surface properties of biotite common in granodiorite and mica gneiss. The motivation for the research was the construction of a repository for Finnish spent nuclear fuel in crystalline rock at a depth of about 500 meters. In this study, molecular modelling was used in order to deepen understanding of sorption phenomena studied typically by mechanistic sorption modelling: ion exchange and surface complexation modelling (SCM). Typically molecular modelling has been used to estimate chemical reactions between atoms or molecules, properties of solid materials, and adsorption behaviour of molecules on solid surfaces. Nowadays, with increased calculation power rather complex cluster or periodic model systems can be calculated, which enables e.g. clay-cation (Ren et al. (2012), Tribe et al. (2012)) and even clay-cation-water (Chatterjee et al. (1999)) interaction studies. In sorption studies, molecular modelling has been utilized typically in connection with surface characterization like X-ray photoelectron spectroscopy by Ebina et al. (1999) and extended X-ray absorption fine structure by Hattori et al. (2009). Also, relation between atomistic phenomena and SCM has been formulated by Wesolowski et al. (2009).

When molecular modelling is used, differences between basal and terminal surface sites can be detected. Quantum chemistry gives atomic level information about reactivity on surfaces, molecular dynamics describes e.g. water diffusion into interlayer spaces of minerals, and possible phase separation around minerals can be investigated using mesoscale modelling (Leach (2002)). All of this information can be used to restrict SCM only for essential reactions. SCM can be applied in extrapolation of K_d (distribution coefficient) values used in performance analysis (PA) calculations, and sorption models can also be applied in reactive transport modelling (RTM). Both the PA and RTM are utilized in evaluation of uncertainties of the release and transport of radionuclides and applied conceptual thinking (Figure 1).

In this paper, molecular modelling results are introduced, and our focus has been on formation of water molecular layer onto biotite surfaces and sorption of nickel onto basal and terminal surfaces. ^{63}Ni is beta emitting radionuclide, and its mobility in soil depends on water content and salinity of soil (Skwarzec et al

(2006), Nouri et al. (2001)). Based on the research of Olin et al. (2008), biotite, $K(Mg,Fe)_3AlSi_3O_{10}(OH,F)_2$, has potential role as a sink for radioactive elements like ^{63}Ni . Further, biotite, , is present as a fracture-fill mineral in the far-field of a planned Finnish repository for spent nuclear fuel. Therefore, it is important to identify the mechanisms for cation exchange and surface complexation reactions in order to gain a deeper insight into the chemical properties of mineral surfaces.

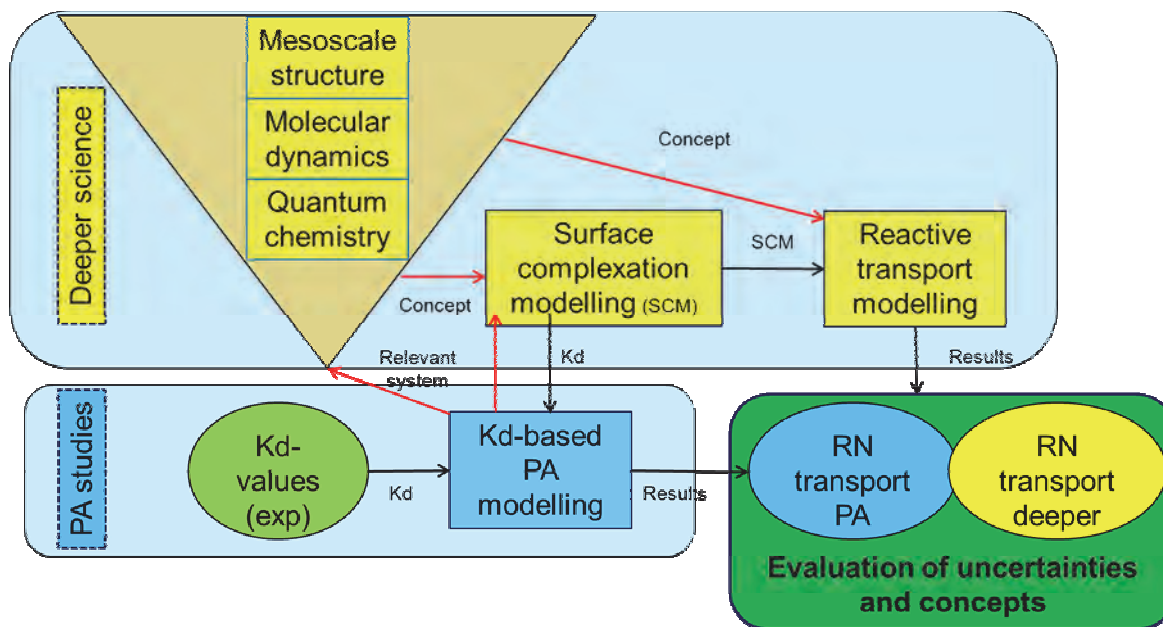


Figure 1: Overall concept of modelling work.

Methods

Density functional calculations were performed with the CASTEP (CAmbridge Serial Total Energy Package by Clark et al. (2005) code implemented into Materials Studio versions 6.0 (Accelrys (2011)). The exchange-correlation was described with generalized gradient approximation GGA-PBE, and the ultrasoft pseudopotentials were used for each element. In the potential of iron, the semicore states were treated as a part of the core. The kinetic cut-off energy for a plane wave expansion of the wave function was 310 eV.

Results

Biotite has a sheet-like structure, where the sheets are connected to each other by potassium cation layer (Accelrys (2011)). According to the density functional calculations, the optimized lattice parameters of the energetically stable biotite structure are $a = 528.4$ pm, $b = 916.2$ pm, $c = 2\,077.3$ pm and $c/a = 3.931$ (Figure 2a). Construction of surface models to molecular modelling studies revealed that the smallest meaningful models are very atomic-rich, which causes long calculation times. In order to simplify model structures, it can be used end-members of biotite: annite and phlogopite. In this study, annite (Accelrys (2011)), where all magnesium ions are substituted by iron ions, was utilized. The unit cell of annite is about half of that of biotite. The optimized lattice parameters are $a = 513.1$ pm, $b = 893.3$ pm, $c = 1\,037.3$ pm, and $c/a = 2.022$ (Figure. 2b), and the Si:Al ratio is 3:1.

The aim of molecular modelling was to deepen understanding of the chemical properties of biotite and corresponding minerals. Therefore, the molecular modelling was used to investigate formation of water molecular layer onto annite surfaces, and reaction of Ni^{2+} species on cation exchange and surface complexation sites. It was supposed that the cation exchange sites are basal surfaces like the (001) surface, and surface complexation sites are terminal surfaces like the (110) surface.

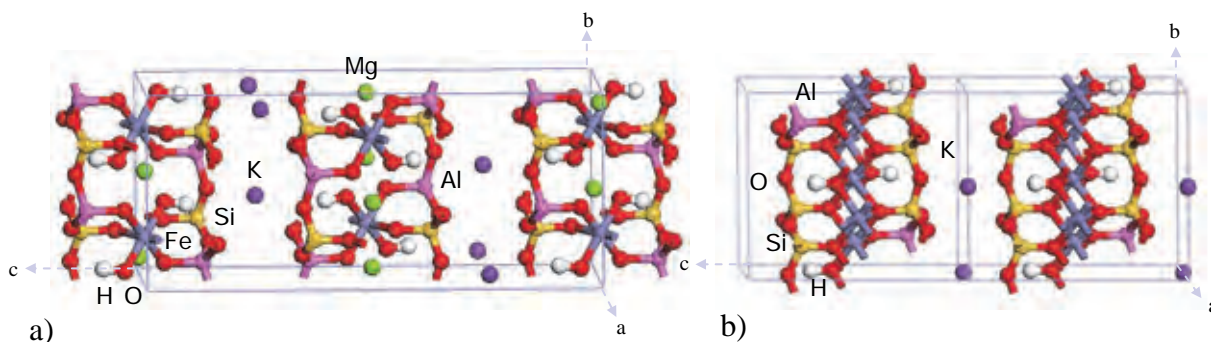


Figure 2: Optimized unit cells for a) biotite, and b) annite.

First, formation of water molecular layer was considered including both the adsorption and possible dissociation of water on the basal (001) and terminal (110) surfaces. On the basal surface, the reactivity of the surface depends on the existence of potassium ions on the surface. Otherwise, the surface structure is rather stable. On the terminal surface, there are no empty vacancies in the coordination sphere of aluminium and/or silicon atoms. However, this oxide surface can be very reactive with water forming hydroxylated surface structure. In the water adsorption studies, water molecules were adsorbed onto the surface one by one, and water molecules were allowed to find their energetically favourable positions on the surface. Also, dissociation of water molecules was allowed on the surfaces. As a result, the formation of the first water molecular layer was described.

On the ideal basal (001) surface, there are no hydroxyl groups originated from the crystal structure of annite, and there are 4.4 K^+ ions/ nm^2 and 11 bridged O atoms/ nm^2 . On this surface, water forms a molecular layer, and no water dissociation happens. The water molecular layer consists of $11 \text{ H}_2\text{O}$ molecules/ nm^2 (Figure 3a).

On the ideal terminal (110) surface, there are 1.9 K^+ ions/ nm^2 and 6.6 H^+ sites/ nm^2 . Based on the calculations, every sixth water molecule dissociates forming surface hydroxyl groups in the adsorption of water onto the surface. On the first water molecular layer, there are $10 \text{ H}_2\text{O}$ molecules/ nm^2 (Figure 3b).

After the structure of water molecular layer was defined, then reaction of $\text{Ni}(\text{H}_2\text{O})_2^{2+}$ species on cation exchange and surface complexation sites was considered. The aim was to define, if a difference between the sites can be detected. It was calculated step-by-step mechanism for the reaction path which consists of a) sorption of $\text{Ni}(\text{H}_2\text{O})_2^{2+}$ above the first water molecule layer, b) desorption of water molecules from the surface, so that $\text{Ni}(\text{H}_2\text{O})_2^{2+}$ can adsorb onto the surface, and c) re-formation of the water molecule layer.

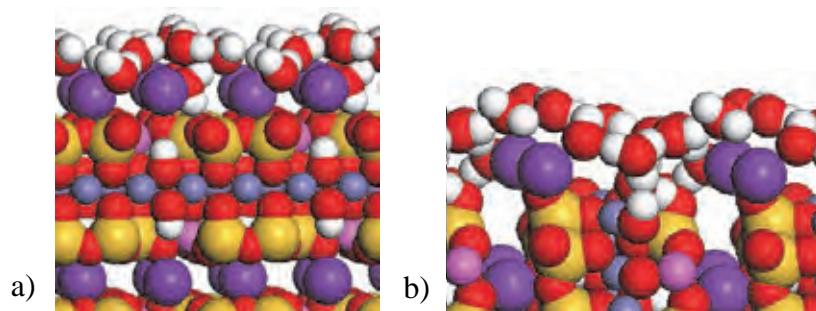
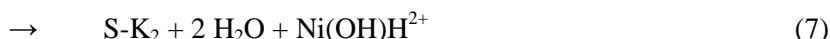
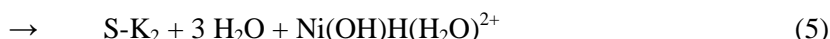
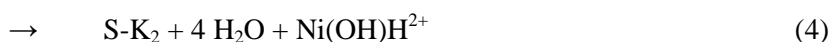
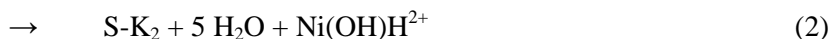
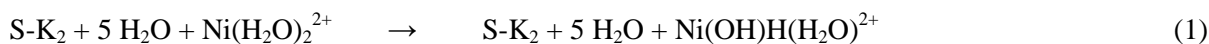


Figure 3: The first water molecular layer on the annite surfaces: a) (001) and b) (110).

On the basal (001) surface, the reaction proceeds according to Scheme 1, where S represents $\text{K}_2\text{Fe}_{12}\text{Si}_{12}\text{Al}_4\text{O}_{40}(\text{OH})_8$ surface structure:



First, $\text{Ni}(\text{H}_2\text{O})_2^{2+}$ species adsorbs onto the water covered surface (Figure 4a). After that about half of the water molecules desorb from the surface (Reactions 1-5), and $\text{Ni}(\text{H}_2\text{O})_2^{2+}$ species gets closer to the mineral surface. Re-arrangement of Ni^{2+} and K^+ ions starts during Reaction 6, and cation exchange reaction achieves the final state during Reaction 8 (Figure 4b). After that re-formation of the water molecular layer happens (Figure 4c). The cation exchange reaction (including also re-formation of the water layer) is spontaneous reaction, which releases energy -0.29 eV. Based on this, the cation exchange reaction between Ni^{2+} and K^+ ions takes place on the basal (001) surface of annite.

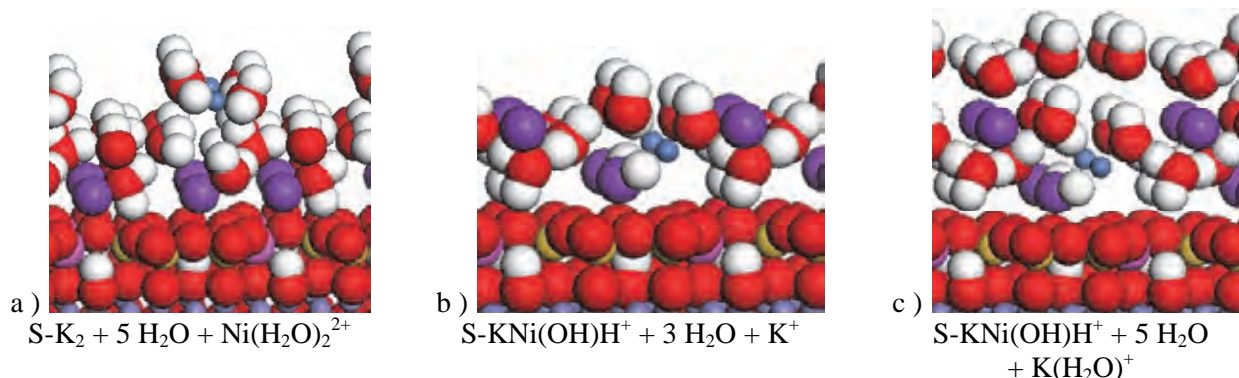


Figure 4: The annite (001) surface: a) $\text{Ni}(\text{H}_2\text{O})_2^{2+}$ above the first water molecule layer, b) Ni^{2+} ion has replaced K^+ ion (cation exchange), and c) the re-formed water molecule layer.

Possibility for the cation exchange reaction was also investigated on the terminal (110) surface. There the reaction proceeds according to Scheme 2, where S represents $\text{K}_6\text{Fe}_{12}\text{Si}_{12}\text{Al}_4\text{O}_{42}(\text{OH})_8$ surface structure:



On this surface, $\text{Ni}(\text{H}_2\text{O})_2^{2+}$ species forms a surface complex with the water molecule layer (Figure 5a). This complex does not dissociate and move to other position on the surface, though desorption of water molecules reduces steric hindrance on the surface (Figure 5b). Therefore, steric shielding around the K^+ ions reduces, and K^+ ions are susceptible for other reactions. Energy needed for this surface re-arrangement reaction is 1.57 eV.

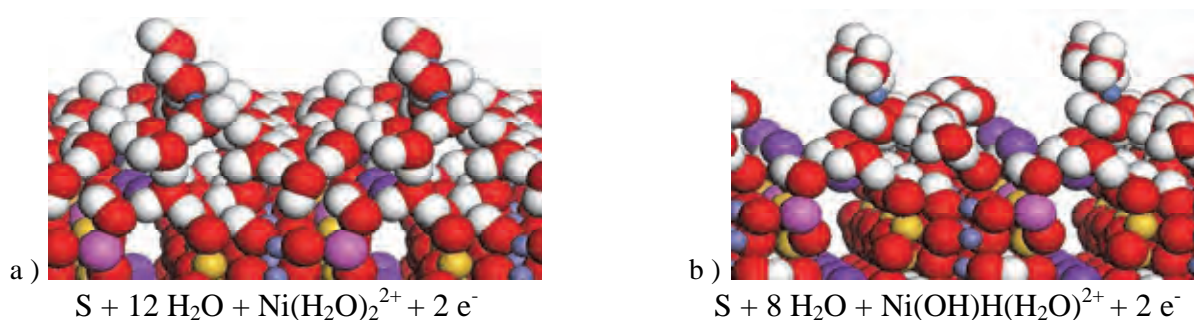


Figure 5: The annite (110) surface: a) $\text{Ni}(\text{H}_2\text{O})_2^{2+}$ above the first water molecule layer, and b) surface complexed $\text{Ni}(\text{H}_2\text{O})_2^{2+}$.

Based on the calculated results, surface reactions are different on the basal and terminal surfaces on biotite and its end-member (annite). Cation exchange reactions between K^+ and Ni^{2+} ions take place on the basal surfaces, and surface complexation reactions on the terminal surfaces. If the ratio between the basal and terminal surfaces can be determined, then reactions needed in the surface complexation modelling can be restricted only essential reactions.

Conclusions

Formation of water molecular layer onto biotite surfaces and sorption of nickel onto basal and terminal surfaces of biotite were investigated using molecular modelling techniques. The difference between surfaces was able to be identified: Surface complexation (proton) happens on the terminal surfaces, and cation exchange (permanent charge) on the basal surface. This information can be utilized in SCM in order to define the existence and nature of surface sites. Molecular modelling also gives valuable information about surface reactions and behaviour of water molecules near surface and near sorbing ions (hydration). The first class uncertainties in sorption studies is related to this basic question of surface sites and reactions, which are relatively easy to fit by macroscopic experimental data, but for which not much direct experimental nano-level data or modelling is available.

Acknowledgement

The research leading to these results has received funding from the European Union's European Atomic Energy Community's (Euratom) Seventh Framework Programme FP7/2007-2011 under grant agreement n° 269658 (CROCK project), Posiva Oy and VTT.

References

- Accelrys (2011). *MS Modeling*, Release 6.0. San Diego: Accelrys Software Inc.
- Chatterjee, A., Iwasaki, T., Ebina, T. and Miyamoto, A. (1999). A DFT study on clay-cation-water interaction in montmorillonite and beidellite. *Computational Materials Science*, 14, 119-124.
- Clark, S. J., Segall, M. D., Pickard, C. J., Hasnip, P. J., Probert, M. J., Refson, K. and Payne, M. C. (2005). First principles methods using CASTEP. *Zeitschrift fuer Kristallographie*, 220(5-6), 567-570.
- Ebina, T., Iwasaki, T., Onodera, Y., Chatterjee, A. (1999). A comparative study of DFT and XPS with reference to the adsorption of caesium ions in smectites. *Computational Materials Science*, 14, 254-260.
- Hattori, T., Saito, T., Ishida, K., Scheinost, A.C., Tsuneda, T., Nagasaki, S. and Tanaka, S. (2009). The structure of monomeric and dimeric uranyl adsorption complexes on gibbsite: A combined DFT and EXAFS study. *Geochimica et Cosmochimica Acta*, 73, 5975-5988.
- Leach, A. R. (2001). *Molecular Modelling, Principles and Applications*, 2nd ed., Pearson Education Limited, Essex.
- Nouri, J., Alloway, B. J. and Peterson, P. J. (2001). The chemical Extractability and Mobility of Ni^{63} in Soil and Sludge. *OnLine Journal of Biological Sciences*, 1(10), 976-985.

Olin, M., Puukko, E., Puhakka, E., Hakanen, M., Lindberg, A., Lehtikoinen, J. (2008). Final results of sorption on biotite. VTT Research Report VTT-R-08147-08.

Ren, X., Yang, S., Tan, X., Chen, C., Sheng, G., Wang, X. (2012). Mutual effects of copper and phosphate on their interaction with γ -Al₂O₃: Combined batch macroscopic experiments with DFT calculations. *Journal of Hazardous Materials*, 237-238, 199-208.

Skwarzec, B., Strumińska, D.I. and Borylo, A. (2006). Radionuclides of iron (⁵⁵Fe), nickel (⁶³Ni), polonium (²¹⁰Po), uranium (²³⁴U, ²³⁵U, ²³⁸U) and plutonium (²³⁸Pu, ²³⁹⁺²⁴⁰Pu, ²⁴¹Pu) on Poland and Baltic Sea environment. *Nukleonika*, 51(Supplement 2) S45-S51.

Tribe, L., Hinrichs, R. and Kubicki, J.D. (2012). Adsorption of Nitrate on Kaolinite Surfaces: A Theoretical Study. *The Journal of Physical Chemistry B*, 116, 11266-11273.

Wesolowski, D. J., Bandura, A. V., Cummings, P. T., Fenter, P. A., Kubicki, J. D., Lvov, S.N., Machesky, M. L., Mamontov, E., Předota, M., Ridley, M. K., Rosenqvist, J., Sofo, J. O., Vlcek, L. and Zhang, Z. (2009). Atomistic origins of mineral-water interfacial phenomena and their relation to surface complexation models. *Geochimica et Cosmochimica Acta*, 73(13), A1429.

REACTIVE TRANSPORT MODELLING OF NICKEL IN FRACTURED BEDROCK

Veli-Matti Pulkkanen^{*}, Anniina Seppälä, Markus Olin

VTT Technical Research Centre of Finland (FIN)

^{*} Corresponding author: veli-matti.pulkkanen@vtt.fi

Abstract

To clarify the connection between the concepts used in performance assessment (PA) models and in data fitting, three different reaction models for sorption of nickel on biotite were coupled to a fracture flow model. In the simplest reaction model, a linear sorption isotherm is used, which is the usual way to treat sorption in PA models. In the second model, the reactions in data fitting have been used directly meaning that an equilibrium surface complexation reaction has been implemented into the fracture flow model as kinetic reactions. Where in this model the surface sorption sites have been divided into a volume of water, in the third model the sites have been divided onto model surfaces giving a different conceptual view to sorption. The three models show somewhat similar sorption behaviour in the case of sorption of nickel and biotite, but give insight into interpreting experimental results for PA models.

Introduction

The final disposal of spent nuclear fuel in Finland is planned according to the geological disposal concept KBS-3, in which approximately 400 meters of bedrock functions as one of the barriers isolating the spent fuel from the surface environment. Evaluating the performance of this barrier in retarding radionuclides in a case of leakage of spent fuel is an important part of the performance assessment and safety analysis of the whole concept. The retardation models in such analysis are usually fairly simple due to the complexity of the whole analysis. They consist of matrix diffusion with linear sorption from water conducting fractures to surrounding bedrock through different types of rock layers. The parameters for the retardation models are usually obtained directly from the fitting of chemical reactions (surface complexation reactions etc.) to experimental data. In this work, reactive transport modelling is used to give insight in the connection between the experimental data fitting and PA models

Sorption of nickel on biotite was chosen to be studied in this work and also in Itälä et al. (2013) and Puhakka et al. (2013). This sorption reaction was selected, because it is relevant to safety (biotite being the main sorbing mineral at Finnish disposal site), but more importantly there is experimental data available on this reaction.

Three reaction models for sorption of nickel on biotite were coupled to a simple fracture flow model using COMSOL Multiphysics as the computational tool. Linear sorption isotherm was chosen to the first model to link the work to PA models in which the linear sorption is usually used. The sorption deciding parameter, K_d , was calculated from the reaction parameters presented in Itälä et al. (2013), in which non-electrostatic surface complexation model gives the best fit for sorption of nickel on biotite. The second model includes the surface

complexation equilibrium reaction in the form that it has been used in the fitting, but the reaction was implemented as kinetic reactions. In the third model, reactions were interpreted as surface reactions that take place on the actual fracture surfaces of the model in contrary to the second model where the surface sites have been considered per volume of water. Cation exchange reactions were also considered at early stages of the reactive transport modelling but were omitted, since the surface reaction fitting to experiments show that their effect on the quality of the fit was negligible.

Modelling

Chemical reactions

The surface complexation reaction can be presented as a volumetric reaction which in equilibrium satisfies the equation

$$K[\text{Ni}^{2+}][\text{sOH}] = [\text{sONi}^+][\text{H}^+] \quad \text{eq. 1}$$

where square brackets stand for the moles of surface sites (sOH and sONi⁺) per volume of water or concentration of dissolved species (Ni²⁺ and H⁺). K is the equilibrium constant. The linear sorption distribution coefficient K_d can be obtained from the reaction by comparing the dissolved nickel concentration [Ni²⁺] to the sorbed nickel [sONi⁺].

Using the moles of surface sites per volume, however, poses a conceptual problem: Let us assume there are second (or higher) powers in the equilibrium equation above. If a certain mass of biotite was put into a volume of water (with fixed concentrations of Ni²⁺ and H⁺) and the volume was doubled, the equilibrium state would change according to the equation. It, however, should not. Therefore, instead of using volumetric variables, it is natural to use surface variables (moles/area) for the surface species sOH and sONi⁺. In these terms the equilibrium condition is

$$K[\text{Ni}^{2+}]\{\text{sOH}\} = \{\text{sONi}^+\}[\text{H}^+] \quad \text{eq. 2}$$

where the wave brackets stand for the moles of surface sites per reactive surface area.

Reactive transport models

The reactive transport equations differ slightly for each of the three reaction model cases. In the linear sorption and volumetric reaction models, dissolved nickel moving in a fracture (aperture 1 mm) can diffuse into the surrounding rock matrix by matrix diffusion and the sorption of nickel takes place in the bedrock. In the third (i.e. surface coverage) model, the surrounding bedrock matrix has been replaced by very thin transverse fractures whose volume corresponds to the porosity in the other two models.

The equation for the transport model with linear sorption and K_d -value reads

$$(\phi + \rho_{\text{biotite}} K_d) \frac{\partial c_{\text{Ni}^{2+}}}{\partial t} + \nabla \cdot (-D_e \nabla c_{\text{Ni}^{2+}}) + \mathbf{u} \cdot \nabla c_{\text{Ni}^{2+}} = 0 \quad \text{eq. 3}$$

where $c_{\text{Ni}^{2+}}$ is the dissolved nickel concentration, ϕ is the porosity, ρ_{biotite} the density of biotite (mass per total volume), D_e the effective diffusion coefficient and \mathbf{u} the velocity of water in the fracture. The velocity of water is zero in the rock matrix, whereas the retardation factor ($\phi + \rho_{\text{biotite}} K_d$) is one in the fracture.

The transport equations with volumetric reactions can be written as

$$\phi \frac{\partial c_i}{\partial t} + \nabla \cdot (-D_e \nabla c_i) + \mathbf{u} \cdot \nabla c_i = \pm \phi R \quad \text{eq. 4}$$

for variables $c_i = c_{\text{Ni}^{2+}}, c_{\text{sONi}^+}$ and c_{sOH} . The H^+ concentration is obtained from pH. The reaction term is $R = k \left(c_{\text{Ni}^{2+}} c_{\text{sOH}} - \frac{1}{K} c_{\text{sONi}^+} c_{\text{H}^+} \right)$, which with time tends to the equilibrium value, and k is the rate constant. The direction of the reaction for each variable sets the sign of the reaction term. For the surface variables, the diffusion and convective terms are zero meaning that the surface sites stay still.

In the reactive transport model with the surface sites as surface coverage, the sorption is also described with kinetic equilibrium reactions. In this case, however, the surface sites are presented as surface variables c_{sONi^+} (moles of sorbed nickel per area) and $c_{\text{s,sOH}}$ (moles of free surface sites per area) which exist only on the fracture surfaces of the model. The transport equation for the soluble nickel becomes

$$\phi \frac{\partial c_{\text{Ni}^{2+}}}{\partial t} + \nabla \cdot (-D_e \nabla c_{\text{Ni}^{2+}}) + \mathbf{u} \cdot \nabla c_{\text{Ni}^{2+}} = 0 \quad \text{eq. 5}$$

and the surface reaction for soluble nickel is presented as a flux boundary condition

$$\mathbf{j} \cdot \mathbf{n} = R \quad \text{eq. 6}$$

(\mathbf{j} is the mass flux and \mathbf{n} the surface normal) on the fracture surfaces, on which nickel sorbs. The reactions term R is of the same form as for volumetric reactions but now the surface variables are used instead of volume variables. The equations for the surface variables are of the form

$$\frac{\partial c_i}{\partial t} = \pm R \quad \text{eq. 7}$$

and they are defined only on the fracture surfaces.

Water flow in the fracture

Water flow in the fracture is slow enough to use Stokes equations instead of Navier-Stokes equations. Computing a realistic flow profile can make the results differ from PA models where the flow is often assumed a plug flow.

Model geometries, initial values, boundary conditions and parameters

The model geometry for the K_d and the volumetric reaction models consists of a planar rock fracture with aperture of 1 mm and a 30 cm thick bedrock block. The length of the model is one meter. In the surface coverage model, the bedrock with a porosity of $3 \cdot 10^{-5}$ was replaced with transverse small fractures (5, 10, 20, 50 or 100 fractures) such that their volume corresponds to the porosity.

Dissolved nickel concentration of $1 \cdot 10^{-7}$ mol/l was set on the inlet boundary of the fracture and the migration of nickel in the fracture and the retardation into the rock was monitored. The initial value for the reacting surface sites, $c_{s,SOH}$, was computed from the surface site density ($n_s = 9$ 1/nm²), the specific surface area ($a_s = 4.7$ m²/g) and the volume ratio (0.28) of biotite and the rock grain density (2 700 kg/m³). The initial value for the surface variable $c_{s,SOH}$ in the surface coverage model was set such that the total number of surface sites correspond to the one in the volumetric reaction model.

The effective diffusion coefficient in the bedrock is $6 \cdot 10^{-14}$ m²/s and in water $2 \cdot 10^{-9}$ m²/s. Flow rate through the fracture has been set to 10 l/year. The sorption parameter values were taken from experiments (see Itälä et al. (2013)) and the order of magnitudes of the other parameters correspond the values used in safety analysis (see POSIVA (2008)).

Results

The results are shown in Figure 1 and Figure 2. In Figure 1a the concentration profiles of the K_d -model, the volumetric reaction model and the surface coverage model with 100 fractures practically coincide. When the number of transverse fractures is decreased, the profiles show step-like behaviour (see Figure 1b). The total amounts of soluble nickel Ni^{2+} and sorbed nickel $sONi^+$, however, change only slightly (see Figure 2).

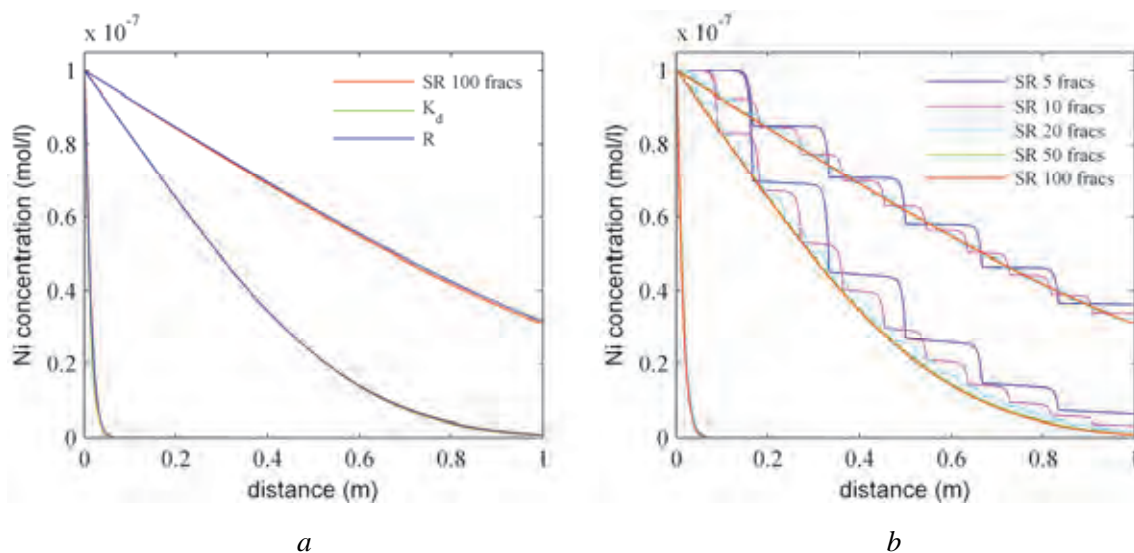


Figure 1: Soluble Ni^{2+} concentration profile at the midline of the fracture at times 0 years (lowest set of lines), 0.2 years (middle) and 1 year (top). The graphs in figure a are from the K_d -model, volumetric reaction model (R) and surface coverage model (SR) with 100 transverse fractures. In figure b, the number of transverse fractures varies.

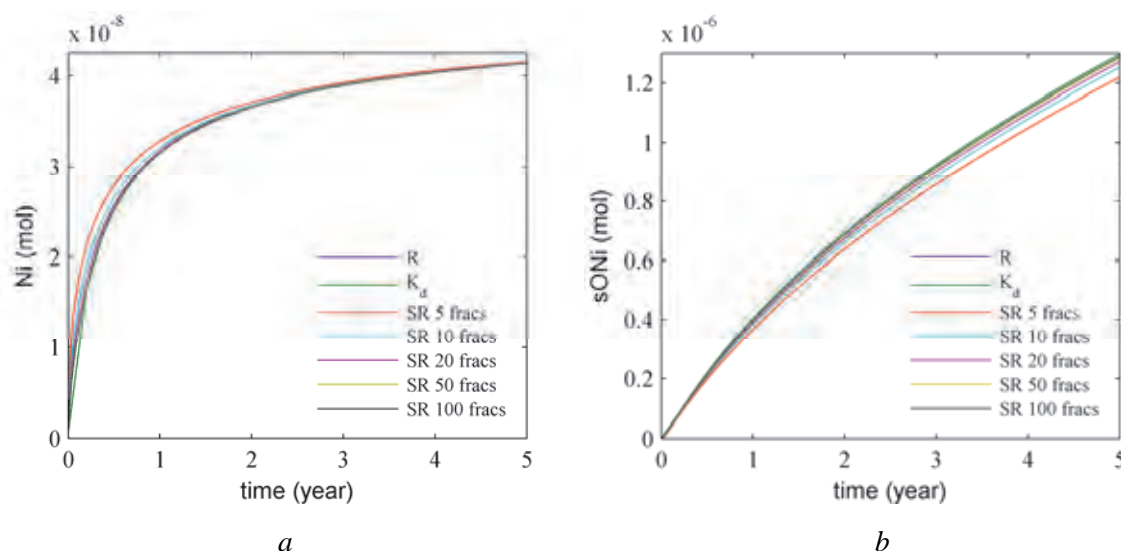


Figure 2: The total amount of soluble nickel Ni^{2+} and sorbed nickel $sONi^+$ in the K_d -model, volumetric reaction model (R) and surface coverage model (SR) as a function of time.

Conclusions and Future work

Sorption reactions from three different conceptual models have been implemented into reactive transport models successfully. The reactive transport models can be used to evaluate the concepts, but in the particular case of sorption of nickel on biotite they show similar behaviour due to the simplicity of the sorption reaction. At least a few more reactions could be added to the volumetric reaction and the surface coverage models to evaluate the effect of the chemical environment in a transport model context.

The model in which the surface reactions have been added to the model as real surface coverage is an attempt to solve the conceptual difficulties in the volumetric reactions models. But, this gives a rise to another problem: what is the number of surface sites per area in the model in comparison to the number of sites on nano- or micro-scale reactive area?

The largest uncertainty in the models is related to the scaling of experimental results to intact rock. Very low masses of biotite per water volume (2 or 4 g/l) have been used in the experiments, whereas the biotite density (mass of biotite per total volume) in intact rock is hundreds of grams per litre (about 800 g/l in this work) and the total rock density is around 2 700 g/l. This means that results obtained for a system with high porosity (~ 1) have been scaled linearly to a system of very low porosity ($<10^{-4}$) without knowledge on the scalability. The number of surface sites per volume of water ranges from $2 \cdot 10^{-5}$ mol/l (2 g/l of biotite and porosity of one) to about 2 000 mol/l (800 g/l of biotite and porosity $3 \cdot 10^{-5}$). Overcoming the problem would mean performing experiments with sample densities ranging from low values (2 g/l) to values as close as possible to the intact rock.

Acknowledgement

The research leading to these results has received funding from the European Union's European Atomic Energy Community's (Euratom) Seventh Framework Programme FP7/2007-2011 under grant agreement n° 269658 (CROCK project), Posiva Oy and VTT.

References

Itälä, A., Tanhua-Tyrkkö, M., and Olin, M. (2013). Surface complexation modelling of biotite – nickel and europium models. Final Workshop Proceedings of the Collaborative Project “Crystalline Rock Retention Processes” (7th EC FP CROCK).

POSIVA 2008-6 (2008). Radionuclide Release and Transport – RNT-2008. POSIVA Report 2008-06, Posiva Oy, Eurajoki, Finland.

Puhakka, E. and Olin M. (2013). Molecular modelling of biotite surface. Final Workshop Proceedings of the Collaborative Project “Crystalline Rock Retention Processes” (7th EC FP CROCK).

SURFACE COMPLEXATION MODELLING OF BIOTITE: NICKEL AND EUROPIUM

Aku Itälä*, Merja Tanhua-Tyrkkö, Markus Olin

VTT Technical Research Centre of Finland (FI)

* Corresponding author: aku.itala@vtt.fi

Abstract

In this study surface complexation model (SCM) is re-fitted on our experimental results (Olin et al., 2008). This work, however, includes the extension of the modelling to 2-p*K* non-electrostatic (NEM) and diffuse-layer (DLM) models. First, two pH titration curves (acid and basic) of Luumäki (pure) biotite surface are fitted to obtain acid-base reaction parameters and site density, which are needed when fitting the sorption data. Second the observed sorption percentages of Ni and Eu on Luumäki biotite are re-fitted using the FITEQL 4.0 software by a combination of cation exchange and 1-p*K*/2-p*K* models. Third, the 1-p*K* and the 2-p*K* modelling approaches are compared and applied to predict K_d values for Olkiluoto biotite and rock samples. The main result of the study is that the non-electrostatic model works better for biotite than the common electrostatic models and that biotites from different formation environments need their own cation exchange/sorption parameters.

Introduction

Biotite ($K(Mg,Fe)_3AlSi_3O_{10}(OH,F)_2$) is a typical mineral in Finnish bedrock and a major sorbent for cations in the Olkiluoto site (Lindberg, 2002). Biotite is present in the pore surfaces as part of the granite matrix in the far-field of the planned Finnish repository for spent nuclear fuel, and thus it can work as a sink for radioactive elements. In this work, the experimental sorption results for nickel and europium on biotite obtained in a previous study have been applied. A mechanistic sorption model (including surface complexation (SCM) and ion exchange (IE)) has been created in this work for nickel and europium on biotite surfaces. The objective was to get good fits for K_d values and to test if one kind of model fit would work on all the different types of biotites/rock materials used. Acid and basic titrations are used in this work for determining surface site density and surface acidity reactions and their constants. K_d values are determined for sorbing elements (Ni^{2+} and Eu^{3+}).

Experimental data

In this study no experimental work was done, but instead the experimental data was retrieved from (Olin, 2008). In that work pH-titrations in oxygen free conditions for Luumäki biotite were provided. In addition sorption data for nickel and europium on Luumäki biotite and on two rocks and on two biotites from Olkiluoto were also provided. In the rocks studied the amount of biotite was 28.8% and the tests were done in oxygen-free conditions. The titrations were done successfully only for biotite from Luumäki whereas the sorption of nickel and europium were done for all the solids. The Ni-63 and Eu-152 tracer concentrations were $2.5 \cdot 10^{-10}$ mol/L and

$9.0 \cdot 10^{-8}$ mol/L, respectively. The background electrolytes applied were 0.05M or 0.5M NaClO₄. The experimental conditions are listed in Table 1.

Table 1: The experimental conditions of the sorption experiments reported in (Olin, 2008).

Solid	Solid/Liquid ratio	Liquid
Luumäki biotite		
Olkiluoto A biotite		
Olkiluoto B biotite	2 g/L or 4 g/L	Ni $2.5 \cdot 10^{-10}$ mol/L and 0.5M or 0.05M NaClO ₄
Olkiluoto A rock		
Olkiluoto B rock		
Luumäki biotite	0.4 g/L,	Eu $1 \cdot 10^{-8}$ mol/L and
Olkiluoto A biotite	2 g/L or	0.5M* or 0.05M NaClO ₄
Olkiluoto B biotite	4 g/L	

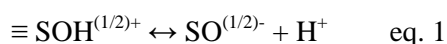
* only for 2g/L

Fitting the titration data

The surface complexation modelling can be divided into two phases. In the first phase the titration of solid sample (here Luumäki biotite) is evaluated to obtain the number of “surface complexation sites” and equilibrium constant for the acid-base reaction and in the second phase the actual complexation of some cation (here nickel or europium) on these surface sites is evaluated together with ion exchange parameters.

In this work the first phase were done with 1-pK and 2-pK models using Diffuse Layer Model (DLM), Constant Capacitance Model (CCM) and Non Electrostatic Model (NEM). The fittings were done for the whole data set and also some cases were tested where some of the end points from both ends of the titration data were left out. It was found that the end points did not have much effect to the fits.

For the 1-pK titration model the equation is:



And for the 2-pK titration model the equations are:

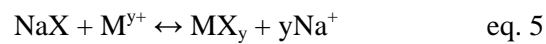
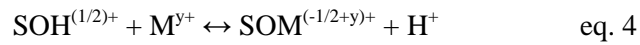


From the fittings, it was seen that the DLM model fitted best the basic side titration while the NEM model fitted best the acid side titrations. When both experimental (acidic and basic titration data together) data were used the best fit was obtained with NEM model. The CCM model gave unreasonable results and was not used after the first phase.

Fitting sorption results

In this study, the idea was to fit the pH-titration data of Luumäki biotite and, after that test if the values obtained from the Luumäki fit could be used to fit the experimental sorption data of two other biotites (Olkiluoto A and Olkiluoto B) and two rocks (only in case of nickel, sorption of europium on these rocks were not included in the experiments reported by Olin (2008)). Only one sorption complex for cations was used, because fittings were good enough compared to other uncertainties.

For the 1-pK sorption model the fitted equations are:



For the 2-pK sorption model the ion exchange reaction was the same but the sorption reaction fitted was:



where M^y is either Eu^{3+} or Ni^{2+} .

Titration of Luumäki biotite

The fitting of experimental Luumäki pH-titration data gave $\log K$ for reaction 1 (1-pK model) to be 5.4 together with a site density of 7 sites/nm² by DLM. And for the 2-pK model (reactions 2 and 3) the results using the DLM were $\log K$ 3.6 and -6.2, respectively, and a site density of 9 sites/nm² while the results using the NEM were 3.6 and -8.7 with 9 sites/nm² site density.

Table 2: Fitted nickel sorption parameters for different experimental conditions.

Data	Model type	NaClO₄ [mol/L]	S/L [g/L]	T(SOH) [mol/L]	T (X[-]) [mol/L]	GK(SONi[+])	GK(NiX2)
Luumäki	2-pK NEM	0.05	2	1.4E-04	2.6E-05	-3.9	24.5
Luumäki	2-pK NEM	0.05	4	2.8E-04	5.2E-05	-3.9	24.1
Luumäki	2-pK NEM	0.5	4	2.8E-04	5.2E-05	-4.3	26.0
Luumäki	2-pK DLM	0.5	4	2.8E-04	5.2E-05	-6.1	26.2
OAB	2-pK NEM	0.05	2	2.9E-05	4.7E-06	-2.9	26.3
OAB	2-pK NEM	0.05	4	5.7E-05	9.4E-06	-2.9	25.9
OAB	2-pK NEM	0.5	4	5.7E-05	9.4E-06	-3.5	27.4
OBB	2-pK NEM	0.05	2	3.8E-05	9.3E-06	-3.2	26.1
OBB	2-pK NEM	0.05	4	7.7E-05	1.9E-05	-3.1	25.3
OBB	2-pK NEM	0.5	4	7.7E-05	1.9E-05	-3.5	26.8
OAR	2-pK NEM	0.05	25	1.0E-04	1.7E-05	-2.4	26.6
OAR	2-pK NEM	0.5	25	1.0E-04	1.7E-05	-3.2	27.9
OBR	2-pK NEM	0.05	14	7.7E-05	1.9E-05	-1.8	26.7
OBR	2-pK NEM	0.5	14	7.7E-05	1.9E-05	-3.1	27.8

Fitting sorption data of nickel

The K_d -results from the fittings, for all cases, are presented in the figures below. For the Olkiluoto biotites and rocks the results show that better fits can be obtained if the evaluation is done without using the sorption log K values of Luumäki, but the sorption parameters (Table 2) are obtained for Olkiluoto biotites separately (see Figures 1-3). If the Luumäki log K values are used, the concentration of surface complexation sites (TSOH) must be increased from the Luumäki case by a factor of 1.8. This is in contradiction to the experimental data that show that Olkiluoto biotites have actually smaller surface area and thus (by assumption) less surface complexation sites. Thus it was decided that the fitting of sorption properties has to be done independently for the Olkiluoto samples.

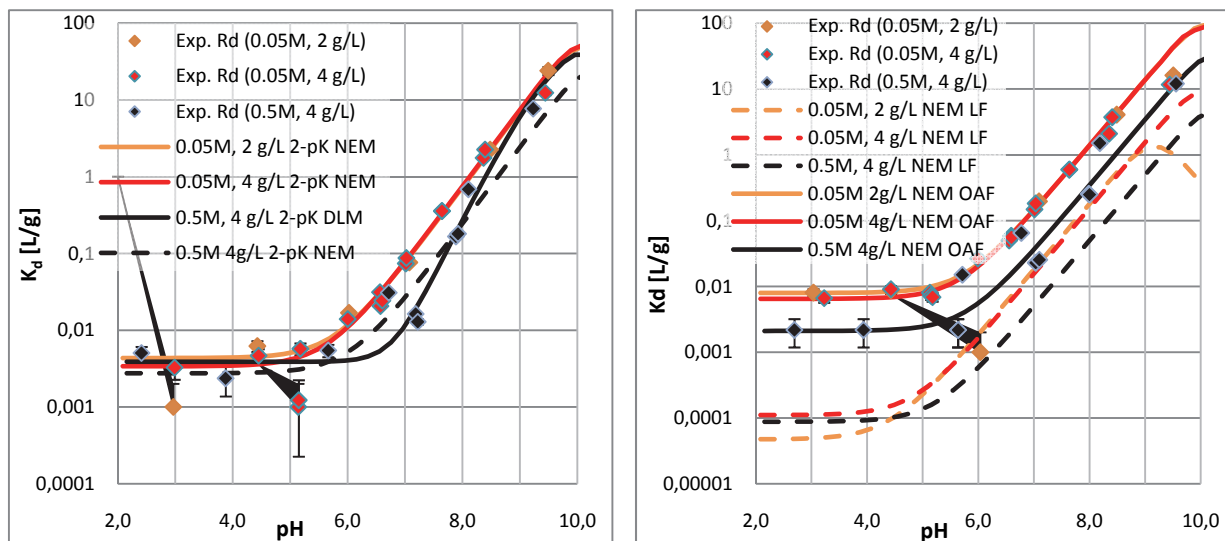


Figure 1: K_d fits of nickel on Luumäki biotite 2 and **Figure 2:** K_d fits for nickel on Olkiluoto A biotite (OAB) 4 g/L, 0.05 and 0.5M.

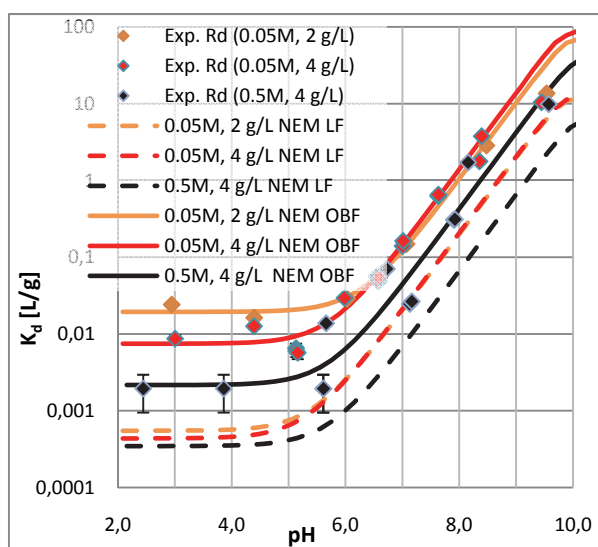


Figure 3: K_d fits for nickel on Olkiluoto B biotite (OBB) 2-4 g/L, 0.05-0.5M.

The use of Olkiluoto biotite fits was also tested for the rock samples (see Figure 4). However it was found out that the use of sorption log K values for pure biotite samples when fitting sorption data on rock samples will underestimate the sorption capability. Thus it was concluded again to make sorption fits separately for rock samples. The results can be seen in Figures 4-5. The experimental data was done in conditions with 25 g/L (Olkiluoto A rock (OAR)) or 14g/L (Olkiluoto B rock (OBR)) solid/liquid ratio and the solution used was 0.05 or 0.5M NaClO₄. The Olkiluoto rock had a fraction of biotite of 29% (Olin et. al., 2008).

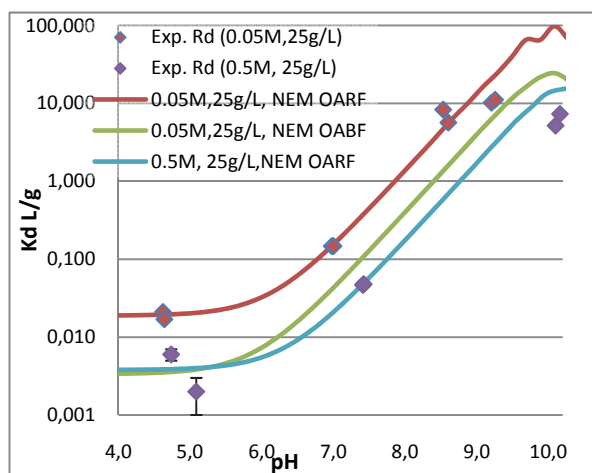


Figure 4: K_d fits of nickel sorption on Olkiluoto A Rock (OAR) 25 g/L, 0.05-0.5M.

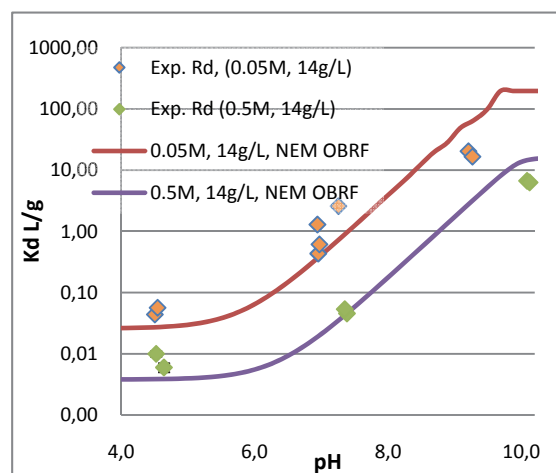


Figure 5: K_d fits for nickel sorption on Olkiluoto B rock (OBR) 14 g/L, 0.05-0.5M.

Fitting sorption data of europium

Europium fitting was more challenging because europium has the tendency to sorb almost 100% to biotite at high pH values. This caused problems to fitting with FITEQL as the output from this program only handles values with a precision of three decimals. The fittings done for europium were not nearly as good as for nickel. In a few cases DLM models gave better fits. The fitted parameters used in the Figures 6-8 are also listed in Table 3; note that sorbed amounts of Europium are shown in europium figures due to very high sorption.

Table 3: Fitted Europium sorption parameters for different experimental conditions.

Data	Model type	NaClO ₄ [mol/L]	S/L [g/L]	T(SOH) [mol/L]	T (X[-]) [mol/L]	GK(SONi[+])	GK(NiX2)
Luumäki	2-pK NEM	0.05	0.4	2.8E-05	5.2E-06	0.1	41.9
Luumäki	2-pK NEM	0.05	2	1.4E-04	2.6E-05	-0.5	39.8
Luumäki	2-pK NEM	0.5	2	1.4E-04	2.6E-05	-1.1	41.5
Luumäki	2-pK NEM	0.05	4	2.8E-04	5.2E-05	-0.6	37.7
OAB	2-pK NEM	0.05	0.4	5.7E-06	9.4E-07	1.2	45.8
OAB	2-pK DLM	0.05	2	2.9E-05	4.7E-06	0.4	43.8
OAB	2-pK NEM	0.5	2	2.9E-05	4.7E-06	-0.3	44.9
OAB	2-pK NEM	0.05	4	5.7E-05	9.4E-06	1.0	42.8
OBB	2-pK NEM	0.05	0.4	7.7E-06	1.9E-06	1.5	44.7
OBB	2-pK DLM	0.05	2	3.8E-05	9.3E-06	0.2	42.6
OBB	2-pK DLM	0.5	2	3.8E-05	9.3E-06	-2.5	44.1
OBB	2-pK NEM	0.05	4	7.7E-05	1.9E-06	1.6	41.4

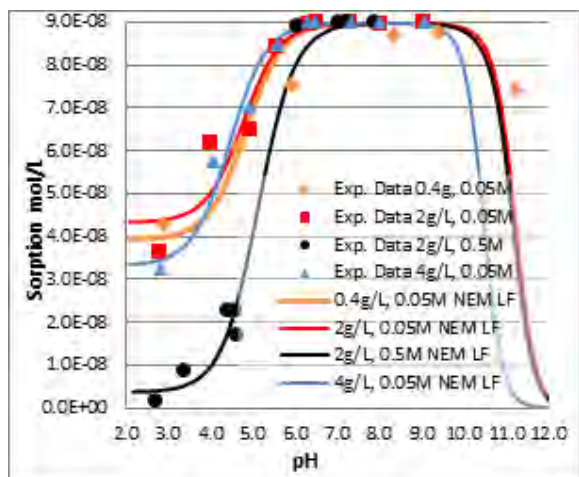


Figure 6: Europium sorption fits for Luumäki biotite 0.4-4g/L, 0.05-0.5M.

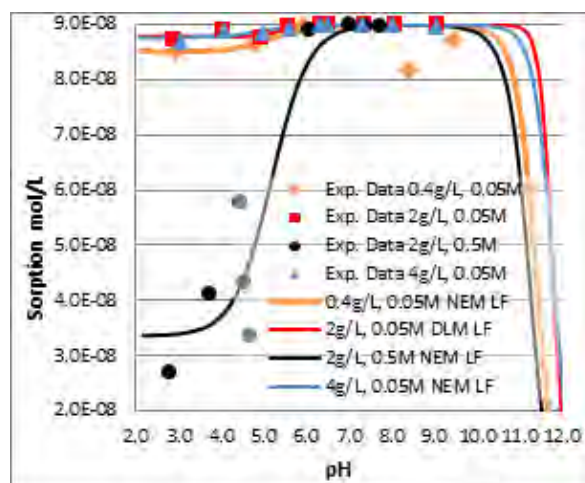


Figure 7: Europium sorption fits for Olkiluoto A biotite 0.4-4g/L, 0.05-0.5M.

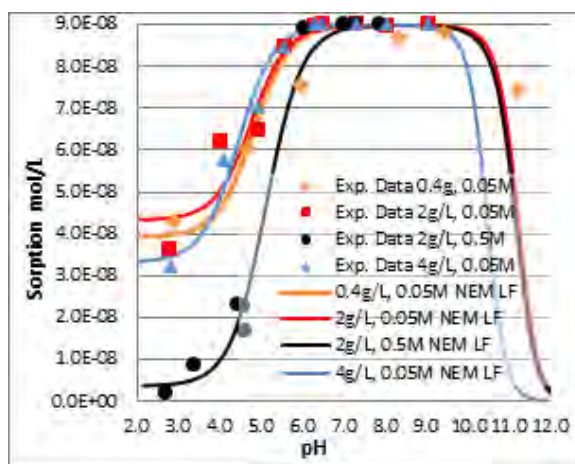


Figure 8: Europium sorption fits for Olkiluoto B biotite 0.4-4g/L, 0.05-0.5M.

Conclusions and Future work

We observed that both acid-base titration results and sorption of nickel and europium on biotite are better fitted by non-electrostatic models (NEM) than applying either diffuse layer or constant capacitance models. The reason behind this observation may be in inappropriate surface charging models (compare for example with the models developed for montmorillonite, which has a similar layer structure as biotite (Bourg et al. 2007)). One of our goals was to see if sorption fit for one biotite material could be used for all the others and the result was that every material needs their own sorption model because they behave differently. Some of the best fitted cases from these results were used in reactive transport modelling.

Acknowledgement

The research leading to these results has received funding from the European Union's European Atomic Energy Community's (Euratom) Seventh Framework Programme FP7/2007-2011 under grant agreement n° 269658 (CROCK project), Posiva Oy and VTT.

References

Bourg, I. C., Sposito, G., Bourg, A.C.M. (2007). Modelling the acid–base surface chemistry of montmorillonite. *J. Colloid Interface Sci.*, 312, 297–310.

Lindberg, A. (2002). Biotiitin muuttuminen kallion läheisyydessä. Posiva Working Report 2002-05. Posiva Oy, Olkiluoto, Finland. (in Finnish)

Olin, M., Puukko, E., Puhakka, E., Hakanen, M., Lindberg, A. and Lehikoinen, J. (2008). Sorption on biotite. Final Annual Workshop Proceedings- 6th EC FP-FUNMIG IP, Forschungszentrum Karlsruhe Report. Forschungszentrum Karlsruhe GmbH, 335-343. <http://bibliothek.fzk.de/zb/berichte/FZKA7461.pdf>

POSSIBLE CAUSES OF UNCERTAINTY IN THE SORPTION DATA FOR PA STUDIES

Markus Olin^{1*}, Antti Poteri¹, Veli-Matti Pulkkanen¹, Lasse Koskinen²

¹ VTT Technical Research Centre of Finland (FI)

² Posiva Oy (FI)

* Corresponding author: markus.olin@vtt.fi

Abstract

Sorption and matrix diffusion are the most important retardation mechanism of radionuclides in fractured bedrock. In PA studies sorption is typically modelled by linear sorption isotherm, K_d approach. Evaluation of uncertainty may be roughly divided into model and data evaluation. We have analysed both modelling and data uncertainties based on our experience on application of surface complexation and molecular level modelling tools. Our main result in this work is the listing of the potential sources of uncertainty.

Introduction

A final repository for spent nuclear fuel has a major demand to restrict the release and transport of radionuclides below the limits specifically given to different barriers and time scales by authorities. It is the duty of waste producer to design the repository in a way these limits and other possible demands are fulfilled in all time scales. Radionuclide transport calculations, usually done for set of radionuclides, in large systems, over long periods and variations of conditions, form an essential part of these studies. Therefore, simplified models are applied in these performance analysis (PA) calculations. The bedrock in Finland is fractured, and therefore, radionuclides migrate via the fracture network consisting of fractures of varying apertures and other properties. In a simple model a fracture of constant aperture is modelled by Darcy's law for flow, K_d approach for sorption and Fickian diffusion into intact rock. Usually PA studies are based on experimentally defined K_d values, selection of which may be supported by surface complexation modelling (SCM). In principle, SCM can be applied in extrapolation of K_d values outside measured conditions, but the modelling must then be supported for example by molecular level modelling, which is not directly applying any macroscopic experimental data. In addition to producing experimental K_d values for PA purposes, the SCM can be applied to produce mechanistic sorption models to be applied in reactive transport modelling (RTM). All these approaches together can be used in evaluation of uncertainties and applied conceptual thinking (Figure 1).

The goals in our work were to evaluate of uncertainties

1. in K_d values
2. of whole K_d based sorption model approach used in PA.

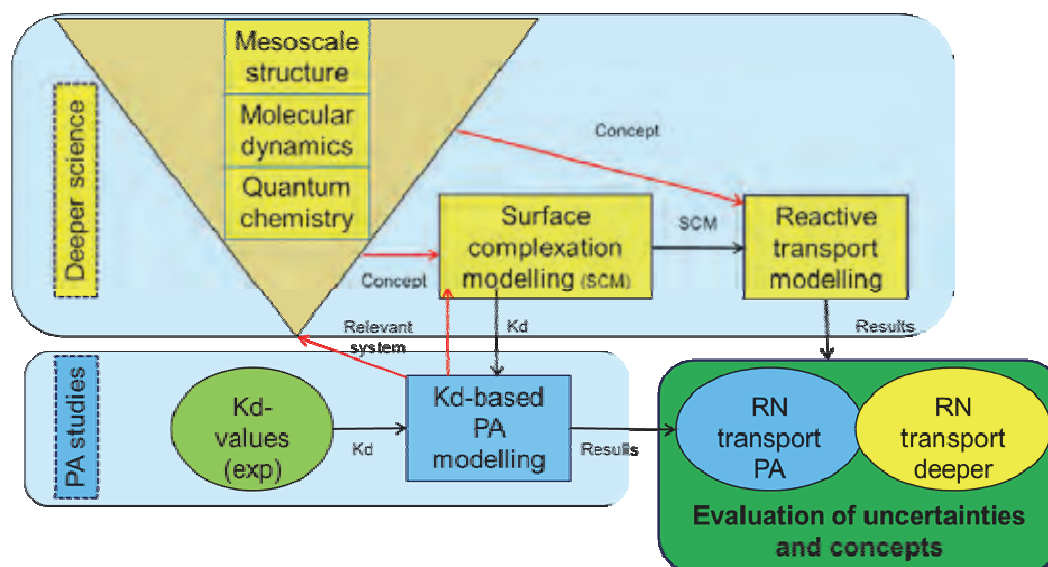


Figure 1: Overall concept of our approach.

Uncertainty evaluation of sorption: models and data

Experimental work

Adsorption of radionuclides onto mineral surfaces is an essential retardation mechanism in granitic bed rocks. Sorption is typically given as a sorption distribution factor K_d measured for a rock sample, in given conditions (pH, salinity, carbon dioxide) and after crushing and possible purifying samples in different ways. Therefore, the uncertainties start to accumulate in sampling and sample preparation. In order to fit the model over large enough condition space, the lab work must be carried out at least varying pH, solid to water ratio, salinity and other case specific parameters. In the PA analysis either experimental K_d values are used as such (after careful selection process) or via mechanistic sorption modelling (SCM and IE), which can produce values with varying uncertainty depending on many topics. However, the K_d values are needed both in fracture surfaces and in intact porous rock, where the solid to water ratio (even 10 000 kg/L) exceeds by several orders magnitude typically applied laboratory values (0.001 – 0.1 kg/L). Also there exist problems related to reactive surface area and in the case of sheet silica like biotite also to orientation of minerals in the studied system.

Modelling work

Our modelling concept was based on multiscale approach (starting from smallest scale):

1. MLM – molecular level modelling: molecular structure, about nanometre scale
2. SCM – surface complexation modelling: laboratory scale mainly
3. RTM – reactive transport modelling: larger parts of a final repository
4. PA – performance analysis, the entire repository even over hundreds of thousands of years

First, we noticed a gap in our modelling between MLM and SCM, which should be coupled via molecular dynamics (MD) and possible even via some mesoscale model. MD is basically adding the statistical physics into

molecular level studies and larger models are also more realistic (only fraction of surface sites may be occupied etc.). However, study times in MD are really short (nanoseconds) compared to equilibrium approach of MLM studies.

The most important information that MLM may offer to SCM studies is the existence and nature of surface sites. Second, the MLM studies may give valuable information about surface reactions and nowadays also about behaviour of water molecules near surface and near sorbing ions (hydration). The first class uncertainties in sorption studies is related to this basic question of surface sites and reactions, which are relatively easy to fit by macroscopic experimental data, but for which not much direct experimental nano-level data (EXAFS or other methods) or modelling is available.

PA studies are able to define the most relevant systems to be studied, and this means mainly radionuclides in our case, because in Olkiluoto conditions the biotite has appeared the most important sorbing mineral. The availability of data in MLM studies for other radionuclides except caesium, nickel and europium was studied very briefly, and data for strontium was found. The developed surface complexation models have two different ways of application, which appear to have basic differences

1. SCM model into RTM: sorption is modelled mechanistically as a part of transport model and in our approach (detailed geometry) sorption model is a kind of boundary condition in the RTM.
2. SCM based K_d 's into PA: sorption is handled traditionally in PA, but instead of direct experimental values, their fit into SCM is applied to produce values. This may extend the approach into conditions not measured and is in that content a kind of an extension instead on interpolation.

Uncertainties in sorption modelling

Selection

Identification and selection of the most important sorbing minerals and their occurrence in rock types (e.g., Olin et al., 2008) may be done for example by applying autoradiography of the thin rock sections for a set of radionuclides together with optical analysis for mineral phases. The uncertainties are coupled in sampling and laboratory work, of which first one probably causes bigger uncertainty.

Sampling

Representative rock and mineral samples are needed for PA applicable results. Sorbing mineral (biotite) must be separated from rock for SCM purposes. In addition, it is possible to apply pure natural (like Luumäki biotite in our case, (Itälä et al., 2013)) or commercial mineral samples. Purified mineral (biotite) goes to characterisation: impurities, specific surface area, cation exchange capacity (CEC). Impurities are a common source for uncertainties: they may alter CEC, surface area, protonation and sorption properties. Specific surface area is a complicated topic, which depends for example on crushing and grinding of samples, and is an important parameter in SCM development.

Selection and preparation of water solutions

Usually simple electrolyte solutions are used for SCM development, but for more PA relevant cases groundwater simulants must be used, and often with real rock samples and not only with purified minerals. All this leads to lot of additional work and therein possible also contradictory results, which apparently increases

uncertainty. The uncertainties here track back to site specific data, which increases rapidly during real construction phase of the repository.

Titration to obtain surface acidity model

The surface acidity model has been a very basic thing in SCM development, because charging is observed in acid-basic titrations and the conceptual model of (oxide) surfaces is based on these reactions. However, the non-electrostatic models (NEM) have been however popular, but in principle they don't have need for surface protonation reactions and they are inconsistent with present understanding of diffusion related phenomena, like anion exclusion and surface diffusion. The uncertainties here are coupled to consistent description of sorption and diffusion, because both diffusivity and porosity models for anions include often anion exclusion, which is interpreted commonly by an electrostatic interaction with negatively charged surfaces. Basically there are two optional models: 1-pK and 2-pK, of which the first one has only two parameters (one binding constant and surface site density).

One big uncertainty is in surface sites

- How many different types are needed?
- Distinction between surface site density and binding constants, which appear as a product in SCM, and may therefore need some additional information to be fitted properly
- Are these types and densities observable also by some other method than fitting of titration data?

K_d measurements as function of pH, salinity, solid-water ratio, etc.

Parameter data of SCMs are based on measured K_d values, which are however measured in different conditions

- typically at least pH is varied, but especially very low and high pH may cause mineral dissolution to appear and therefore is a source of uncertainty
- salinity is varied both in electrolyte solutions and by groundwater simulants, but usually experimental work at low salinity (below say 0.01 M) has appeared difficult, while the modelling is difficult in saline (over 0.5 M) solutions due to complex interaction of species
- solid-fluid ratio is often varied only little, which increases uncertainty when models are applied in PA conditions.

In order estimate experimental uncertainty, there is need for many repetitions under many conditions (e.g., varying contact time), but this type data is rare, and uncertainty evaluation is based on standard single laboratory measurement methods, which may not reveal possible "out-layers".

Model fitting to data

SCM is a non-linear theory and addition of surface charging models and realistic groundwater conditions make it still more non-linear. Fitting is often done against percentage sorbed,

- which causes problems and uncertainties at high sorption, near 100 per cent sorbed
- commonly used programs like FITEQL have only percentage options

- in modern codes, like COMSOL Multiphysics, no such limitation exists, but this far we have not applied COMSOL in fitting of sorption data.

Prediction or interpolation to not measured systems

SCM model have aimed to be used

- either as predictive sorption models, which can effectively substitute direct measurements, or
- as a smart K_d , which has some explicit dependencies on pH, salinity and solid-fluid fraction.

Prediction outside measured conditions or materials, have appeared to be difficult like in this work (see

Conclusions and Future work

The chosen multiscale approach to extrapolate K_d values for conditions without measured data and evaluation of uncertainties in PA studies appears promising, but very tedious and time consuming work. However, we have been able to identify by molecular methods surface complexation (proton) and cation exchange (permanent charge) sites on biotite structure (Puhakka & Olin, 2013). We have observed that both acid-base titration results and sorption of nickel and europium on biotite are better fitted by non-electrostatic models (NEM) than applying either diffuse layer or constant capacitance models (Itälä et al., 2013). The reason behind this observation may be in wrong surface charging models (compare with montmorillonite, which has layer structure, models developed recently, Bourg et al. (2007)).

Acknowledgement

The research leading to these results has received funding from the European Union's European Atomic Energy Community's (Euratom) Seventh Framework Programme FP7/2007-2011 under grant agreement n° 269658 (CROCK project), the Finnish Research Programme on Nuclear Waste Management (KYT) 2011-2014 (LS-TUPER project), Posiva Oy and VTT Technical Research Centre of Finland.

References

- Bourg, I.C., Sposito G. and Bourg A.C.M. (2007). Modelling the acid–base surface chemistry of montmorillonite. *J. Colloid Interface Sci.*, 312, 297–310.
- Olin, M., Puukko, E., Puhakka, E., Hakanen, M., Lindberg, A. and Lehtikoinen, J. (2008). Sorption on biotite. Final Annual Workshop Proceedings- 6th EC FP-FUNMIG IP, Forschungszentrum Karlsruhe Report. Forschungszentrum Karlsruhe GmbH, 335-343. <http://bibliothek.fzk.de/zb/berichte/FZKA7461.pdf>
- Itälä, A., Tanhua-Tyrkkö, M. and Olin, M. (2013). Surface complexation model for nickel and europium on biotite. To be published 2nd Workshop Proceedings of the Collaborative Project “Crystalline Rock Retention Processes” (7th EC FP CROCK).

Puhakka, E. and Olin, M. (2013). Molecular level modelling of biotite surface – support in forming surface complexation models. To be published 2nd Workshop Proceedings of the Collaborative Project “Crystalline Rock Retention Processes” (7th EC FP CROCK).

STUDY OF SELENIUM SORPTION ON ÄSPÖ DIORITE

Kateřina Videnská^{1,2*}, Václava Havlová¹, Jani Vejsadů¹

¹ÚJV Řeř, a.s., Husinec-Řeř 130, 250 68, Řeř (CZ)

²Institute of Chemical Technology, Technická 5, 166 28 Prague (CZ)

* Corresponding author: hvl@ujv.cz

Abstract

Selenium belongs among long-lived fission products being present in the spent nuclear fuel (SNF). Because of the long lifetime, the complex selenium chemistry, its high mobility and mainly anionic character, selenium contributes significantly to the risk associated with the storage of radioactive waste in deep geological repositories. The presented work is focused on interaction of anionic species (SeO_4^{2-} , SeO_3^{2-}) with Äspö diorite. The Äspö synthetic granitic water was used as liquid phase. The batch sorption experiments were conducted on crushed rock under aerobic and anaerobic conditions. Two diorite fractions with different grain size were used in experiment, contact time of liquid and solid phases was 112 days and ratio of solid and liquid phase was 10:1. Results demonstrated different sorption behaviour of studied anionic species and influence of redox conditions on distribution coefficient values (K_d). K_d of selenate converged to zero under both conditions and influence of grain size was not observed. On the other hand K_d of selenite reached higher values under anaerobic conditions (2.2 mL/g) than under aerobic conditions (1.6 mL/g). However, generally speaking it can be said that sorption of selenium on diorite Äspö was very low, probably due to composition of synthetic granitic water Äspö.

Introduction

Selenium (Se-79) is β -emitting radionuclide with long half-live ($T_{1/2} = 3.77 \cdot 10^5$ yrs.) and belong among the long-lived fission products of spent nuclear fuel. It has to be taken into account in safety assessment of deep geological repository due its anionic and redox sensitive character. Selenium exists in several oxidation states. The specie Se(-II) and elemental Se(0) occur in reducing environment and they are immobile species with low solubility. Therefore the presence of selenium in these oxidation states is desirable in the conditions of geological repository. Se(IV) and Se(VI) are soluble and mobile species, they occur under oxidation conditions at forms SeO_3^{2-} and SeO_4^{2-} . Retention of selenite and selenate on natural sorbent was investigated widely. The results showed different behaviour of selenite and selenate. Selenate behaved as non-sorbing, conservative specie and is considered more mobile than selenite (Puraren et al. 2009).

This study is focused on investigation of selenium sorption on diorite Äspö and study of influence of diorite grain size on radionuclide retention. Also influence of aerobic and anaerobic conditions was studied. The special attention was focused to iron as a potential reducing agent because, in many published works, presence of Fe-minerals in natural sorbent led to decrease of selenite concentration in solution. Selenite was sorbed onto surface of natural material (granite, bentonite, hematite, goethite, pyrite, magnetite) by surface complexation or redox reaction (Rovira, et al. 2008; Eichler et al. 2011). In the diorite, minority minerals (biotite, magnetite) can hold iron in their structure (Byegard et al. 1998).

Experimental

Solid and liquid phase

The Äspö diorite is a medium-grained and porphyritic quartz monzodiorite/granodiorite. The main components of diorite are plagioclase, K-feldspar, quartz, biotite and calcite. Minority minerals are muscovite, titanite, apatite, fluorite, zircon and magnetite. The mineralogical analysis showed that iron in diorite rock is partitioned between biotite, epidote, titanite and magnetite (Byegard et al. 1998). The used diorite was sampled from borehole KA2368A-01 from Äspö underground lab. The samples originated from depth 13.04 – 13.52 m and 13.52 – 14.00 m. Those were sampled in such a way the contact with the O₂ in the atmosphere was as short as possible. Then the samples were moved to the anaerobic box in KIT INE where they were crushed and sieved into two fractions with different grain size, still under anoxic atmosphere. The grain size of fraction AD-A was 0.5 – 1 mm and the grain size of fraction AD-B was 1 – 2 mm. The aliquots were then distributed to each project partner for the analyses.

In UJV Rez labs part of the material was moved to the anaerobic box where was kept under anaerobic conditions with O₂ < 1 ppm. The material was washed in de-ionised water to remove fine particles and dried.

The synthetic granitic water Äspö (AGW) was used as a liquid phase for preparation of experimental solutions. Chemical composition of synthetic granitic water Äspö is shown in Table 1.

Table 1: *Composition and pH of synthetic granitic water Äspö.*

Component	Concentration [mg/L]
pH	7.26
Na	1889.9
K	10.6
Ca	1122.2
Mg	99.7
Cl	4909
SO ₄ ²⁻	393.7
HCO ₃ ⁻	11.6
F	1.41
Sr	20.2
Br	21.6

An appropriate aliquots of Na₂SeO₃ and Na₂SeO₄ (p.a., Sigma Aldrich, USA) were dissolved in AGW in order to prepare solution with concentration of 2·10⁻⁵ mol/L.

Sorption experiments

The static batch method was used in order to study selenium sorption on solid material. Batch experiments with crushed diorite were conducted in laboratory under normal atmosphere at 25 ± 1 °C and under anaerobic atmosphere in glove box. All experiments were performed in triplicate. Reaction mixtures were prepared by mixing crushed crystalline rock and synthetic granitic water Äspö containing defined amount of selenium. The ratio of solid and liquid phase was 1:10. The mixtures vials under aerobic conditions were shaken throughout experiment constantly. On the other hand, the vials in the glove box were shaken once a week. Samples, taken regularly were centrifuged (10 min, 12000 rpm) and selenium concentration in liquid phase was determined using inductively coupled plasma mass spectrometry (ICP-MS). Sorption distribution coefficients K_d were calculated on the basis of measured Se concentration in solution. Sorption distribution coefficient of selenium is defined as follows:

$$K_d = \frac{(c_0 - c) \cdot V}{c \cdot m} \quad (\text{mL/g}), \quad \text{eq. 1}$$

where c_0 is the initial concentration of selenium in solution (mol/L), c is the concentration of selenium in liquid phase after sorption (mol/L), V is volume of liquid (mL) and m is solid mass (g).

Eh and pH were also measured in liquid phases.

ICP-MS measurement

The determination of selenium was performed using an ICP-MS method (spectrometer Elan DRC-e, Perkin-Elmer, Concord, Canada). The most abundant isotope ^{80}Se was used for the measurement and the spectral interferences due to $^{40}\text{Ar}_2^+$ were removed by methane as reaction gas. Germanium served as the internal standard. Before measurement the samples were diluted (1 + 9) by 0.28 mol/L HNO_3 solution (Suprapur®, Merck, Darmstad, Germany) and spiked by germanium solution to obtain final concentration 500 µg/L Ge. Calibration solution (0, 100, 200 and 500 µg/L Se respectively) were prepared by dilution of 1000 mg/L H_2SeO_4 stock solution (Analytika Prague, Ltd.) and were also spiked by internal standard (Eichler et al. 2011, 2012).

Results and discussion

Sorption experiments on crushed granite under aerobic conditions

The batch sorption experiments with two crystalline fractions were used as solid phase under aerobic conditions lasted 112 days. Results of batch sorption experiments with selenite are presented in Table 2 and Table 4. The K_d -values showed similar behaviour of selenite for both studied fractions, the K_d -values increased very slightly, after 112 days of phases contact. K_d reached 1.3 mL/g in case of fraction AD-A and 1.6 mL/g in case of fraction AD-B (see Figure 1A). The results showed only very limited selenite sorption. Only 12 % of selenite was sorbed on diorite fraction AD-A, 14 % of selenite was sorbed on diorite fraction AD-B respectively. The obtained results are lower in comparison with publications, studying sorption of selenite on natural sorbents. For example Papelis et al (2001). observed that the sorption yield of selenium on granite is about 50% , Ticknor et al. (1996) obtained the K_d -value of 4 mL/g on granite under oxidising conditions, Vilks et al. (2011) published K_d -values for bentonite in the range of 14 – 16 mL/g under oxidising conditions and Carbol et al. (1997)

mentioned K_d of 40 mL/g under slightly reducing conditions. The low sorption of selenite on diorite Äspö is probably caused by composition of synthetic granitic water Äspö. The groundwater used contains high concentrations of chloride and sulphate. Their content is significantly higher than concentration of SeO_3^{2-} in experimental solution and this fact may negatively influence the retention of selenium. Jan et al. (2008) observed that the cations (Ca^{2+} , Mg^{2+}) in experimental solution might interact with negatively charged surface of crystalline rock (granite) and reduced repulsion between rock surface and selenium species, which led to less negatively charged environment and to selenium sorption. However high concentration of chloride in synthetic granitic water Äspö may probably compete with selenium and decrease sorption of selenium species.

In the experiment the influence of grain size on selenite sorption was studied. Two fractions of diorite Äspö were used as solid phases (fraction AD-A: 0.5 – 1 mm, fraction AD-B: 1 – 2 mm) and although the specific surface area of diorite in fraction AD-A is probably twice, the maximal K_d values of both fractions were comparable and the effect of diorite grain size on selenium retention was not observed. Jan et al. (2007) described similar situation, they observed slight variation in K_d with the size of grains (6 – 8 mL/g).

Results of sorption experiments with selenate under aerobic conditions are presented in Table 3 and Table 5. Values of K_d , approaching zero, confirm assumption that selenate is non sorbing, mobile species (see Figure 2A). The pH and Eh values were measured throughout the experiment and slightly increasing trend in pH values was observed in case of both selenite and selenate. After 112 days of experiment the pH values increased from 7.2 to 7.4 (see Figures 2A and 2B).

Table 2: Electrochemical properties and K_d values of sodium selenite on granitic fraction AD-A under aerobic conditions.

t [days]	K_d [mL/g]	sorbed Se [%]	pH	Eh (SHE) [mV]
0.9	0.4	4.2	7.29	398
1.9	0.6	5.5	7.26	404
3.9	0.5	4.6	7.34	410
6.9	0.6	5.7	7.32	416
13.9	0.8	7.3	7.43	425
27.9	1.0	8.7	7.42	434
56.9	1.3	11.7	7.41	427
84.1	1.5	12.7	7.46	436
112.1	1.3	11.6	7.39	436

Table 3: Electrochemical properties and K_d values of sodium selenate on granitic fraction AD-A under aerobic conditions.

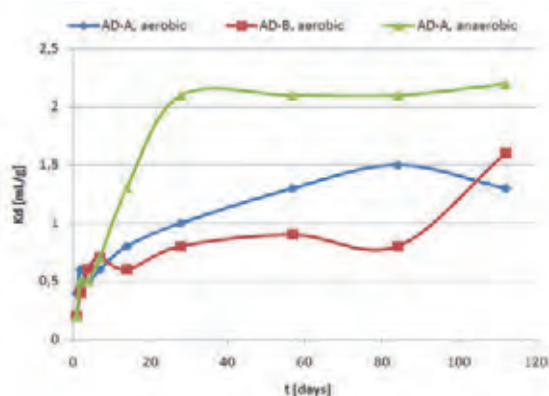
t [days]	K_d [mL/g]	sorbed Se [%]	pH	Eh (SHE) [mV]
0.9	0.2	1.6	7.21	419
1.9	0.0	0.0	7.23	452
3.9	0.0	0.0	7.29	451
6.9	0.0	0.0	7.26	450
13.9	0.0	0.4	7.35	455
27.9	0.0	0.0	7.42	455
56.9	0.3	2.6	7.35	427
84.1	0.0	0.0	7.42	443
112.1	0.0	0.0	7.35	448

Table 4: Electrochemical properties and K_d values of sodium selenite on granitic fraction AD-B under aerobic conditions.

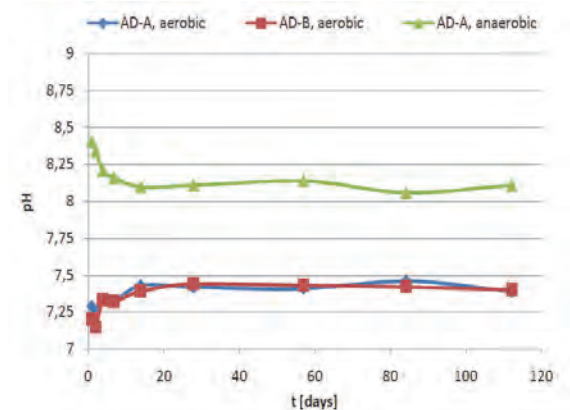
t [days]	K_d [mL/g]	sorbed Se [%]	pH	Eh (SHE) [mV]
0.9	0.2	2	7.2	460
1.9	0.4	4	7.15	458
3.9	0.6	5.6	7.33	458
6.9	0.7	6.2	7.32	457
13.9	0.6	5.7	7.39	455
27.9	0.8	7.2	7.44	454
56.9	0.9	7.9	7.43	443
84.1	0.8	7.5	7.42	440
112.1	1.6	13.9	7.40	434

Table 5: Electrochemical properties and K_d values of sodium selenate on granitic fraction AD-B under aerobic conditions.

t [days]	K_d [mL/g]	sorbed Se [%]	pH	Eh (SHE) [mV]
0.9	0.0	0.1	7.16	417
1.9	0.0	0.0	7.17	422
3.9	0.0	0.0	7.30	429
6.9	0.0	0.0	7.30	432
13.9	0.0	0.4	7.37	436
27.9	0.0	0.0	7.42	440
56.9	0.1	0.5	7.43	447
84.1	0.0	0.0	7.35	442
112.1	0.0	0.0	7.40	442



A



B

Figure 1: Results of selenite sorption experiment under aerobic and anaerobic conditions: A) K_d values of selenite on two diorite fractions, B) pH of studied system.

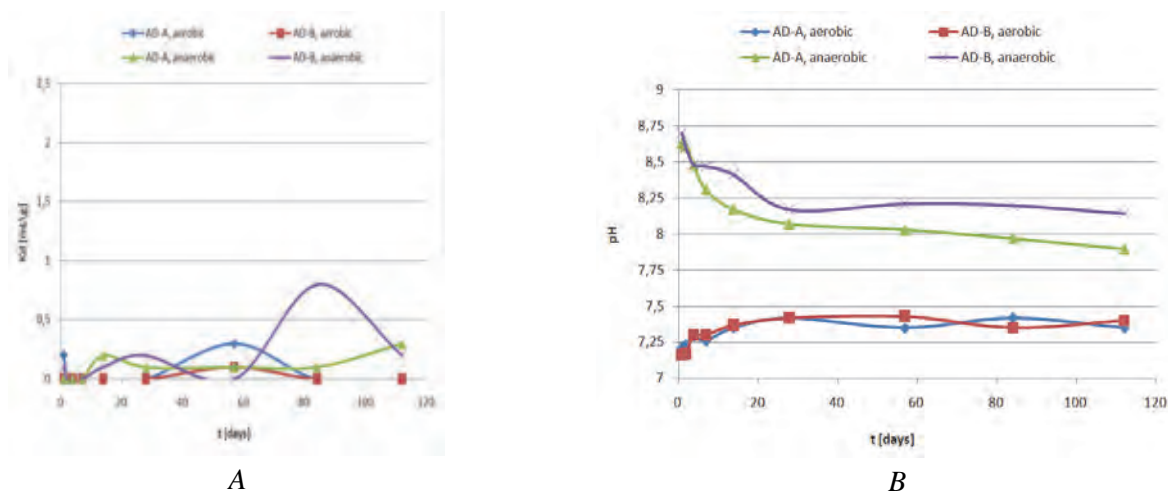


Figure 2: Results of selenate sorption experiment under aerobic and anaerobic conditions: A) K_d values of selenate on two diorite fractions, B) pH of studied system.

Sorption experiments on crushed granite under anaerobic conditions

Sorption experiments conducted under anaerobic conditions show similar results as experiments under aerobic conditions. K_d of selenite, displayed in Table 6, were in case of granitic fraction AD-A only slightly higher than in case of aerobic experiment. Sorption of selenite was also very low, however reaching slightly higher values than for sorption experiments under aerobic conditions (see Figure 1A). Sorption experiment with sodium selenite and granitic fraction AD-B is under way.

Very low sorption of selenate was observed on both granitic fractions. The results showed that conduction of experiment under anaerobic conditions influenced K_d of selenate (see Table 7 and Table 8, Figure 2A) only a little. The K_d -values are similar for both studied fractions: influence of grain size on selenate sorption was not observed. However, K_d reached very slightly higher values than for selenate sorption under aerobic conditions.

The pH and Eh values were measured throughout the experiment and slightly decreasing trend in pH values was observed in case of selenite and selenate. After 112 days of experiment the pH values decreased from 8.4 to 8 (see Figures 1B and 2B). On the other hand, the influence of atmospheric CO_2 absence was observed, pH of solutions under anaerobic conditions were higher than pH of solutions under aerobic conditions. The measurement of Eh does not show any trend of Eh in case of selenite or selenate.

Table 6: Electrochemical properties and K_d values of sodium selenite on granitic fraction AD-A under anaerobic conditions.

t [days]	K_d [mL/g]	sorbed Se [%]	pH	Eh (SHE) [mV]
1.0	0.2	1.7	8.41	-2
2.0	0.5	5	8.34	-33
4.0	0.5	4.4	8.21	3
7.0	0.7	6.9	8.16	-74
16.0	1.3	11.1	8.1	2
28.0	2.1	17	8.11	-21
56.0	2.1	17.7	8.14	80
84.0	2.1	17.2	8.06	-14
112.1	2.2	17.8	8.11	55

Table 7: Electrochemical properties and K_d values of sodium selenate on granitic fraction AD-A under anaerobic conditions.

t [days]	K_d [mL/g]	sorbed Se [%]	pH	Eh (SHE) [mV]
1.0	0.0	0.0	8.63	*
2.0	0.0	0.0	8.61	49
4.0	0.0	0.0	8.48	-31
7.1	0.0	0.1	8.31	50
14.0	0.2	1.9	8.17	73
29.0	0.1	1.2	8.07	*
56.0	0.1	0.6	8.03	-15
84.0	0.1	0.6	7.97	23
112.0	0.3	2.8	7.90	-20

* value wasn't measured due to technical problems

Table 8: Electrochemical properties and K_d values of sodium selenate on granitic fraction AD-B under anaerobic conditions.

t [days]	K_d [mL/g]	sorbed Se [%]	pH	Eh (SHE) [mV]
1.0	0.1	0.6	8.7	20
2.0	0.0	0.0	8.60	-37
4.0	0.0	0.2	8.48	134
7.2	0.0	0.0	8.47	-55
14.2	0.1	0.7	8.41	-7
28.0	0.2	1.5	8.17	19
60.0	0.0	0.0	8.21	80
86.0	0.8	7.3	8.20	90
119.0	0.2	2.3	8.14	12

Conclusion

The sorption of selenite and selenate onto crushed diorite Äspö was studied under aerobic and anaerobic condition as a function of grain size of diorite rock and aerobic/anaerobic conditions. The sorption of selenite was very low in case of both studied conditions and of both studied fractions. The influence of grain size of used sorbent was not observed, namely due to use of rather coarse fractions. The highest K_d -values of selenite were observed after 112 days of experiment: 1.6 mL/g (fraction AD-B) under aerobic conditions and 2.2 mL/g (fraction AD-A) under anaerobic conditions. K_d -values of selenate were converged to zero in case of both studied fractions and under both conditions.

Acknowledgement

The research leading to these results has received funding from the European Union's European Atomic Energy Community's (Euratom) Seventh Framework Programme FP7/2007-2011 under grant agreement n° 269658 (CROCK project).

References

- Byegard, J., Johansson, H., Skalberg, M. and Tullborg, E. L. (1998) The interaction of sorbing and non-sorbing tracers with different Äspö rock types. Technical Report TR-98-18, Swedish Nuclear Fuel and Waste Management Co.
- Carbol, P. and Engkvist, I. (1997) Compilation of radionuclide sorption coefficients for performance assessment. SKB rapport R-97-13, Swedish Nuclear Fuel and Waste management Co.
- Eichler, Š., Mestek, O. (2011) Speciační analýza selenu s využitím HPLC a ICP/MS pro výzkum distribuce selenu v bariérách jaderného úložiště. Chemické listy, 105, 24-26.

Eichler, Š., Vosmanská, M., Hofmanová, E., Koplík, R. and Mestek, O. (2012) Analýza anorganických specií selenu s využitím HPLC a ICP/MS pro sledování mobility selenu v inženýrských bariérách jaderného úložiště. *Chemické listy*, 106, 189-194.

Jan, Y. L., Wang, T. H., Li, M. H., Tsai, S. Ch., Wei, Y. Y. and Teng, S. P. (2008) Adsorption of Se species on crushed granite: A direct linkage with its internal iron-related minerals. *Applied Radiation and Isotopes*, 66, 14-23.

Jan, Y. L., Wang, T. H., Li, M. H., Tsai, S. Ch., Wei, Y. Y., Hsu, Ch. N. and Teng, S. P. (2007) Evaluating adsorption ability of granite to radioselenium by chemical sequential extraction. *Journal of Radioanalytical and Nuclear Chemistry*, 273, 299-306.

Papelis, Ch. (2001) Cation and anion sorption on granite from the Project Shoal Test Area, near Fallon, Nevada, USA. *Advances in Environmental Research*, 5, 151-166.

Puranen, A., Jonsson, M., Dahn, R. and Cui, D. (2009) Immobilization of selenate by iron in aqueous solution under anoxic conditions and the influence of uranyl. *Journal of Nuclear Materials*, 392, 519-524.

Rovira, M., Giménez, J., Martínez, M., Martínez-Lladó, X., de Pablo, J., Martí, V. and Duro, L. (2008) Sorption of selenium(IV) and selenium(VI) onto natural iron oxides: Goethite and hematite. *Journal of Hazardous Materials*, 150, 279-284.

Ticknor, K. V., Vandergraaf, T. T., McMurry, J., Boisvenue, L. and Wilkin, D.L. (1996) Parametric studies of factors affecting Se and Sn sorption. AECL EACL report TR-723, COG-95-554, Whiteshell Laboratories, Pinawa, Canada.

Vilks, P. (2011) Sorption of Selected Radionuclides on Sedimentary Rocks in Saline Conditions – Literature Review. TR-2011-12, Nuclear Waste Management Organization, Canada.

APPLICATION OF ELECTROMIGRATION METHOD ON LONG ROCK SAMPLES: DETERMINATION OF MIGRATION PARAMETERS (F_f , D_e)

Petr Vecernik¹, Vaclava Havlová^{1*}, Martin Löfgren²

¹UJV Rez, a. s., Hlavni 130, 250 68, Rez (CZ)

²Niressa AB, Stockholm (SWE)

* Corresponding author: hvl@ujv.cz

Abstract

Through-electromigration method (TEM) is an efficient method enabling successful determination of migration parameters (formation factor F_f and effective diffusion coefficient D_e). The method was successfully tested for Äspö diorite with rather low water accessible porosity around 0.2 %. Migration parameters (F_f , D_e), gained by both resistivity and through-electromigration methods, revealed a good consistency for 4 samples with different lengths. Effective diffusion coefficient D_e for I, used as a tracer, varied in the range of 1.1×10^{-14} - 4.6×10^{-13} $\text{m}^2 \cdot \text{s}^{-1}$. Formation factor $F_f(\text{TEM})$ reached values in the range 5.5×10^{-6} - 2.3×10^{-4} . The difference between the apparent formation factor F_f^a and $F_f(\text{TEM})$ decreased with increasing formation factor, presumably due to decreasing impact of surface diffusion. Such an observation was in clear consistency with previous measurements on samples from Forsmark and Oskarshamn. The overestimation of apparent formation factor F_f^a towards $F_f(\text{TEM})$ points towards proclaimed anion exclusion.

Introduction

Diffusion of radionuclides from fractures into adjacent altered or fresh rock is considered to be one of the important retardation processes for safety assessment of radioactive waste in a deep geological repository. Diffusion within crystalline rocks with low porosity (< 1 %) is a slow process that results in the need to use samples of limited length in the laboratory in order to receive results in reasonable time scales. The usage of short samples brings some contradictions: even though the experiments can deliver the results within a month, samples in fact do not represent real rock conditions, namely due to possible interconnections of pores that would not be connected in real rock massive. This causes increased pore connectivity and possible overestimation of laboratory diffusion results.

Moreover, it is known from the literature that the disturbed zone on the sample surface, produced by sawing and drilling, can extent up to 15 mm from the edge (Möri, 2008; results of LTD experiment in Grimsel Test Site), giving rise or increased tracer diffusivity through the sample. It was reported in the literature, that formation factor F_f decreases with increasing sample length (Valkiainen et al., 1996) as non-realistic connectivity vanishes with less disturbed samples. Electromigration methods (Löfgren, 2004; Löfgren and Neretnieks, 2006; Löfgren et al., 2009) enables speeding up laboratory diffusion experiments, gaining rock migration parameters (F_f , D_e) in relatively short times (hours). The aim of the study presented was to test the use of the apparatus, previously tested, for longer samples (10 – 100 mm) in order to obtain migration data for less disturbed rock and to study the dependence of migration parameters on sample length.

Theory

The theory of electromigration experiments has been based on through-electromigration (TEM) method, described in Löfgren (2004), Löfgren and Neretnieks (2006) and in Löfgren et al. (2009) where the methodology was applied in UJV Rez, a. s. labs. The details were presented in Vecernik et al. (2012).

Samples and experimental methodology description

Rock samples obtained and characterisation

For details of processing the samples from Äspö Hard Rock laboratory see Delivery 1.1.

Four discs (~45 mm diameter) with different length (10 mm, 30 mm and 100 mm) thickness were used for electromigration experiments. For sample identification see Table 1.

Samples from borehole KA2368A (AD-1, AD-3) were received as O₂ disturbed samples, i.e. samples that were not held under anaerobic atmosphere. Sample AD-31 (30 mm thick) and AD-100 were originally received in an autoclave, being held under Ar atmosphere. As transfer and operation of the electromigration cell into a glove box Ar controlled atmosphere is not possible, all the analyses and electromigration measurements were performed under oxic conditions.

Table 1: *Sample origin, identification and size.*

Sample	Borehole	Log No.	Borehole length (m)	Diameter (mm)	Length (mm)
AD-1	KA2368A-01	# 1.27	10.65-11.12	45.22	12.40
AD-3	KA2368A-01	# 1.27	10.65-11.12	45.25	11.45
AD-31	KA2370A-01	# 2.30	11.63-12.13	45.29	33.11
AD-100	KA2370A-01	# 2.30	11.63-12.13	45.31	99.20

Samples from both boreholes are Äspö diorite. Sample photos are presented on Figures 1, 2, 3, 4.



Figure 1: Sample AD-1 for electromigration measurement.



Figure 2: Sample AD-3 for electromigration measurement.



Figure 3: Sample AD-31 for electromigration measurement.



Figure 4: Sample AD-100 for electromigration measurement.

Sample saturation and porosity measurements

Rock samples were saturated using a vacuum saturation method, presented by Melnyk and Skeet (1986). The method determines the amount of connected pores that are available for water molecules.

Electromigration measurements

The TEM method was developed in cooperation with the author (Löfgren et al., 2009) and the UJV Rez, a. s. electromigration cell concept was carefully described in joint publication by Löfgren et al. (2009). In this arrangement the TEM cell consists of four compartments, as presented in Figure 5. The rock sample (usually 10 mm long) is placed in a special rubber seal and mounted between two compartments (200 ml). The apparatus was also tested for the longer samples (30 mm; Vecernik et al, 2012).

In 2012/2013 the system was updated in order longer samples can be used (see Figure 6 and 7). Even though the concept and the measurement procedure is still the same, the electromigration cell now consists of modular parts that enable emplacement of samples with different length (30–100 mm). Samples of 10 mm can be also measured, however longer samples are more suitable due to the apparatus length.

The procedure of through-electromigration (TEM) measurements, as it was presented in Vecernik et al., (2012), is applied for both systems and for all the samples. Both inlet and outlet compartments ($V = 200$ ml) were filled with 0.05 M NaCl. The potential gradient over the sample was gained by placing an electrode in each electrolyte and connecting the electrodes to a direct current power supply. To avoid the electrolysis at the anode and cathode, the electrodes are placed in separated compartments. Furthermore, the high and low pH electrolytes formed in the anode and cathode compartments are used to neutralise each other, by drop wise intermixing them.

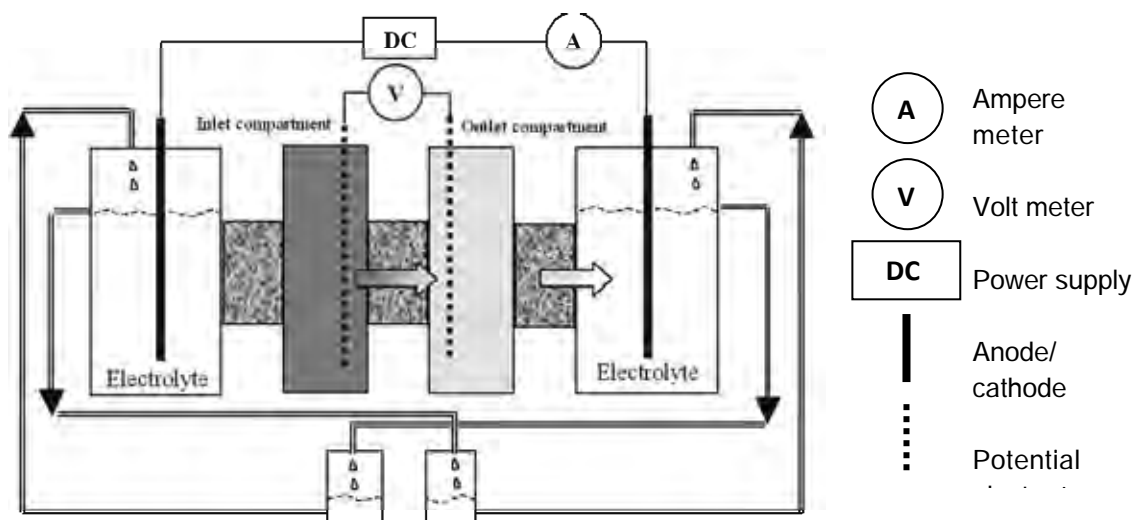


Figure 5: The scheme of through-electromigration cell. Reproduced from Löfgren et al., (2009).

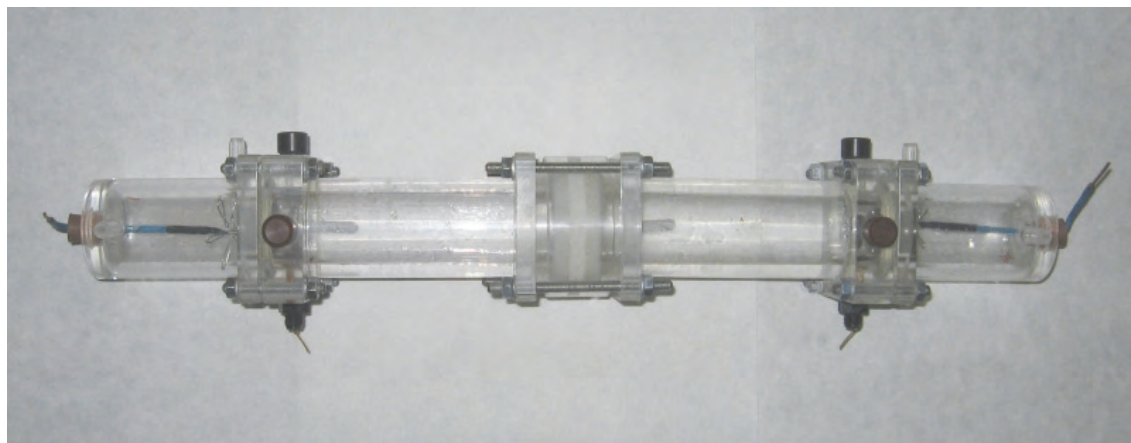


Figure 6: The photo of inlet compartment, outlet compartment and sample mounted between as a part of the through-electromigration apparatus (UJV Rez, a. s. concept; reproduced from Löfgren et al., 2009).

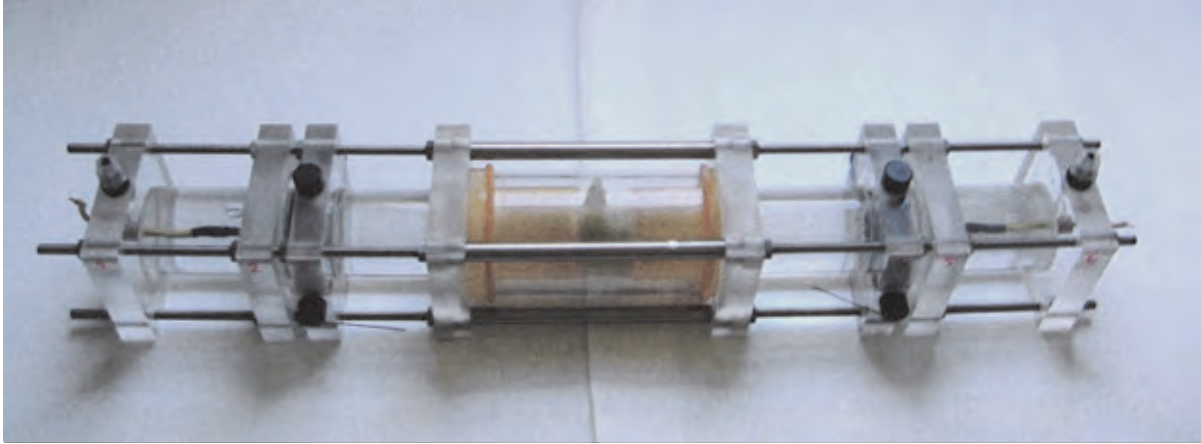


Figure 7: The photo of modified electromigration cell, enabling to use the samples of variable length (30 – 100 mm; UJV Rez, a. s. concept).

Current and voltage values are then collected, enabling calculation of resistivity value for saturated sample ρ_r ($\Omega\cdot\text{m}$). When resistivity ρ_r is constant in time, the apparent formation factor F_f^a can be calculated according to eq. 1.

$$F_f^a = \frac{\rho_w}{\rho_r} = \frac{\kappa_r}{\kappa_w} \quad \text{eq. 1}$$

where ρ_w is pore water (electrolyte) resistivity ($\Omega\cdot\text{m}$), κ_r is electrical conductivity of saturated sample ($\text{S}\cdot\text{m}^{-1}$) and κ_w is electrical conductivity of the electrolyte ($\text{S}\cdot\text{m}^{-1}$).

After the direct current (DC) measurement is terminated, the electrodes are connected with slight modification to alternating current (AC) circuit and F_f^a is calculated, following the same approach as reported above. The electrolytes are sampled afterwards from all compartments. Their pH and conductivity are measured.

Through-electromigration experiment with a tracer is possible to accomplish after system equilibration and resistivity stabilization. In this case I⁻ was used in the NaI form. Iodide corresponding to the concentration 0.005 M is inserted into high concentration reservoir ($t = 0$). The current and voltage measurements are performed in the same manner as presented above. In addition, the tracer concentration is measured in low concentration cell.

Using non-active I⁻, an ion selective electrode (Theta 90, CZ) is used for concentration measurement (measurement range 10^{-6} – 10^{-1} M; calibration from 10^{-6} – 10^{-4} M). The concentration increase is recorded with time. Assuming that tracer concentration increase is linear at steady state, the effective diffusion coefficient can be calculated. Afterwards, the formation factor F_f can be calculated, using eq. 2 and knowing tracer diffusion coefficient in free water D_w (e.g. Miller, 1983).

$$F_f = \frac{D_e}{D_w} \quad \text{eq. 2}$$

where F_f is TEM formation factor (-), D_e is effective diffusion coefficient ($\text{m}^2\cdot\text{s}^{-1}$), D_w is diffusion coefficient in free water ($\text{m}^2\cdot\text{s}^{-1}$).

As indicated above, the formation factor is not only estimated from the tracer breakthrough curve. It is also estimated by measuring the rock resistivity and electrolyte resistivity (see eq. 1). However, the rock resistivity is affected by so called surface conduction, which can be described as ionic conduction by cations in the electrical double layer at the pore walls. Such surface bound migration is not normally included in the concept of formation factor. Accordingly “formation factors” derived in this manner is called the apparent formation factor. By subtracting the contribution from surface conduction, the formation factor F_f can be estimated (Crawford and Sidborn, 2009).

$$F_f = F_f^a - \frac{\kappa_s}{\kappa_w} \quad \text{eq. 3}$$

where κ_s is surface conductivity ($\text{S}\cdot\text{m}^{-1}$)

Results

Porosity measurements

Porosity was calculated on the basis of measurements and methodology of Melnyk and Skeet (1986). The method also enables one to calculate sample density ($\text{kg}\cdot\text{m}^{-3}$). Porosity of AD-100 was not measured due to sample size that enabled to measure it on the same device as the previous samples. As the AD-100 is the joint sample to AD-31 we presume the same porosity.

Table 2: Porosity and density measurements for Äspö rock samples.

Sample	Porosity value (%)	Density ($\text{kg}\cdot\text{m}^{-3}$)
AD-1	0.22±0.01	2 650±60
AD-3	0.21±0.01	2 660±60
AD-31	0.29±0.01	2 741±62

Electromigration measurements

In Figures. 8, 9, 10 and 11 iodide breakthrough curves for the samples are presented, emphasizing the part at steady state condition for further F_f (TEM) and D_e (TEM) calculations. D_e was calculated from steady state part of the curve, using the procedure from Löfgren et al. (2009). The breakthrough curve for AD-100 has to be presented in different scale due to slower I transfer in the same time scale in comparison with other samples.

F_f was calculated according to eq. 2, using $D_w = 2 \times 10^{-9} \text{ m}^2 \cdot \text{s}^{-1}$ from Miller (1983). F_f^a was calculated from eq. 1. In Table 3 all formation factors are listed.

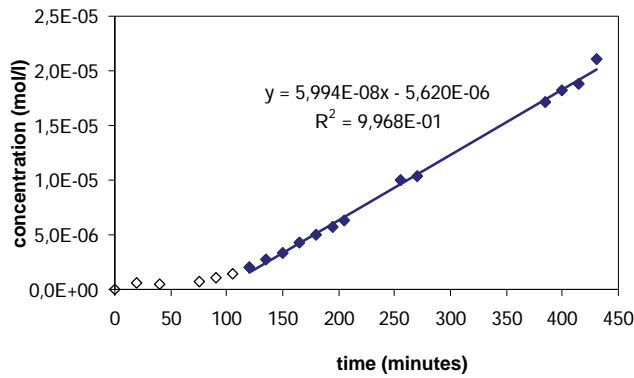


Figure 8: TEM experiment: Iodide breakthrough curve for sample AD-1 (10 mm length). Full diamonds represent steady state conditions.

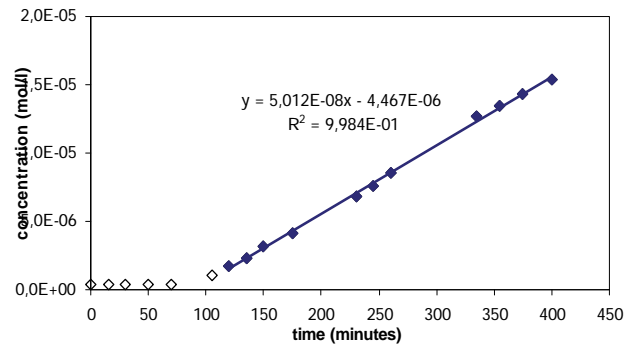


Figure 9: TEM experiment: Iodide breakthrough curve for sample AD-3 (10 mm length). Full diamonds represent steady state conditions.

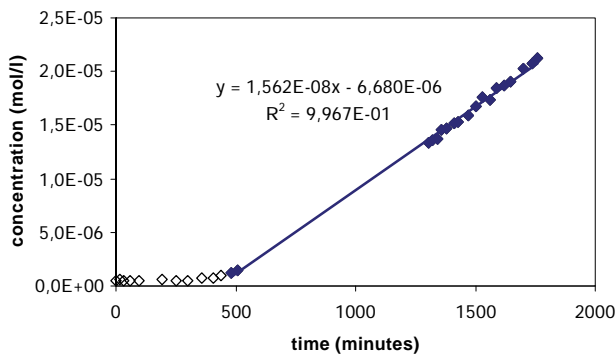


Figure 10: TEM experiment: Iodide breakthrough for sample AD-31 (30 mm length). Full diamonds represent steady state conditions.

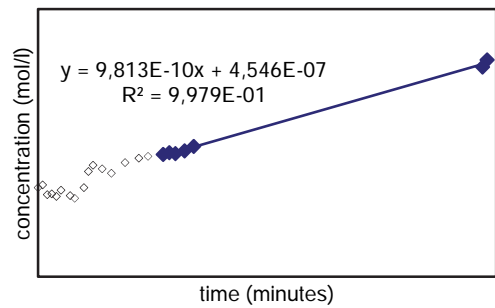


Figure 11: TEM experiment: Iodide breakthrough for sample AD-100 (100 mm length). Full diamonds represent steady state conditions.

Table 3: TEM Formation factor F_f and apparent formation factor F_f^a for samples from Äspö hard rock laboratory measured by electromigration methods.

Sample	AD-1	AD-3	AD-31	AD-100
D_e ($m^2 \cdot s^{-1}$)	4.64×10^{-13}	3.90×10^{-13}	2.70×10^{-13}	1.10×10^{-14}
F_f (TEM)	2.3×10^{-4}	1.8×10^{-4}	1.3×10^{-4}	5.51×10^{-6}
F_f^a (DC)	6.1×10^{-4}	5.70×10^{-4}	6.5×10^{-4}	1.78×10^{-4}
F_f^a (AC 10 Hz)	7.7×10^{-4}	7.4×10^{-4}	7.4×10^{-4}	1.56×10^{-4}
F_f^a (AC 100 Hz)	7.9×10^{-4}	7.5×10^{-4}	7.5×10^{-4}	1.61×10^{-4}
F_f^a (AC 1 kHz)	8.2×10^{-4}	7.8×10^{-4}	7.7×10^{-4}	1.68×10^{-4}
F_f^a (AC 2 kHz)	8.2×10^{-4}	7.8×10^{-4}	7.8×10^{-4}	1.69×10^{-4}

Discussion

Porosity measurements revealed that the Äspö diorite samples have rather low porosity (0.21 %).

Migration parameters (F_f , D_e), gained by both resistivity and through-electromigration methods, revealed decreasing trend for 4 samples with different lengths (see Table 3). Such behaviour was expected due to less disturbed character of long sample (100 mm). Effective diffusion coefficient D_e for anionic I varies within one order of magnitude (1.10×10^{-14} – 4.64×10^{-13} $m^2 \cdot s^{-1}$). The D_e value for the longest sample is one order lower than the diffusivity values for other samples (see Table 3).

Furthermore, the measured values of formation factors complemented the data, presented in Vecernik et al. (2012). F_f (TEM) was calculated from D_e . F_f^a were calculated, using DC and AC electrical circuits. The measurement confirmed overestimation of F_f by DC and AC measurements in comparison with TEM measurement, previously published in Löfgren (2004) or Löfgren et al. (2009). The trends are visible in Table 4 and on Figure 12. However, the value for F_f (TEM) for AD-100 sample was rather low (5.51×10^{-6}), almost two orders lower than for shorter samples. This should be re-evaluated as the sample measured was only one, even though slow tracer movement through the sample (Figure 11) pointed towards lower diffusion coefficient (see Table 3).

Comparing the F_f^a results for long sample AD-100 for AC and DC measurements, the differences between values are rather small ($\pm 0.13 \times 10^{-4}$). Relative uncertainty of 11.9% could be the reason that overestimation of F_f^a (DC) value in comparison with F_f^a (AC). The trend for other sample was opposite (see Table 3). However, it is clearly visible that the difference between the apparent formation factor F_f^a and F_f (TEM) decreased with increasing formation factor, most probably due to a smaller relative impact of surface conduction.

The overestimation of F_f^a towards F_f (TEM) for long sample AD-100 is rather high (up to factor 32), even comparing with Löfgren (2004) where samples with similar length were used (Forsmark granite, porosity ranging from 0.1–0.4 %). However, the high overestimation of F_f^a towards F_f (TEM) values might be explained by pronounced anion exclusion of I tracer in the pore system that can be more evident for longer sample than for

the shorter ones. The results confirm also the presumption by Löfgren (2004) that the overestimation factor could increase with decreasing formation factor (see Figure 12).

Table 4: Ratio of $F_f^a/F_f(TEM)$ under different measurement conditions.

Sample	AD-1	AD-1	AD-31	AD-100
DC	2.6	3.2	4.9	32.3
AC 10 Hz	3.3	4.1	5.5	28.4
AC 100 Hz	3.4	4.2	5.6	29.1
AC 1 kHz	3.5	4.3	5.7	30.4
AC 2 kHz	3.6	4.3	5.8	30.7

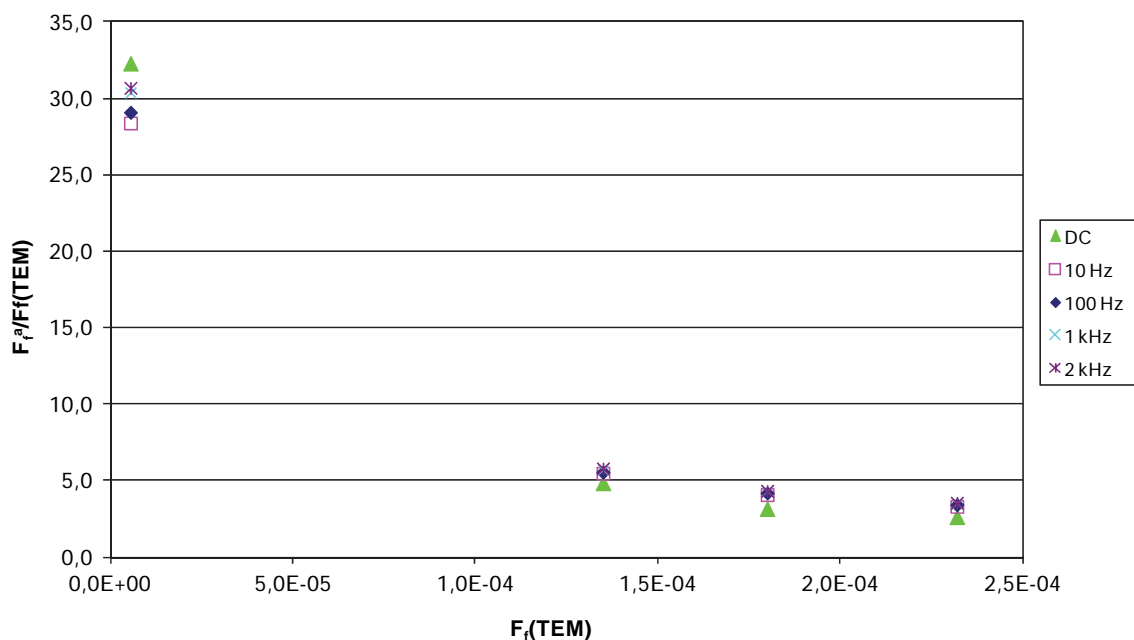


Figure 12: Ratio of apparent formation factor F_f^a to TEM formation factor F_f with increasing $F_f(TEM)$.

Using the electromigration method and anionic species, the influence of anion exclusion can be also studied, by using 3H . The results will be discussed in the poster by Havlová et al. (2013).

Conclusions

A modified electromigration apparatus was successfully tested for samples with different length under reference conditions. The experiments enable one to measure migration parameters (geometric formation factor F_f , apparent formation factor F_f^a and effective diffusion coefficient D_e for iodine), for Äspö diorite, even using samples with different length (10 mm, 30 mm, 100 mm). The results showed a rather consistent range of data, revealing differing migration parameters with sample length. However, one has to take into account that only a limited number of disc samples were available and therefore the data set is very small.

Formation factor F_f (TEM), determined by through-electromigration method with anion (I) tracer is important for performance modellers namely in comparison with F_f gained using conservative tracer (^3H), comparing the extent of anionic exclusion. Formation factor F_f^a gained by resistivity measurement is important namely for laboratory verification of in-situ resistivity measurement in boreholes.

Acknowledgement

The research leading to these results has received funding from the European Union's European Atomic Energy Community's (Euratom) Seventh Framework Programme FP7/2007-2011 under grant agreement n° 269658 (CROCK project) and from the Czech Ministry of Trade and Industry under the contract FR-TII/362.

References

- Crawford, J. and Sidborn M. (2009). Bedrock transport properties Laxemar. Site descriptive modelling SDM-Site Forsmark. SKB R-08-48, Svensk Kärnbränslehantering AB, Stockholm, Sweden.
- Havlová, V. and Vecernik, P. (2013). Diffusion of species through Äspö diorite. Poster, 1st Workshop Proceedings, 7th EC FP - CROCK CP, 22nd – 24th May 2012, Stockholm, Sweden.
- Löfgren, M. (2004). Diffusive properties of granitic rock as measured by in-situ electrical methods. Doctoral thesis, Royal Institute of Technology Stockholm.
- Löfgren, M. and Neretnieks, I. (2006). Through electromigration: A new method of obtaining formation factors and investigating connectivity. *J. of Contam. Hydrol.* 87, 237-252.
- Löfgren, M., Vecernik, P. and Havlová, V. (2009). Studying the influence of pore water electrical conductivity on the formation factor, as estimated based on electrical methods. SKB R-09-57, Svensk Kärnbränslehantering AB, Stockholm, Sweden.
- Melnyk, T. W. and Skeet, A. M. M (1986). An improved technique for the determination of rock porosity. *Can. J. Earth Sc.*, 23, 1068-1074.
- Miller, D.G. (1982). Estimation of diffusion coefficients of ions in aqueous solution. LLNL Report UCRL-533319. Lawrence Livermore National Laboratory, Livermore, California, USA.
- Möri, A. (2009). In situ matrix diffusion in crystalline rocks – An experimental approach. PhD thesis, University Bern.

Ohlsson, Y. (2000). Studies of Ionic Diffusion in Crystalline Rock. Doctoral thesis at the Royal Institute of Technology, Stockholm, Sweden. ISBN 91-7283-025-5.

Valkiainen, M., Alto, H., Lehtonen, H. and Uusheimo, K. (1996). The effect of thickness in through-diffusion experiments. Final Report, VTT Research Notes 1788, VTT Vuorimiehentie 5, Finland.

Vecernik, P., Havlová, V. and Löfgren, M. (2012). Determination of rock migration parameters (F_f , D_e): Application of electromigration method on samples of different length. S+T presentation. 1st Workshop Proceedings, 7th EC FP - CROCK CP, 22nd – 24th May 2012, Stockholm, Sweden.

URANIUM (VI) SORPTION ONTO ROCK SAMPLES FROM AREAS OF THE PROPOSED HLW AND SNF REPOSITORY IN RUSSIA (NIZHNEKANSKY MASSIVE)

Natalia Kuzmenkova¹, Vladimir Petrov^{2*}, Irina Vlasova², Vladislav Petrov³, Valery Poluektov³,
Stepan Kalmykov²

¹ Vernadsky Institute of Geochemistry and Analytical Chemistry, Russian Academy of Science, Moscow (RUSSIA)

² Lomonosov Moscow State University, Chemistry Department, Moscow (RUSSIA)

³ Institute of Geology of Ore Deposits, Petrography, Mineralogy and Geochemistry, Russian Academy of Sciences (IGEM RAS), Moscow (RUSSIA)

* Corresponding author: vladimir.g.petrov@gmail.com

Abstract

Rock samples from two areas of Nizhnekansky massive (Russia) have been studied in terms of mineralogical composition along with sorption of U (VI). Rock samples were crushed and sieved to size 1-2 mm. Results show insignificant differences between the samples in terms of sorption rate and pH-dependence. After 10-15 days 90-95 percent of uranium available was sorbed at pH of 5. The maximum sorption is observed at pH range from 4 to 8.

Introduction

It is decided that the Russia concept for high level wastes (HLW) and spent nuclear fuel (SNF) disposal is based on their isolation into the deep underground crystalline rock formations. Three candidate areas of the Nizhnekansky Granite Massive, namely “Kamenny”, “Itatsky” and “Eniseysky”, are considered as the most promising locations for the future HLW and SNF repository. Sorption properties of granites for various radionuclides are of great importance for evaluation of radionuclide migration through the granite body of the repository and, thus, for the Safety Case. In this work sorption behaviour of uranium (VI) onto granite samples from aforementioned areas is studied.

Experimental

Characterization

Core materials from two candidate areas (area **Kamenny**, drilling depth down to 700 m, and area **Itatsky**, drilling depth down to 500 m) have been studied in terms of petrographic and mineralogical characterization; definition of filtration, elastic, petro-physical and strength properties; and estimation of hydrothermal-metasomatic transformation of rocks.

Sorption experiments

Batch sorption experiments were performed in glove box with inert atmosphere (N₂) to exclude the possible speciation to U(VI) carbonate complexes. Sodium perchlorate was used as a background electrolyte (0.01 M). Initial concentration of uranium was 1·10⁻⁷ mol/L and isotope ²³³U (T_{1/2} = 1.59·10⁵ years) was used for liquid-scintillation counting. The solid to liquid ratio was 1:4. Rock samples were crushed and sieved. The fraction 1-2 mm was used.

Results and discussion

Characterization

Petrographic characterization of rock samples are summarized in Table 1. The intensity of metasomatic transformations for almost all samples is minor or absent. Only sample K-698.4 shows quite high transformation intensity that results in difference of structure and mineralogical composition in comparison with other samples. All samples from Kamenny area have lower content of dark minerals than from Itatsky area, contain potash feldspar and show higher intensity of low temperature hydrothermal-metasomatic transformations.

Sorption of U(VI)

Kinetics of U(VI) sorption onto investigated rock samples show similar behaviour. Maximum of sorption percentage (>90-95 %) is reached in 10-15 days for all samples. Dependence of uranium sorption on time is shown in Figure 1 for samples I-408.2 and K-106.8 from Itatsky and Kamenny areas, respectively. Similar dependencies were observed for other rock samples as well.

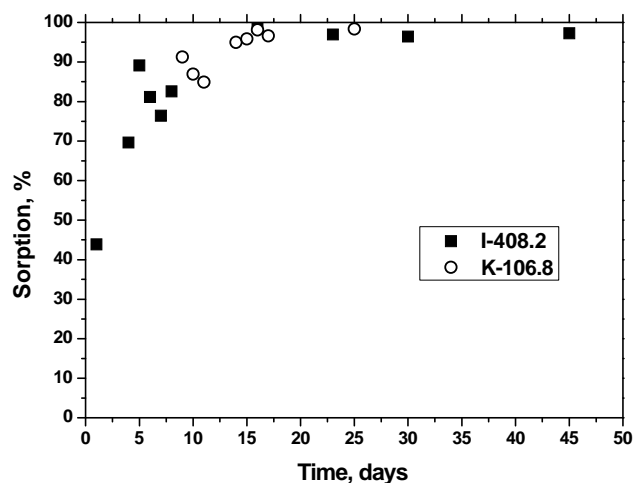


Figure 1: Sorption of U(VI) onto samples K-106.8 and I-408.2 versus time.

Table 1: Petrographic characterization of rock samples from Nizhnekansky massive

Sample	Rock	Structural (Str) and Textural (Tex) characteristic	Mineralogical composition* (%), Intensity of hydrothermal-metasomatic transformations (IHMT)
Kamenny area			
K-106.8	Biotite granodiorite	Str: massive, no gneissic elements. Tex: gipidyomorphogranular, weakly porphyritic grain size: 2-5 mm, >5, 10-40, unevenly granular	Bi>Hrb 15, Qtz 20, Pfs 20, Pl 45-50, Sph, NM, Chl, CM 5 IHMT-minimum
K-343.7	Leucocratic biotite granite	Str: massive, spotty, no gneissic elements Tex: granitic to porphyritic, locally poikilitic; grain size: 2-5 mm, unevenly granular	Bi, Chl 5, Qtz 30, Pfs 35-40, Pl 25, Ap, Zr, Chl, CM, Ser, NM 5 IHMT-medium
K-524.3	Biotite granodiorite - tonalite	Str: massive, locally banded Tex: hypidiomorphic, granular grain size: 1-2 mm, 2-5 mm unevenly granular	Bi, Chl 10-15, Qtz 15-20, Pfs 5-10, Pl 60, Ap, Zr, NM 2-3 IHMT-minimum
K-689.4	Metasomatic-altered spessartite	Str: massive, spotty Tex: microprismatic grained, microporphyritic, panidiomorphic, granular, metasomatic; grain size: <1 mm, evenly granular	Hrb, Px, Chl, Ep, CM 50-55, Ab, Fsp 35-40, Ap, Sph, NM 5 IHMT-medium
Itatsky area			
I-92.1	Quartz tonalite - biotite-hornblende diorite	Str: massive and gneissic. Tex: hypidiomorphic, granular, weakly porphyritic; grain size: 1-2 mm, 2-5 mm, unevenly granular	Bi>Hrb 15-20, Qtz 15, Pfs 5, Pl 55-60, Sph, NM, Zr 2-3 IHMT-0 (original rock)
I-239.9	Hornblende-biotite tonalite	Str: massive, no gneissic elements Tex: hypidiomorphic, granular; grain size: 1-2 mm, 2-5 mm, unevenly granular	Bi< Hrb, Ep 15, Qtz 20, Pfs 5, Pl 55-60, Sph, NM, Ap 5 IHMT-0 (original rock)
I-408.2	Hornblende diorite	Str: massive Tex: hypidiomorphic, granular; grain size: 1-2 mm, evenly granular	Bi<Hrb 30, Qtz 5, Pfs 5, Pl 55-60, Sph, Ap, NM, Zr 5 IHMT-minimum
I-501.8	Hornblende - biotite plagiogranite	Str: massive, with weak gneissic Tex: granitic to porphyritic; grain size: 1-2 mm, 2-5 mm, unevenly granular	Bi<Hrb 15, Qtz 25, Pfs 5-10, Pl 50-55, Ap, Sph, NM 2 IHMT-minimum

* Ab – albite, Ap – apatite, Bi – biotite, Chl – chlorite, CM – clay minerals (kaolin, illite, montmorillonite, et al.), Ep – epidote, Fsp – metasomatic non-transparent feldspars, Hrb – hornblende, NM – non-transparent minerals (magnetite, leucoxene, hematite), Px – piroxene, Pfs – potash feldspar (microcline, orthoclase), Pl – plagioclase, Ser – sericite, Sph – sphen, Qtz – quartz, Zr - zircon

Hexavalent uranium sorption dependencies on pH are shown in Figure 2 for the same samples K-106.8 and I-408.2 at different sampling times. Sorption increases with time in the whole investigated pH range. Shape of the observed pH-dependence of sorption onto I-408.2 sample is typical for U(VI): increase of sorption from acidic to near neutral pH region (pH >4), plateau from pH ~5 to ~8, further decrease of sorption due to hydrolysis of uranyl-cation. The average pH value of pore water for used rock samples is about 8 which is close to the decreasing edge of U(VI) sorption pH-dependence.

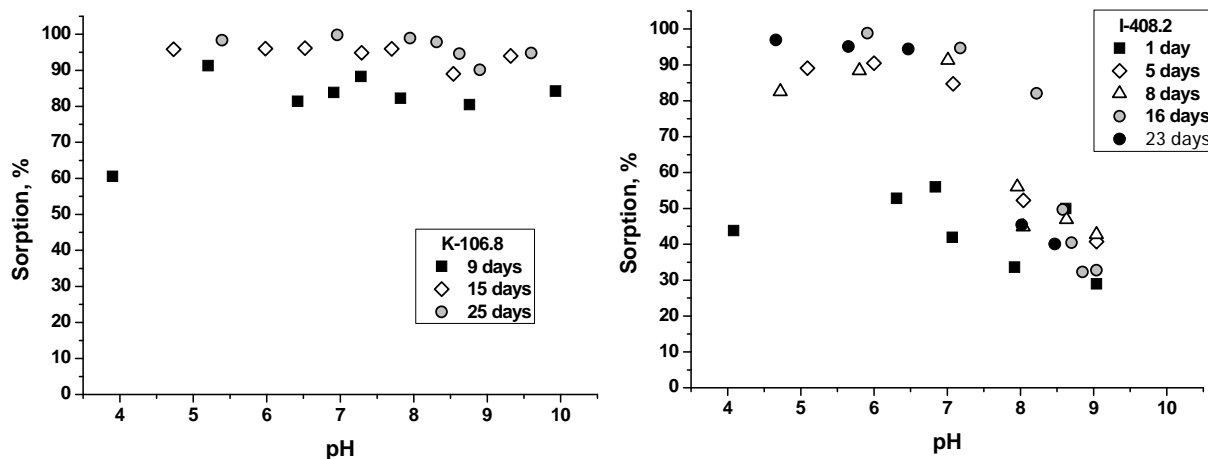


Figure 2: Sorption of U(VI) onto samples K-106.8 and I-408.2 versus pH.

Conclusions and Future work

Different rock samples from two sites of Nizhnekansky Granite Massive were characterized in terms of mineralogical composition. It was observed that all investigated samples have low metasomatic transformations. Sorption of U(VI) have similar time- and pH-dependencies with low deviations at pH values > 8 for all samples from Itatsky area. It was observed that in case of Kamenny area sorption doesn't decrease significantly till pH 10.

Experiments with sliced rock samples to determine minerals crucial for U(VI) sorption are ongoing. Further mathematical treatment of obtained data is required for application in U(VI) migration modelling.

Acknowledgement

This work was supported by the Ministry of Education and Science of Russian Federation (contract 14.U02.21.1527).

ANALYSIS OF SORPTION ONTO GRANITES AND GRANITE MINERALS: THE CASE OF CAESIUM

Tiziana Missana* and Miguel García-Gutiérrez

CIEMAT, Departamento de Medioambiente, Av. da Complutense 40, 28040, Madrid (ES)

* Corresponding author: tiziana.missana@ciemat.es

Abstract

During the CROCK project, a large Caesium sorption data set was obtained: Cs sorption onto granites and granite minerals of various origins was studied with the aim of evidencing the real degree of uncertainty of distribution coefficients and to improve the understanding of its retention in crystalline rocks. In all the tests, experimental conditions were kept as similar as possible, and the effects of several parameters (time, Cs concentration, pH and water salinity) were analysed.

Firstly, Cs retention was studied in several granites and an exhaustive study of Cs retention onto biotite, which is reported to be the most relevant sorbent mineral in granite, was performed. In the second part of the project, additional tests with muscovite, K-feldspar (FdK) and mixtures of quartz, plagioclase and K-feldspar (Q3) or quartz and plagioclase (Q2) were carried out. These tests were performed to establish the possible relevance of other mineral phases in contributing to Cs retention.

Introduction

The determination of a distribution coefficient (K_d) is needed to quantify the retention properties of a material, and to evaluate contaminant mobility in the environment. However, in heterogeneous materials, as granite, large discrepancies in retention data, obtained from different sources, still exist.

Crystalline rocks are envisaged as possible host rocks for deep geological repositories of radioactive waste, therefore a defensible choice of K_d values for the performance assessment of these repositories is needed. The sound estimation of retention parameters in granite strongly requires a better insight on radionuclide retention processes.

In the first part of the project, detailed analyses of Cs adsorption on several granites (Missana and Garcia, 2012a) and biotites (Missana and Garcia, 2012b) were carried out, considering both saline and low saline waters. Experimental conditions were kept as similar as possible in all tests to reduce experimental variability.

In all granites and biotites, Cs sorption showed a non-linear behaviour, small dependence on pH, and significant dependence on the ionic strength. This indicates ionic exchange as the most probable mechanism for Cs retention in these solids. A simplified three-site exchange model could satisfactorily fit all the experimental sorption isotherms and, in particular, the sorption behaviour as a function of Cs concentration that, in the case of Cs, is one of the main sources of K_d variability.

However, the quantitative differences in sorption values at a given concentration could not be explained by comparing the distribution coefficients. Therefore, in the present study, a comparison of sorption values normalized to the BET surface area and a specific analysis of the possible contribution of different minerals to Cs sorption in the crystalline rock has been done.

Experimental

Five different granite samples were used for the experiments reported here. Three come from the Grimsel Test Site (GTS, Switzerland): one comes from the FEBEX tunnel (from here to hereafter referred to as Grimsel FEBEX granite, *GFeb*, which corresponds to the central Äare type granite; the other two come from the MIGRATION tunnel, which corresponds to a granodiorite type and will be referred to hereafter to as Grimsel MIGRATION granite, *GMig*. A darker biotite-rich zone of this granite was identified and separately crushed to perform additional sorption tests: it is referred to as *b-GMig* granite. Two rock types are from Spain: the first is from Los Ratones mine, *Rat*, granite (Gómez, 2002) and the second from the El Berrocal site, *Ber*, granite (Miller et al, 2000). Additional tests were carried out with a set of granite minerals, i.e. biotite, muscovite, potassium feldspar (FdK), and mixtures of quartz, plagioclase and K-feldspar (Q3) or quartz and plagioclase (Q2).

The size fractions and the BET (Brunauer–Emmett–Teller) surface areas of these materials are summarized in Table 1. The average mineralogical compositions of granites used in this study are given in Table 2.

Table 1: Size fraction and BET area of the granites used in the experiments

Country of origin	Sample Name	Description	Size fraction (mm)	BET (m ² /g)
Switzerland	GFeb	FEBEX Granite, Fraction 1 (F1)	< 0.5	0.089±0.02
	b-GMig	MIGRATION Granite (black)	<0.064	4.097 ±0.005
	GMig	MIGRATION Granite	<0.064	2.871±0.005
Spain	RAT	RATONES Granite	< 1	0.488±0.005
	Ber	BERROCAL Granite	<0.5	2.780±0.005
	Biotite (RAT)	RATONES Biotite	<0.5	1.148±0.005
	Muscovite (B)	BERROCAL Muscovite	<0.5	0.402±0.005
	FdK	Potassium feldspate	0.125<x<0.250	8.001±0.005
	Q2	Quartz+plagioclase	0.125<x<0.250	1.290±0.005
	Q3	Quartz+plagioclase+FdK	0.125<x<0.250	1.089±0.005

In all sorption experiments, a simplified aqueous phase was used, simulating a low saline granitic groundwater: *low* saline water (LSW). The composition of this water is summarized in Table 3. In order to evaluate the solid-rock interactions, the compositions of waters after 1-month contact time with the solids were analysed. For Cs adsorption, the quantity of potassium in water can be very relevant; therefore it was specifically checked. Table 4 shows the potassium content in the LSW after 1-month contact time with all the solids used in the tests.

Table 2: Average mineralogical composition of the granites used in the experiments.

Country (%) Mineral	Switzerland		Spain	
	<i>GFeb</i>	<i>GMig</i>	<i>Rat</i>	<i>Ber</i>
Quartz	30-36	25-31	33-35	40-43
Plagioclase /Albite	19-23	26-32	29-32	28-31
K-Feldspar	31-37	22-26	26-28	15-18
Biotite /Chlorite	6-8	10-12	2-3	2-3
Muscovite	1-2	3-4	5-6	7-9

Table 3: Chemical composition of water used in the experiments.

Element (mg/L)	LSW
Na ⁺	8.3
Ca ²⁺	7
Mg ²⁺	<0.03
K ⁺	<0.03
Cl ⁻	28
SO ₄ ²⁻	<0.1
F ⁻	<0.1
Al	<0.03
Fe	<0.03
Cs	<0.02
Si	Nd
Alk (meq/L)	<0.05

The tracer used in this study was ¹³⁷Cs (as CsCl in 0.1 HCl). The half-life of ¹³⁷Cs is 30.2 years. The activity of Cs in solution was measured by γ -counting with a NaI detector (Packard Autogamma COBRA 2). Sorption isotherms were carried out under aerobic conditions, using a contact time of 14 days and at pH of 7 \pm 1.

From the initial aqueous solution, 10 mL were introduced in polyethylene centrifuge tubes and 100 mg of the rock/mineral was added. After the addition of the tracer, the pH was adjusted, if necessary. Tubes were maintained under continuous stirring and then they were centrifuged (26362g, 30 min). After the separation of solids, three aliquots of the supernatant from each tube were extracted for the analysis of final activity. The rest of solution was used to check pH.

Table 4: Potassium in LSW after 1 month contact with the solid.

SOLID	K ⁺ (mol/L)
GFeb-F1	8.5E-05
b-GMig	2.6E-04
GMig	2.5E-04
RAT	5.4E-05
Ber	5.1E-04
Biotite (RAT) obta	8.5E-05
Moscovite (B)	1.5E-05
FdK	3.3E-04
Q2	7.2E-05
Q3	1.5E-04

The distribution coefficients (ml/g) were calculated using this formula:

$$K_d = \frac{C_{S_{ADS}}}{C_{S_{FIN}}} \cdot \frac{V}{m} \quad \text{eq. 1}$$

where $C_{S_{ADS}}$ is the adsorbed Cs, $C_{S_{FIN}}$ the final concentration of Cs in the liquid phase, V the volume of the liquid and m the mass of the solid. The values were then normalized to the BET surface area (m^2/g) and expressed in cm.

Results and Discussion

Figure 1 shows the sorption isotherms obtained for the different granites. Data are represented as normalized $\text{Log}(K_d)$ values (with respect to the BET surface area) as a function of logarithm of aqueous Cs concentration at the equilibrium ($\text{Log}C_{S_{FIN}}$).

It is interesting that, at a given Cs concentration once sorption values are normalized to the BET area, they differ only within one order of magnitude, with the highest variation being at very low Cs loadings. At medium-high concentrations, the differences in $\text{Log}(K_d)$ tend to decrease (values are very similar), with the only exception being the *GFeb* granite.

Caesium adsorption is nonlinear, in all the cases, indicating the existence of more than one sorption site. The density of the first type of sorption sites (T1), predominating at the lowest Cs loadings, can be derived directly from the isotherms (when the first saturation is observed).

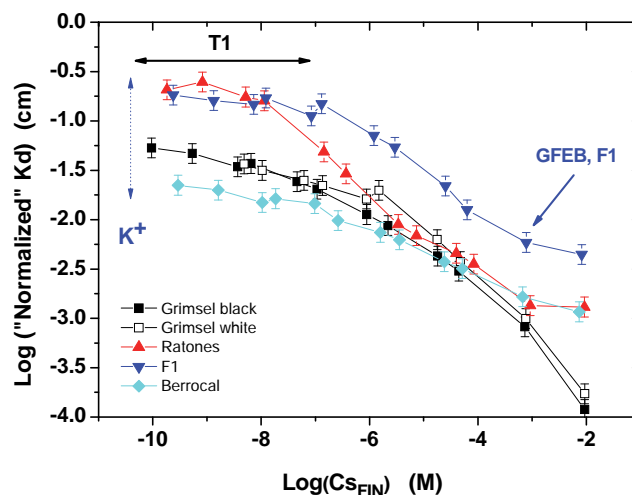


Figure 1: Caesium isotherms in different granites. K_d data normalized to the BET surface area.

T1 sites present low capacity but very high affinity for Cs (K_d values are the highest). T1 sites behave similarly to frayed edge sites (FES), present in micaceous materials to which cations like Cs^+ , K^+ , Rb^+ , Li^+ , NH_4^+ , present high selectivity.

Thus, is interesting to analyse the effects of the presence of potassium on Cs uptake, especially on T1 sites. Caesium is adsorbed following this order: $\text{Rat} \approx \text{GFeb} - \text{F1} > \text{GMig} > \text{Ber}$. This sequence nicely agrees with the inverse aqueous content of potassium (Table 4). Thus, at low Cs loadings, the main cause of variability on K_d values will be represented by potassium content in water.

At higher Cs loadings, the normalized sorption values are very similar in granites samples, with the exception of the *GFeb* granite. The *GFeb* sample shows slightly higher adsorption and a slight different shape in the isotherm.

By analysing one by one the sorption isotherms, it can be observed that the density of T1 sites is not the same in all granites. Particularly in *GFeb*, the density of T1 sites is clearly higher. The observed differences in Cs sorption between granites can be related to chemical/mineralogical differences in the rocks.

Figure 2 shows sorption isotherms of Cs for different minerals (muscovite, biotite, and potassium feldspar) as well as in (not quantified) mixtures of quartz and plagioclase (Q2) and quartz, plagioclase and potassium feldspar (Q3). In all mineral (and mixtures) Cs sorption is not linear.

A similar normalized K_d correlation to aqueous Cs concentration (within one order of magnitude) is observed between all studied cases. As already observed, the main differences are observed at a very low Cs concentration, due to potassium ion competition for sorption in high affinity sites, T1. Again, in general, higher Cs adsorption is observed in the presence of less potassium.

At medium-high loadings the normalized sorption values are similar for all the solids, with slightly higher values for those containing FdK. Furthermore, the density of T1 sites is clearly higher in the presence of potassium feldspar (FdK and Q3) and consequently the shape of the isotherms in the presence of this mineral is slightly different.

Thus, the small differences observed in the isotherms of *GFeb* granite are most probably caused by its highest FdK (31-37 %) content.

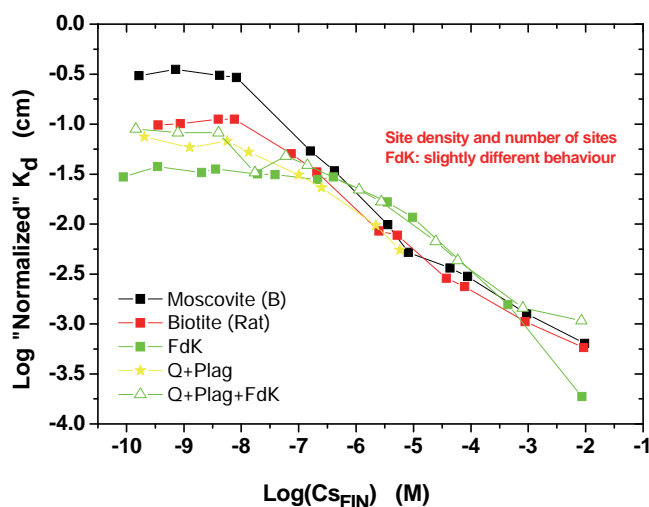


Figure 2: Caesium isotherms in different minerals. K_d data normalized to the BET surface area.

Conclusions and Future work

The adsorption of Cs in several different granites and granite minerals has been studied considering the effects of pH, ionic strength, Cs concentration (Missana and Garcia 2013). Caesium adsorption was non-linear, in all analysed materials, indicating the existence of more than one sorption site. The first type of sorption sites (T1), predominating at the lowest Cs loadings has low capacity but high affinity for the radionuclide. The capacity of these T1 sites is slightly different from a solid to another but significantly higher for potassium feldspar. Due to this fact, the shape of Cs isotherms in materials with higher content in potassium feldspar is visibly different.

Once the distribution coefficients in the different granites are normalized to the BET values, and plotted against varying Cs concentration, the K_d coefficient curves vary only within an order of magnitude. The major differences are found at very low Cs loadings, when competitive effects with potassium are very important. Similar considerations are valid also for minerals and mineral mixtures considered in this work.

At medium-high Cs loadings, the normalized sorption values are very similar, with the unique exception of the *GFeb* granite, which present the highest potassium feldspar content.

The determination of selectivity coefficients of Cs with respect to the main competitive ions K and Na is being carried out using exchanged materials at different ionic strengths. This study also will allow establishing the nature of Cs retention (pure ionic exchange or other complexation mechanisms).

Acknowledgement

The research leading to these results has received funding from the European Union's European Atomic Energy Community's (Euratom) Seventh Framework Programme FP7/2007-2011 under grant agreement N° 269658 (CROCK project)

References

Gómez, P. (2002). Impacto de la Mina Ratones (Albalá, Cáceres) sobre las aguas superficiales y subterráneas: modelización hidrogeoquímica. ENRESA Technical Report 06/2002.

Miller, W., Russel, A., Chapman, N., McKinley, J. C. and Smellie J. (2000). Geological Disposal of Radioactive Waste and Natural Analogues. Elsevier.

Missana, T. and García-Gutiérrez, M. (2012a). Comparison of the caesium adsorption on different crystalline rocks. First CROCK Workshop proceedings, KIT Scientific Reports 7629.

Missana, T. and García-Gutiérrez, M. (2012b). Analysis of caesium sorption behaviour on biotites of different origin. First CROCK Workshop proceedings, KIT Scientific Reports 7629.

Missana, T. and García-Gutiérrez, M. (2013). Summary of the experiments for the EC-CROCK Project. Caesium adsorption onto granite minerals. Technical Report CIEMAT/CROCK/1/2013.

RN MIGRATION IN A SINGLE FRACTURE FROM ÄSPÖ, SWEDEN: EXPERIMENTS AND REACTIVE TRANSPORT MODELLING

Florian Huber^{1*}, Paolo Trincherò³, Jorge Molinero³ and Thorsten Schäfer^{1,2}

¹Karlsruhe Institute of Technology (KIT), Institute for Nuclear Waste Disposal (INE),
P.O. Box 3640, 76021 Karlsruhe (GER)

²Institute of Geological Sciences, Department of Earth Sciences,
Freie Universität Berlin, Berlin (GER)

³Amphos21 Consulting S.L., Barcelona (ESP)

* Corresponding author: florian.huber@kit.edu

Abstract

In the context of nuclear waste disposal reactive transport modelling represents an important tool for long-term predictions of radionuclide migration. In this work, the computational tool FASTREACT (FrAmework for STochastic REActive Transport) (Trincherò et al., 2011) is applied which is able to solve for multicomponent reactive transport. This approach is tested for the first time to model experimental laboratory data on Np(V) migration experiments. For this, Np migration laboratory experiments have been conducted using a single fractured drill core from the Äspö Hard Rock Laboratory, Sweden.

Introduction

High level nuclear waste (HLW) as consequence of e.g. the energy production in nuclear power plants need to be stored safely over long time periods (several 100k years) since they represents a considerable menace to the biosphere due to their radio toxicity. Nowadays the disposal of this nuclear waste in deep geological formations is the preferred option. Crystalline rock, such as granites, are the preferred host rock formation in the Scandinavian countries Sweden and Finland for a high level nuclear waste disposal. Among the long lived fission products comprising the HLW, Np-237 represents an important constituent having half-life time of 2.1×10^5 a. The mobility of Np strongly depends on the environmental boundary conditions like e.g. pH and Eh which govern the aqueous speciation. Under oxidizing conditions and in absence of strongly complexing ligands like e.g. CO₃²⁻, Np forms the stable positively charged pentavalent neptunyl ion NpO₂⁺. Under these conditions Np is considered to be mobile in ground water since it does not possess a pronounced tendency to sorb as a result of its low charge. Due to its redox sensitivity Np can be transformed to lower oxidation states under reducing conditions. The reduction of Np(V) to Np(IV) is accompanied with a considerable decrease in solubility, significantly reducing the mobility (Bondietti and Francis, 1979).

In the framework of safety assessments for geological disposal of high nuclear waste, large scale interdisciplinary models are powerful tools aiming at supporting regulatory decision making as well as providing input for repository engineering activities. Striking aspects of these kinds of models are their very large temporal and spatial modelling scales (the former spanning from thousands up to one million years, the latter covering areas of several square kilometres) and the need to integrate different processes, which in turns take

place over different scales. It turns out that these kinds of models may be very computationally demanding and often unfeasible. This is precisely the case for reactive transport models, which need to simultaneously account for the effects of physical heterogeneity and complex nonlinear reactions (e.g., mineral dissolution and precipitation, adsorption and desorption, microbial reactions and redox transformations). This problem is usually overcome by adopting a compromise: either (1) defining simplified geometries (e.g., representative vertical cross-sections, in the best of the cases) with a detailed description of geochemical processes; or (2) carrying out complex three-dimensional flow models with simplified geochemical formulations (usually Kd-based).

In this work, we present a computational tool that aims at solving multicomponent-reactive transport problems with a computationally efficient approach where complex systems are reduced to sets of one-dimensional models. This approach is tested on experimentally determined Np(V) laboratory migration data through a natural fracture in an Äspö diorite drill core.

Materials & Methods

Migration experiments

All experiments have been conducted in a glove box under Ar atmosphere ($O_2 \sim 1-2$ ppm) at room temperature ($\sim 21^\circ C$). In the present study natural Grimsel ground water (GGW) was used which was stored in Teflon coated aluminium barrels under argon atmosphere previous to the experiments. Water chemistry was analysed via ICP-MS and colloid concentrations determined by laser induced breakdown detection (LIBD). The chemical composition is listed in Table 1. The Grimsel ground water represents a low mineralized, meteoric ground water which possesses a low ionic strength of about ~ 1 mM and is therefore suitable to mimic a possible melt-water intrusion scenario in the Äspö system. Both Eh and pH measurements were conducted yielding values of +150 - +200 mV and 9.6 respectively. Prior to the experiments the drill core was “equilibrated” by flushing GGW through the core over a duration of ~ 6 weeks. The data presented in Table 1 also documents that the “equilibration” step was sufficient to establish hydro-chemical conditions very similar to the Grimsel ground water in the Äspö core. However, the concentration of divalent cations is higher in the core effluent compared to the inlet solution, which indicates that e.g. cation exchange processes and/or dissolution processes are still ongoing.

A radionuclide cocktail was prepared in a glove box under Ar atmosphere on basis of natural Grimsel ground water. Among several other radionuclides present in the cocktail, only the results for $^{237}Np(V)$ are presented here. A $^{237}Np(V)$ concentration of $\sim 1.25 \times 10^{-6}$ M has been used in the radionuclide cocktail. As conservative tracer tritium (HTO) was used. The pH and Eh were measured in the cocktail yielding values of 9.6 and an Eh of $\sim +50$ mV, respectively. For the pH measurements a semi-micro Ross electrode (81-03, Orion Co.) coupled to a digital pH meter (720A, Orion Co.) was applied. At least 4 buffers have been used to calibrate the electrode prior to the measurement. A Pt combined electrode (Metrohm) was used for determining the redox potential in the cocktail. Since the cocktail contained redox sensitive elements, like e.g. Np which are prone to eigencolloid formation, an aliquot of the cocktail was ultracentrifuged for 1h at 90'000 rpm (Beckman Coulter, XL-90, rotor-type 90Ti) to check for any colloidal phases. Only 0.1% (Np) of the total concentration in the cocktail may be present as colloidal phase.

Table 1: Chemical composition of the Äspö GW, Grimsel GW and Grimsel GW after different contact times to the fracture within the equilibration phase of the core.

	Äspö GW	Grimsel GW (barrel #3) (MI shearzone)	Grimsel GW (sample CFMH1-0c) (MI shearzone)	Grimsel GW Contact core #8	Grimsel GW Contact core #8
	Sep.-Nov. 2007	22. May 2007	12. Febr. 2008	4. March 2008	1. April 2008
pH	7.5 ± 0.1	9.6	9.67	9.89	9.8
E _{h(SHE)}	~ 62 ± 20 mV	-170mV	n.d.	~ +154mV	~ +203mV
[Mg ²⁺]	76.4 mg·L ⁻¹	14.1 µg·L ⁻¹	12.6 µg·L ⁻¹	36.3 µg·L ⁻¹	46.7 µg·L ⁻¹
[Ca ²⁺]	0.87 g·L ⁻¹	5.4 mg·L ⁻¹	5.3 mg·L ⁻¹	9.0 mg·L ⁻¹	9.4 mg·L ⁻¹
[Fe ^{2+,3+}]	< D.L.	< D.L.	< D.L.	< D.L.	< D.L.
[Mn ²⁺]	532 µg·L ⁻¹	23.2 µg·L ⁻¹	< D.L.	2.86 µg·L ⁻¹	1.25 µg·L ⁻¹
[Sr ²⁺]	15.4 mg·L ⁻¹	197 µg·L ⁻¹	181.5 µg·L ⁻¹	285.1 µg·L ⁻¹	290.2 µg·L ⁻¹
[Cs ⁺]	3.5 µg·L ⁻¹	n.d.	0.79 µg·L ⁻¹	0.64 µg·L ⁻¹	0.31 µg·L ⁻¹
[La ³⁺]	0.03 µg·L ⁻¹	n.d.	< D.L.	< D.L.	< D.L.
[U]	0.35 µg·L ⁻¹	n.d.	n.d.	0.098 µg·L ⁻¹	0.128 µg·L ⁻¹
[Al ³⁺]	9.2 µg·L ⁻¹	126.8 µg·L ⁻¹	42.9 µg·L ⁻¹	29.9 µg·L ⁻¹	64.7 µg·L ⁻¹
[Na ⁺]	1.2 g·L ⁻¹	12.9 mg·L ⁻¹	14.7 mg·L ⁻¹	50.3 mg·L ⁻¹	53.7 mg·L ⁻¹
[Cl ⁻]	4.9 g·L ⁻¹	5.3 mg·L ⁻¹	6.7 mg·L ⁻¹	n.d.	10.6 mg·L ⁻¹
[Si]	4.9 mg·L ⁻¹	4.2 mg·L ⁻¹	5.6 mg·L ⁻¹	8.9 mg·L ⁻¹	9.3 mg·L ⁻¹
[SO ₄ ²⁻]	268 mg·L ⁻¹	5.0 mg·L ⁻¹	5.8 mg·L ⁻¹	n.d.	8.8 mg·L ⁻¹
[F ⁻]	1.3 mg·L ⁻¹	5.9 mg·L ⁻¹	6.3 mg·L ⁻¹	n.d.	10.3 mg·L ⁻¹
[Br ⁻]	n.d.	n.d.	n.d.	n.d.	n.d.
[NO ₃ ²⁻]	< D.L.	< D.L.	< D.L.	n.d.	< D.L.
[HCO ₃ ⁻]	125.6 mg·L ⁻¹	4.5 mg·L ⁻¹	3.0 mg·L ⁻¹	n.d.	n.d.

The core used in this study comes from a drill hole (KOV01) in Oskarshamn (Sweden) from 774.7-775.2 drill core length. Prior to characterization the core was sealed on the outside by sticking it in a custom made Plexiglas column (Figure 1). To gain information about geometry and orientation of the fracture, total porosity and fracture aperture distribution, the drill core was scanned using X-ray computed tomography (CT). For a detailed description of the drill core used in the migration experiments see (Huber et al., 2012). Here only a brief description is presented. The spatial dimensions of the core are 0.1352 m in length and 0.5048 m in diameter.

The experimental setup used in the migration study is depicted in Figure 1. The drill core was equipped with fittings at the inlet and outlet and connected to a pump. The continuity of the water flux was checked independently using a balance collecting the eluted fluid volume. All tubing, valves and fittings used in the migration setup were made of PEEK (Upchurch Scientific) material to exclude any unwanted RN sorption. A possible metal ion sorption onto the PEEK tubing was tested and found to be negligible. Pulse injection of the

RN cocktail was done by means of an injection device with a volume of 1 mL. Samples of the effluent were collected with a fraction collector (Gilson, FC203b). Subsequently, aliquots of every sample collected was diluted in 2% HNO₃ (Merck, ultrapure) for elemental analysis by inductively-coupled mass spectrometry (ICPMS) (PerkinElmer Elan 6100). Sample evaporation due to unavoidable exposure of the open samples vials in the fraction collector to the Ar atmosphere for some time (a maximum of a few hours) were found to be of no concern.

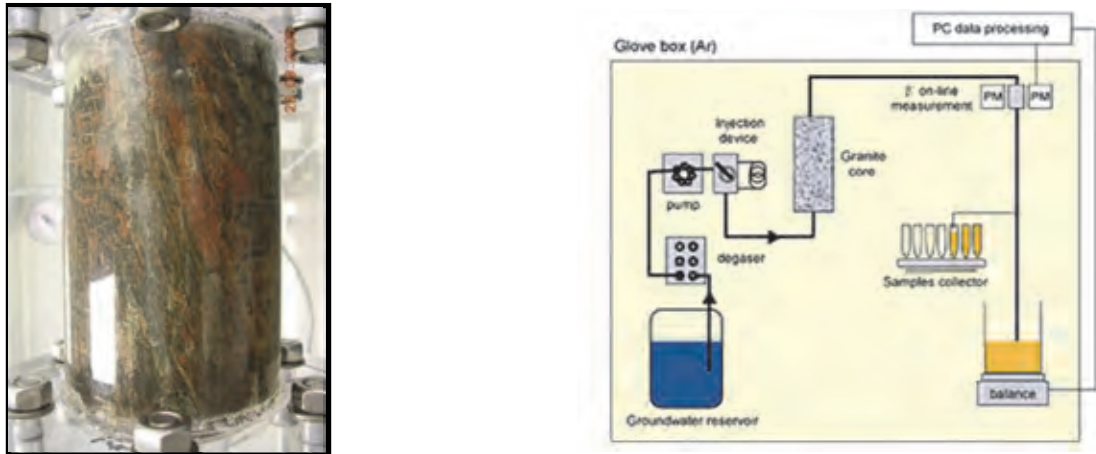


Figure 1: Left: The fractured diorite drill core used in the experiments. Right: Setup of the migration experiments.

HTO was diluted in Ultima Gold scintillation cocktail (PerkinElmer) and measured by liquid scintillation counting (LSC) whereas Np concentration was determined with inductively-coupled mass spectrometry (ICP-MS). Two experiments have been carried out to test the reproducibility of the results. The flux in both experiments was 50 $\mu\text{L}/\text{min}$.

Theoretical background and methodological approach

The FASTREACT approach is founded on the theory of Stochastic-Convective (SC) models (Shapiro and Cvetkovic, 1988) assuming steady state fluid flow and neglecting local-scale dispersion. Under the given assumptions, a complex 3D transport problem can be reduced to a set of streamlines which can be treated independently (Cirpka and Kitanidis, 2000). Disregarding local-scale dispersion assumes that no mass is exchanged between adjacent streamlines consequently limiting this approach to advection dominated systems (Peclet numbers > 1). The stream tube approach makes it attractive for the solution of reactive transport problems since it is computationally less expensive to solve for a set of 1D models than for a multidimensional model.

The application of FASTREACT involves a step-wise process described as follows:

- Infer travel time probability density functions (PDF) at given control locations for streamlines in the system to be modelled. This is usually done using particle tracking simulations on existing flow fields
- Parameterization and calculation of a reference 1D reactive transport simulation
- Coupling between the reference simulation and the set of streamlines

The computation of the breakthrough curve at a given control plane is done in FASTREACT as follows (eq. 1):

$$C^f(t) = \frac{1}{Q} \sum_{i=1}^{n_p} (Q_{inj}/n_p) c_i(t, \tau_i) = \frac{Q_{inj}}{Q} \frac{\sum_{i=1}^{n_p} c_i(t, \tau_i)}{n_p} \quad \text{eq. 1}$$

where c_i is the concentration at the intersection between the i -th streamtube and the control plane, and τ_i is the related travel time.

The equation can be rewritten in terms of probability as (eq.2):

$$C^f(t) = \frac{Q_{inj}}{Q} \sum_{i=1}^N c(t, \tau_k^{RS}) p(\tau_k^{RS}) \Delta\tau \quad \text{eq.2}$$

where $p(\tau_k^{RS})$ and $\Delta\tau$ are the probability of residence time τ_k^{RS} and the time-bin width respectively and N is the number of nodes of the reference simulation. For further details on the mathematical formalisms used in FASTREACT the reader is referred to the literature .

Conceptual geochemical models

Ideally, results of particle tracking simulations on an existing flow field should be equivalent to the experimental conservative tracer breakthrough curve. The available 3D fracture flow model of the Äspö diorite core (Huber et al., 2012) was used in the particle tracking simulations in this study but failed in reproducing the tracer breakthrough perhaps due to different boundary conditions between the experiments and the model (e.g. in the spatial distribution of tracer injection at the fracture inlet). It was thus decided to fit a probability density function (PDF) to the conservative tracer breakthrough curve to obtain a travel time distribution of the particles needed in the next step of the FASTREACT modelling. For the reference 1D reactive transport simulation the geochemical code PhreeqC (Parkhurst and Appelo, 1999) was used. In the last step the results of the 1D reference simulation and the travel time PDF are coupled to obtain the temporal evolution of the geochemical parameter of interest (in this case the Np concentration and thus the Np breakthrough curve) at the desired reference plane (here the outlet of the fracture).

To model the Np reactive transport we tested different approaches with increasing complexity ranging from simplified K_d based sorption models (first order reversible sorption/desorption kinetics) to more complex, mechanistically based surface complexation models (SCM) (Wang et al., 2001) for sorption of NpO_2^+ onto one ($\text{Fe}_2\text{O}_3 \cdot 2\text{H}_2\text{O}$ (HFO)), two (HFO and biotite (Bt)) and three (HFO, Bt and kaolinite) mineral phases (see Table 2 and 3 for further information on the surface complexation models). First, the surface distribution coefficient K_a is derived from the experimental Np breakthrough curve using eq. 3 (Wels et al., 1996):

$$R_f = 1 + a_w K_a \quad \text{eq. 3}$$

here a_w is the flow wetted surface area [m^2/m^3] and K_a is the surface distribution coefficient [m]. The retardation factor R_f is determined by the ratio of the Np peak maximum elution time and the HTO peak maximum elution time yielding a value of 1.8. The flow-wetted surface area describes the ratio of total surface area of the fracture [m^2] to the total volume of the fracture [m^3]. From the fracture surface area (0.01165 m^2) and fracture volume (2.7 mL) determined by (Huber et al., 2012) one obtains a value of 4307 [m] for a_w . By rearranging eq.1 a K_a value of 0.18 [l/m^2] is obtained.

Next, PhreeqC batch models have been set-up reproducing the experimental K_a . Since the K_a values calculated using the surface area derived from the μ CT measurements of the drill core used in this study is too low (the actual *reactive* surface area of the fracture is unknown) it was decided to use it as fitting parameter by coupling FASTREACT/PhreeqC to the parameter estimation code PEST (Gallagher and Doherty, 2007). Multiple batch models have then been used to simulate the reactive transport for the given geochemical conditions (e.g. one or more mineral phases as mentioned above). In case of the first-order reversible sorption/desorption kinetics model, the sorption and desorption rate was fitted. The sorption and desorption reactions in this approach are described as given in eq. 4:

$$s = K_D \times c \text{ and } K_D = k_f/k_r \quad \text{eq.4}$$

Where s is the sorbed concentration (mol/L), K_D is the distribution coefficient [-], c is the dissolved concentration, k_f is the forward reaction rate (sorption) and k_r is the backward reaction rate (desorption).

Table 2: Thermodynamic constant for the speciation used in the surface complexation models.

Aqueous reaction	log K
$\text{NpO}_2^+ + \text{H}_2\text{O} = \text{NpO}_2\text{OH} + \text{H}^+$	-8.9
$\text{NpO}_2^+ + 2\text{H}_2\text{O} = \text{NpO}_2(\text{OH})_2^- + 2\text{H}^+$	-23.0*
$\text{NpO}_2^+ + \text{CO}_3^{2-} = \text{NpO}_2\text{CO}_3^-$	4.6
$\text{NpO}_2^+ + 2\text{CO}_3^{2-} = \text{NpO}_2(\text{CO}_3)_2^{3-}$	7.0
$\text{NpO}_2^+ + 3\text{CO}_3^{2-} = \text{NpO}_2(\text{CO}_3)_3^{5-}$	8.5
$\text{CO}_3^{2-} + \text{H}^+ = \text{HCO}_3^-$	10.33
$\text{CO}_3^{2-} + 2\text{H}^+ = \text{H}_2\text{CO}_3$	16.67
$\text{Na}^+ + \text{CO}_3^{2-} = \text{NaCO}_3^-$	0.51
$\text{Na}^+ + \text{H}^+ + \text{CO}_3^{2-} = \text{NaHCO}_3$	10.48

Equilibrium constants are taken on thermodynamic data from Data0.comV8.R6 file of the EQ3/6 database. * constant taken from (Fuger, 1992)

Table 3: Surface complexation models used in the study.

Solid phase	BET [m ² /g]	log K ₊ ^a	log K ^a	log K ₁ ^b	log K ₂ ^b	log K ₃ ^b
ferrihydrite	600	7.29	-8.93		-2.72	
biotite	7.5	8.33	-9.73			-11.60
			-7.20		-4.17	
kaolinite	24.5	8.33	-9.73		-4.04	
			-7.20	4.09		

A site density of 2.31 sites/nm² is assigned to all solid phases. ^a Acidity constants taken from (Turner and Sassman, 1996). ^b Binding constants K₁-K₃ correspond to the following surface reactions (M^{z+} = NpO₂⁺): K₁, ≡XOH-M^{z+}; K₂, ≡XOH + M^{z+} = XO-M^(z-1) + H⁺; K₃, ≡XOH + M^{z+} + H₂O; table modified after (Wang et al., 2001).

Results and Discussion

Figure 2 depicts the experimental cumulative breakthrough curves for Np in conjunction with the model results. Np shows a complex migration behaviour in the experiment reflected by the shape of the breakthrough curve. As shown in Figure 2, the peak maximum of Np is shifted to later times compared to HTO. A retardation factor of ~1.8 is derived from the breakthrough curve (BTC) for Np. The shape of the Np BTC shows a steep rising edge of the BTC followed by a pronounced tailing which is still on-going after the stop of the experiment. Np migration seems to be influenced by an interaction with the fracture surface leading to a retardation. According to the Np speciation under the geochemical conditions prevailing in the experiment, the retardation of Np may be explained by sorption processes of the positively charged NpO₂⁺ with the negatively charged fracture surface. Regarding the surface charge of the diorite, we conducted streaming potential measurements on the Äspö diorite yielding zeta-potentials of ~ -55 mV at a pH of ~9.7. Np recovery is ~76% at the end of the experiment, but the tailing seems to be still ongoing thus a quantitative Np recovery is reasonable to expect. The high Np recovery is in line with measured Eh values (~ +200 mV) of the effluent solution and thermodynamic modelling using the constant by (Wang et al., 2001) yielding no Np reduction and NpO₂⁺ (~55%) (and NpO₂CO₃⁻ (43%)) as dominating species which is known to sorb only weakly. Several migration laboratory studies in fractured media have shown the weakly sorbing properties of the free neptunyl ion evidenced by high recoveries (Roemer et al., 2002; Vandergraaf et al., 1996; Vejmelka et al., 2000; Vejmelka et al., 2001). In contrast, Np migration studies in Äspö diorite under Äspö ground water conditions and much higher residence times (Kienzler et al., 2009) found very low recoveries referred to a reduction of Np(V) to Np(IV) due to the strongly reducing conditions in the ground water applied.

Results of the FASTREACT modelling exercise are shown in Figure 2 for HTO and in Figure 3 for Np. The experimental HTO BTC is captured well by FASTREACT due to the fitting of the PDF.

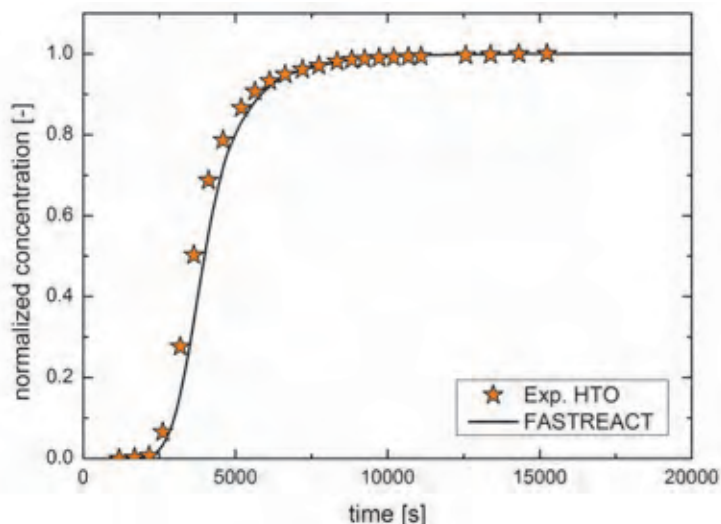


Figure 2: Simulated HTO breakthrough curve by FASTREACT using the fitted PDF in comparison to the cumulative experimental HTO breakthrough curve (orange stars).

It is obvious that by using the K_a derived from the migration experiments ($K_a = 0.18$) in the different SCM models (Figure 3 (left)), it is not at all possible to adequately describe the Np BTC. While the position of the peak maximum is captured relatively well the models completely fail both in describing the Np BTC peak concentration and tailing. Due to the strong sorption properties of HFO and the low sorption capacities of biotite the results of the 1-mineral-model and the 2-mineral-model are very equal to each other, whereas the 3-mineral-model shows some deviation to the other two models as a consequence of the additional sorption capacity of kaolinite which is stronger than biotite and weaker than the HFO. All three models dramatically overestimate the maximum peak concentration and do not show any pronounced tailing.

In case of the 1st order kinetic model, the model fit describes the ascending part of the curve quite well, and also shows a pronounced tailing (Figure 3 (right)) but the overall fit is again not satisfactory. Moreover, no process understanding may be gained by this approach since no mechanistically process description of the sorption processes is applied.

Since the actual reactive surface area of the core is unknown PEST is used to fit the surface area (which correlates to the total number of sorption sites) trying to improve the SCM model results. Figure 3 (right) depicts the first results of the fitting exercise for the 1-, and 2-mineral model, respectively. The results are fitting the experimental data better compared to the model results without the adjustment of the surface area but are still not matching the experimental BTC satisfactorily. The final 3-mineral-model may further increase the results based on preliminary results but it is still in progress. Regarding the pronounced tailing of the Np breakthrough curve it seems likely that a kinetic description of the sorption and desorption process is necessary. It is a well-known fact that the desorption process often shows slower kinetics which in consequence lead to solute retardation and pronounced tailing of breakthrough curves. Regarding the relatively high flux ($50\mu\text{L}/\text{min}$) in the experiments it seems reasonable that no equilibrium between the sorption and desorption step has been reached within the experimental duration causing the observed tailing in the breakthrough curve. Since PhreeqC is only able to treat the SCM applied as an equilibrium process, it is not possible to describe the different kinetic rates for the sorption and desorption step as it may be the case for the Np migration behaviour in our experiments. To tackle this problem a further option to be tested in the modelling exercise is the coupling of

FASTREACT to the reactive transport code HBGC123D (Gwo et al., 2001) with which the SCM can be treated in a kinetic way rather than as an equilibrium process as used so far.

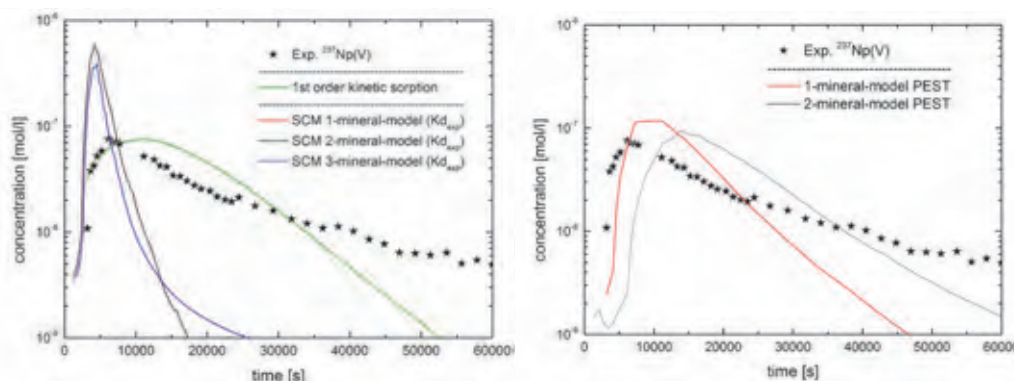


Figure 3: Left: Comparison between experimental Np breakthrough curve and model results on basis of the experimentally derived K_d . Note that the 1-mineral-model and the 2-mineral model are giving the same results. Right: Results of the FASTREACT/PEST fitting for the 1- and 2-mineral-model, respectively.

To sum up, the FASTREACT approach coupled to PhreeqC has been shown to represent an effective computational tool for the interpretation of complex reactive transport simulations taking into account real fracture geometry.

Acknowledgement

The authors gratefully acknowledge the funding received from the European Union's European Atomic Energy Community's (EURATOM) Seventh Framework Program FP7/2007-2011 under grant agreement n° 269658 (CROCK project).

References

- Bondietti, E.A. and Francis, C.W. (1979). Geologic Migration Potentials of Technetium-99 and Neptunium-237. *Science*, 203(4387), 1337-1340.
- Cirpka, O. A. and Kitanidis, P. K. (2000). An advective-dispersive stream tube approach for the transfer of conservative-tracer data to reactive transport. *Water Resources Research*, 36(5), 1209-1220.
- Fuger, J. (1992). Thermodynamic Properties of Actinide Aqueous Species Relevant to Geochemical Problems. *Radiochimica Acta*, 58-9, 81-91.
- Gallagher, M. and Doherty, J. (2007). Parameter estimation and uncertainty analysis for a watershed model. *Environmental Modelling & Software*, 22(7), 1000-1020.
- Gwoa, J. P., D'Azevedob, E. F., Frenzelc, H., Mayesc, M., Yehd, G. T., Jardinec, P. M., Salvagee, K. M., Hoffmanc, F. M. (2001). HBGC123D: a high-performance computer model of coupled hydrogeological and biogeochemical processes. *Computers & Geosciences*, 27(10), 1231-1242.

Huber, F., Enzmann, F., Wenka, A., Bouby, M., Dentz, M., and Schäfer, T. (2012). Natural micro-scale heterogeneity induced solute and nanoparticle retardation in fractured crystalline rock. *Journal of Contaminant Hydrology*, 133(0), 40-52.

Kienzler, B., Vejmelka, P., Romer, J., Schild, D. and Jansson, M. (2009). Actinide Migration in Fractures of Granite Host Rock: Laboratory and in Situ Investigations. *Nuclear Technology*, 165(2), 223-240.

Parkhurst, D. L. and Appelo, C. A. J. (1999). User's guide to PHREEQC (Version2)-A computer program for speciation, batch-reaction, one-dimensional transport, and inverse geochemical calculations. *Water-Resources Investigations Report 99-4259*, U.S.Geological Survey.

Römer, J., Kienzler, B., Vejmelka, P., Soballa, E., Görtzen, A. and Fuß, M. (2002). Actinide migration experiment in the HRL ÄSPÖ, Sweden : results of laboratory and in situ experiments, *Wissenschaftliche Berichte / Forschungszentrum Karlsruhe in der Helmholtz-Gemeinschaft ; ... Forschungszentrum Karlsruhe GmbH, Karlsruhe*.

Shapiro, A. M. and Cvetkovic, V.D. (1988). Stochastic-Analysis of Solute Arrival Time in Heterogeneous Porous-Media. *Water Resources Research*, 24(10), 1711-1718.

Trincherro, P., Molinero, J. and Román-Ross, G. (2012). A streamline-BASED approach for the solution of multicomponent reactive transport problems. *SKB report R-10-45*.

Turner, D. R. and Sassman, S. A. (1996). Approaches to sorption modelling for high-level waste performance assessment. *Journal of Contaminant Hydrology*, 21(1-4), 311-332.

Vandergraaf, T. T., Drew, D. J. and Masuda, S. (1996). Radionuclide migration experiments in a natural fracture in a quarried block of granite. *Journal of Contaminant Hydrology*, 21(1-4), 153-164.

Fanghänel, T., Kienzler, B., Korthaus, E., Römer, J., Schüßler, W. and Artinger, R. (2000). Sorption and Migration of Radionuclides in Granite (HRL ASPO, Sweden),6488, FZKA.

Vejmelka, P., Kienzler, B., Römer, J., Marquardt, Ch., Soballa, E., Geyer, F., Kisely, T. and Heathman, D. (2001). Actinide Migration Experiment in the HRL ÄSPÖ, Sweden: Results of Laboratory and in Situ Experiments. *Forschungszentrum Karlsruhe*.

Wang, P.M., Anderko, A. and Turner, D.R. (2001). Thermodynamic modelling of the adsorption of radionuclides on selected minerals. I: Cations. *Industrial & Engineering Chemistry Research*, 40(20), 4428-4443.

Wels, C., Smith, L. and Vandergraaf, T. T. (1996). Influence of specific surface area on transport of sorbing solutes in fractures: An experimental analysis. *Water Resources Research*, 32(7), 1943-1954.

STUDY OF SELENIUM SORPTION ON ÄSPÖ DIORITE SURFACE USING SPECTROSCOPIC METHODS

Kateřina Videnská^{1,2*}, Václava Havlová¹, Michaela Vařinová Galiová^{3,4}, Petr Sajdl²

¹ÚJV Řeř, a.s., Husinec-Řeř 130, 250 68 Řeř (CZ)

²Institute of Chemical Technology, Technická 5, 166 28 Prague (CZ)

³Masaryk University, Kotlářská 2, 611 37 Brno (CZ)

⁴Masaryk University, Central European Institute of Technology (CEITEC), Kamenice 5, 625 00 Brno (CZ)

* Corresponding author: hvl@ujv.cz

Abstract

Selenium belongs among long-lived fission products present in spent nuclear fuel (SNF). Due to the long lifetime of the radioisotope, the complex selenium chemistry, its high mobility and prevailing anionic character, selenium contributes significantly to the risk associated with the storage of radioactive waste in deep geological repositories. The presented work is focused on study of Äspö diorite surface after contact with solution of selenite and selenate. The aim of experiments was identifying potential retention mechanisms of selenium on diorite and observing correlation between sorbed selenium and iron present in Äspö diorite. The spectroscopic technique The Electron Spectroscopy for Chemical Analysis (ESCA) and Laser Ablation Inductively Coupled Plasma Mass Spectrometry (LA-ICP-MS) were used. These methods provide information about distribution of selenium on rock surface. The results partially confirmed the initial assumption that retention mechanism of selenium species was in correlation to the presence of Fe minerals. However, the methods did not confirm presence of reduce Se species. Therefore it can be assumed that the mechanism of Se sorption is surface complexation.

Introduction

Selenium radionuclide ⁷⁹Se ($T_{1/2} = 3.77 \cdot 10^5$ yrs.) represents long-lived fission product being produced in spent nuclear fuel. Its formation has to be considered carefully in safety assessment of deep geological repository (DGR) for radioactive waste. Selenium occurs in aqueous solutions in four oxidation states (-II, 0, +IV, +VI) depending on redox conditions. The anions SeO_3^{2-} and SeO_4^{2-} form mostly soluble compounds and can therefore be regarded as non-sorbing and mobile species. On the other hand Se(-II) forms poorly soluble compounds and Se(0) is found in nature as pure selenium (Puraren et al. 2009). Retention of mobile selenium species onto natural sorbents with Fe(II)-containing minerals has been observed in the species reduction and subsequent precipitation of Se(0) and Se(-II). The natural materials (siderite, pyrite, clay or calcite) were used as natural sorbent (Piqué et al. 2010; López et al. 2008). The retention of selenium by surface complexation was observed on hematite, goethite or magnetite. Selenium forms on the surface were studied in many publications (Duc et al. 2006; Zhang and Sparks, 1990). The retention of selenium species on natural sorbent was also investigated widely by spectroscopic method. These methods provide information about oxidation state of sorbed elements and could be used to study of retention mechanism of multivalent, redox sensitive elements. For example the technique X-ray photoelectron spectroscopy (XPS) was used to study of selenium retention on mackinawite and

pyrite. The analysis identified the lower oxidation state of selenium on Fe-minerals surface (Montavon et al. 2009; Han et al. 2011; Puraren et al. 2010). The other methods X-ray absorption near edge structure (XANES) and Extended X-ray absorption fine structure analysis (EXAFS) were used to study of magnetite, montmorillonite, pyrite, calcite or mackinawite surface and selenium retention was identified by these methods (Diener et al. 2012; Charlet et al. 2007; Aurelio et al. 2010).

In presented work, the sorption of selenium species was studied on Äspö diorite using the static batch method and the spectroscopic technique LA-ICP-MS and ESCA (also known as XPS) were used to analysed surface of Äspö diorite after contact with solution of selenite or selenate at synthetic granitic water. These methods can provide information about distribution of ions over the studied surface and about oxidation states of measured species. The aim was to determining possible fixation of selenium on the diorite constituents with high concentration of iron. In the diorite, iron is present in minority minerals (biotite, epidote, titanite and magnetite) (Byegard et al. 1998), therefore the special attention was focused to iron as potential reducing agents.

Experimental

Solid and liquid phase

The diorite rock used was sampled from borehole KA2368A-01. The samples originated from depth 10.65 – 11.12 m were cut into thin slices (10×10×2 mm) for aerobic experiments. For anaerobic experiments small rock pieces were slices, using pliers and directly in the anaerobic box. The synthetic granitic water Äspö was used as a liquid phase. Chemical composition of synthetic granitic water Äspö is shown in Table 1.

Sorption experiments

Reaction mixtures for spectroscopic analysis were prepared by inserting rock cubes (dimension 1×1×0.2 cm) into 10 mL synthetic granitic water Äspö containing defined amount of selenium. Concentrations of Na₂SeO₃ or Na₂SeO₄ in synthetic granitic water were 2·10⁻³ mol/L. The cubes were immersed in solution for 7 days; the mixtures were shaken once a day. Surface of diorite cubes was then wiped with pulps after removal from experimental solution and the samples were dried in a desiccator. The experiment was carried out under aerobic conditions. The surface was analysed by ESCA and LA-ICP-MS methods.

Table 1: Composition and pH of synthetic granitic water Äspö.

Component	Concentration [mg/L]
pH	7.26
Na	1889.9
K	10.6
Ca	1122.2
Mg	99.7
Cl	4909
SO ₄ ²⁻	393.7
HCO ₃ ⁻	11.6
F	1.41
Sr	20.2
Br	21.6

ESCA measurement

The samples were measured by ESCA Probe P (Omicron Nanotechnology, Taunusstein, Germany). Emission of electrons from sample surface was induced by beam with energy of 1486.7 eV (Al anode). The XPS spectra were measured in the CAE mode (Constant Analyser Energy), the pass energy constant was set to 50 and 30 eV. Only electrons of this energy arrived at the detector. The pass energy 50 eV was used to measure the overview spectrum which was used to determination of elements with higher concentration than several at. %. The pass energy 30 eV was used to measurement detailed spectra in the range of binding energy E_b 49 – 68 eV and in some other ranges needed for detailed comparison of lines of present elements. Charge compensation was carried out by electrons with low energy level 1 – 3.5 eV. Data processing was carried CASA XPS program. The limit of detection of selenium was 0.02 at. %, the limit of detection of iron was 0.1 at. %.

The mapping of selenium distribution was carried out using a grid of points (3 × 3 points) with 0.8 mm in diameter. The measured points were located at distance of 0.7 mm in x and y axes. Selenium, sodium and iron intensities were detected in order to reveal the selenium distribution.

LA-ICP-MS measurement

Distribution of selenium on the diorite surface was investigated by LA-ICP-MS. The ablation events were carried out using an UP 213 (New Wave Research, Inc., Fremont, CA, USA) laser ablation system consisting of commercial Q-switched Nd:YAG laser operated at the wavelength of 213 nm and with pulse duration of 4.2 ns. The sample was placed into Super cell (New Wave Research, Inc., Fremont, CA, USA) having volume of 33 cm³. An XY-stage was used to move the sample along a programmed trajectory and a CCD camera was used to monitor the ablation event. The ablated material was transported into inductively coupled plasma by a carrier gas (helium, flow rate of 1 L/min) mixed with argon (flow rate of 0.6 L/min) prior to the torch. The laser ablation system was attached to an Agilent 7500ce (Agilent Technologies, Santa Clara, CA, USA) quadrupole

ICP-MS equipped with a collision-reaction cell for potential interference suppression. Optimization of LA-ICP-MS parameters (gas flow rates, sampling depth, voltage of ion optics) was performed using glass reference material NIST SRM 612 to maximize the S/N ratio and minimum oxide formation (ThO^+/Th^+ counts ratio 0.2%) and U^+/Th^+ counts ratio 1.1%.

The mapping of selenium distribution was carried out using a grid of points (15×20 points) with $100 \mu\text{m}$ in diameter. The ablated points were located at the distance of $200 \mu\text{m}$ in both axes (x, y). The each spot was ablated for 10 s at laser pulse frequency of 10 Hz and 13 J/cm^2 fluence. A delay time of 8 s between individual ablation events was set to wash out the ablation chamber, and thus decrease of the isotope signal onto a background level. The potential interferences were minimized via 1 mL/min and 2 mL/min flow rate of hydrogen and helium, respectively. $^{27}\text{Al}^+$, $^{31}\text{P}^+$, $^{42,43,44}\text{Ca}^+$, $^{55}\text{Mn}^+$, $^{56,57}\text{Fe}^+$, $^{77,78,80,82}\text{Se}^+$, $^{86,88}\text{Sr}^+$ and $^{133}\text{Cs}^+$ intensities were detected in order to reveal the selenium distribution.

Results and discussion

LA-ICP-MS measurement of diorite rock

The results of LA-ICP-MS analysis of Äspö diorite after 7 days of contact with selenite solution are shown in Figure 1. The surface maps reveals trend of increased intensity of selenium in presence of iron. The part 1A shows analysed surface of diorite, 1B shows iron distribution and 1C shows selenium distribution on diorite. High content of iron (Figure 1B) is in correlation with dark spots on the Figure 1A, corresponding to Fe-minerals. The distribution of iron (isotope ^{57}Fe) is correlated to distribution of selenium (isotope ^{77}Se). This result indicates that there are spots were increased content of Se^- is in direct correlation with presence of Fe. Even though there are also some other spots with increased Se concentration, with low Fe concentration, some pattern of Se sorption can be spotted. Comparing Figure 1A and 1C, those spots can be attributed to mica grains. However, such a trend is less visible for sodium selenate (see Figure 2), even though some of the mica spots can be assigned Se sorbing. However, the LA-ICP-MS analysis have not provided information about oxidation state of sorbed selenium and about content of selenium on analysed surface yet.

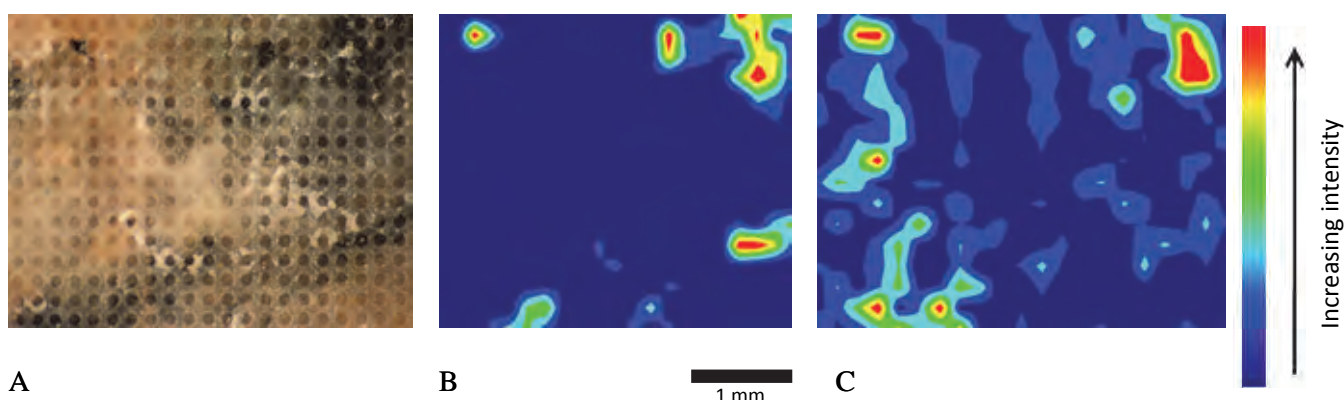


Figure 1: LA-ICP-MS surface map of diorite sample after contact with $2 \cdot 10^{-4} \text{ mol/L Na}_2\text{SeO}_3$ solution: A) analysed surface, B) iron (^{57}Fe) distribution, C) selenium (^{77}Se) distribution.

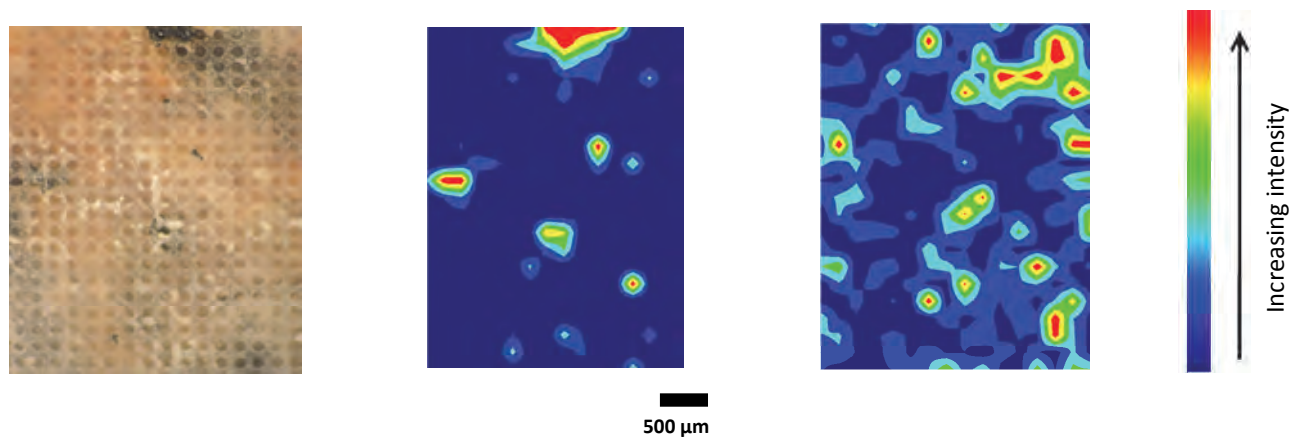


Figure 2: LA-ICP-MS surface map of diorite sample after contact with $2 \cdot 10^{-3}$ mol/L Na_2SeO_4 solution: A) analysed surface, B) iron (^{57}Fe) distribution, C) selenium (^{77}Se) distribution.

ESCA measurement of diorite rock

Diorite samples were immersed in solution of selenite and selenate in synthetic granitic water. The aim of using this method was identification of influence of iron present in diorite on selenium sorption. In the first step, pure selenium species (Na_2SeO_4 , Na_2SeO_3 and Se^0) were analysed by ESCA. The results provided more detailed information about position of selenium specie peaks in spectrum (see Figure 3). Position of peak in spectrum informs about oxidation state of sorbed element. The results of the standard measurement showed that peak of Se^0 is in the range of E_b 54.7 – 55.7 eV and peaks of Se^{IV} and Se^{VI} are in the range of E_b 58 – 61.6 eV. The significant peak observed at selenite and selenate spectra around E_b 64 eV is assigned to sodium Na 2s.

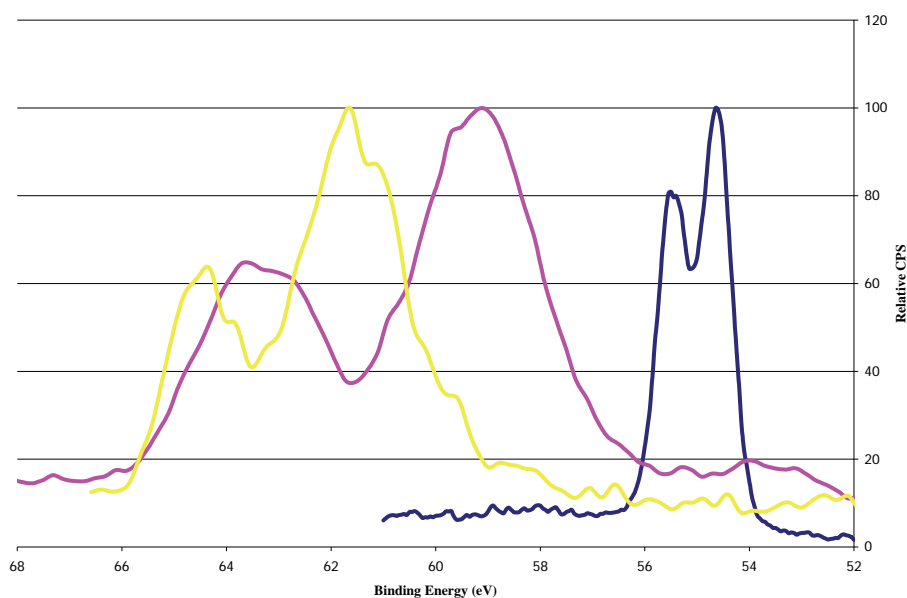


Figure 3: ESCA spectra of measured selenium standards $\text{Se}(0)$, Na_2SeO_3 , Na_2SeO_4 . Blue line: spectrum of $\text{Se}(0)$, purple line: spectrum of $\text{Se}(IV)$ 3d and Na 2s, yellow line: spectrum of $\text{Se}(VI)$ 3d and Na 2s.

In the second step, nine positions on diorite cubes were measured and results of ESCA are summarized in Table 2 and Table 3. For illustration purposes, two spectra of samples after contact with selenite and selenate solutions are shown in Figures 4 and 5. The ESCA measurement did not prove any Se oxidation changes on the diorite surface. Selenium was in both cases determined in the oxidation state, which corresponds to the experimental solution used. If reduced selenium forms are present on analysed surface, its content might be under ESCA detection. However, the amount of Se species, sorbed on the surface, was evaluated in atomic % as surface maps which should illustrate distribution on diorite (see Figure 6 and Figure 7). Moreover, the Fe distribution is also presented. The Figures 6A and 7A show placement of measured spots, the Figures 6B and 7B show distribution of iron, the Figures 6C and 7C show distribution of selenium.

The Table 2 and Figure 6 show results of diorite sample after contact with solution of sodium selenite. Two spots (positions 3 and 4) with high content of iron were analysed on studied sample. The content of iron was 0.46 at.%, respectively 1.28 at.%. The high content of selenium was analysed in these positions and in neighbour position. On the other hand the high content of selenium was analysed in position 8 and 9, although no content of iron was determined in these spots.

The Table 3 and Figure 7 show results of analyses of diorite sample after contact with solution of sodium selenate. The high content of iron was measured in position 8, and increased content of iron was measured in positions 1 and 2, where higher content of selenium was also detected. However, to correlation is not clear, as in the previous case with LA ICP MS measurement.

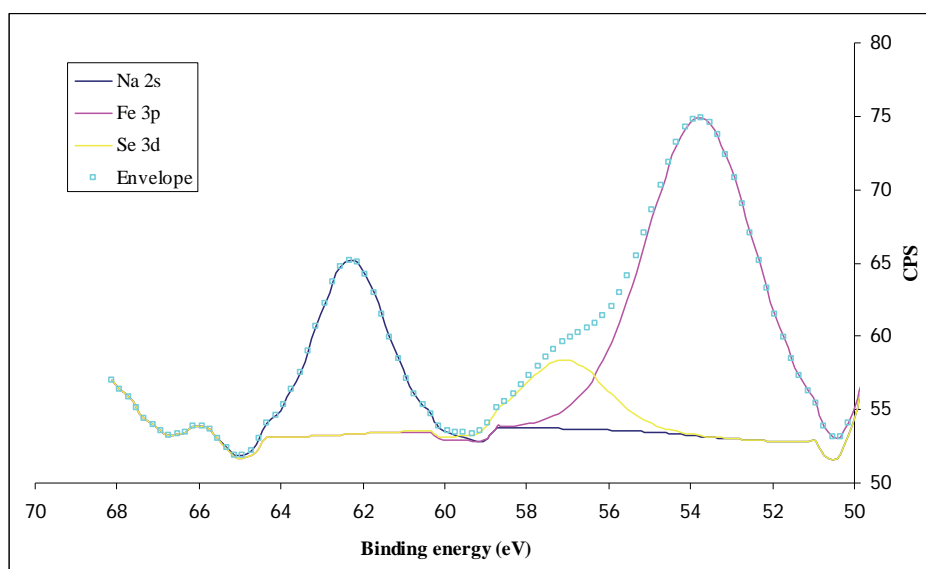


Figure 4: ESCA spectrum of sample after contact with Na_2SeO_3 solution. Yellow line: selenium (Se 3d, $E_b = 57.5$ eV), purple line: iron (Fe 3p, $E_b = 53.7$ eV), dark blue line: sodium (Na 2s, $E_b = 62.5$ eV), blue squares: multi-peak spectral envelope resolving into three components (Se, Na, Fe).

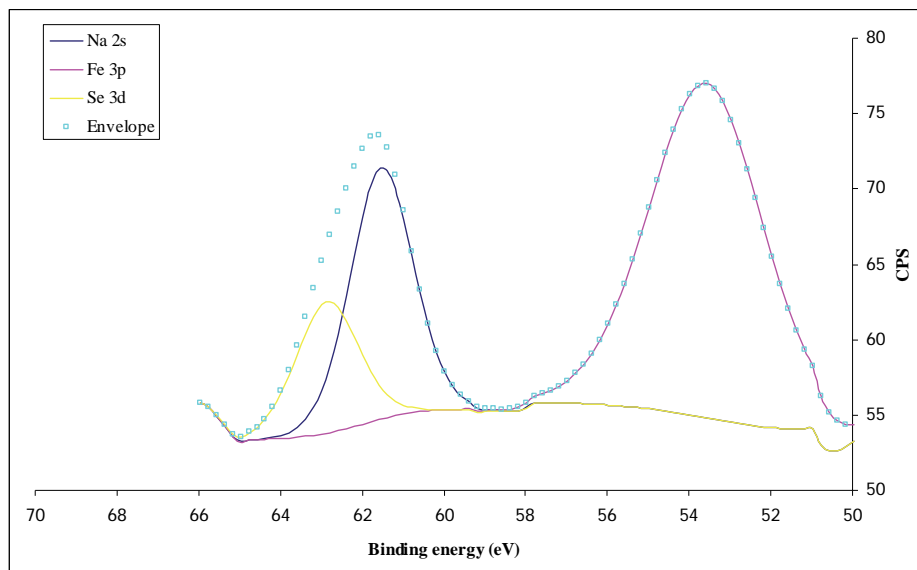


Figure 5: ESCA spectrum of sample after contact with Na_2SeO_4 solution. Yellow line: selenium ($\text{Se } 3d$, $E_b = 62.5 \text{ eV}$), purple line: iron ($\text{Fe } 3p$, $E_b = 53.5 \text{ eV}$), dark blue line: sodium ($\text{Na } 2s$, $E_b = 61.5 \text{ eV}$), blue squares: multi-peak spectral envelope resolving into three components (Se , Na , Fe).

Table 2: Results of ESCA analysis of diorite surface after contact with sodium selenite.

Position	Fe content (at. %)	Se content (at. %)
1	0	0.01
2	0	0.19
3	0.46	0.18
4	1.28	0.20
5	0	0.17
6	0	0.17
7	0	0.19
8	0	0.59
9	0	0.07

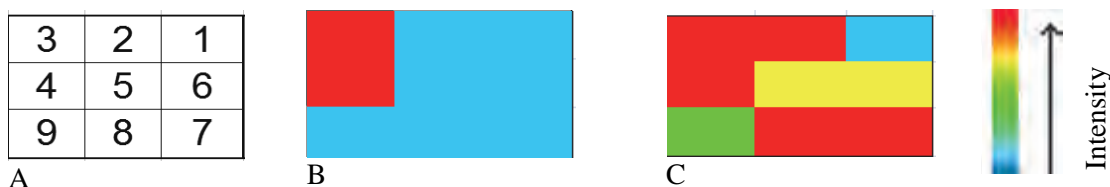


Figure 6: ESCA surface map of diorite sample after contact with $2 \cdot 10^{-3} \text{ mol/L Na}_2\text{SeO}_3$ solution: A) measured positions, B) Fe distribution, C) Se distribution.

Se sorption is widely described as reduction on Fe surface (Se lower oxidation state absence can push the results towards the possibility that complexation might be the main reason for Se sorption on Äspö diorite (Puranen et al. 2009; López et al. 2008; Duc et al. 2006; Rovira et al. 2008; Missana et al. 2009). However complexation mechanisms are also mentioned For example sorption of selenite on goethite or magnetite is described by surface complexation (see eq. 1 and 2). Rovira et al (2008). describes formation of mixture of monodentate inner-sphere deprotonated and protonated surface complexes FeOHSeO_2 and FeOSeO_2^- on goethite. Selenate forms on goethite $\text{FeOH}^{2+}\text{-SeO}_4^{2-}$ complex²². The iron oxide surface monodentate inner-sphere complexes are formed on goethite surface ($\alpha\text{-Fe}^{3+}\text{O(OH)}$) (Rovira et al. 2008; Missana et al. 2009)).

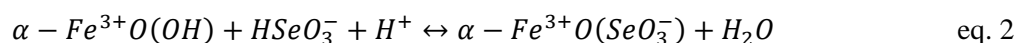
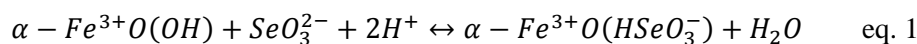


Table 3: Results of ESCA analysis of granitic surface after contact with sodium selenate.

Position	Fe content (at. %)	Se content (at. %)
1	0.06	0.29
2	0.05	0.12
3	0	0.01
4	0	0.02
5	0	0.12
6	0	0.03
7	0	0.19
8	0.39	0.16
9	0	0.05

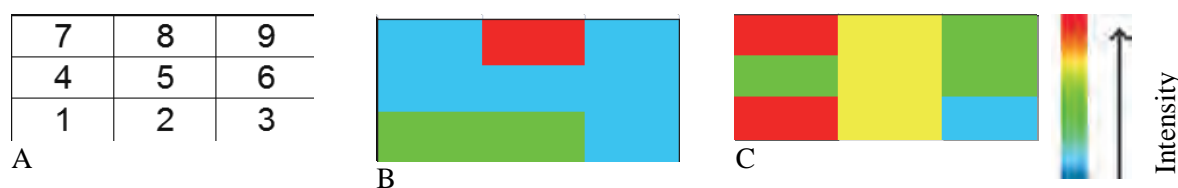


Figure 7: ESCA surface map of granite sample after contact with $2 \cdot 10^{-3}$ mol/L Na_2SeO_4 solution: A) measured positions, B) Fe distribution, C) Se distribution.

Similar retention mechanism of selenite (1, 2) is reported also for magnetite. The result is an inner-sphere monodentate species (Kim et al. 2012; Jordan et al. 2009). The selenium speciation depends on pH. Under neutral-alkaline pH the complexes FeO-HSeO_3 and FeO-SeO_3^- are formed, under lower pH magnetite is dissolute and Fe-Se species are produced. Similar complexes might be formed even with Fe, present on mica. The study on Se retention on mica is ongoing. Moreover aluminol sites were presented to be potential sites for sorption in silicate mixtures (Hurel and Marmier, 2006). This might also explain the unconformity in Se presence on sites with low Fe content.

Furthermore, another fact can have an influence on Se sorption: As it was indicated in Videnska et al (2011), under $\text{pH} > 8$ calcium selenite complex can be formed (see Figure 8). As calcite is reported to be one of the main components of the Äspö diorite (altogether with plagioclase, K-feldspar, quartz, biotite; minor: muscovite, titanite, apatite, fluorite, zircon and magnetite), formation of calcium selenium complexes can also explain the Se retention on the diorite surface.

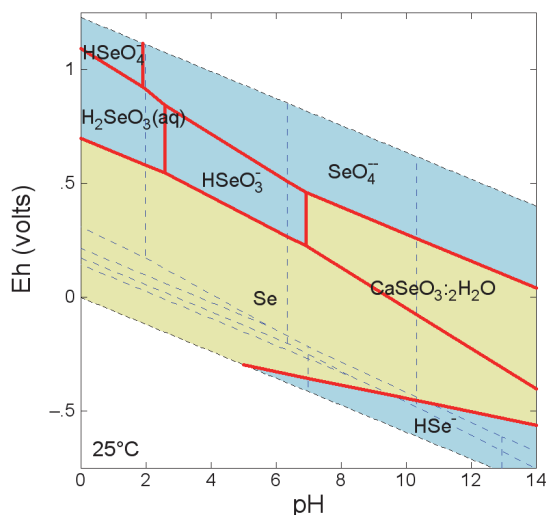


Figure 8: Speciation of Se in Äspö synthetic groundwater. $c(\text{Se}) = 2 \cdot 10^{-3} \text{ mol/L}$.

Conclusion

The surface of Äspö diorite was analysed after contact with solution of sodium selenate and sodium selenite. The spectroscopic methods ESCA and LA-ICP-MS were used. These methods provide multi-elements analysis of studied sample surface. The content of selenium and iron was measured on diorite surface. The influence of Fe-mineral in diorite on selenium species retention was investigated, as iron is widely mentioned as potential reductive agent of selenium. Iron is present in diorite in the structure of minority minerals (e.g. biotite, epidote, titanite and magnetite). Basically, the Se sorption on the diorite sorption was low. The LA-ICP-MS showed to some extent some relationship between presence of iron on diorite surface and retained selenium species, namely for Se(IV). This result was particularly confirmed by ESCA analysis of diorite surface. However, surface complexation with other species, e.g. with Ca, can be responsible for Se sorption on the surface.

Acknowledgement

The research leading to these results has received funding from the European Union's European Atomic Energy Community's (Euratom) Seventh Framework Programme FP7/2007-2011 under grant agreement n° 269658 (CROCK project).

References

- Aurelio, G., Fernández-Martínez, A., Cuello, G. J., Román-Ross, G., Alliot, I. and Charlet, L. (2010) Structural study of selenium(IV) substitutions in calcite. *Chemical Geology*, 270, 249-256.
- Byegard, J., Johansson, H., Skalberg, M. and Tullborg, E. L. (1998) The interaction of sorbing and non-sorbing tracers with different Äspö rock types. Technical Report TR-98-18, Swedish Nuclear Fuel and Waste Management Co.
- Charlet, L., Scheinost, A. C., Tournassat, C., Greneche, J. M., Géhin, A., Fernández-Martínez, A., Coudert, S., Tisserand, D. and Brendle, J. (2007) Electron transfer at the mineral/water interface: Selenium reduction by ferrous iron sorbed on clay. *Geochimica et Cosmochimica Acta*, 71, 5731-5749.
- Diener, A., Neumann, T., Kramar, U. and Schild, D. (2012) Structure of selenium incorporated in pyrite and mackinawite as determined by XAFS analyses. *Journal of Contaminant Hydrology*, 133, 30-39.
- Duc, M., Lefevre, G. and Fédoroff, M. (2006) Sorption of selenite ions on hematite. *Journal of Colloid and Interface Science*, 298, 556-563.
- Han, D. S., Batchelor, B. and Abdel-Wahab, A. (2011) Sorption of selenium (IV) and selenium (VI) to mackinawite (FeS): Effect of contact time, extent of removal, sorption envelopes. *Journal of Hazardous Materials*, 186, 451-457.
- Hurel, Ch. and Marmier, N. (2006) Sorption Of Selenium (IV) On Mineral Mixtures: Role Of Minor Phases In The Modelling Part. *Mat. Res. Soc. Symp. Proc.*, 932.
- Jordan, N., Lomenech, C., Marmier, N., Giffaut, E. and Ehrhardt, J. J. (2009) Sorption of selenium(IV) onto magnetite in the presence of silicic acid. *Journal of Colloid and Interface Science*, 329, 17-23.
- Kim, S. S., Min, J. H., Lee, J. K., Baik, M. H., Choi, J. W. and Shin, H. S. (2012) Effects of pH and anions on the sorption of selenium ions onto magnetite, *Journal of Environmental Radioactivity*, 104, 1-6.
- López de Arroyable Loyo, R., Nikitentko, S. I., Scheinost, A. C. and Simonoff, M. (2008) Immobilization of Selenite on Fe₃O₄ and Fe/Fe₃C Ultrasmall Particles. *Environmental Science and Technology*, 42, 2451-2456.
- Missana, T., Alonso, U., Scheinost, A.C., Granizo, N., García-Gutiérrez, M. (2009) Selenite retention by nanocrystalline magnetite: Role of adsorption, reduction and dissolution/co-precipitation processes. *Geochimica et Cosmochimica Acta*, 73, 6205-6217.
- Montavon, G., Guo, Z., Lützenkirchen, J., Alhajji, E., Kedziorek, M. A. M., Bourg, A. C. M. and Grambow, B. (2009) Interaction of selenite with MX-80 bentonite: Effect of minor phases, pH, selenite loading, solution composition and compaction. *Colloids and Surfaces A: Physicochem. Eng. Aspects*, 332, 71-77.
- Piqué, A., Grandia, F., Sena, C., Arcos, D., Molinero, J., Duro, L. and Bruno, J. (2010) Conceptual and numerical modelling of radionuclide transport in near-surface systems at Forsmark. SKB rapport R-10-30, Swedish Nuclear and Waste Management Co, Stockholm, Sweden.
- Puranen, A., Jonsson, M., Dahn, R. and Cui, D. (2009) Immobilization of selenate by iron in aqueous solution under anoxic conditions and the influence of uranyl. *Journal of Nuclear Materials*, 392, 519-524.

Puranen, A., Jonsson, M., Dahn, R. and Cui, D. (2010) Reduction of selenite and selenate on anoxically corroded iron and the synergistic effect of uranyl reduction. *Journal of Nuclear Materials*, doi: 10.1016/j.jnucmat.2010.08.031.

Rovira, M., Giménez, J., Martínez, M., Martínez-Lladó, X., de Pablo, J., Martí, V. and Duro, L. (2008) Sorption of selenium(IV) and selenium(VI) onto natural iron oxides: Goethite and hematite. *Journal of Hazardous Materials*, 150, 279-284.

Videnská K., Havlová V. and Vejsadů J. (2011) Speciation of Se in Äspö synthetic groundwater . S+T presentation. 1st Workshop Proceedings, 7th EC FP - CROCK CP, 22nd – 24th May 2012 Stockholm, Sweden.

Zhang, P. and Sparks, D. L. (1990) Kinetics of Selenate and Selenite Adsorption/Desorption at the Goethite/Water Interface. *Environ. Sci. Technol.*, 24, 1846-1856.

TC(VII) SORPTION ON NATURAL GRANITIC ROCKS AND SYNTHETIC MAGNETITE

Yury Totskiy^{1*}, Thorsten Schäfer^{1,2}, Florian Huber¹, Dieter Schild¹, Horst Geckeis¹,
Stepan Kalmykov³

¹ Institut für Nukleare Entsorgung (INE), Karlsruher Institut für Technologie (KIT) (DE)

² Institute of Geological Sciences, Department of Earth Sciences, Freie Universität Berlin, (DE)

³ Lomonosov Moscow State University (MSU) (RU)

* Corresponding author: yuri.totskiy@kit.edu

Abstract

Technetium-99 is one of the most hazardous radioactive component of high-level waste due to its high fission yield and long half-life ($2.1 \cdot 10^5$ years), but its mobility and migration studies on host rock formations under natural conditions are scarce. Sorption of Tc(VII) onto crystalline rock materials from Äspö Hard Rock Laboratory (Sweden) and Nizhnekansky massif (Russia) is investigated to understand retention mechanisms under (a) natural conditions expected in the deep-geological formation and (b) geochemical perturbations (oxidation) possibly introduced by e.g. the far future glaciations. Distribution coefficients for varying conditions are determined. Both materials after oxidation on air sorb almost the same Tc amount. High Tc immobilization is achieved via its reduction to insoluble Tc(IV) species proved by XPS. Due to low exchangeable Fe(II) concentration found in the granite material this process is much slower and less effective than in case of sorption on synthetic magnetite. Desorption under reducing conditions was almost negligible and independent of contact time, whereas after atmospheric oxidation Tc desorption significantly increased.

Introduction

⁹⁹Tc is one of the main long-lived U and Pu fission products in spent nuclear fuel (SNF) and also can be generated by medical laboratories and research institutions. Because of relatively high fission yield (*ca.* 6%) and long half-life ($2.1 \cdot 10^5$ years) technetium is considered as one of the most hazardous radioactive component of high-level waste (HLW). The most stable Tc form under aerobic atmosphere is pertechnetate (TcO_4^-), which is very soluble under fully oxidizing conditions (Um and Serne, 2005; Zachara et al., 2007b). Under anaerobic conditions Tc(VII) is reduced to Tc(IV) and the solubility is limited by $\text{TcO}_2 \cdot 1.6\text{H}_2\text{O}(\text{s})$.

The generally accepted concept of spent nuclear fuel and high-level waste long-term storage is its disposal in deep- geological formations at a depth of more than 300 – 500 meters. When radionuclides with period of potential danger of over 500 years are disposed, the repository host rock as part of the multi-barrier system plays an important role as protective barrier to retard the radionuclide migration. Thus, the selection of the host rock formation with appropriate geochemical and hydro-geological properties is a key challenge in the task of nuclear waste disposal siting.

In 1993, by the request of Ministry of Atomic Energy (Minatom) the search for an appropriate site of underground facility for high-level radioactive waste disposal was initiated in Russian Federation. In 2002, on

the basis of the research performed and taking into account criteria established by the International Atomic Energy Agency (IAEA) and the waste isolation concept chosen, a “Declaration of Intentions” (DOI) was prepared and adopted by the State Atomic Energy Corporation, Rosatom. The DOI covers plans to construct an underground research laboratory, into Nizhnekansky granitoid massif, Krasnoyarsky Krai. In this massif, three potential locations for the laboratory has been considered (Yeniseisky, Itatsky and Kamenny, see Figure 1). In 2008, the revised DOI stated that the Yeniseisky site is the favourite candidate for further investigations, and the probable candidate for final disposal repository. The other sites should be considered as reserve options.



Figure 1: Location of Nizhnekansky granitoid massif and three proposed sites for SNF final geological disposal (Yeniseisky, Itatsky and Kamenny sites. Based on (Jardine, 2005).

The Äspö Hard Rock Laboratory (HRL) is an underground research laboratory in Sweden for *inter alia* in-situ studies of processes in crystalline formations concerning deep geological disposal of spent nuclear fuel. Crystalline host rocks contain fractures, which are potential migration pathways in cases of radionuclide releases from a repository. Radionuclide transport processes depend strongly on the hydrological and geochemical conditions (pH, Eh, ionic strength) of bedrock. Furthermore, depending on the fracture structure (fracture filling material, fault gauge, hydrothermal alteration) fracture surfaces likely vary in mineralogical composition compared to the rock matrix and, besides advective transport, matrix diffusion may contribute significantly to radionuclide retention. Technetium mobility in natural systems strongly depends on the redox state. Both batch type sorption and column experiments with Hanford sediments (Um and Serne, 2005; Zachara et al., 2007b) have revealed that ⁹⁹Tc is highly mobile and shows virtually no retardation under fully oxidizing conditions. Consequently, it can be used to trace tank waste migration through a vadose zone.

In an early work by (Bondietti and Francis, 1979) on a variety of natural samples showed considerable retention (by TcO_4^- reduction) in accordance with Eh/pH conditions. This relation was described with the equation: $E^0(\text{TcO}_4^-/\text{TcO}_2) = 0.738 - 0.0788\text{pH} + 0.0197$.

Because of the variability in natural systems, distribution coefficients and apparent diffusion coefficients for natural systems found in the literature vary by orders of magnitude, and are rarely documented together with the Eh/pH conditions studied. Furthermore, Tc redox kinetics strongly depend on the availability of reactive Fe(II) in host rock (surface complexed, precipitated, ion exchangeable) (Fredrickson et al., 2009; Heald et al., 2007; Jaisi et al., 2009; Peretyazhko et al., 2008a; Peretyazhko et al., 2008b; Zachara et al., 2007a).

In the case of Tc(VII), Äspö in-situ and laboratory migration studies (CHEMLAB-2) done prior to the CROCK project (Kienzler et al., 2003; Kienzler et al., 2009) using Äspö derived natural groundwater revealed ~ 1% Tc recovery (after 254 days) of the injected quantity. Batch type studies, done in parallel, derived K_d values of $\sim 2.1 \cdot 10^{-3}$ M for ^{99}Tc ($t_{\text{contact}} = 14$ d), whereas altered material showed significantly lower values. These results show contact time/residence time dependency on retardation and/or reduction kinetics.

The present work is a continuation of Tc sorption study, started by (Totskiy et al., 2012) for crushed Äspö diorite (ÄD) samples.

Materials and methods

Äspö diorite (ÄD)

Crystalline rock material was delivered from CROCK drilling site of Äspö HRL (Sweden). Details of the sampling procedure and material characterization are presented in the S&T contribution of (Schäfer et al., 2012). The bore cores (#1.32 and #1.33) of Äspö diorite were used for investigations. Preparation and handling of Äspö rock samples were described in the previous CROCK S&T contribution (Totskiy et al., 2012).

Nizhnekansky massif granite (NK)

Granitoid drill core material from Nizhnekansky (NK) massif was available from Kamenny (depth of sampling down to 700 m) and Itatsky (depth of sampling down to 500 m) sites. Cores were transferred to the Institute of Geology of Ore Deposits, Petrography, Mineralogy and Geochemistry RAS (IGEM RAS, Russia) under oxic conditions, cut by circular saw, then part of the material was transferred to the Karlsruhe Institute of Technology, Institute for Nuclear Waste Disposal (KIT-INE, Germany). At KIT-INE, the material was broken up by jaw crusher into small grains and sieved to obtain the 1-2 mm grain size fraction. This material was characterized with XRD and BET for mineralogical composition and surface area interpretations. Thereafter, material was used for sorption experiments. Tc(VII) sorption kinetics was investigated using material only from a core from Itatsky site (core from approx. depth of 92 m). A detailed description of the NK material used in this study can be found in (Petrov et al., 2012).

Magnetite

Magnetite was synthesized in accordance with the procedure described in (Schwertmann and Cornell, 2000) and produced at KIT-INE by oxidation of Fe(II) solution under argon atmosphere. The amount of 80 g of $\text{FeSO}_4 \cdot 7\text{H}_2\text{O}$ was dissolved in 560 mL of MilliQ water (bubbled beforehand with Ar) in an 1 L glass beaker, and

heated to the temperature of 90° C (controlled by a thermocouple) in the water bath. Once the reaction temperature was reached, 250 mL of oxygen-free solution containing 44.9 g KOH and 6.46 g KNO₃ was added using drop-funnel approx. 20 min. Then the reactor was heated additional 30 min and cooled overnight. The product was purified by dialysis throughout 3 months with daily water change and then characterized by XRD, BET, XPS and SEM+EDX.

Synthetic groundwater simulants

Synthetic Äspö groundwater simulant (ÄGWS) for batch-type sorption experiments was prepared to mimic the CROCK drilling site outflow groundwater composition (sample CROCK-2) (see (Schäfer et al., 2012)). All chemicals used were of analytical grade; deionized Milli-Q water was used for dilution. ÄGWS has comparable composition to groundwater sampled from borehole KA3600-F-2 in a 50 L barrel at the CP-CROCK site (Heck and Schäfer, 2012). Chemical compositions of the used ÄGWS and natural groundwater samples can be found in (Totskiy et al., 2012).

Synthetic groundwater for NK material (NKGWS) was prepared in accordance with (Petrov et al., 2012) by dissolution of 62.5 mg/L NaHCO₃ and 187.5 mg/L Ca(HCO₃)₂ in MilliQ water. The total amount of dissolved solids is 250 mg/L and pH = 6.5. Sustainability of the chemical mixture under argon atmosphere was tested by classical HCl titration of a reference sample during a sorption experiment.

The Background electrolyte for Tc sorption experiments on magnetite was 0.2 M NaCl.

Radionuclides

Technetium behaviour investigations were mainly performed by using ⁹⁹Tc isotope in form of 13mM NaTcO₄ stock solution. For experiments with low Tc concentrations, which can't be measured using ⁹⁹Tc, it was decided to apply ^{95m}Tc as an isotope with shorter half-life and strong gamma lines in the spectrum. For this purpose natural Mo foil (50 µm, 350±5 mg) was irradiated by protons at ZAG Zyklotron AG (Karlsruhe, Germany), transported to KIT-INE and processed to separate technetium according the technique of (Boyd et al., 1960). The foil was dissolved in 1 mL concentrated H₂SO₄ with addition of 2.5 mL 30% H₂O₂, then the solution was slowly neutralized with saturated NaOH. The obtained alkaline solution was passed through a column of anion exchanger Dowex 1x8 with total volume *ca.* 3 mL. The column was washed first with 20 mL 1 M K₂C₂O₄ to remove residues of molybdate and after rinsing with 20 mL of MilliQ water pertechnetate was eluted with 30 mL 1 M HClO₄. The last fraction was collected in 2 mL vials, which were measured with γ-spectrometry and samples with *ca.* 90% of ^{95m}Tc were merged and neutralized with concentrated NaOH.

For iron exchange studies ⁵⁹Fe (t_{1/2} = 44.495 d) isotope was used. The isotope was produced by neutron activation of four iron foils (total mass ≈ 500 mg) at the Technical University of Munich (Heinz Maier Leibnitz Neutron Source FRM-II).

Batch-type sorption/desorption studies

Batch-type sorption experiments were carried out in 20 mL liquid scintillation counter (LSC) vials (HDPE, type Zinsser) inside the Ar glovebox with O₂ concentrations ≤ 1 ppm at room temperature (20 ± 2° C). Solid-liquid ratio was 2 g of granitic rock and 8 mL of GWS in case of natural materials or 2 g/L of iron oxide for magnetite batches. For each condition and kinetics point, two separate samples were prepared and closed during the

equilibration to prevent oxidation of Fe(II) species at mineral surfaces. All sorption experiments were conducted at pH equal to 8. Investigations of Tc behaviour were carried out using 13mM NaTcO₄ stock solution, added to GWS, for final concentrations of 10⁻⁵ M, 10⁻⁸ M and 10⁻⁹ M of Tc(VII). For measurement of ⁹⁹Tc content in supernatants after sorption 1 mL aliquots were taken, added to 10 mL of LSC cocktail Ultima Gold and analysed with LSC (PerkinElmer Quantulus). To differentiate between colloidal phases and true solution species a phase separation by ultracentrifugation (90,000 rpm for 1 h) was applied.

Redox potential was measured in the Ar glovebox by using a Metrohm (Ag/AgCl, KCl (3 M)) electrode and recording values every hour; the Eh values presented in this work are corrected for the standard hydrogen potential (SHE).

Samples of sorption experiments were taken to desorption experiments after three month contact time. The Tc containing supernatant was removed and 8 mL of fresh liquid phase (NKGWS in the case of NK material) added. For surface analysis small diorite fragments with unpolished faces after cutting by circular saw were equilibrated with 10⁻⁵ M Tc(VII) in GWS for 2 months, washed with MilliQ water for a few seconds to prevent salt precipitation and then investigated with X-ray photoelectron spectroscopy (XPS) system PHI 5600-CI (Physical Electronics Inc.) to determine Tc redox speciation.

Available iron content

In order to estimate the cation exchangeable Fe(II) amount on mineral surfaces, a method proposed by (Heron et al., 1994) was applied using 10 mL 1 M CaCl₂ (pH = 7) in contact with 2 g of granite for 24 h. Afterwards, an aliquot was taken for Fe(II) quantification by the ferrozine technique (Viollier et al., 2000).

Radioactive tracer of ⁵⁹Fe was taken for the first iron exchange study on ÄD material. ÄGWS with admixture of ⁵⁹Fe with carrier (total iron concentration 2·10⁻⁶ M) in Fe(II) or Fe(III) form was added to granite (12 mL of liquid per 3 g of solid phase) and then the kinetics of iron concentration change in the solution was measured with γ -spectrometry.

Core migration

Unoxidized Äspö diorite core #2.2 (0.53-0.97 m, borehole KA2370A-01) was used for a migration experiment. The sample contains a natural fracture at ~0.70 m that was opened during on-site handling at the Äspö HRL. A core segment containing the natural fracture (length ~4.2 cm) was cut and sealed into a Plexiglas column under Ar atmosphere with connectors to the fracture in- and outlet. The core was sealed in an Ar filled plastic bag as second confinement, transferred to the Federal Institute for Materials Research and Testing (BAM, Berlin) and characterized by 3D computer tomography (μ CT). The fracture volume after segmentation was estimated to be 0.415 mL. More detailed information on core #2.2 preparation and characterization can be found in (KIT-INE, 2012).

For tracer migration experiments 1 mL of ÄGWS containing HTO and ³⁶Cl admixtures was eluted through the core by ~50 mL of ÄGWS using a syringe pump under different flow rates (10 mL/h, 1.5 mL/h and 0.2 mL/h). The eluate was gathered with a fraction collector (Gilson FC 203b) and measured with LSC. General set-up of the core migration experiment is presented in Figure 2. For a reactive transport investigation the same experiment was performed with injection of Tc containing ÄGWS. Experiments under low Tc concentrations (~10⁻¹⁰ M) were possible due to the availability of ^{95m}Tc, measured with γ -spectrometry.

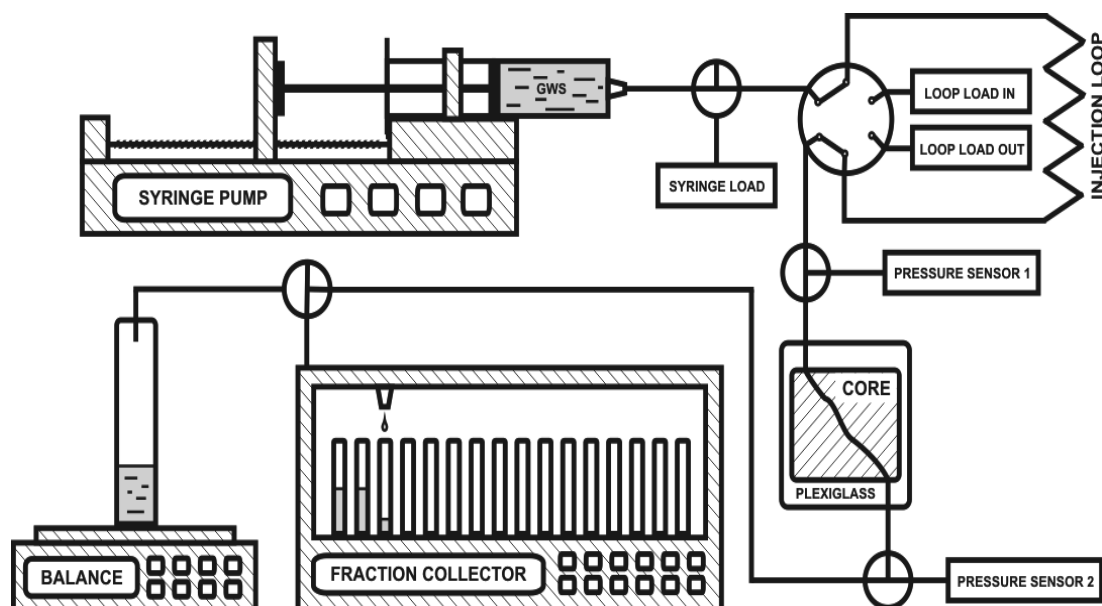


Figure 2: Core migration apparatus scheme.

Results and discussions

Sorption

Batch-type sorption study on NK material was performed under comparable conditions to a previous work with ÄD (Totskiy et al., 2012). The term “sorption” implies here to the total Tc immobilization due to various processes – surface complexation (sorption) itself and reduction of pertechnetate by Fe(II) species followed by potential precipitation of Tc(IV) as insoluble $\text{TcO}_2 \cdot 1.6\text{H}_2\text{O}(\text{s})$. Tc sorption evolution with different Tc concentrations is shown in Figure 3.

After three weeks of equilibration time plateau values of sorption within the analytical uncertainty were reached for all tested Tc concentrations. In the case of the lowest concentration (10^{-9} M) the final Tc retention was ~45%, and for the highest concentration used (10^{-5} M) ~18%. These values are quite similar to the results found for the sorption onto oxidized ÄD, performed under similar conditions – ~40% for the initial Tc concentration of 10^{-9} M and ~10% for 10^{-5} M, respectively. Only for the intermediate Tc concentration (10^{-8} M) sorption values differ considerably – ~20% for NK and ~40% for ÄD. Observed sorption decreases towards the last kinetic points (190 days contact time) for 10^{-9} M Tc samples. This can be explained by oxygen intrusion into the glovebox and partial re-oxidation of a Tc(IV) species. Data on ion-exchangeable Fe(II) extraction ($0.1 - 1 \mu\text{g/g}$ of Fe(II) for NK granite, and $1 - 3 \mu\text{g/g}$ for oxidized ÄD) indicate that the investigated NK cores were stronger oxidized by air than ÄD or cores had a lower overall redox buffer capacity. The difference in sorption of the intermediate Tc concentration used, might serve as reasoning for the assumptions made above. According to N_2 -BET analyses NK granite has higher surface area with $0.32 \text{ m}^2/\text{g}$ than ÄD with $0.16 \text{ m}^2/\text{g}$, respectively. However, since mineral surfaces are not saturated with Tc, surface area does not limit Tc sorption and Fe(II) content is considered to be the more important factor in the immobilization process.

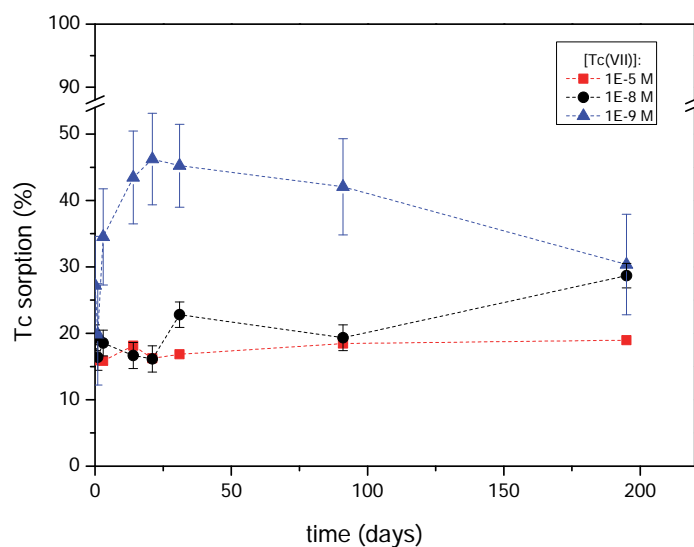


Figure 3: Sorption kinetics with different Tc(VII) concentrations on NK granitic rocks.

The formation of Tc colloidal phase was not detected while comparing ultracentrifuged samples with non-centrifuged. Similar results were obtained for ÄD material. This supports the hypothesis of either negligible formation of eigencolloids or its low stability under considered groundwater conditions.

Redox potential measurements of Tc ÄGWS after one month equilibration time with oxidized and un-oxidized ÄD are shown in Figure 4 together with Pourbaix diagrams calculated for the ÄGW composition with HYDRA/MEDUSA software.

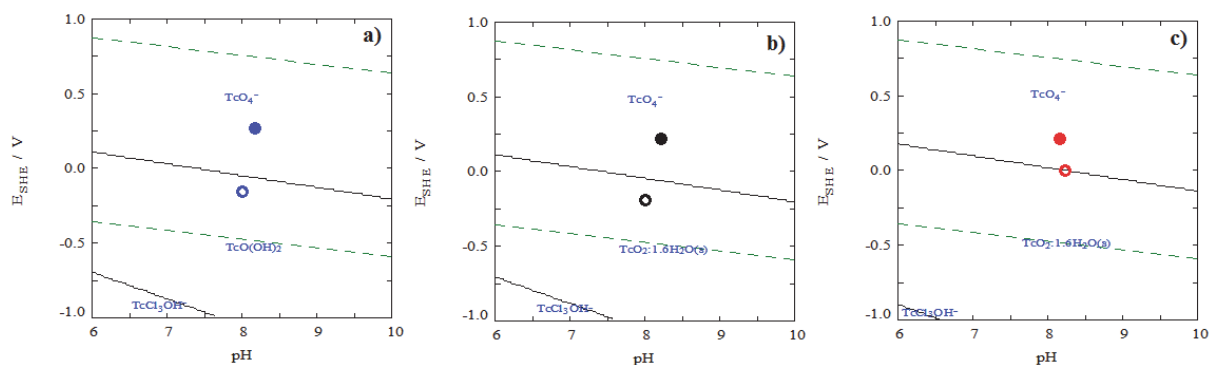


Figure 4: Pourbaix diagrams for ÄGW containing 10^{-9} M (a), 10^{-8} M (b) and 10^{-5} M (c) Tc. Empty and filled circles indicate experimental points of un-oxidized and oxidized ÄD, respectively.

Redox potential values after one week of Tc sorption on NK material are similar (within error margins) to oxidized ÄD (~300 mV) and do not differ significantly for varying Tc concentrations. The same trend of decreasing Eh values were measured as already observed in the ÄD system. After one month of equilibration redox potentials were ~ 240 mV. According to Pourbaix diagrams Tc reduction in the supernatant is thermodynamically feasible only in the case of un-oxidized material, whereas equilibrated with oxidized granitic rocks GW stabilizes Tc(VII). Tc reduction in the oxidized case may take place on the material surface or in pores, where Fe(II) concentration is possibly higher.

Distribution coefficient (K_d) was calculated using equation

$$K_d = \frac{C_0 - C_f}{C_f} \times \frac{V}{m_{solid}} \quad \text{eq. 1}$$

where C_0 and C_f are the initial and final aqueous activities of radionuclide (Bq/mL), respectively, V is the volume of aqueous phase (mL) and m_{solid} – the solid mass (g). This equation is traditional for sorption estimation and has been used in recent works (Kaplan et al., 2008; Powell et al., 2002). Typical K_d values, obtained for Tc sorption onto Äspö and Nizhnekansky massif rock materials as result of the present work are presented in Table 1.

XPS analysis of ÄD disc fragments, after exposing them to 10^{-5} M Tc(VII) in ÄGWS for two months, revealed that Tc is located in dark, mafic regions of rock material (Figure 5), whereas on light minerals it could not be detected. According to the binding energy data found in the XPS spectrum (Figure 6), technetium is reduced (from +7 to +4) most probably on Fe(II)-containing mica surfaces (biotite). Reduced Tc is probably present as $\text{TcO}_2 \cdot 1.6\text{H}_2\text{O}(\text{s})$. Tc(VII) was not detected on the material after sorption.

Table 1: Experimental K_d values for Tc sorption initially introduced as Tc(VII) onto ÄD and NK materials.

Tc concentration, M	Distribution coefficient K_d , mL/g		
	Unoxidized ÄD	Oxidized ÄD	Oxidized NK
10^{-5}	1.2	0.5	0.8
10^{-8}	500	3	0.8
10^{-9}	1000	3	3.5



Figure 5: ÄD sample for XPS. Red circle indicates region where Tc(IV) was found.

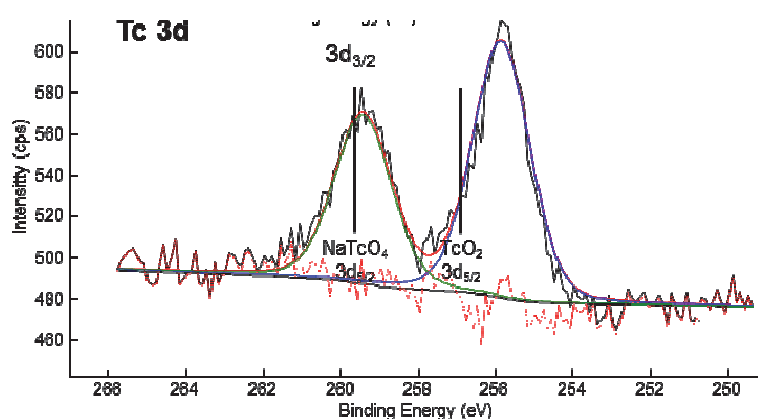


Figure 6: XPS narrow scan of Tc 3d spectrum after sorption onto ÄD surface.

To prove the assumption of Tc(VII) reduction by a Fe(II) species as a pathway of Tc immobilization, technetium sorption experiment onto freshly synthesized magnetite as a reference material was also carried out. Synthesized magnetite was fully characterized with Raman spectrometry, XDR (both proved, that it is pure magnetite), XPS (29% Fe(II) with ideal value of 33%), SEM (100 – 200 nm particle size) and BET (10.96 m²/g surface area).

From results of sorption kinetic experiments (Figure 7) one can clearly deduce, that pertechnetate immobilization is much faster and more effective on magnetite, than on natural granite samples. Sorption reaches the plateau ~100% after about one week contact time with distribution coefficient $K_d > 10^4$ for all investigated cases (three different Tc concentrations at pH 7 and 8).

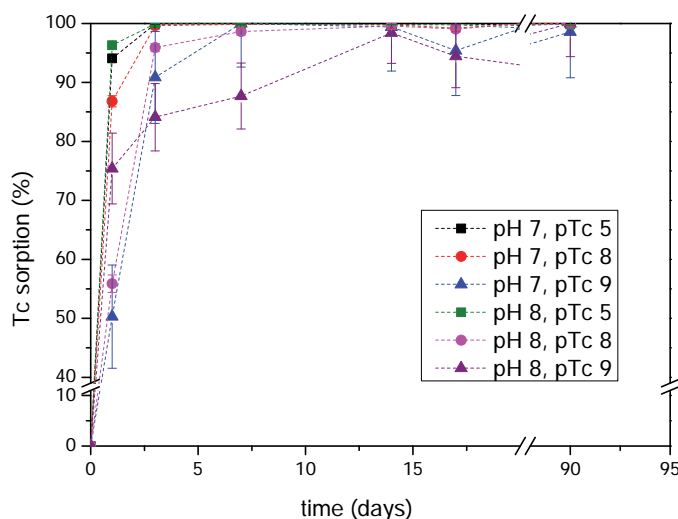


Figure 7: Sorption kinetics for different initial Tc concentrations onto magnetite.

Technetium oxidation state on magnetite was again determined with XPS analysis. It was proved, that Tc is reduced by Fe(II) and occurs only as Tc(IV) (Figure 9). No traces of Tc(VII) were found on the magnetite surfaces. Fe(II)/Fe(III) ratio in magnetite remained constant during the experiment due to excess of Fe(II). Total Fe(II) amount was about $7.5 \cdot 10^{-3}$ mol/L versus the highest Tc concentration of 10^{-5} mol/L. Redox potential in all samples was on the Tc(IV)/Tc(VII) borderline within the measurement error, Eh values were from +80 mV to +110 mV.

The next step in this direction will be (a) to perform Tc sorption onto magnetite isostructural maghemite (pure Fe(III) end-member) to investigate the pure sorption without reduction, and (b) to measure full sorption isotherms over larger Tc concentration ranges in order to capture sorption behaviour with XAFS investigations as well. Also trace concentration studies below the Tc(IV) solubility limit by ^{95m}Tc will be performed.



Figure 8: Magnetite sample for XPS. Red circle marks the place of analysis.

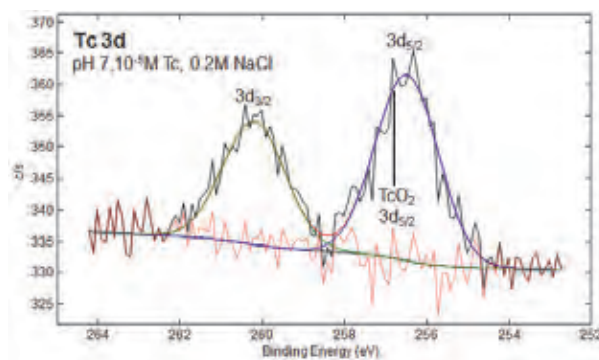


Figure 9: XPS narrow scan of Tc 3d spectrum after sorption onto magnetite.

Desorption experiments

Desorption experiments, which covered one month of equilibration time on initially three months contacted sorption samples, show very low desorption in all studied cases for both ÄD and NK materials, regardless of oxidized or un-oxidized material used. For the case of ÄD samples two types of natural groundwaters – Äspö and Grimsel GWs (representing glacial melt water composition with low ionic strength) were used. Desorption achieved values of up to 7% after one day contact time. This level remained relatively stable up to 30 days of equilibration and resulted washing out of soluble Tc(VII) species without further contribution from surface associated Tc(IV).

Pre-oxidation of the ÄD samples on air for one month before addition of ÄGWS changed the Tc desorption behaviour drastically (Figure 10). Both sorption experiments, with originally oxidized and un-oxidized materials were treated by air revealed the same desorption behaviour possibly indicating a comparable Tc surface species. To explain the strong desorption dependence on initial Tc concentration a hypothesis of matrix diffusion was proposed, but this phenomenon still requires further investigations. Similar studies for the NK material are in progress.

ÄD core migration experiments

Conservative tracer tests for hydraulic characterization of a natural fracture were performed by HTO and the effect of potential anion exclusion was monitored in parallel through addition of ³⁶Cl. Typical breakthrough curves (BTC) for both radionuclides at different flow rates are shown in Figure 11. The long tailing of the BTC is most likely due to channelling through the fracture with different flow rates as identified by μ CT measurements. A significant contribution of the experimental set-up to the observed tailing could be excluded by additional tests bypassing the core.

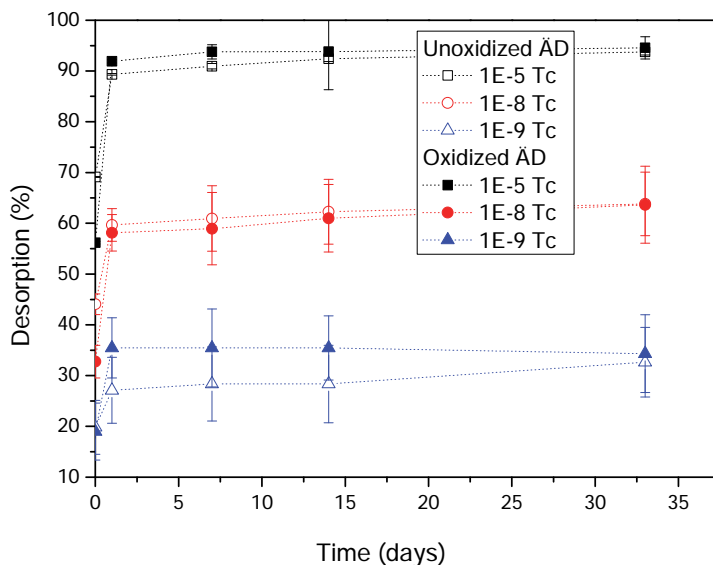


Figure 10: Desorption kinetics of Tc sorption experiments performed with oxidized and un-oxidized ÄD material after one month pre-oxidation under atmospheric conditions.

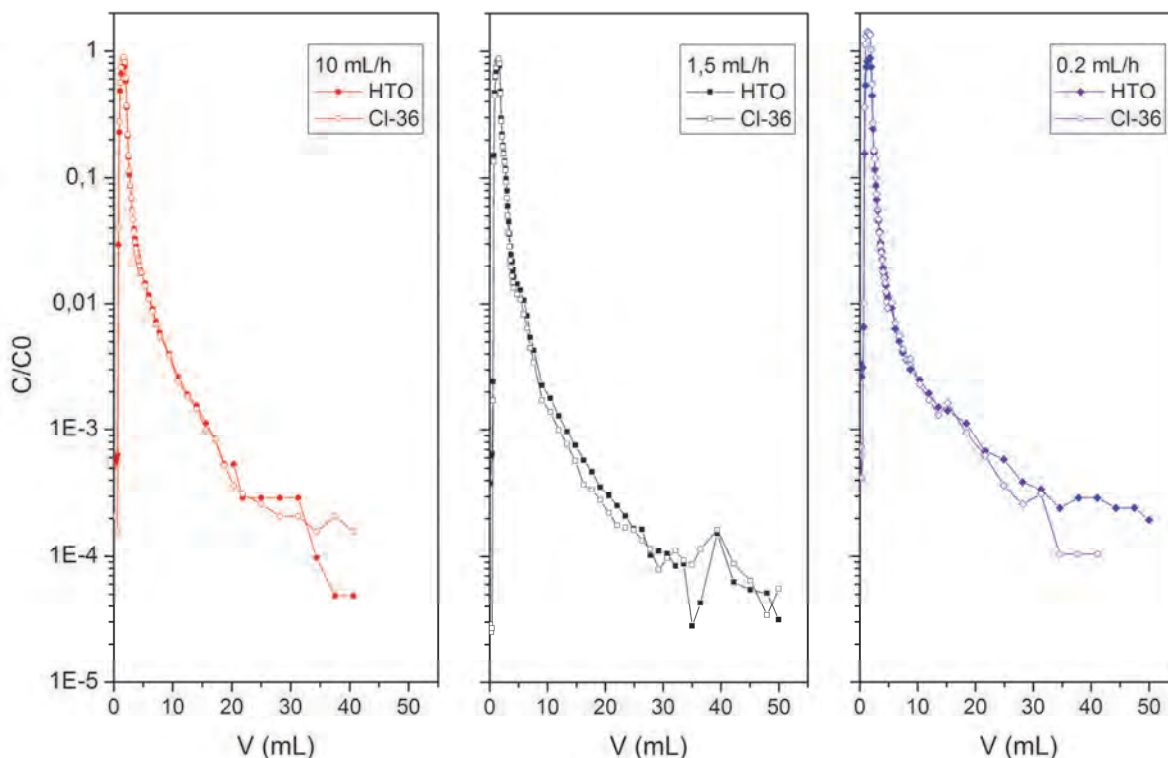


Figure 11: HTO and ³⁶Cl breakthrough curves for natural fracture in Äspö core #2.2.

Based on pressure measurements on the both ends of the core during the experiments under three different flow rates (10, 1.5 and 0.2 mL/h), permeability ($3.4 - 4.0 \cdot 10^{-14} \text{ m}^2$) and hydraulic conductivity ($2.5 - 3.0 \cdot 10^{-10} \text{ m/s}$) were calculated. The comparison of HTO and ³⁶Cl BTC for different flow velocities clearly shows an influence of fracture residence time on breakthrough tailing. As far as HTO and ³⁶Cl show similar behaviour, anion exclusion effect was not observed in the fracture investigated. Currently, Tc migration studies using ^{95m}Tc(VII) at trace concentrations below the Tc(IV) solubility are in progress and will be presented in a later occasion.

Conclusions

According to the experimental work, Tc behaviour on both ÄD and NK oxidized materials is quite similar, but it differs dramatically with non-oxidized ÄD samples. Oxidized rocks can sorb up to 40% – 50% of Tc trace concentrations (10^{-9} M) and up to 10% – 20% of Tc at a relatively high (10^{-5} M) concentration. Varying values between ÄD and NK samples at an intermediate (10^{-8} M) concentration indicates that NK samples contain less available Fe(II), than ÄD. This is also confirmed with extractions of ion-exchangeable Fe(II) (0.1 – 1 µg/g for NK granites and 1 – 3 µg/g for ÄD). Apparently, the Tc(VII) concentration is directly influencing the sorbed amount of Tc on un-oxidized and oxidized material, which can be correlated with the ion-exchangeable Fe(II) buffer available. The Tc(VII) reduction by ferrous iron resulting in insoluble Tc(IV) species was proved by XPS analysis. There was no indication of surface complexation in these cases. In accordance with this observation fast and effective sorption of only Tc(IV) onto magnetite as a reference system was found. Distribution coefficient values for further migration modelling were determined.

Technetium desorption from granites under natural conditions is insignificant for all investigated cases, but after artificial oxidation of samples technetium mobility is increased.

Further activities, continued after the finalization of the CP-CROCK project will include continuation of technetium migration experiment with the natural core, batch-type sorption on maghemite, precise surface spectroscopic study and reactive transport modelling.

Acknowledgement

The research leading to these results has received funding from the European Union's European Atomic Energy Community's (Euratom) 7th Framework Programme FP7/2007-2011 under grant agreement n° 269658 (CROCK project) and the Federal Ministry of Economics and Technology (BMWi) collaborative project VESPA (Behaviour of long-lived fission and activation products in the near field of a repository and possible retention mechanisms) under contract n° 02 E 10800.

We would like to express our thanks to M. Rothmeier (KIT-INE), N.V. Kuzmenkova (MSU), I.E. Vlasova (MSU) and V.G. Petrov (MSU) for great help in sample preparations, N. Finck (KIT-INE) for help in XRD measurements and S. Heck (KIT-INE) for laboratory supply.

References

- Bondietti, E. A. and Francis, C. W. (1979). Geologic Migration Potentials of Technetium-99 and Neptunium-237. *Science*, 203(4387), 1337-1340.
- Boyd, G. E., Larson, Q. V. and Motta, E. E., (1960). Isolation of Milligram Quantities of Long-Lived Technetium from Neutron Irradiated Molybdenum. *Journal of the American Chemical Society*, 82(4), 809-815.
- Fredrickson, J. K., Zachara, J. M., Plymale, A. E., Heald, S. M., McKinley, J. P., Kennedy, D. W., Liu C. and Nachimuthu, P. (2009). Oxidative dissolution potential of biogenic and ablogenic TcO₂ in subsurface sediments. *Geochimica Et Cosmochimica Acta*, 73(8), 2299-2313.

Heald, S. M., Zachara, J. M., Jeon, B. H., McKinley, J. P., Kukkadapu, R. and Moore, D. (2007). XAFS Study of the Chemical and Structural States of Technetium in Fe (III) Oxide Co-Precipitates. In AIP Conference Proceedings, 882, 173.

Heck, S. and Schäfer, T. (2012). Short Note: CP CROCK groundwater sample characterization.

Heron, G., Crouzet, C., Bourg, A. C. M. and Christensen, T. H. (1994). Speciation of Fe(II) and Fe(III) in contaminated aquifer sediments using chemical extraction techniques. Environ. Sci. Technol., 28, 1698-1705.

Jaisi, D. P., Dong, H., Plymale, A. E., Fredrickson, J. K., Zachara, J. M., Heald, S. and Liu, C. (2009). Reduction and long-term immobilization of technetium by Fe (II) associated with clay mineral nontronite. Chemical Geology, 264(1), 127-138.

Jardine, L.J. (2005). Development of a Comprehensive Plan for Scientific Research, Exploration, and Design: Creation of an Underground Radioactive Waste Isolation Facility at the Nizhnekansky Rock Massif. UCRL-TR-213167.

Kaplan, D. I., Roberts, K., Coates, J., Siegfried, M. and Serkiz, S. (2008). Saltstone and concrete interactions with radionuclides: sorption (K_d), desorption, and reduction capacity measurements. SRNS-STI-2008-00045, SRNL.

Kienzler, B., Vejmelka, P., Römer, J., Fanghänel, E., Jansson, M., Eriksen, T. E. and Wikberg, P. (2003). Swedish-German actinide migration experiment at ÄSPÖ hard rock laboratory. Journal of Contaminant Hydrology, 61(1), 219-233.

Kienzler, B., Vejmelka, P., Romer, J., Schild, D., Jansson, M. (2009). Actinide Migration in Fractures of Granite Host Rock: Laboratory and in Situ Investigations. Nuclear Technology, 165(2), 223-240.

KIT-INE, 2012. Characterization of experimental material. CROCK Deliverable 1.2.

Peretyazhko, T., Zachara, J. M., Heald, S. M., Jeon, B. H., Kukkadapu, R. K., Liu, C., Moore, D. and Rescha, C. T. (2008a). Heterogeneous reduction of Tc(VII) by Fe(II) at the solid-water interface. Geochimica Et Cosmochimica Acta, 72(6): 1521-1539.

Peretyazhko, T., Zachara, J. M., Heald, S. M., Kukkadapu, R. K., Liu, C., Plymale, A. E. and Resch, C. T. (2008). Reduction of Tc (VII) by Fe (II) sorbed on Al (hydr) oxides. Environmental science & technology, 42(15), 5499-5506.

Petrov, V. G., Vlasova, I. E., Kuzmenkova, N. V., Petrov, V. A., Poluektov, V. V., Grivot, A. and Lalmykov, S. N. (2012). Characterisation of rock samples from areas of the proposed. Russian HLW and SNF repository (Nizhnekansky massive) and first sorption studies. 1st Workshop Proceedings of the Collaborative Project „Crystalline Rock Retention Processes“ (7th EC FP CP CROCK), 37-42.

Powell, B. A., Fjeld, R. A., Coates, J. T., Kaplan, D. I. and Serkiz, S. M. (2002). Plutonium oxidation state geochemistry in the SRS subsurface environment. WSRC-TR-2003-00035, SRC.

Schäfer, T., Stage, E., Büchner, S., Huber, F. and Drake, H. (2012). Characterization of new crystalline material for investigations within CP CROCK. 1st CROCK Workshop Proceedings.

Schwertmann, U. and Cornell, R.M. (2000). *Iron Oxides in the Laboratory*. Wiley.

Totskiy, Y., Geckeis, H. and Schäfer, T. (2012). Sorption of Tc(VII) on Äspö Diorite (ÄD). 1st Workshop Proceedings of the Collaborative Project "Crystalline Rock Retention Processes" (7th EC FP CP CROCK), 97-105.

Um, W. and Serne, R.J. (2005). Sorption and transport behaviour of radionuclides in the proposed low-level radioactive waste disposal facility at the Hanford site, Washington. *Radiochimica Acta*, 93(1), 57-63.

Viollier, E., Inglett, P. W., Hunter, K., Roychoudhury, A. N. and Van Cappellen, P. (2000). The ferrozine method revisited: Fe(II)/Fe(III) determination in natural waters. *Applied Geochemistry*, 15(6), 785-790.

Zachara, J. M., Heald, S. M., Jeon, B. H., Kukkadapu, R. K., Liu, C., McKinley, J. P., Dohnalkova, A. C. and Moore, D. A. (2007a). Reduction of pertechnetate [Tc(VII)] by aqueous Fe(II) and the nature of solid phase redox products. *Geochimica Et Cosmochimica Acta*, 71(9), 2137-2157.

Zachara, J. M., Serne, J., Freshley, M., Mann, F., Anderson, F., Wood, M., Jones, T. and Myers, D. (2007b). Geochemical processes controlling migration of tank wastes in Hanford's vadose zone. *Vadose Zone Journal*, 6(4), 985-1003.

INTERACTION OF URANIUM(VI) AND NEPTUNIUM(V) WITH ÄSPÖ DIORITE UNDER ANOXIC CONDITIONS

Katja Schmeide*, Sylvia Gürtler, Frank Bok, Vinzenz Brendler

Helmholtz-Zentrum Dresden-Rossendorf, Institute of Resource Ecology,
P.O. Box 51 01 19, 01314 Dresden, Germany

* Corresponding author: k.schmeide@hzdr.de

Abstract

The interaction of uranium(VI) and neptunium(V) with diorite obtained from Äspö Hard Rock Laboratory (HRL, Sweden) has been studied by means of batch sorption experiments under anoxic conditions (N₂ atmosphere) as a function of contact time (5 to 108 d) applying a synthetic Äspö groundwater (pH 7.8, $I = 0.18$ M) as background electrolyte. In the case of uranium(VI), sorption isotherms have been recorded by varying the total uranium(VI) concentration between 3×10^{-9} and 6×10^{-5} M. For the sorption of uranium and neptunium on anoxic diorite (1 – 2 mm fraction), distribution coefficients were determined with $K_d = (3.8 \pm 0.6)$ L/kg and $K_d = (93 \pm 65)$ L/kg, respectively. Desorption experiments have been performed using synthetic Äspö groundwater. For redox speciation of actinides in sample solution or desorbed from the diorite, solvent extraction has been applied.

Introduction

Risk assessments predicting the fate and transport of actinides under environmentally relevant conditions require extensive knowledge about their interaction with complexing ligands, their sorption and redox behaviour, their solubility, as well as their ability to form colloids. Both the speciation and the mobility of actinides in aquatic systems strongly depend on their oxidation state due to the different precipitation, complexation, sorption and colloid formation behaviour of the various oxidation states (e.g., Silva and Nitsche, 1995; Choppin, 2006; Kim, 2006).

Under oxidizing geochemical conditions, uranium and neptunium occur in the hexavalent and pentavalent oxidation state, respectively, thereby being highly soluble and mobile. Under reducing conditions as prevalent in deep geological environments, the tetravalent oxidation state predominates. The tetravalent actinides are regarded as much less mobile due to the low solubility of their hydrous oxides and their pronounced hydrolysis tendency even at low pH (Neck and Kim, 2001; Opel et al., 2007) which leads to precipitation (except for strongly acidic conditions) and/or results in high sorption affinity to mineral surfaces. However, it is also known that in the presence of inorganic or organic complexing ligands or aquatic colloids also tetravalent actinides may become mobile due to formation of soluble complexes or stable colloids as shown for neptunium(IV) (Artinger et al., 2000; Schmeide et al., 2010).

Granitic subsurface environments are considered as potential host rock formations for the deep underground disposal of radioactive waste (Bäckblom, 1991). Sorption on mineral surfaces of the host rock is one important retardation process for radionuclides to be considered in long-term safety assessments for radioactive waste

repositories. Diorite, as representative crystalline rock material from the Äspö HRL (Sweden), was applied for the present study. It was sampled, transported, crushed and stored under anoxic conditions. Details with regard to sampling procedure and material characterization can be found in (Schäfer et al., 2012). The objective of the present sorption experiments was to quantify the retention capacity of this anoxic, unaltered diorite towards the redox-sensitive actinides uranium and neptunium and to compare the sorption data with experimental results obtained directly at the Äspö HRL, where the sorption/migration of radionuclides can be investigated under in situ conditions (e.g., Jansson and Eriksen, 1998; Vejmelka et al., 2000; Widestrand et al., 2001; Kienzler et al., 2003, 2009; Park et al., 2012). Thus, to perform the sorption experiments under conditions that approximate to near-realistic environmental conditions on-site, a synthetic Äspö groundwater, prepared under anoxic conditions, was applied as background electrolyte.

In our previous work (Schmeide et al., 2012), the sorption of uranium(VI) and neptunium(V) onto diorite was studied by means of batch sorption experiments in dependence on solid-to-liquid ratio (2 to 200 g/L), grain size (0.063 – 0.2 mm, 0.5 – 1 mm, 1 – 2 mm), temperature (25 and 10°C) and atmosphere (N₂ or $p\text{CO}_2 = 10^{-3.5}$ atm) using a synthetic Äspö groundwater (pH 7.8, $I = 0.18$ M) as background electrolyte. The K_d values were found to decrease with increasing grain size of the diorite and with decreasing temperature. The K_d values determined under oxic conditions are lower than those determined under anoxic conditions. Since these experiments proved a solid-to-liquid ratio of 200 g/L optimal for the sorption experiments and the 1 – 2 mm grain size fraction as representative, these experimental conditions were also applied for the present sorption studies.

Thus, the interaction of uranium(VI) and neptunium(V) with crushed diorite (1 – 2 mm, 200 g/L) in synthetic Äspö groundwater has been studied over a longer time period (up to 108 d) under anoxic conditions (N₂ atmosphere). For uranium(VI), sorption isotherms (3×10^{-9} M to 6×10^{-5} M UO₂²⁺) have been recorded.

Experimental

Material

A new diorite batch for sorption experiments was prepared by crushing further diorite discs from the drill core #2.30 in an inert gas box (N₂ atmosphere) with a hammer and sieving the crushed material with stainless steel sieves whereby the fraction 1 – 2 mm was obtained. This fraction was washed with degassed Milli-Q water (Milli-RO/Milli-Q-System, Millipore, Molsheim, France) to remove any dust and then, dried. Its Kr-BET surface area, determined by using a surface area and pore size analyser (mod. Coulter SA 3100, Beckman Coulter, Fullerton, USA), amounts to 0.125 ± 0.012 m²/g.

A synthetic Äspö groundwater was prepared, based on the composition of the natural Äspö groundwater KA3600-F-2 (Schäfer et al., 2012), in an inert gas box. All salts (Na₂B₄O₇ · 10 H₂O, NaCl, MgSO₄ · 7 H₂O, CaCl₂ · 2 H₂O, SrCl₂ · 6 H₂O (all p.a., Merck), LiF (suprapur, Merck), KBr (Uvasol, for IR spectroscopy, Merck)), with the exception of NaHCO₃, were dissolved in O₂- and CO₂-free Milli-Q water. Then, this solution was additionally deoxygenated by bubbling N₂ through the solution for about 1 h and after that, NaHCO₃ (p.a., Merck) was added. The composition of the synthetic groundwater is shown in Table 1.

Table 1: Composition of the synthetic Äspö groundwater applied in this work.

Element/Ion	Concentration (mol/L)
Li	7.4×10^{-5}
Na	8.2×10^{-2}
K	2.7×10^{-4}
Mg	4.1×10^{-3}
Ca	2.8×10^{-2}
Sr	2.3×10^{-4}
B	4.0×10^{-5}
F ⁻	7.4×10^{-5}
Cl ⁻	1.4×10^{-1}
Br ⁻	2.7×10^{-4}
SO ₄ ²⁻	4.1×10^{-3}
CO ₃ ²⁻ /HCO ₃ ⁻	1.9×10^{-4}
<i>I</i>	0.18
pH	7.8

Batch sorption and desorption experiments

The sorption and desorption experiments were performed in an inert gas box (N₂) at room temperature. Exclusively the 1 – 2 mm grain size fraction of diorite was used for sorption experiments, the solid-to-liquid ratio was always 200 g/L.

Three different procedures were applied for the sorption experiments.

- i) During pre-equilibration of the diorite in Äspö groundwater (10 d), the background electrolyte was exchanged 4 times. For this, the samples were centrifuged at 2880×g for 15 min (Sigma 3K18, Sigma, Germany) and 8 mL of the supernatant solution were replaced with fresh Äspö groundwater. No additional pH corrections during pre-equilibration. Start of the sorption experiment by replacing a certain amount of background electrolyte with Äspö groundwater spiked with radionuclide (²³³U(VI) or ²³⁷Np(V)), previously equilibrated at pH 7.8 for 3 d. During the sorption process, pH values were measured/adjusted at rare intervals (e.g., during 107 d sorption time, the pH value was adjusted 6 times to pH 7.8 whereby only small amounts of diluted HCl were added).
- ii) During pre-equilibration (10 d), the background electrolyte was not exchanged (also no pH corrections). Start of the sorption experiment by adding an aliquot of the radionuclide stock solution, with immediate pH adjustment of the sample solution to pH 7.8. Rare pH adjustments during sorption process (similar to procedure i)).

- iii) In the case of two sorption experiments (the 108 d experiments for uranium and neptunium), pre-equilibration and start of sorption were performed according to procedure i). The pH values were neither measured nor adjusted during sorption (the samples were closed during the sorption experiments).

During pre-equilibration and sorption, the samples were continuously shaken on a horizontal shaker. After the specified sorption time, the final pH values of the samples were determined. The solid and liquid phases were separated by centrifugation and subsequent filtration of the supernatants (450 nm; polyethersulfone). Prior to filtering, the filters were rinsed with 1 mL of the sample solutions. Regular tests showed that actinide concentration in associated supernatants and filtrates was identical. The actinide concentration in solution was determined by liquid scintillation counting (LSC, Winspectral α/β , Wallac 1414, Perkin Elmer). Conventional distribution coefficients (K_d values) were determined by using the following equation:

$$K_d \text{ (L/kg)} = \frac{c_0 - c_{\text{eq}}}{c_{\text{eq}}} \frac{V}{m} \quad \text{eq. 1}$$

where c_0 and c_{eq} (mol/L) are the initial and equilibrium actinide concentration in solution, V (L) represents the solution volume and m (kg) the mass of solid. By dividing the K_d values by the specific surface area (A , m^2/g) of the respective diorite fraction, K_a values (cm) are obtained. The sorption experiments were performed at least in duplicate.

Subsequent to sorption experiments, desorption of uranium and neptunium from the loaded rock material was studied. For this, the supernatants of the sorption samples were removed after the specified contact time and fresh Äspö groundwater was added. Samples were taken after 1, 3 and 7 d and analysed by LSC. The redox state of uranium and neptunium, remained in the supernatant solution after sorption or desorbed from the diorite, was checked by means of solvent extraction using 0.5 M 2-thenoyltrifluoroacetone (TTA; puriss. p.a., Fluka, Taufkirchen, Germany) in xylene (puriss. p.a., Fluka) (Bertrand and Choppin, 1982). After finalization of the sorption experiments, redox potentials of the sorption samples were measured using a combined platinum Ag/AgCl redox electrode (Schott, Mainz, Germany) recording values every half hour over a period of about 4 to 5 h. The E_h values given in the paper correspond to the minima of the E_h evolution during the measurements and are corrected for the standard hydrogen potential (SHE).

Thermodynamic modelling

The actinide speciation in Äspö groundwater was calculated with the speciation code EQ3/6 (Wolery, 1992) applying uranium(VI) and neptunium(V) thermodynamic data compiled in the OECD/NEA Thermochemical Database (Guillaumont et al., 2003) with addition of thermodynamic data of the $\text{Ca}_2\text{UO}_2(\text{CO}_3)_3(\text{aq})$ complex (Bernhard et al., 2001).

An E_h -pH diagram for uranium was calculated with the geochemical speciation code "Geochemist's Workbench" (Rockware[®], Release 8.0.12) using the default data base thermo.dat accompanying the code, supplemented by the thermodynamic data mentioned above. It was calculated for the experimental conditions applied in this study whereby the formation of solid uranium phases was suppressed.

Results and Discussion

Our previous experiments to the uranium(VI) sorption onto diorite in Äspö groundwater (Schmeide et al., 2012) have shown that the speciation of uranium(VI) in solution and consequently, its sorption onto diorite is strongly influenced by the groundwater composition. From the ions leached out of diorite, calcium and carbonate ions have the strongest influence. $\text{Ca}_2\text{UO}_2(\text{CO}_3)_3(\text{aq})$ determines the aqueous chemistry of uranium in the neutral to alkaline pH range (cf. Figure 1) due to its large formation constant ($\log \beta_{213}^{\circ} = 30.45 \pm 0.35$ (Bernhard et al., 2001)). In agreement with the speciation calculation, $\text{Ca}_2\text{UO}_2(\text{CO}_3)_3(\text{aq})$ was found to be the dominating species in Äspö groundwater at pH 7.8 by time-resolved laser-induced fluorescence spectroscopy (Schmeide et al., 2012). As predominant surface species on diorite, $\text{UO}_2(\text{CO}_3)_3^{4-}$ was identified by in situ time-resolved attenuated total reflection Fourier-transform infrared (ATR FT-IR) spectroscopy (Schmeide et al., 2012).

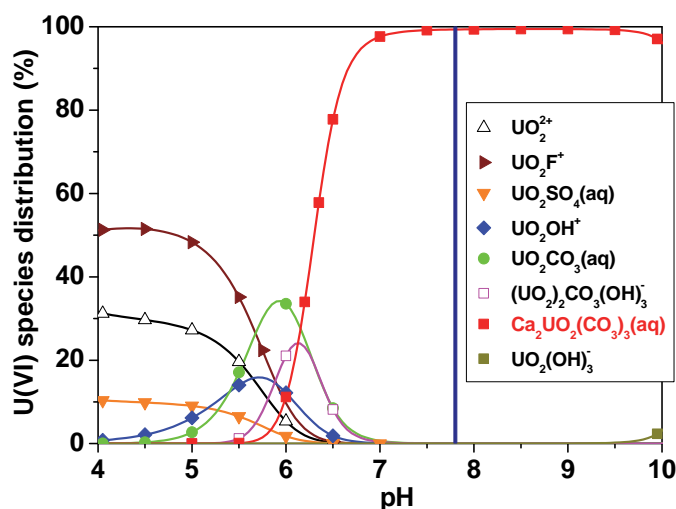


Figure 1: Uranium(VI) speciation in Äspö groundwater ($[\text{U}]_{\text{total}} = 1 \times 10^{-6} \text{ M}$, N_2). Species below 5% are not plotted.

In Figure 2, the uranium(VI) sorption onto diorite in Äspö groundwater is shown in dependence on sorption time. For each sorption time studied, separate sorption samples were prepared. Mostly the sorption procedure i) was applied. The results shown for a sorption time of 21 d, however, contain sorption results obtained by applying the sorption procedure i) (4 samples) or ii) (2 samples). No strong differences are observable for sorption results obtained by the two procedures. The sorption samples equilibrated for 107 d or for 108 d show the peculiarity that in each case one sorption sample fits to the results of the sorption samples obtained after shorter sorption time and one sorption sample shows a much higher uranium sorption. The reason for this scatter is not clear. It might be attributed to a heterogeneity of the natural rock material whose relatively large grains (1 – 2 mm), applied for sorption experiments, can differ in the inventory of sorbing minerals and/or the iron(II) content.

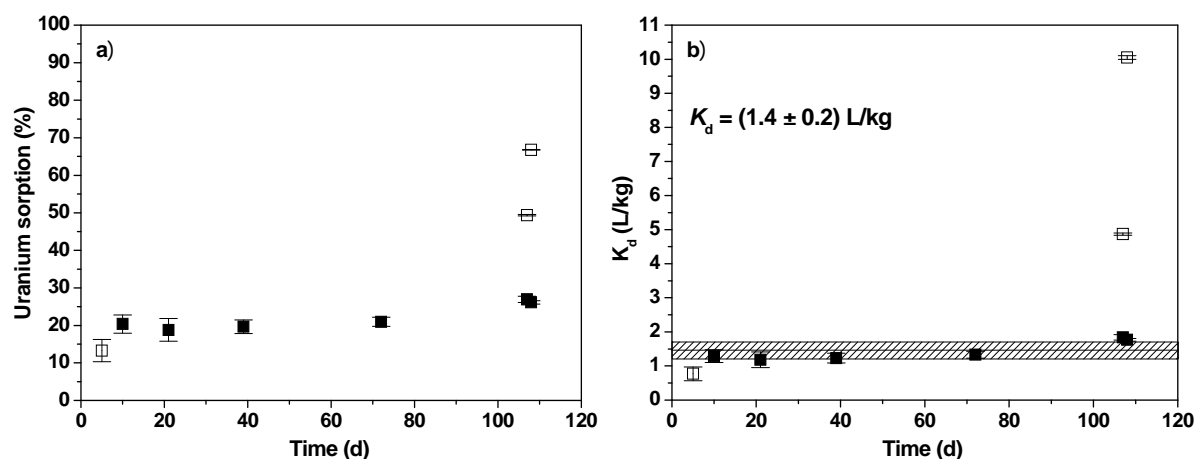


Figure 2: Uranium sorption onto diorite as a function of time shown on a percentage scale (a) and as K_d value (b) ($[U]_{total} = 1 \times 10^{-6}$ M, Äspö groundwater, $S/L = 200$ g/L, $pH = 8.02 \pm 0.09$, N_2). Error bars: 2σ . For the sorption samples equilibrated for 107 d or 108 d, not the mean values, but the sorption data of the individual samples are shown. For the calculation of the mean K_d value, only the sorption data represented by filled symbols were used.

The carbonate content of the sorption samples equilibrated for 107 d (with pH adjustments) and 108 d (without pH adjustments) was determined with 1.7×10^{-4} M and 1.9×10^{-4} M, respectively, on average (error: ± 3 %). That means that pH adjustments usually applied during sorption experiments, which theoretically could lead to an enhanced leaching of the rock material or could change the carbonate concentration of the solution, have no strong influence on sorption results. The final pH values of the two samples studied for 108 d, where the sorption procedure iii) was applied (no pH adjustments), amounted to pH 7.98 and 8.09 (8.04 ± 0.08) which is in the range of the other samples.

Generally, Figure 2 shows that sorption equilibrium is reached relatively fast (after 10 to 20 d). On average, a K_d value of (1.4 ± 0.2) L/kg is determined for uranium sorption onto the 1 – 2 mm fraction of the diorite. This value confirms the low sorption affinity of uranium(VI) to diorite shown previously (Schmeide et al., 2012) under conditions where the aqueous $Ca_2UO_2(CO_3)_3$ complex predominates. The K_d value corresponds to a K_a value of 0.0011 cm which is in agreement with the data determined by Holgersson et al. (2013).

45 to 50% of the sorbed uranium can be desorbed with Äspö groundwater. This part occurs predominantly as uranium(VI) (~94%) as shown by TTA solvent extraction. Figure 3 shows the E_h -pH diagram for uranium in Äspö groundwater. For the redox potentials of the uranium/diorite/Äspö groundwater sample solutions, monitored at the end of each sorption experiment, an average amount of 160 ± 30 mV was determined. This value lies in the stability field of $Ca_2UO_2(CO_3)_3(aq)$. That means that in the Äspö groundwater system uranium is stabilized against reduction. Brooks et al. (2003) have shown that calcium uranyl carbonate complexes inhibit microbial reduction of uranium under certain conditions. However, whether or not uranium(IV) is formed directly at the diorite surface to some extent cannot be decided from the results of the desorption experiments. X-ray photoelectron spectroscopy (XPS) has to be applied to clarify the oxidation state of sorbed uranium. Kienzler et al. (2009) and Alonso et al. (2012) identified iron-bearing phases of Äspö crystalline rock as main sorbing mineral phases for uranium by XPS and ion beam technique micro-Particle Induced X-ray Emission (μ PIXE), respectively.

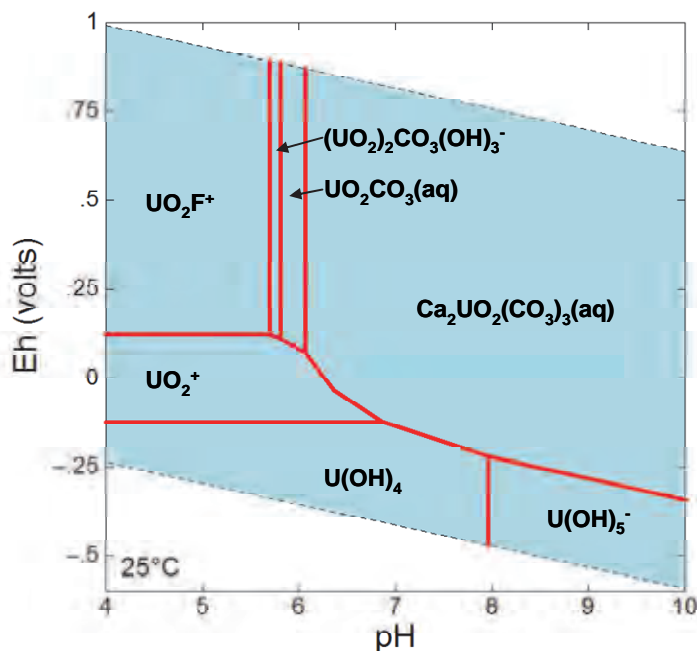


Figure 3: E_h -pH diagram for uranium in Äspö groundwater ($[U]_{total} = 1 \times 10^{-6} M$, N_2).

The uranium(VI) sorption onto diorite in Äspö groundwater was also studied as a function of the uranium(VI) concentration (Figure 4). The data obtained were fitted applying the Freundlich isotherm (Freundlich, 1906). The Freundlich isotherm is described by equation (eq. 2):

$$a_{eq} = c_{eq}^{n_F} \cdot k_F \quad \text{eq. 2}$$

where a_{eq} (mol/kg) is the amount of uranium(VI) adsorbed on the solid phase, c_{eq} (mol/L) is the equilibrium concentration of uranium(VI) in solution, k_F (L/kg) is the Freundlich coefficient and n_F (–) is the Freundlich exponent.

The distribution coefficient K_d is defined as follows:

$$K_d \text{ (L/kg)} = \frac{a_{eq}}{c_{eq}} \quad \text{eq. 3}$$

The K_d value for the uranium(VI) sorption onto diorite was calculated using the logarithmic form of equation 2. Setting $n_F = 1$, k_F is equal to K_d .

The sorption isotherm for the uranium(VI) sorption onto diorite is shown in Figure 4. With initial uranium(VI) concentrations between 3×10^{-9} and 2×10^{-5} M the amount of adsorbed uranium increases linearly with a slope of 0.88 (n_F). The sorption data obtained for the highest initial uranium(VI) concentration studied (6×10^{-5} M) point to a potential precipitation of uranium at the diorite surface and thus, was not included in the fit of the data. The K_d value, determined using the Freundlich equation and a fixed slope of 1, amounts to (3.8 ± 0.6) L/kg. The weak uranium(VI) sorption onto diorite in Äspö groundwater is confirmed.

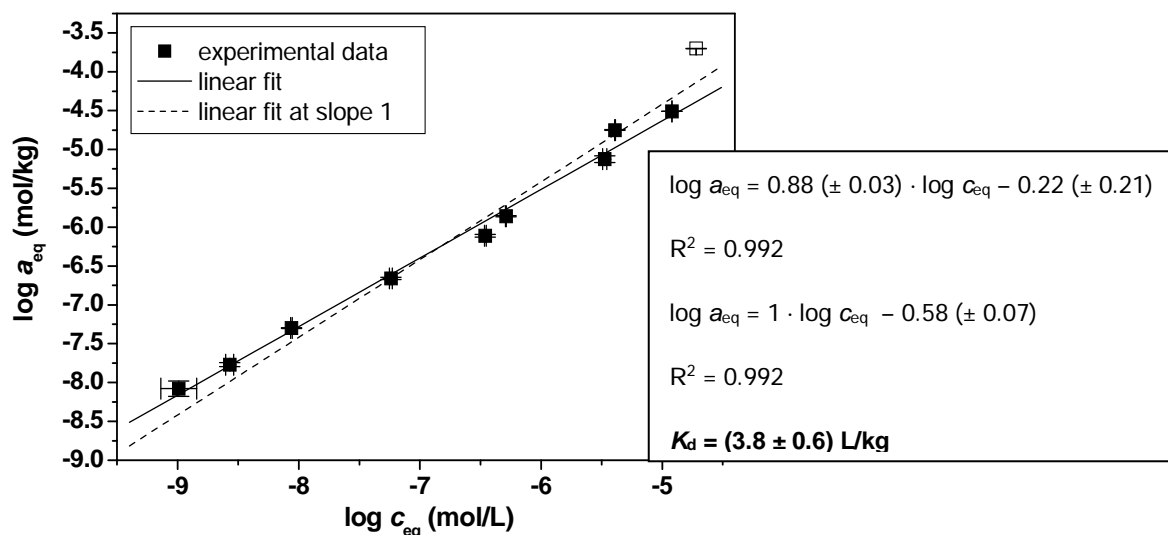


Figure 4: Freundlich isotherm of the uranium(VI) sorption onto diorite as a function of uranium(VI) concentration ($[U]_{total} = 3 \times 10^{-9} - 6 \times 10^{-5} M$, Äspö groundwater, $S/L = 200 \text{ g/L}$, $pH = 8.03 \pm 0.02$, N_2 , sorption time 60 d). Error bars: 2σ . For linear fits, only the sorption data represented by filled symbols were used.

In contrast to the uranium(VI)/diorite/Äspö groundwater system, the effect of the groundwater composition on neptunium(V) speciation in solution (cf. Figure 5) is weak in the neptunium(V)/diorite/Äspö groundwater system. The free uncomplexed neptunyl ion (NpO_2^+), predominating in Äspö groundwater at pH 7.8, was verified by ATR FT-IR spectroscopy (Schmeide et al., 2012). This species was also confirmed by UV-VIS-NIR spectroscopy and TTA extraction.

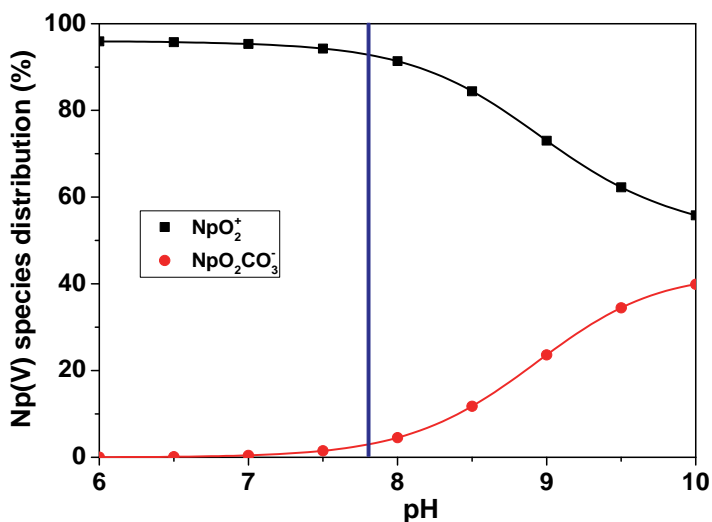


Figure 5: Neptunium(V) speciation in Äspö groundwater ($[Np]_{total} = 1 \times 10^{-6} M$, N_2). Species below 5% are not plotted.

In Figure 6, the neptunium(V) sorption onto diorite in Äspö groundwater is shown in dependence on sorption time. Again, for the individual sorption samples mostly the sorption procedure i) was applied. Only for the sorption samples studied for 21 d, the sorption procedure i) (4 samples) or ii) (2 samples) was applied. The difference obtained for these samples is within the experimental error. The sorption results obtained after 107

and 108 d, where the sorption procedure i) and iii), respectively, was applied, show a slight difference. The final pH values of the two samples studied for 108 d were determined with 8.06 and 8.11 (8.09 ± 0.04) which again is in the range of the other samples. Generally, Figure 6 shows that, compared to the respective uranium system, a longer sorption time is necessary to reach equilibrium (≥ 40 d). The neptunium sorption onto diorite is very strong with $> 90\%$ up to 98% . This strong neptunium retention can be attributed to a reduction of neptunium(V) to the less soluble neptunium(IV) by the iron(II) at the diorite surface. The iron(II) content of the Äspö diorite is reported with 2.51 wt.%, the content of total iron was determined with 4.39 wt.% (Schäfer et al., 2012). The ion-exchangeable iron(II) content of anoxic diorite was determined with about 4 – 6 $\mu\text{g/g}$ (Totskiy et al., 2012). The iron-bearing phases of Äspö granite rock were identified as main sorbing mineral phases for neptunium by Kienzler et al. (2009). Also Park et al. (2012) found for a fractured granite core in the Chemlab2 probe at the Äspö HRL that most of neptunium was retained onto granite and altered minerals by reduction to neptunium(IV) in the presence of iron(II) minerals. $\mu\text{-XAFS}$ measurements, performed by Denecke et al. (2009) after a radiotracer experiment in a fractured granite bore core from Äspö HRL, showed that neptunium, originally introduced as neptunium(V) into the column, is present in the granite in its reduced neptunium(IV) form. In some areas a correlation of the neptunium(IV) distribution with the iron distribution was found, in others not. This was attributed to different residence times, i.e., reaction times in fissures and fractions, respectively, having different sizes. More clearly, a correlation of neptunium(IV) with zinc was found. The neptunium(IV) was found to be present as particles, tens of μm in size.

Thus, in the case of the Np sorption system, the term ‘sorption’ means the total amount of neptunium associated with the solid phase after centrifugation. It is probably an overlapping of different processes: sorption as well as precipitation of neptunium(IV) hydrous oxide since its solubility is exceeded (solubility product of $\text{Np}(\text{OH})_{4(\text{am})}$ or $\text{NpO}_2 \cdot x\text{H}_2\text{O}_{(\text{am})}$ (Neck et al., 2001): $\log K_{\text{sp}}^\circ = -56.5 \pm 0.4$). The K_d values, given in Figure 6b, show a relatively strong scatter, especially where the sorption percentages approach 100%. However, the deviation is smaller than one order of magnitude. A mean K_d value of (93 ± 65) L/kg was determined for the neptunium sorption onto the 1 – 2 mm diorite fraction. This shows that the retention capacity of anoxic diorite towards neptunium is higher than towards uranium. Similar results were reported by Kienzler et al. (2009), who determined distribution coefficients, K_s , with (0.16 ± 0.025) cm and (0.026 ± 0.050) cm for the neptunium and uranium sorption, respectively, on flat samples of freshly broken Äspö granite after 14 d of immersion.

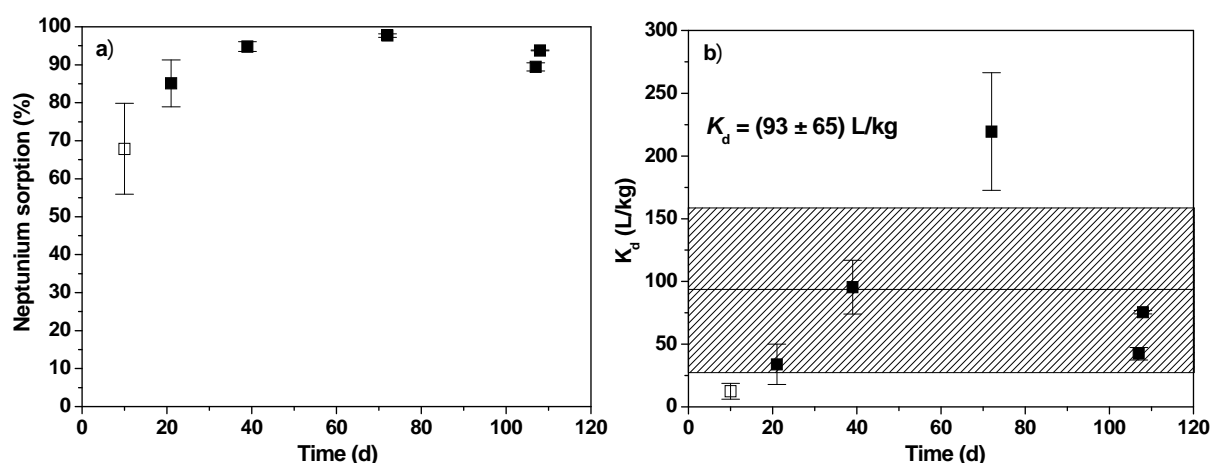


Figure 6: Neptunium sorption onto diorite as a function of time shown on a percentage scale (a) and as K_d value (b) ($[\text{Np}]_{\text{total}} = 1 \times 10^{-6}$ M, Äspö groundwater, $S/L = 200$ g/L, $\text{pH} = 7.99 \pm 0.10$, N_2). Error bars: 2σ . For the calculation of the mean K_d value, only the sorption data represented by filled symbols were used.

The neptunium sorption determined during the present long-time sorption experiments is much stronger than that obtained during previous neptunium sorption experiments (Schmeide et al., 2012) which were performed also under anoxic conditions but the sorption time was only 10 d. Obviously, during these experiments redox effects were minimized due to the short contact times. The assumption, that also under anoxic conditions initially neptunium(V) is sorbed onto diorite which is subsequently reduced to neptunium(IV), is supported by the fact that during the neptunium sorption study on diorite by in situ ATR FT-IR spectroscopy (Schmeide et al., 2012) the absorption band at 789 cm^{-1} increased. This absorption band was attributed to a NpO_2^+ surface species. Since very short sorption times are used for in situ ATR FT-IR experiments (about 90 min), a reduction of neptunium(V) to neptunium(IV) on the diorite surface to a significant extent cannot take place. Such a reduction would imply the disappearance of the neptunyl band in the IR spectrum, however, this was not observed. The reaction kinetics, i.e. the time necessary to reduce neptunium(V) to neptunium(IV) and its sorption onto the minerals, was emphasized as important factor also in other sorption/migration studies (Vandergraaf et al., 1996; Vejmelka et al., 2000; Denecke et al., 2009; Park et al., 2012).

The redox potential of the neptunium/diorite/Äspö groundwater sample solutions, determined at the end of each sorption experiment, amounts to $190 \pm 30\text{ mV}$ in average. Desorption experiments showed that only 5 to 6% of the sorbed neptunium can be desorbed with Äspö groundwater. The small amount of neptunium, that can be desorbed, was identified as neptunium(V) by TTA solvent extraction. The part of neptunium, that cannot be desorbed under these conditions but remains immobilized, is probably neptunium(IV). In previous experiments, 0.1 M or 1 M HCl were used for desorption of the neptunium. In those cases, neptunium was desorbed from the diorite to a larger extent and part of the desorbed neptunium was identified as neptunium(IV). In further experiments, XPS measurements will be applied to study the oxidation state of the sorbed neptunium.

Conclusions and future work

From the present results and from results reported by Schmeide et al. (2012), the following conclusions can be drawn. The speciation of uranium(VI) in solution and consequently, its sorption onto diorite is strongly influenced by the groundwater composition. Calcium and carbonate ions have the strongest influence by forming the weakly sorbing $\text{Ca}_2\text{UO}_2(\text{CO}_3)_3(\text{aq})$ complex. This complex was verified to be the dominating uranium species in Äspö groundwater at pH 7.8 by time-resolved laser-induced fluorescence spectroscopy. By in situ time-resolved ATR FT-IR spectroscopy, the surface species on diorite was identified as $\text{UO}_2(\text{CO}_3)_3^{4-}$. For the uranium(VI) sorption onto the 1 – 2 mm diorite fraction, a K_d value of $(3.8 \pm 0.6)\text{ L/kg}$ was determined. This value shows a low sorption affinity of uranium(VI) to diorite.

In the case of neptunium(V), the effect of the groundwater composition on its solution speciation and sorption behaviour is weak. For the neptunium sorption onto the 1 – 2 mm diorite fraction, a K_d value of $(93 \pm 65)\text{ L/kg}$ was determined. This strong interaction of neptunium with diorite can be attributed to iron(II) at the diorite surface which induces a substantial reduction of neptunium(V) to the sparingly soluble neptunium(IV) under anoxic conditions. The reduction of radionuclides to sparingly soluble mineral phases reduces migration risks. To verify the strong reduction of neptunium(V) to neptunium(IV) and its sorption/precipitation at the diorite surface, XPS measurements are planned.

Due to the different solution speciation and especially redox speciation at the diorite surface, sorption and mobility of the two actinides in a diorite environment under anoxic conditions are not comparable. The retention capacity of anoxic diorite towards neptunium is much higher than towards uranium. Consequently, a higher migration risk is expected for uranium(VI).

Acknowledgement

The research leading to these results has received funding from the European Union's European Atomic Energy Community's (Euratom) Seventh Framework Programme FP7/2007-2011 under grant agreement n° 269658 (CROCK project). We also thank KIT-INE for providing the diorite, Ch. Müller for technical support and A. Ritter and C. Eckardt (HZDR, Dresden) for cation and anion analyses and BET determinations.

References

- Alonso, U., Missana, T., Patelli, A., Rigato, V. and Ceccato, D. (2012). Uranium retention under anoxic conditions on Äspö diorite: First micro-scale analyses. In: 1st Workshop Proceedings of the Collaborative Project "Crystalline Rock Retention Processes" (7th EC FP CP CROCK), KIT Scientific Reports 7629, KIT Scientific Publishing, Karlsruhe, 189-194.
- Artinger, R., Marquardt, C.M., Kim, J.I., Seibert, A., Trautmann, N. and Kratz, J.V. (2000). Humic colloid-borne Np migration: Influence of the oxidation state. *Radiochim. Acta*, 88, 609-612.
- Bäckblom, G. (1991). The Äspö hard rock laboratory – a step towards the Swedish final repository for high-level radioactive waste. *Tunn. Undergr. Space Technol.*, 4, 463-467.
- Bernhard, G., Geipel, G., Reich, T., Brendler, V., Amayri, S. and Nitsche, H. (2001). Uranyl(VI) carbonate complex formation: Validation of the $\text{Ca}_2\text{UO}_2(\text{CO}_3)_3(\text{aq.})$ species. *Radiochim. Acta*, 89, 511-518.
- Bertrand, P. A. and Choppin, G. R. (1982). Separation of actinides in different oxidation states by solvent extraction. *Radiochim. Acta*, 31, 135-137.
- Brooks, S. C., Fredrickson, J. K., Carroll, S. L., Kennedy, D. W., Zachara, J. M., Plymale, A. E., Kelly, S. D., Kemner, K. M. and Fendorf, S. (2003). Inhibition of bacterial U(VI) reduction by calcium. *Environ. Sci. Technol.*, 37, 1850-1858.
- Choppin, G.R. (2006). Actinide speciation in aquatic systems. *Marine Chem.*, 99, 83-92.
- Denecke, M. A., Brendebach, B., De Nolf, W., Falkenberg, G., Janssens, K. and Simon, R. (2009). Spatially resolved micro-X-ray fluorescence and micro-X-ray absorption fine structure study of a fractured granite bore core following a radiotracer experiment. *Spectrochim. Acta Part B*, 64, 791-795.
- Freundlich, H. (1906) Concerning adsorption in solutions. *Z. Phys. Chem. Stoechiom. Verwandtschafts.*, 57, 385-470.
- Guillaumont, R., Fanghänel, T., Fuger, J., Grenthe, I., Neck, V., Palmer, D. A. and Rand, M. H. (2003). Update on the chemical thermodynamics of uranium, neptunium, plutonium, americium and technetium. *Chemical Thermodynamics*, vol. 5. (OECD Nuclear Energy Agency, ed.) Elsevier, Amsterdam.
- Holgersson, S. (2013). Cs, Ra and U sorption on rock samples from Äspö. Presentation during Final Workshop of the CROCK project, May 14-16, 2013, Karlsruhe, Germany.

Jansson, M. and Eriksen, T.E. (1998). CHEMLAB in-situ diffusion experiments using radioactive tracers. *Radiochim. Acta*, 82, 153-156.

Kim, J.I. (2006). Significance of actinide chemistry for the long-term safety of waste disposal. *Nucl. Eng. Technol.*, 38, 459-482.

Kienzler, B., Vejmelka, P., Römer, J., Fanghänel, T., Jansson, M., Eriksen, T. E. and Wikberg, P. (2003). Swedish-German actinide migration experiment at Äspö hard rock laboratory. *J. Contam. Hydrol.*, 61, 219-233.

Kienzler, B., Vejmelka, P., Römer, J., Schild, D. and Jansson, M. (2009). Actinide migration in fractures of granite host rock: Laboratory and in situ investigations. *Nucl. Technol.*, 165, 223-240.

Neck, V. and Kim, J. I. (2001). Solubility and hydrolysis of tetravalent actinides. *Radiochim. Acta*, 89, 1-16.

Neck, V., Kim, J. I., Seidel, B. S., Marquardt, C. M., Dardenne, K., Jensen, M. P. and Hauser, W. (2001). A spectroscopic study of the hydrolysis, colloid formation and solubility of Np(IV). *Radiochim. Acta*, 89, 439-446.

Opel, K., Weiß, S., Hübener, S., Zänker, H. and Bernhard, G. (2007). Study of the solubility of amorphous and crystalline uranium dioxide by combined spectroscopic methods. *Radiochim. Acta*, 95, 143-149.

Park, C. K., Kienzler, B., Vejmelka, P. and Jeong, J. T. (2012). Modelling and analysis of the migration of HTO and ²³⁷Np in a fractured granite core at the Äspö hard rock laboratory. *Radiochim. Acta*, 100, 197-205.

Schäfer, T., Stage, E., Büchner, S., Huber, F. and Drake, H. (2012). Characterization of new crystalline material for investigations within CP CROCK. In: 1st Workshop Proceedings of the Collaborative Project “Crystalline Rock Retention Processes” (7th EC FP CP CROCK), KIT Scientific Reports 7629, KIT Scientific Publishing, Karlsruhe, 63-72.

Schmeide, K. and Bernhard, G. (2010). Sorption of Np(V) and Np(IV) onto kaolinite: Effects of pH, ionic strength, carbonate and humic acid. *Appl. Geochem.*, 25, 1238-1247.

Schmeide, K., Gürtler, S., Müller, K., Steudtner, R., Joseph, C., Bok, F. and Brendler, V. (2012). Sorption of U(VI) and Np(V) onto diorite from Äspö HRL. In: 1st Workshop Proceedings of the Collaborative Project “Crystalline Rock Retention Processes” (7th EC FP CP CROCK), KIT Scientific Reports 7629, KIT Scientific Publishing, Karlsruhe, 169-180.

Silva, R. J. and Nitsche, H. (1995). Actinide environmental chemistry. *Radiochim Acta*, 70/71, 377-396.

Totskiy, Y., Geckeis, H. and Schäfer, T. (2012) Sorption of Tc(VII) on Äspö diorite (ÄD). In: 1st Workshop Proceedings of the Collaborative Project “Crystalline Rock Retention Processes” (7th EC FP CP CROCK), KIT Scientific Reports 7629, KIT Scientific Publishing, Karlsruhe, 97-105.

Vandergraaf, T. T., Drew, D. J. and Masuda, S. (1996). Radionuclide migration experiments in a natural fracture in a quarried block of granite. *J. Contam. Hydrol.*, 21, 153-164.

Vejmelka, P., Fanghänel, T., Kienzler, B., Korthaus, E., Römer, J., Schübler, W. and Artinger, R. (2000). Sorption and migration of radionuclides in granite (HRL Äspö, Sweden). FZKA 6488, Wissenschaftliche Berichte, Forschungszentrum Karlsruhe, Karlsruhe.

Widestrand, H., Andersson, P., Byegard, J., Skarnemark, G., Skalberg, M. and Wass, E. (2001). In situ migration experiments Äspö Hard Rock Laboratory, Sweden: Results of radioactive tracer migration studies in a single fracture. *J. Radioanal. Nucl. Chem.*, 250, 501-517.

Wolery, T.J. (1992). EQ3/6. A software package for the geochemical modelling of aqueous systems. Lawrence Livermore National Laboratory Report UCRL-MA-110662, Part 1, Livermore, USA.

REAL SYSTEM ANALYSIS

John Smellie*

CONTERRA (SE)

* Corresponding author: john.smellie@conterra.se

Abstract

The main objective for Conterra is to supply all relevant background sources of the analytical and field porewater data, together with interpretations, from the recent Swedish site characterisation programme with a focus on matrix diffusion. All data are from the Forsmark and Laxemar sites with the majority collected from the period 2003-2008. Depths sampled mostly range from about 200-500 m with some extending to about 1,000 m. To compensate for the absence of near-surface samples during the main investigation periods, seven additional samples from Forsmark not previously reported were taken more recently in 2011 at depths less than 100 m.

Introduction

For Work Package 3 Conterra has provided AMPHOS and KEMAKTA with relevant background sources of the analytical and field porewater data, together with interpretations, from the Swedish site characterisation programme (Waber et al., 2008, 2009, 2011, 2012; Waber and Smellie, 2008, 2009, 2012; Smellie, 2012a). This information is also referred to in Deliverable D3.1 and D3.2 (Smellie, 2011) and the updated Deliverable D3.1 and D3.2 (Smellie 2012a).

Generally, and to varying degrees, both sites have been subjected to the same palaeoclimatic conditions following the last glaciation, i.e. since the last deglaciation (18,000-8000 BC). The climatic changes and resulting different groundwater types introduced into the bedrock, extending since the last deglaciation stage to present day meteoric conditions, are well documented (Laaksoharju 2008, 2009). In chronological order the most important are dilute glacial meltwaters, brackish waters (Littorina/Baltic Sea) and recent fresh waters. These successive water intrusions during Holocene, Pleistocene and pre-Pleistocene times have interacted to a various extent with the resident porewaters which therefore can be considered an archive of the past hydrogeological (and therefore hydrogeochemical) history at the Forsmark and Laxemar sites.

Depending on the distance to the nearest water conducting fracture and the depth of the rock sample, the porewater preserves signatures of exchange with fracture groundwaters during Holocene, Pleistocene and pre-Pleistocene times. Furthermore, solute transport in the intact rock matrix appears to be dominated by diffusion, and matrix diffusion was identified to occur at least over several decametres into the rock matrix.

Porewater extraction and analysis

Porewater that resides in the connected pore space of crystalline rock cannot be sampled by conventional techniques and therefore are extracted by indirect methods based on rock material. This approach has been successfully carried out and porewater can be characterised by out-diffusion and diffusive isotope exchange techniques. The calculation of the concentration of chloride (or any other chemically conservative element) in the porewater (from out-diffusion concentrations) is inversely proportional to the water content in the rock sample in question. The uncertainty of the indirectly derived porewater concentrations thus strongly depends on the accuracy of the water content determination and the degree to which the measured values represent in-situ conditions.

Of high quality are data relating to the conservative species Cl and Br (e.g. indication of groundwater origin), the stable isotopes of ^{18}O and ^2H (e.g. indication of climate types), and also a suite of non-conservative major ions which are subsequently corrected for any water/rock reactions incurred during the out-diffusion extraction process (e.g. in particular Mg can be an important indication of marine derived waters). Petrophysical parameters, such as measured water content, bulk density, and water-loss porosity determined by both gravity and isotope exchange, are also determined.

Experimentally derived data

As mentioned above, solute transport in the intact rock matrix at both sites appears to be dominated by diffusion, and matrix diffusion has been identified to occur into the rock matrix. At Forsmark, experimentally derived average pore diffusion coefficients of Cl^- for the major rock types at a temperature of 25 °C are: metagranite to granodiorite = $1.2 \times 10^{-10} \text{ m}^2/\text{s} \pm 0.40 \times 10^{-10} \text{ m}^2/\text{s}$ (n = 21), granodiorite to tonalite = $8.1 \times 10^{-11} \text{ m}^2/\text{s}$ (n = 1), aplitic granite = $9.4 \times 10^{-11} \text{ m}^2/\text{s} \pm 4.2 \times 10^{-12} \text{ m}^2/\text{s}$ (n = 5) and fine-grained granite = $1.1 \times 10^{-10} \text{ m}^2/\text{s} \pm 0.38 \times 10^{-10} \text{ m}^2/\text{s}$ (n = 3). At Laxemar, the average pore diffusion coefficients of Cl^- for the major rock types at a temperature of 25 °C are: Ävrö granite = $6.3 \times 10^{-11} \text{ m}^2/\text{s} \pm 2.9 \times 10^{-11} \text{ m}^2/\text{s}$ (n = 9), quartz monzodiorite = $8.4 \times 10^{-11} \text{ m}^2/\text{s} \pm 5.5 \times 10^{-11} \text{ m}^2/\text{s}$ (n = 3), diorite = $3.8 \times 10^{-11} \text{ m}^2/\text{s} \pm 4.1 \times 10^{-12} \text{ m}^2/\text{s}$ (n = 2).

Acknowledgement

The research leading to these results has received funding from the European Union's European Atomic Energy Community's (Euratom), Seventh Framework Programme FP7/2007-2011 under grant agreement n° 269658 (CROCK project).

References

Laaksoharju M., Smellie J., Tullborg E-L., Gimeno M., Hallbek L., Molinero J., Waber N. (2008). Bedrock hydrogeochemistry Forsmark. Site descriptive modelling SDM-Site Forsmark. SKB R-Report (R-08-47), SKB, Stockholm, Sweden.

Laaksoharju M., Smellie J., Tullborg E-L., Wallin B., Drake H., Gascoyne M., Gimeno M., Gurban I., Hallbeck L., Molinero J., Nilsson A-C., Waber N. (2009). Bedrock hydrogeochemistry Laxemar, Site descriptive model, SDM-Site Laxemar. SKB R-Report (R-08-93) SKB, Stockholm, Sweden.

Smellie, J. (2011). Real system analysis. Deliverables D3.1 and D3.2 published in the CP CROCK web homepage.

Smellie, J. (2012a). Real system analysis: Update. Deliverables D3.1 and D3.2 published in the CP CROCK web homepage.

Smellie, J. (2012b). Real system analysis - 1st CROCK Workshop (May 22-24, 2012, Stockholm, Sweden), Paper.

Waber HN., Gimmi T., Smellie JAT. (2008). Porewater in the rock matrix. Site descriptive modelling, SDM-site Forsmark. SKB R-Report (R-08-105), SKB, Stockholm, Sweden.

Waber HN., Smellie JAT. (2008). Characterisation of porewater in crystalline rocks. Applied Geochemistry, 23, 1834-1861.

Waber HN., Smellie JAT. (2009). Forsmark site investigation. Borehole KFM02B. Part I: Diffusion experiments and porewater data. SKB P-Report (P-09-14), SKB, Stockholm, Sweden.

Waber HN., Gimmi T., Smellie JAT., deHaller A. (2009). Porewater in the rock matrix. Site descriptive modelling. SDM-Site Laxemar. SKB R-Report (R-08-112), SKB, Stockholm, Sweden.

Waber HN., Gimmi T., Smellie JAT. (2011). Effects of drilling and stress release on transport properties and porewater chemistry of crystalline rocks. Journal of Hydrology, 405, 316-332.

Waber HN., Gimmi T., Smellie JAT. (2012). Reconstruction of palaeoinfiltration during the Holocene using porewater data (Laxemar, Sweden). Geochimica et Cosmochimica Acta. 94, 109-127.

Waber HN., Smellie JAT. (2012). Forsmark site characterisation. Borehole KFM22 and KFM23: Derivation of porewater data by diffusion experiments. SKB P-Report (P-12-18), SKB, Stockholm, Sweden.

CHARACTERIZATION OF ROCK SAMPLES FROM ÄSPÖ USING GAS ADSORPTION

Stellan Holgersson*

Department of Chemical and Biological Engineering, Division for Nuclear Chemistry, Chalmers University of Technology (SE)

* Corresponding author: stehol@chalmers.se

Abstract

Drill cores from the Äspö Laboratory have been obtained and characterized with a gas adsorption instrument for specific surface area, using Kr gas and interpreted with the Brunauer-Emmet-Teller (BET) model. Before the measurements each drill core were sawn into 1.5cm long samples, by the use of a low speed saw. In addition, the porosity was measured by the dry/wet weighing method. The apparent density of the samples was also determined. Some of the samples were crushed and sieved into four fractions: 1-0.5mm, 0.5-0.25mm, 0.25-0.125mm and 0.125-0.063mm. These samples were also characterized with BET and also for specific pore volume (porosity), using N₂ gas and interpreted with the Barrett-Joyner-Halenda (BJH) model. The results for crushed material fractions were interpreted with a model for the interdependency of specific surface area and porosity, by assuming a disturbed zone in the geological material. It is suggested that the origin of the disturbed zone can be the mechanical treatment of the rock particles or inherited porosity zones in the rock, or a combination of both. When extrapolating this model to the BET surface area for intact discs this shows that the measured porosity of the intact material is much larger than predicted by the model. This is interpreted as a macroporosity which contributes very much to the porosity of the intact samples but contributes very little to the BET area.

Introduction

In the CROCK project, one task is to measure sorption R_d (m³/kg) values for some selected radioactive tracers at different laboratories, using the same geological material. The material was sampled in the form of drill-cores at the Äspö laboratory, near Oskarshamn, Sweden (KIT-INE, 2011). Special care was taken to preserve the reducing conditions for the samples, both at sampling and the subsequent handling and measurements. The overall aim of this task is to try to reduce the experimental uncertainties in R_d values, in order to obtain more exact calculations of radiotracer migration in a performance assessment of a nuclear waste repository in granitic rock. A preliminary characterization of the geological material in the form of specific surface area (SSA) and porosity is necessary in order to: 1) normalize the sorption data that will be obtained from batch sorption measurements of crushed and sieved material, and 2) to normalize and interpret the sorption and diffusion data that will be obtained from diffusion experiments. The normalization to a specific surface area corrected R_d value (then usually called R_a), is a fundamental step in order to make a meaningful comparison of the data from the different forms of the geological material used in this investigation. First thereafter, phenomena influencing sorption that are not related to SSA (and porosity) of the material may be identified. The characterization thus reduces errors that otherwise will be introduced due to averaging over values of what is essentially non-

comparable R_d data, due to, what can be expected, hugely different SSA of the different size fractions of the material.

The specific surface area have been identified as a key parameter for extrapolating the results from laboratory experiments to the field-scale (André *et al.*, 2009, Dubois *et al.*, 2011), in order to obtain surface area normalized R_a (m) values. Also, the available porosity may not be constant between different size fractions up to the intact rock. It is also an essential parameter in the interpretation of sorption R_d values obtained from diffusion experiments. The porosity may therefore also be a key parameter to understand how sorption should be extrapolated from laboratory to field-scale. The interdependency of specific surface area and porosity for pure minerals have been the object of separate investigations (see Brantley and Mellott, 2000, Dubois *et al.*, 2012) and in this work, the rock is now investigated for similar interdependency.

Objective and scope

The first objective of this work is to prepare geological samples for subsequent batch sorption and diffusion experiments within the CROCK project Work Package(WP) 2. A number of drill cores were sampled at the Äspö laboratory. Priority for Chalmers drill-core samples were cores sampled perpendicular to a fracture. One drill-core was then sawn into smaller slices of 3cm length, starting from one fracture. One half (each sample then 1.5cm) of the sliced core will be used in subsequent diffusion experiments in the WP2 of the CROCK project, the other half will be crushed and used in batch sorption experiments. The scope of the investigation is limited to one drill core of about 29cm, giving material for, in total, 8 diffusion experiments and 8 different samples for batch experiments. The second objective for this work is to obtain specific surface area for the 1.5cm long drill core samples, by measurements with gas adsorption. Also, specific surface area for samples of crushed and sieved rock is to be obtained. The third objective is to obtain the porosity for the crushed samples, by measurements with gas adsorption. Measurement of the porosity of an intact core slice with this method have been found impossible, due to either: a) the very low volumes involved or b) the volume is macroporous with pore size above the measurement capability of this method ($>0.5\mu\text{m}$) (Dubois *et al.* 2012). Therefore, the dry/wet weighing method is used for these samples. Extrapolation methods of porosity from crushed samples up to intact 1.5cm disc samples, using a model of specific surface area and specific volume interdependency is here used for comparison with porosity measurements of intact disc samples. Another porosity measurement is to be made with HTO diffusion, in WP2 of this project.

Experimental

Sampling of drill cores

Altogether 18 samples of drill cores were obtained for Chalmers from the Äspö facility. The sampling took place during May 2011 in the tunnel gallery NASA2376A, located at a depth of approximately 300m below surface (KIT-INE, 2011). Two boreholes were drilled, KA2368A-01 and KA2370A-01, both directed perpendicular to the tunnel wall. The drill cores were of 42mm diameter and the rock type was found to be predominately Äspö diorite (ÄD), sometimes with minor components of Fine-grained granite (FGG) and Ävrö granite (ÄG) (KIT-INE 2011). The drill core samples obtained for Chalmers are described in Tables 1 and 2 below.

Table 1: Description of drill core samples at Chalmers, from first borehole (KIT-INE, 2011).

Drill core from KA2368A-01		
label	drilling length (m)	note
1.11	4.77-4.90	fracture half
1.12	4.90-5.40	fracture half
1.20	8.13-8.26	sealed fracture, re-opened, complete
1.30	12.11-12.66	sealed fracture, re-opened, complete

Table 2: Description of drill core samples at Chalmers, from second borehole (KIT-INE, 2011).

Drill core from KA2370A-01		
label	drilling length (m)	note
2.4	1.3-1.69	fracture half
2.5	1.69-1.93	fracture half
2.7	2.45-2.89	fracture half
2.10	3.81-4.35	fracture, complete
2.19	7.30-7.57	possible fracture half
2.20	7.57-7.91	two fracture halves, one complete, contains $\ddot{A}G$
2.23	8.47-8.91	two fracture halves, contains $\ddot{A}G$
2.24	8.91-9.24	fracture half, contains $\ddot{A}G$
2.26	9.54-9.81	fracture half
2.27	9.81-10.20	fracture half, contains $\ddot{A}G$
2.37	13.69-14.05	two fracture halves, one complete
2.38	14.05-14.60	two fracture halves, one complete

At the drilling site, the samples were put into Al-foil coated plastic bags, flushed with N₂ gas and sealed immediately after they were obtained from drilling. The samples were transported to Chalmers and put into an N₂ flushed glove-box (MBraun InLab, [O₂(g)]~1ppm, T~20°C) for storage.

Sample preparation

It was decided to use sample 1.30 from first borehole (Table 1) for the subsequent experiments. The sample is of total length of about 55 cm, with sealed and re-opened fractures at 12.11, 12.40 and possibly also at 12.66m. Only the first half of the sample was used (12.11-12.40m), thus this particular section sample has two sealed and re-opened fractures, one in each end of the sample. The core sample was first sawn into sections of 3cm length using a low speed saw (Buehler IsoMet 1000) set to 300-325rpm with a $\varnothing=17.5$ cm diamond wafering blade (Buehler 20LC) and cooled by water bath. The cutting was made inside the N₂ flushed glove-box and the cooling water degassed and stored in N₂ atmosphere. The 3cm sections were then further sawn into 1.5cm length, one half to be used in diffusion, the other half in batch sorption experiments. This gave in total sixteen 1.5cm pieces plus one odd section at the end. Pictures of the fracture surfaces at 12.11 and 12.40m are shown in Figure 1 and 2.

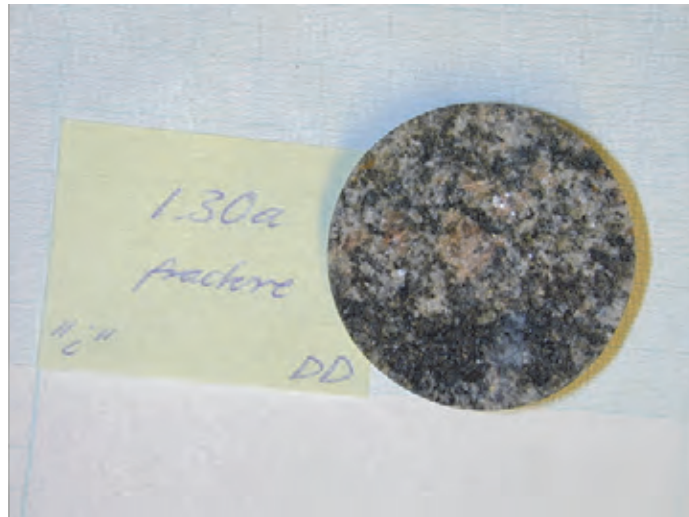


Figure 1: Fracture surface at the end of drill core section at 12.11m in borehole KA2368A-01, viewed in drilling direction.



Figure 2: Fracture surface at the end of drill core section at 12.40m in borehole KA2368A-01, viewed in tunnel direction.

Some of these sections were used for obtaining crushed material with the following procedure, also made inside a glove-box. The samples were put into three plastic bags and over these a clean tissue and then smashed into pieces with a hammer. The coarse pieces were then crushed further, using an agate mortar and pestle. Four fractions were collected with plastic and nylon mesh sieves (CISA brand): 63-125 μm , 125-250 μm , 250-500 μm and 500-1000 μm . The fractions were washed several times with 95% ethanol for removing finer particles. Ethanol washing is an established standard procedure in preparation of geological samples and has also been shown to be a preservative of carbonate containing minerals rather than a solvent for them (Serrano *et al.*, 2008). Highly ionic compounds, such as alkaline chlorides and hydroxides, are soluble in ethanol, but are anyway also soluble in water.

Specific surface area measurements

Samples were measured with a gas adsorption instrument (ASAP 2020, Micromeritics) using Kr gas (99.998%, Air Liquide). Before measurements, samples were dried at the vacuum station of the instrument at room temperature for at least 25 hours (crushed samples) or several days (sections of drill cores). The samples for specific surface area were measured using a 10 point Kr sorption isotherm with p/p_0 from 0.05 to 0.2. For drill cores, only the three first points of the isotherm were used since a deviating non-linear behaviour of the isotherm developed when more points were included. The results were interpreted with the instrument software using the BET model (Brunauer *et al.* 1938). For samples of drill core sections a special made glass sample holder of 455mL measured free space (Figure 3) was used, with a glass insert. For crushed samples, standard 1/2-inch glass tubes of 16mL volume (Micromeritics p/n 240-61003-00) and filler rods (Micromeritics p/n 240-61016-00) were used.



Figure 3: The specially made holder for gas adsorption measurements of drill-core sections.

Porosity measurements

Crushed samples were measured with the same gas adsorption instrument (ASAP 2020, Micromeritics) that was used for the specific surface area measurements but now using N₂ gas (99.999%, AGA/Linde). Before measurements, the samples were dried at the vacuum station of the instrument at room temperature for at least 25 hours. The samples for porosity were measured using N₂ adsorption up to saturation pressure and then desorption with, in total about 90 pressure points (the number varies from different measurements). The results were interpreted as mesoporosity (pore width from 2 to 50nm) with the instrument software using the BJH model (Barrett *et al.* 1951). For some samples also t-plots were made for checking any presence of microporosity (pore width below 2nm) (Lippins *et al.* 1964). Sample holders were the same as for specific surface area measurements. The porosity of the intact 1.5cm section samples were measured using the dry/wet weighing method. For this measurement the sample was dried at 30°C for several days in a vacuum oven and weighed for dry weight. Thereafter, the sample was placed on the rim of a tray with synthetic groundwater (see below) inside a plastic exsiccator. After 3-5 hours of evacuation, the sample was toppled into the bath and

vacuum released. The tray with the immersed sample was placed in an ultrasonic bath for one hour. After 3 days the sample was taken up and dried externally with a swipe and weighed for wet weight.

Density measurements

The density of the rock material was determined by weighing dried intact discs of well-defined cylindrical geometry, where the dimensions were measured with a calliper gauge. Four measurements of each section thickness were made, while five sections were used for one diameter measurement each.

Preparation of synthetic groundwater

The recipe for synthetic groundwater is based on analysed water from borehole KA3600F-2, which was found to be comparable to the water in KA2368A-01 (Heck and Schäfer). The groundwater was used here only for porosity measurements of the 1.5m drill core sections, which should anyway be saturated with the groundwater at the start of the subsequent diffusion experiments in WP2. The recipe is shown in Table 3. The method for preparation is as follows. Ultrapure water was used (Millipore Milli-Q 185).

Concentrate 1. In a 1L measure flask, the following salts were dissolved in water: 3.665g LiCl (>98%, Scharlau extra pure), 2.002g KCl (99+%, Acros p.A.), 6.0553g SrCl₂ · 6H₂O (99%, Merck p.A.).

Concentrate 2. In a 1L measure flask, the following salts were dissolved in water: 2.988g NaBr (<99% Mallinckrodt a. R.), 8.170g NaHCO₃ (>99.7% SigmaAldrich ACS R.), 0.312g NaF (99.99% SigmaAldrich) 0.285g B₂O₃ (Merck p.A.).

Concentrate 3. 3.3652 g of Na₄SiO₄ (AlfaAesar) was dissolved in a 100mL measure flask.

Synthetic groundwater. In a 1L measure flask, the following salts were dissolved in water: 4.218g NaCl (99.5% Merck p.A.), 0.581g MgCl₂ · 6H₂O (>99% SigmaAldrich ACS R.), 4.163g CaCl₂ · 2H₂O (>99.5% Merck p.A.), 0.583g Na₂SO₄ (>99% SigmaAldrich ACS R.). To this, 10mL of concentrate 1, 10mL of concentrate 2 and 0.92mL of concentrate 3 was added. The flask was almost filled with water and then transferred to a beaker for pH adjustment (pHC 3006-9 electrode, pHM240, Radiometer). The pH was adjusted to 7.8, using 1M HCL and/or NaOH (Titrisol, Fluka). The water was transferred back to the measure flask, filled up to the mark and then transferred to and stored in a washed plastic vessel.

Density measurement. The density of the synthetic groundwater was determined with a 50mL pycnometer, which was calibrated for volume three times with pure water at 24°C (density 997.2995kg/m³, CRC Handbook 1979). Thereafter, three weight measurements with groundwater were made.

Table 3: Recipe of synthetic groundwater, based on analyses of water from KA3600F-2 (Heck and Schäfer).

Component	conc (ppm)
Li	6
Na	1894
K	10.5
Mg	69.4
Ca	1135
Sr	19.9
Fe	0.2
Mn	0.338
F	1.41
Cl	4999
Br	23.2
SO ₄	394.4
Si	4.7
HCO ₃	11.68
B	0.885
pH	7.81

Results

Specific Surface Area Measurements

a) crushed material

Four fractions have been measured for each of the 1.5cm section samples (labelled a-h) that were crushed. All samples are taken from core 1.30 (Table 1). Results of the specific surface area (SSA) of crushed fractions of Äspö diorite are shown in Table 4, below.

Table 4: Results for specific surface area (SSA) measurements of crushed and sieved fractions of Äspö diorite, utilizing a seven point BET Kr gas adsorption isotherm.

Sample	Core section (m)	1-0.5mm	0.5-0.25mm	0.25-0.125mm	0.125-0.063mm
		SSA (m ² /g)	SSA (m ² /g)	SSA (m ² /g)	SSA (m ² /g)
a	12.385-12.4	0.1021±0.0008	0.1544±0.0010	0.2285±0.0014	0.3999±0.0015
b	12.355-12.37	0.0953±0.0008	0.1516±0.0010	0.2507±0.0011	0.3585±0.0015
c	12.325-12.34	0.0850±0.0006	0.1516±0.0008	0.2188±0.0009	0.2980±0.0017
d	12.295-12.31	0.0928±0.0005	0.1328±0.0005	0.2048±0.0006	0.3008±0.0006
e	12.265-12.28	0.0806±0.0004	0.1288±0.0005	0.1747±0.0005	0.2675±0.0008
f	12.235-12.25	0.0766±0.0003	0.1252±0.0003	0.1926±0.0004	0.2676±0.0005
g	12.205-12.22	0.0956±0.0004	0.1404±0.0004	0.1770±0.0006	0.3136±0.0009
h	12.175-12.19	0.0714±0.0009	0.1092±0.0019	0.1760±0.0023	0.2778±0.0011
average		0.0874±0.0107	0.1368±0.0158	0.2029±0.0280	0.3105±0.0468

b) intact sections of material

The results of measurements of SSA of drill-cores are shown in Table 5 below. Note that the samples labelled with **lower case (a,b)** in Table 5 were later crushed and sieved for fractions (the SSA data presented in Table 4

above), while those labelled with **capital letters** are used intact in diffusion experiments in WP2. Larger solid pieces are usually more difficult to measure and since the measured seven points isotherm here for the intact 1.5cm section samples deviates (evaluated as goodness of fit) at the higher pressure points, only the three-four first or sometimes even two first points were used for evaluation of SSA. The C value of the isotherm should also be positive and in between 5-2000, according to recommendations (Webb and Orr, 1997) and this almost succeeded here, with one exception.

Table 5: Results for specific surface area (SSA) of 1.5cm thick sections of drill core of Äspö diorite (core #1.30, Table 1). utilizing a two, three or four point Kr gas isotherm.

Sample	Core section (m)	SSA (m ² /g)	Number of pressure points	Isotherm C value	Goodness of fit
a	12.385-12.4	0.0092±0.0003	4	162	0.999
A	12.37-12.385	0.0069±0.0002	3	503	1.000
b	12.355-12.37	0.0074±0.0003	4	442	0.998
B	12.34-12.355	0.0078±0.0002	4	280	0.999
c	12.325-12.34	0.0075	2	422	1.000
C	12.31-12.325	0.0061	2	421	1.000
d	12.295-12.31	0.0055±0.0002	4	-106	0.999
D	12.28-12.295	0.0051	2	478	1.000
e	12.265-12.28	0.0077±0.0003	3	147	0.999
E	12.25-12.265	0.0044	2	155	1.000
f	12.235-12.25	0.0073±0.0004	3	94	0.999
F	12.22-12.235	0.0062±0.0002	3	111	0.999
g	12.205-12.22	0.0068±0.0000	3	64	1.000
G	12.19-12.175	0.0050±0.0002	3	72	0.999
h	12.175-12.19	0.0068±0.0003	3	57	0.999
H	12.16-12.175	0.0048	2	48	1.000
I	12.11-12.16	0.0080	2	127	1.000
average		0.0066±0.0013			

Specific Pore Volume Measurements

a)crushed material

Four fractions have been measured for each of the 1.5cm section samples (labelled a-h) that were crushed. All samples are taken from core 1.30 (Table 1). Results of the specific pore volume (SPV) of crushed fractions of Äspö diorite are shown in Table 6, below. Some samples were evaluated with t-plots for the possible presence of microporosity, but this was found to be negligible (1-2% of mesoporosity).

Table 6: Results for specific spore volume (SPV) measurements of crushed and sieved fractions of Äspö diorite, utilizing about 90 points BJH N₂ gas adsorption isotherm.

Sample	Core section (m)	1-0.5mm	0.5-0.25mm	0.25-0.125mm	0.125-0.063mm
		SPV (mL/g)	SPV (mL/g)	SPV (mL/g)	SPV (mL/g)
a	12.385-12.4	$3.19 \cdot 10^{-4}$	$5.32 \cdot 10^{-4}$	$7.28 \cdot 10^{-4}$	$1.61 \cdot 10^{-3}$
b	12.355-12.37	$3.42 \cdot 10^{-4}$	$7.19 \cdot 10^{-4}$	$9.72 \cdot 10^{-4}$	$1.30 \cdot 10^{-3}$
c	12.325-12.34	$5.60 \cdot 10^{-4}$	$5.48 \cdot 10^{-4}$	$8.22 \cdot 10^{-4}$	$1.11 \cdot 10^{-3}$
d	12.295-12.31	$6.12 \cdot 10^{-4}$	$5.40 \cdot 10^{-4}$	$7.74 \cdot 10^{-4}$	$1.13 \cdot 10^{-3}$
e	12.265-12.28	$6.99 \cdot 10^{-4}$	$5.27 \cdot 10^{-4}$	$7.31 \cdot 10^{-4}$	$1.03 \cdot 10^{-3}$
f	12.235-12.25	$5.61 \cdot 10^{-4}$	$4.88 \cdot 10^{-4}$	$7.94 \cdot 10^{-4}$	$1.15 \cdot 10^{-4}$
g	12.205-12.22	$6.40 \cdot 10^{-4}$	$6.37 \cdot 10^{-4}$	$7.66 \cdot 10^{-4}$	$1.26 \cdot 10^{-3}$
h	12.175-12.19	$6.62 \cdot 10^{-4}$	$5.15 \cdot 10^{-4}$	$7.25 \cdot 10^{-4}$	$1.05 \cdot 10^{-3}$
average		$5.49 \pm 1.43 \cdot 10^{-4}$	$5.63 \pm 0.76 \cdot 10^{-4}$	$7.89 \pm 0.82 \cdot 10^{-4}$	$1.20 \pm 0.19 \cdot 10^{-3}$

b) intact sections of material

The results of measurements of SPV of drill-cores are shown in Table 7 below. The method was dry/wet weighing, utilizing the measured density of synthetic groundwater ($1003.8 \pm 0.2 \text{ kg/m}^3$) and measured densities of each section, given in Table 8. The measured average section diameter was $45.25 \pm 0.08 \text{ mm}$.

Table 7: Results for specific pore volume (SPV) of 1.5cm thick sections of drill core of Äspö diorite (core #1.30, Table 1), utilizing dry/wet weighing and measured densities (Table 8).

Sample	Core section (m)	Water uptake (mL)	Section length (mm)	SPV (mL/g)
A	12.37-12.385	0.1983	16.48 ± 0.22	$2.78 \cdot 10^{-3}$
B	12.34-12.355	0.2361	15.58 ± 0.20	$3.49 \cdot 10^{-3}$
C	12.31-12.325	0.1325	14.28 ± 0.14	$2.12 \cdot 10^{-3}$
D	12.28-12.295	0.1265	13.48 ± 0.08	$2.13 \cdot 10^{-3}$
E	12.25-12.265	0.1474	16.20 ± 0.20	$2.08 \cdot 10^{-3}$
F	12.22-12.235	0.1634	15.48 ± 0.18	$2.43 \cdot 10^{-3}$
G	12.19-12.175	0.1614	14.91 ± 0.16	$2.52 \cdot 10^{-3}$
H	12.16-12.175	0.1704	14.43 ± 0.15	$2.72 \cdot 10^{-3}$
average				$2.53 \pm 0.47 \cdot 10^{-3}$

Table 8: Results for density of 1.5cm thick sections of drill core of Äspö diorite (core #1.30, Table 3-1).

Sample	Core section (m)	Section weight (g)	Section length (mm)	density (kg/m ³)
A	12.37-12.385	71.180	16.45±0.80	2690
B	12.34-12.355	68.550	15.78±0.37	2702
C	12.31-12.325	62.203	14.24±0.41	2716
D	12.28-12.295	59.064	13.39±0.30	2743
E	12.25-12.265	70.186	16.04±0.55	2721
F	12.22-12.235	67.879	15.65±0.33	2697
G	12.19-12.175	65.256	15.18±0.22	2674
H	12.16-12.175	63.523	14.65±0.19	2695
average				2705±21

Discussion

First, it is clear from Table 4 that the SSA increase with decreasing particle size, which can be expected to show a linear increase for a homogenous material. However, Table 6 shows that the SPV *also* increase with decreasing particle size, which is certainly not expected for a homogenous material (the SPV should be constant). The conclusion is therefore that the material is non-homogenous.

The results are shown as a plot of specific pore volume as function of specific surface area in Figure 4, below.

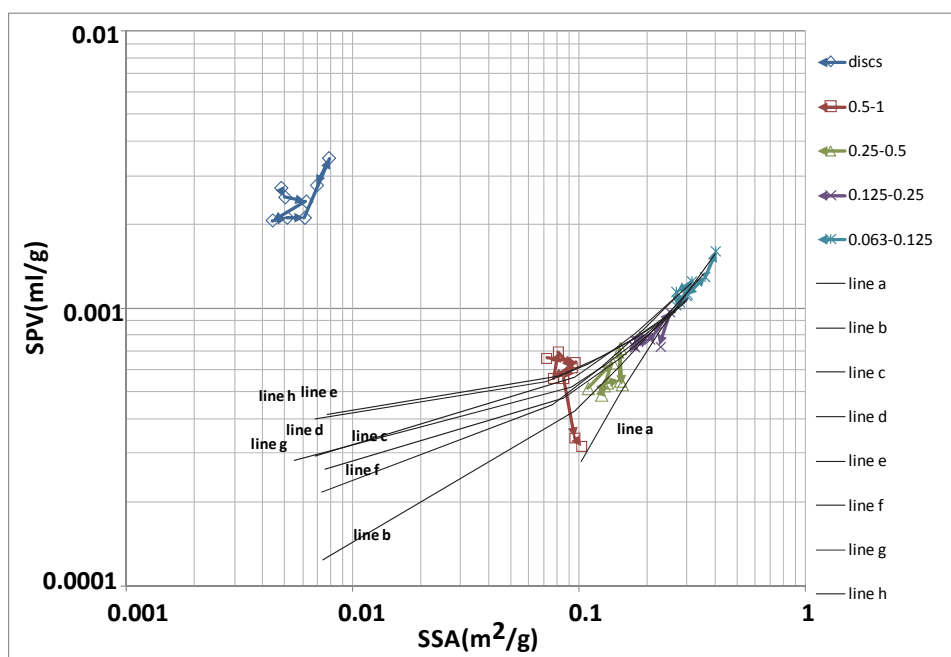


Figure 4: The specific pore volume (SPV) versus specific surface area (SSA) for crushed fractions 0.5-1, 0.25-0.5, 0.125-0.25 and 0.063-0.125mm. values for intact discs also shown. Arrows indicate the sequence of samples taken, in drilling direction. Lines show a linear fitting of data for crushed samples "a" to "h" (the "knees" are due to the log versus log scale).

The data for crushed samples show a linear dependency between SSA and SPV. A model has been developed that assumes that the crushed particles are non-homogenous and consist of a non to low-porous core surrounded with a porous shell (Figure 5).

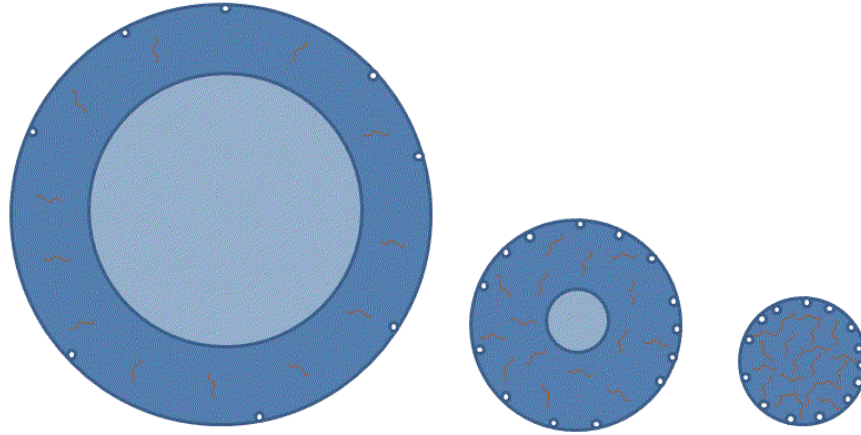


Figure 5: Schematic representation of different particle sizes, comprising of a porous shell (dark) of fixed thickness with "pores" (holes and streaks) and a low- or non-porous core (light). For small enough particles it can be assumed that there will be no core left.

The porous shell is assumed to be of constant thickness for all particle sizes. The model equation is

$$A_{sp} = \frac{2V_{sp}}{r_{pore}} + \frac{F_p}{r_s \cdot \rho} - \frac{F_p}{r_s \cdot \rho} \cdot \sqrt[3]{\frac{V_{sp} \cdot \rho - \varepsilon_s}{\varepsilon_c - \varepsilon_s}} \quad (\text{Eq.1})$$

A_{sp} and V_{sp} are the experimentally determined specific surface area and pore volume, respectively. F_p is a form factor, here assumed to be 3, assuming an ideal sphere and no surface roughness. ρ is the apparent density (an extended equation with the absolute density is also available, but was found not to be necessary to describe the data, because of the relatively low porosities involved). The fitting parameters are the pore radius r_{pore} , the shell thickness r_s , shell porosity ε_s and core porosity ε_c . The pore radius r_{pore} is the "average" radius of cylindrical pores (capillaries) that are assumed to represent the porosity. The length of these pores cancels out and is therefore not a part of the equation. The shell thickness r_s is the constant depth of the porous zone, shown in Figure 5. The model (Eq.1) is based on hundreds of independent measurements of specific surface area and specific volume for different size fractions of pure minerals found in granitic rock (Dubois *et al.* 2012). For this application the third term is assumed to be small and is neglected, giving a linear equation.

Linear fittings to data are shown in Figure 4. It can be seen that the predicted SPVs by the model for intact rock samples, using the measured SSAs for these, are much lower than those actually measured. The water uptake by rock is much larger than what can be expected from the individual pure minerals which the rock consists of. In the case of larger pieces (>cm size) of pure minerals, the porosity is usually below the lower detection limit of gas adsorption (Dubois *et al.* 2012). However, in the case with rock, there must be another explanation namely that the porosity is macroporous and is therefore

instead above the upper detection limit of gas adsorption, because the pores are too wide to be measured. The upper limit of gas adsorption pore volume measurements is about $5 \cdot 10^{-7}$ m in pore diameter, in order to have the gas to condense inside the pores. One must then assume larger pores (in the $> \mu\text{m}$ range) or rather micro-fractures in rock that contribute largely to the SPV, but in the same time contribute very little to SSA. A simple calculation with the assumption of cylindrical channels of, for example, 0.1mm diameter verify that a good number of these can make up the SPV measured here, while at the same be negligible for the measured SSA, which is then dominated by the mesoporosity.

The measured porosity of the intact sections of drill-cores with the dry/wet weighing should be compared with measurements of porosity with the HTO diffusion method in WP2. There has previously been found a very good accordance with the two methods for drill-core samples of granitic rock (see, for example, Holgerson and Albinsson, 2002, Johansson *et al.* 1998) and it is likely that the here measured porosities for intact sections of rock will be confirmed with HTO diffusion.

Conclusions

Some characteristics of Äspö drill cores, in the form of 1.5cm sections and four different size fractions of crushed material, have been determined. The specific surface area (SSA) was found to increase from the intact sections of material (mean $\text{SSA} = 0.0066 \pm 0.0013 \text{m}^2/\text{g}$) to the finest fraction of 0.063-0.125mm (mean $\text{SSA} = 0.3105 \pm 0.0468 \text{m}^2/\text{g}$), which is in accordance with the expected effect of crushing the material, which creates new surfaces and may also access previously closed porosity. The specific pore volume (SPV) was also found to increase for the crushed fractions, apparently in a linear dependency of SSA. This can be explained with a model where the particles are assumed to consist of a disturbed zone with high porosity surrounding a core of low porosity. The model have been found valid for at least ten different pure minerals commonly found in granitic rock (Dubois *et al.* 2012) and seems now to be confirmed also for granitic rock samples. A deviation from the model is found when comparing the SPV dependency on SSA for intact sections of granitic rock. The measured SPV for intact sections ($\text{SPV} = 2.53 \pm 0.47 \cdot 10^{-3} \text{mL/g}$) is about 10 times larger than what can be expected from extrapolation of the size series of crushed material ($\text{SPV} = 1.20 \pm 0.19 \cdot 10^{-3} \text{mL/g}$ for the 0.063-0.125mm fraction to $\text{SPV} = 5.49 \pm 1.43 \cdot 10^{-4} \text{mL/g}$ for the 0.5-1.0mm fraction), using measured SSA for intact section. The conclusion is that intact rock contains macroporosity that is above the upper detection limit of the gas adsorption method. It is likely (but not proved here) that this macroporosity disappear upon crushing the material. The macroporosity in intact material will contribute to a relatively fast diffusion through rock, compared to the slow diffusion in individual pure minerals. Due to an expected very small surface area, however, it will thereby not contribute much to sorption capacity. Instead the mesoporosity will most probably dominate uptake by sorption. The presence of two diffusion paths in drill core sections of granitic rock has previously been shown (Johansson *et al.* 1998).

Acknowledgements

Henrik Drake, Thorsten Schaefer, Sebastian Büchner and the MiRo drilling team are gratefully acknowledged for help with sampling of the drill cores.

The research leading to these results has received funding from the European Union's European Atomic Energy Community's (Euratom) Seventh Framework Programme FP7/2007-2011 under grant agreement n° 269658 (CROCK project) and SKB, the Swedish Nuclear Fuel and Waste Management Company.

References

- André, M., Malmström, M.E. and Neretnieks, I.: Specific surface area measurements on intact drillcores and evaluation of extrapolation methods for rock matrix surfaces. *Journal of Contaminant Hydrology* 110, 1-8. (2009).
- Barrett, E.P., Joyner, L.G. and Halenda, P.P.: The determination of pore volume and area distributions in porous substances. I. Computations from nitrogen isotherms. *J. Am. Chem. Soc.* 73 (1), 373-380 (1951).
- Brantley, S.L. and Mellott, N.P.: Surface area and porosity of primary silicate minerals. *American Mineralogist*, 85, 1767 (2000).
- Brunauer, S., Emmet, P.H. and Teller, E.: Adsorption of gases in multimolecular layers. *J. Am. Chem. Soc.* 60 (2), 309-319 (1938).
- CRC Handbook, 59th Ed. (1979).
- Dubois, I.E., Holgersson, S., Allard, S. and Malmström, M.E.: Dependency of BET surface area on particle size for some granitic minerals. *Proc. Radiochim. Acta* 1, 75-82 (2011).
- Dubois, I.E., Holgersson, S., Allard, S. and Malmström, M.: Interdependency of specific surface area and specific volume for some granitic minerals (Manuscript to be submitted 2012).
- Heck, S. and Schäfer, T.: CP CROCK groundwater sample characterization. EU CROCK Project internal document.
- Holgersson, S. and Albinsson, Y.: Diffusion of HTO and cement pore fluids through host rock. *Radiochimica Acta* 90, 99-108 (2002).
- Johansson, H., Siitari-Kauppi, M., Skålberg, M. and Tullborg, E.L.: Diffusion pathways in crystalline rock- examples from Äspö-diorite and fine-grained granite. *Journal of Contaminant Hydrology* 35, 41-53 (1998).
- KIT-INE: Provision of new fracture bearing drill core samples obtained, handled, transported and stored under anoxic conditions, including first documentation. Deliverable D-N°1-1, published in the EU CROCK Project homepage (2011).
- Lippens, B.C., Linsen, B.G. and de Boer, J.H.: Studies on pore systems in catalysts. 1. The adsorption of nitrogen. *J. Catalysis* 3, 32-37 (1964).
- Serrano, O., Serrano, L. and Mateo, M.A.: Effects of sample pre-treatment on the delta C-13 and delta O-18 values of living benthic foraminifera. *Chemical Geology* 257, 221-223 (2008).
- Webb, P.A. and Orr, C.: Analytical methods in fine particle technology. Micromeritics Instrument Corporation, 1997.

HTO, Cs, Ra AND U SORPTION ON AND DIFFUSION IN ROCK SAMPLES FROM ÄSPÖ

Stellan Holgersson*

Department of Chemical and Biological Engineering, Division for Nuclear Chemistry, Chalmers University of Technology (SE)

* Corresponding author: stehol@chalmers.se

Abstract

Drill cores from the Äspö Laboratory have been obtained and sawn into 1.5cm long samples, by the use of a low speed saw. Eight samples were used in diffusion experiments with radiotracers HTO, Cs and Ra. In the case with HTO, through diffusion were evaluated, while for the other tracers, in-diffusion data were used for evaluation of effective diffusivity and sorption distribution coefficients, R_d . By the assumption that HTO is non-sorbing, the porosity was evaluated. Some of the rock samples were crushed and sieved into four fractions: 1-0.5mm, 0.5-0.25mm, 0.25-0.125mm and 0.125-0.063mm. These samples were used in batch sorption experiments for up to 1 month. Wall sorption and pH measurements were also made in separate batches. Cs and Ra sorption in the batch experiments both show the expected behaviour of increasing sorption R_d with diminishing particle size. This seems to be successfully compensated for by normalizing sorption to specific surface area (SSA) to give Ra sorption coefficients that are essentially the same for all fractions. Cs data for 1 month were: 1.84 ± 0.44 ; 1.89 ± 0.24 ; 2.39 ± 0.48 ; $2.91 \pm 0.40 \cdot 10^{-4} \text{m}$, for the respective size fractions. Ra data for 1 month were: 0.60 ± 0.20 ; 0.84 ± 0.50 ; 1.07 ± 0.51 ; $1.09 \pm 0.30 \cdot 10^{-4} \text{m}$, for the respective size fractions. These data are preliminary, since further equilibration with solid phase is expected. Diffusion experiments with HTO in discs of drill core sections show that the porosity is larger than expected from extrapolation of porosity data from crushed fractions (see Holgersson, 2013). This is probably due to a macro-pore system, or a system of small fractures, that is not measurable with the Kr gas adsorption method, due to too wide "pores" for the gas to condensate in them. Results from Cs and Ra in-diffusion also indicate that these ions are transported in an entirely different pore system, where also sorption of these ions takes place.

Introduction

In the EU-CROCK project, one task is to measure sorption R_d (m^3/kg) values for some selected radiotracers in different laboratories, using the same geological material. The material was sampled in the form of drill-cores at the Äspö laboratory, near Oskarshamn, Sweden (KIT-INE, 2011). Special care was taken to preserve the reducing conditions for the samples, both at sampling and the subsequent handling and measurements. The overall aim of this task is to try to reduce the experimental uncertainties in R_d values, in order to perform more exact calculations of radiotracer migration in a performance assessment of a nuclear waste repository in granitic rock. An initial

characterization of the geological material in the form of surface area and porosity is necessary in order to: 1) normalize the sorption data that will be obtained from batch sorption measurements of crushed and sieved material, and 2) to normalize and interpret the sorption and diffusion data that will be obtained from diffusion experiments. The results of the characterization have been reported for Work Package (WP) 1 of the CROCK project (Holgerson, 2013) and this paper accounts for results from diffusion and batch sorption experiments made in WP2.

Objective and scope

The objective of this work is to obtain sorption coefficients for the Äspö rock material by utilizing two different experimental methods: batch sorption experiments, with crushed material of different size fractions, and diffusion experiments with intact sections of drill cores. The methods are complementary. Batch sorption is the most common method, because it is relatively simple to multiply for many samples. However, because of the mechanical treatment of the rock material it has also been put into question for its ability to give accurate and representative R_d values for the intact rock (André *et al.* 2009). Diffusion experiments can be regarded as somewhere in between batch sorption and in-situ tracer experiments, since it utilizes larger pieces of solid material. This material has nevertheless also been sampled by drilling and then sawn into a precise geometry, which is a requirement for this type of experiments. The objective for this work is to obtain consistent results of R_d for some selected radiotracers for these two laboratory methods only. It may also give an indication of how to extrapolate R_d to in-situ conditions, but this is outside of the objective of this work.

A number of drill cores were sampled in the Äspö laboratory (KIT-INE, 2011). The priority for Chalmers drill-core samples were cores sampled perpendicular to a fracture and a detailed description of the samples collected for Chalmers has been reported (Holgerson, 2013). The scope of the present investigation is limited to one selected section of a drill core of about 29 cm (Figure 1), which was sawn into smaller slices of 3cm length, starting from one fracture and ending at another fracture. These were further sawn into two halves (each sample then 1.5cm); one half was used in diffusion experiments, the other half was crushed and used in batch sorption experiments. This gave material for, in total, 8 diffusion experiments (labelled A-H) and 8 different samples for batch experiments (labelled a-h), each crushed and sieved into four size fractions. (There is one further sample (labelled I), a core end-piece facing a fracture, where it is yet not decided if it should be used in batch or in diffusion experiments). In addition to R_d values for Cs and Ra for 8 diffusion experiments and 8 times 4=32 sorption experiments, other collected data were the effective diffusivities D_e for the radiotracers and the porosity of the rock, the latter by the assumption that tritiated water (HTO) acts as an inert tracer in the through diffusion experiments.

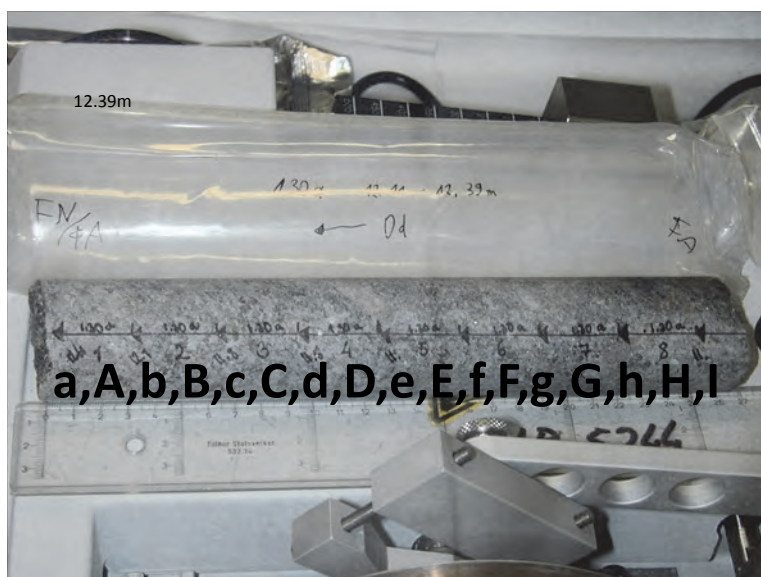


Figure 1: Drill core section (12.11-12.39m) from borehole KA2368A-01, used for all experiments. The section ends at two fractures. Left-hand fracture is a natural and re-sealed fracture while right-hand fracture may be artificial. For pictures of the fracture surfaces, see Holgersson 2013. The approximate sections obtained for diffusion (A-H) and sorption (a-h) experiments are indicated.

Theory

Sorption experiments

Most of the underlying theory can be found in textbooks and have also been collected together in other work concerning batch sorption (Andersson *et al.*, 2008). From a purely experimental view, what is measured is usually not the distribution of a single species of element A (e.g. the uncomplexed free metal ion) but the total sum of all aqueous species (AX, AY...) of element A, between the liquid and the solid phase



The distribution coefficient D , or more commonly in transport calculations R_d , can then be defined as

$$[A]_{ads}/[A]_{aq} = ([AS] + [AXS] + [AYS] + \dots) / ([A] + [AX] + [AY] + \dots) = R_d \quad (\text{Eq.2})$$

The distribution coefficient is dimensionless if the concentrations are expressed in same units. However, since the solid is usually measured by its mass and not by its volume and because of experimental limitations, R_d values are obtained in the unit volume per mass (m^3/kg):

$$R_d (\text{m}^3/\text{kg}) = [A]_{ads} \cdot V / [A]_{aq} \cdot m = ([A]_{tot} - [A]_{aq}) \cdot V / [A]_{aq} \cdot m \quad (\text{Eq.3})$$

In the experiments, $[A]_{ads}$ is obtained indirect: it is measured as the difference between total added tracer $[A]_{tot}$ and aqueous concentration at equilibrium $[A]_{aq}$ and is in concentration per volume solution

units and hence, it has to be multiplied with solution volume V and divided by solid mass m for considering the solid content.

The evaluation of sorption coefficients R_d (m^3/kg) was made by a methodology which is largely identical with the SKB Method Description (SKB MD 540.002) for batch sorption measurements with minerals. The only deviation here from this Method Description is how wall sorption data is interpreted and used for correcting results for the actual batch measurements. Wall sorption is the amount of tracer that sorbs on the walls of the container used in the batch sorption experiments. In the modified evaluation method used here, R_d values for the wall is extracted from separate wall sorption measurements and these values, here designated L_d , are subsequently used for correcting the batch sorption results. The equation for calculating R_d (m^3/kg) is:

$$R_d = (C_{st} \cdot V_{st} \cdot V_{smp,n} / A_{smp,n} - V_0 + \sum V_{smp,i} - L_d - V_{smp,n} / A_{smp,n} \cdot \sum A_{smp,i}) / 10^6 / m \quad (\text{Eq.4})$$

- C_{st} (cpm/mL) is the concentration of radiotracer stock solution
- V_{st} (mL) is the volume of tracer initially added
- $V_{smp,n}$ (mL) is volume of sample, taken at sampling n
- $A_{smp,n}$ (cpm) is count rate of sample, taken at sampling n
- V_0 (mL) is the initial volume of solution
- L_d (mL) is R_d for container wall times the mass of container wall involved in wall sorption, as measured in separate wall sorption experiments
- m (kg) is the dry mass of solid phase

The summation terms runs from 1 to $n-1$ which means, all samples previously taken. Note that the mass of the wall involved in wall sorption is unknown, therefore the wall sorption coefficient R_d times mass of wall is collected together as L_d . A detailed deduction of (Eq.4) can be found elsewhere (Andersson, *et al.*, 2008).

Diffusion experiments

The diffusive flux F (particles/ m^2/s) of a substance through a cross-sectional area of a volume of a medium, in this case water, is proportional to the concentration C (particles/ m^3) gradient in the direction x (m), perpendicular to the cross-sectional area of water:

$$F = -D \cdot \frac{\partial C}{\partial x}, \quad (\text{Fick's First Law}). \quad (\text{Eq.5})$$

The proportionality constant D is called the diffusivity of the substance and it has the unit m^2/s . By considering instead a volume of water filling a porous solid phase, the flux is:

$$F = -D_p \cdot \frac{\partial C}{\partial x}. \quad (\text{Eq.6})$$

The pore diffusivity D_p (m^2/s) is defined as

$$D_p = D \cdot G. \quad (\text{Eq.7})$$

G is the empirical and dimensionless geometrical factor, which is usually <1 . The factor is sometimes written out as

$$G = \frac{\delta}{\tau^2}. \quad (\text{Eq.8})$$

δ is the constrictivity and τ^2 is the tortuosity. These terms may need some explanation. In a capillary model of a porous medium the pores can be assumed to be straight channels and the cross-section width of the pores can be assumed to be much larger than the mean path length of the random movement of the particles. In this case the pore diffusivity would be the same as the diffusivity in water. However, pores are usually not straight, instead they are tortuous. The tortuosity will decrease the pore diffusivity, compared with the diffusivity in water, by increasing the length of the pores. If the pores are narrower and comparable in scale to the mean path length they are said to be constricted. Pore constrictions make the direction of particle movement less random. In this way constrictions will force particles to move in a certain direction and thereby increase the pore diffusivity, compared with the diffusivity in water. In measurements of pore diffusion it is difficult, or rather impossible, to separate these two terms.

Fick's first law (Eqs. 5 and 6) is valid only for gradients independent of the thickness Δx of the cross-section, so called steady-state diffusion. Initially, however, the gradient will vary within Δx . By doing a mass-balance for a time increment over a volume element and using Fick's first law for the mean flux in the middle of the element the result is:

$$\frac{\partial C}{\partial t} = D_p \cdot \frac{\partial^2 C}{\partial x^2}, \quad (\text{Fick's Second Law}). \quad (\text{Eq.9})$$

A substance diffusing in a porous system can also have surface-chemical interactions with the solid, or in other words, it can adsorb on to (and desorb from) the solid. In that case (Eq.9) has to be modified with an additional term:

$$\frac{\partial C}{\partial t} = D_p \cdot \frac{\partial^2 C}{\partial x^2} - \frac{dC_s}{dt}. \quad (\text{Eq.10})$$

C_s (particles/m³) is the concentration of adsorbed substance expressed as particles per volume solution. Combining this equation with a linear adsorption isotherm, it can be shown that:

$$\frac{\partial C}{\partial t} = \frac{D_p \cdot \varepsilon_p}{(\varepsilon_p + K_d \cdot \rho)} \cdot \frac{\partial^2 C}{\partial x^2}. \quad (\text{Eq.11})$$

ε_p and ρ (kg/m³) are the porosity and the apparent density (including pore volume) of the solid phase, respectively. Just as the geometrical factor, these entities must be considered as average values for a particular sample of solid phase.

K_d (m³/kg) is the sorption constant (the requirement of a linear isotherm), defined by

$$K_d = \frac{C_s}{C}. \quad (\text{Eq.12})$$

Here the concentration C_s (particles/kg) is now expressed as particles per mass of solid. The quantity:

$$D_p \cdot \varepsilon_p \equiv D_e, \quad (\text{Eq.13})$$

is called the effective diffusivity D_e (m²/s) and is the proportionality constant at steady- state diffusive flux through a cross-sectional area of the porous medium.

In (Eq. 11) the dimensionless quantity:

$$\varepsilon_p + K_d \cdot \rho \equiv \alpha, \quad (\text{Eq.14})$$

This is defined as the capacity factor α and it is a measure of the total uptake capacity (chemical and physical) of the porous medium for the diffusing substance.

The final form of Fick's second law for 1-dimensional diffusion in a porous medium, as used in this work, is therefore

$$\frac{\partial C}{\partial t} = \frac{D_e}{\alpha} \cdot \frac{\partial^2 C}{\partial x^2}. \quad (\text{Eq.15})$$

Analytical solutions of this differential equation for an experimental configuration can be found if certain boundary conditions can be formulated (Crank, 1975). With appropriate experimental configuration, it is possible to extract D_e and α separately. In the case when $K_d=0$ (an assumption made for HTO), $\alpha=\varepsilon_p$ and it is thus also possible to extract G with the help of water diffusivity data. If, however, $K_d>0$, then it is only possible to extract $G \cdot \varepsilon_p \equiv G_F$, this parameter is called the formation factor.

The experimental configuration selected for the diffusion experiments with rock discs is shown in Figure 2. The design uses two identical plastic containers, each with 38mL volume capacity, clamping between them the disc. The tracer is loaded in one container and the through-diffusion is measured in the other container. The boundary conditions for this configuration are the constant concentrations C_0 in the loading reservoir and the $C(t)$ in the sampling reservoir, which is low and thereby effectively zero and constant in comparison with C_0 . Maximum 1% through-diffusion is a usual rule-of-thumb for the application of the analytical solution.

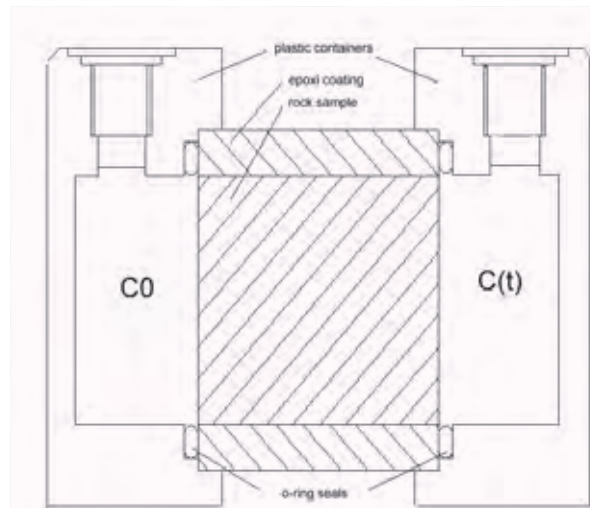


Figure 2: Drawing of the through-diffusion cell. C_0 = high tracer concentration, $C(t)$ =low tracer concentration.

The solution to (Eq.15) for this experimental configuration is (Crank, 1975):

$$\frac{C(t)}{C_0} = \frac{A}{V} \cdot \left(\frac{D_e \cdot t}{l} - \frac{\alpha \cdot l}{6} - \frac{2 \cdot \alpha \cdot l}{\pi^2} \cdot \sum_{n=1}^{\infty} \frac{(-1)^n}{n^2} \cdot \exp\left(\frac{-D_e \cdot n^2 \cdot \pi^2 \cdot t}{\alpha \cdot l^2} \right) \right) \quad (\text{Eq.16})$$

A and V are the disc area and the sampling container volume, respectively. l is the disc thickness. The fitting parameters are D_e and α . This design is excellent for obtaining diffusion parameters for non- to low-adsorbing tracers ($0 < R_d < 0.001$). However, for more adsorbing tracers ($R_d > 0.001$) it is a very time-consuming method. Any through-diffusion would be hard to detect after one year, even though the rock material has been cut into slices of about 1cm.

For more adsorbing tracers, an uptake method is therefore preferable. The uptake method is nevertheless also possible to use with the through-diffusion cell, namely by the measurement of the disappearance of tracer in the loading container. The loading concentration is then not assumed to be constant. Instead the boundary condition for equal flux across the solution/rock interface prevails. In this case through-diffusion can be assumed to be negligible.

The solution to (Eq. 15) for such a configuration is (Crank, 1975):

$$\frac{C(t)}{C(0)} = 1 - \frac{(C(0) - C_{\infty})}{C(0)} \cdot \left(1 - \sum_{n=1}^{\infty} \frac{(2z + 2z^2) \cdot \exp\left(\frac{-4D_e \cdot q_n^2 \cdot t}{l^2 \cdot \alpha}\right)}{1 + z + (q_n \cdot z)^2} \right) \quad (\text{Eq.17})$$

$C(t)$ and $C(0)$ are the tracer concentrations in solution at time t and at $t=0$, respectively now both measured only on the left, high-concentration side in Figure 2. C_{∞} is the constant equilibrium concentration. In (Eq.17) z is defined as:

$$z = \frac{C_{\infty}}{(C(0) - C_{\infty})} \cdot \quad (\text{Eq.18})$$

In (Eq.17), l is the length of the disc and q_n are the positive non-zero roots to:

$$\tan q_n = -z \cdot q_n \cdot \quad (\text{Eq.19})$$

C_{∞} can be expressed as:

$$C_{\infty} = \frac{C(0) \cdot V}{(V + V_{disc} \cdot \alpha)} \cdot \quad (\text{Eq.20})$$

Here V and V_{disc} are the solution and rock disc volumes, respectively. In (Eq.17), the fitting parameters are D_e and α .

Experimental

All experiments were made in an N₂ flushed glove-box (MBraun InLab, [O₂(g)]~1ppm, T~20°C). The synthetic groundwater that was used has previously been described (Holgerson, 2013). Samples were measured with a High Purity Ge detector (Canberra GammaAnalyst) for ¹³⁴Cs gamma radiation counts (E_{γ} : ¹³⁴Cs=605keV). 0.1mL samples for gamma measurement were taken to 6mL plastic tubes and samples diluted with 0.4mL 0.5M HNO₃ to the exact sample geometry that the detector was previously calibrated for. ²²⁶Ra and HTO were measured with an alfa/beta-discriminating Liquid Scintillation Counter (LSC) (Perkin-Elmer/Wallac Guardian 1414), using 7mL vials and with addition of 6mL LSC cocktail, for HTO the Emulsifier Safe, for ²²⁶Ra the alfa/beta discriminating Ultima Gold AB (both Perkin-Elmer). It should be noted that there was not enough time to allow complete secular equilibrium between ²²⁶Ra and its daughters in the samples before measurement. This will take 65 days and therefore the measurements will be repeated and updated results presented elsewhere at a later occasion. It should therefore be noted that this disequilibrium also contributes to uncertainties in the derived data for ²²⁶Ra sorption and diffusion.

Batch sorption experiments

The crushed and sieved rock material (Holgersson, 2013) was weighed in 0.1g portions into polypropylene plastic tubes (Sarstedt 60.546) of 6mL volume capacity. To this, 5mL synthetic groundwater was added. During an initial period of four weeks, 4.5mL of the water was exchanged once every week. Finally, after another outtake of 4.5mL, the water was replaced with mixed radiotracer solution of ^{134}Cs and ^{226}Ra in synthetic groundwater (pH7.8). Total radiotracer concentrations were $1 \cdot 10^{-7}\text{M}$ and $1 \cdot 10^{-8}\text{M}$, respectively. The tubes were then lightly shaken. Sampling of 2 times 0.1mL from each tube was made by first centrifuging the tubes at 1000 g for 15min. Samplings were made after 2 weeks and 1 month. After each sampling, the tubes were lightly shaken for mixing water and solid phases again. Two separate series of batch experiments were also run: one for wall sorption (with radioactive tracers) and one for pH measurements (without radioactive tracers).

Diffusion experiments

The eight samples of sawed 1.5cm thick sections of rock material (Holgersson, 2013) were cast into an epoxy resin (Laminering 275, Nils Malmgren company), where the faces of each sections were protected with tape. The cast form of Teflon gives a circular rim of epoxy resin of about 1cm thickness around the rock samples (Fig. 3.1), in order to give an additional (non-porous) surface for o-rings to fixate the samples in the diffusion cells. The excess of epoxy resin on top of the flat surfaces was sanded away with 120 or 220 grade sand paper. After the measurement of porosity with the dry/wet weighing method (Holgersson, 2013), the water-saturated rock samples were mounted into the diffusion cells and 37-38mL of synthetic groundwater was filled into each container. After two weeks, HTO tracer (about 0.1MBq) was added in one of the containers. After 1h, to allow mixing by diffusion of tracer to entire container volume, the C_0 concentration was measured with an outtake of 0.1mL on the high concentration side. During a following period of about 1 month, nine samples were taken on the low concentration side with 1mL outtake each. The sample volumes were replaced with synthetic groundwater. After the completion of the HTO through diffusion, the containers were emptied and flushed several times with fresh synthetic ground water. After one week of standing with fresh water, the water on one side was replaced with $^{134}\text{Cs}+^{226}\text{Ra}$ mixed radiotracer. After 1h, to allow mixing with any remaining water in the cells, the C_0 concentration was measured with an outtake of 0.1mL on the high concentration side. During a period of about 1 month, seven samples were taken on the high concentration side, each consisting of 0.1mL for gamma counting and 0.1mL for alfa counting. The sample volumes were replaced with synthetic groundwater. No wall sorption measurements were made in the diffusion cells.

pH measurements

Separate batch tubes with the 32 different Äspö-diorite fractions were prepared for pH-measurements. These measurements were made at the same time as samplings were made in the main series of batch experiments. A glass combination electrode and pH-meter were used (Radiometer pHC 3006-9, pHM240) and pH 4 and 7 buffers (AVS Titrinorm) for the electrode adjustment.

Results

Batch sorption experiments

Cs batch sorption

The results for ^{134}Cs wall sorption measurements gave an uptake on the tubes of about 5%, giving an $L_d=0.32\pm0.06\text{mL}$ at 1 month. See (Eq.4) above for the wall sorption correction method used. The results of batch sorption of ^{134}Cs onto four size fractions of crushed Äspö rock material (drill core sections "a" to "h") are presented in Tables 1-4 below.

Table 1: Results for sorption coefficients R_d (m^3/kg) and the specific surface area normalized R_a (m) in batch sorption of Cs onto crushed and sieved fraction 0.063-0.125mm of Äspö diorite (average of triplicate experiments) from 8 drill core sections, labelled a-h. Sampled after 14 days and 1 month.

	R_d (m^3/kg) $\cdot 10^2$		R_a (m) $\cdot 10^4$ ⁽¹⁾	
	14d	1m	14d	1m
a	8.78 \pm 0.35	10.5 \pm 1.6	2.19 \pm 0.09	2.62 \pm 0.40
b	8.37 \pm 0.22	9.15 \pm 1.10	2.33 \pm 0.06	2.55 \pm 0.31
c	6.33 \pm 0.18	8.33 \pm 1.75	2.12 \pm 0.06	2.80 \pm 0.59
d	7.11 \pm 0.56	7.18 \pm 0.05	2.36 \pm 0.19	2.39 \pm 0.02
e	6.70 \pm 0.23	7.99 \pm 0.52	2.50 \pm 0.08	2.99 \pm 0.19
f	7.08 \pm 0.37	8.88 \pm 1.16	2.64 \pm 0.14	3.32 \pm 0.43
g	8.91 \pm 1.29	9.64 \pm 1.61	2.84 \pm 0.41	3.07 \pm 0.51
h	9.49 \pm 0.73	9.84 \pm 0.30	3.42 \pm 0.26	3.54 \pm 0.11
average	7.85\pm1.11(15%)	8.94\pm1.08(12%)	2.55\pm0.42(16%)	2.91\pm0.40(14%)

¹⁾ calculated by using measured specific surface area (Holgerrson, 2013).

Table 2: Results for sorption coefficients R_d (m^3/kg) and the specific surface area normalized R_a (m) in batch sorption of Cs onto crushed and sieved fraction 0.125-0.25mm of Äspö diorite (average of triplicate experiments) from 8 drill core sections, labelled a-h. Sampled after 14 days and 1 month.

	R_d (m^3/kg) $\cdot 10^2$		R_a (m) $\cdot 10^4$	
	14d	1m	14d	1m
a	4.53 \pm 0.61	5.68 \pm 0.30	1.98 \pm 0.27	2.48 \pm 0.13
b	4.44 \pm 0.77	5.17 \pm 0.30	1.77 \pm 0.31	2.065 \pm 0.12
c	3.68 \pm 0.28	4.16 \pm 0.29	1.68 \pm 0.13	1.90 \pm 0.13
d	3.66 \pm 0.19	3.92 \pm 0.51	1.79 \pm 0.09	1.91 \pm 0.25
e	3.57 \pm 0.20	3.71 \pm 0.30	2.04 \pm 0.11	2.12 \pm 0.17
f	4.09 \pm 0.21	5.06 \pm 0.19	2.12 \pm 0.11	2.63 \pm 0.10
g	3.68 \pm 0.19	4.77 \pm 0.23	2.08 \pm 0.11	2.69 \pm 0.13
h	4.59 \pm 0.12	5.81 \pm 1.16	2.61 \pm 0.07	3.30 \pm 0.66
average	4.03\pm0.43(11%)	4.78\pm0.79(16%)	2.01\pm0.29(14%)	2.39\pm0.48(20%)

Table 3: Results for sorption coefficients R_d (m^3/kg) and the specific surface area normalized R_a (m) in batch sorption of Cs onto crushed and sieved fraction 0.25-0.5mm of Äspö diorite (average of triplicate experiments) from 8 drill core sections, labelled a-h. Sampled after 14 days and 1 month.

	R_d (m^3/kg) $\cdot 10^2$		R_a (m) $\cdot 10^4$	
	14d	1m	14d	1m
a	2.31±0.36	2.73±0.20	1.50±0.23	1.77±0.13
b	2.29±0.23	3.03±0.68	1.51±0.15	2.00±0.45
c	1.97±0.54	2.58±0.32	1.30±0.36	1.70±0.21
d	1.93±0.03	2.33±0.40	1.46±0.03	1.76±0.30
e	1.64±0.25	2.16±0.35	1.27±0.20	1.68±0.27
f	2.31±0.24	2.69±0.51	1.85±0.19	2.15±0.40
g	2.14±0.23	2.49±0.15	1.52±0.17	1.77±0.11
h	2.34±0.30	2.54±0.69	2.14±0.27	2.33±0.64
average	2.12±0.25(12%)	2.57±0.26(10%)	1.57±0.29(18%)	1.89±0.24(13%)

Table 4: Results for sorption coefficients R_d (m^3/kg) and the specific surface area normalized R_a (m) in batch sorption of Cs onto crushed and sieved fraction 0.5-0.5-1mm of Äspö diorite (average of triplicate experiments) from 8 drill core sections, labelled a-h. Sampled after 14 days and 1 month.

	R_d (m^3/kg) $\cdot 10^2$		R_a (m) $\cdot 10^4$	
	14d	1m	14d	1m
a	1.14±0.19	1.30±0.17	1.12±0.18	1.27±0.17
b	1.36±0.14	1.27±0.40	1.42±0.15	1.34±0.41
c	1.15±0.15	1.78±0.31	1.35±0.17	2.09±0.36
d	1.18±0.08	1.30±0.09	1.27±0.08	1.40±0.09
e	1.31±0.36	1.80±0.25	1.62±0.44	2.23±0.31
f	1.39±0.11	1.56±0.28	1.81±0.14	2.03±0.36
g	1.50±0.58	1.81±0.60	1.56±0.60	1.89±0.63
h	1.19±0.45	1.74±0.29	1.67±0.63	2.43±0.40
average	1.28±0.13(10%)	1.57±0.24(15%)	1.48±0.23(16%)	1.84±0.44(24%)

Ra batch sorption

The results for ^{226}Ra wall sorption measurements gave an uptake on the tubes of about 25%, giving an $L_d=1.38\pm 0.21\text{mL}$ at 1 month. See (Eq.4) above for the wall sorption correction method used. The results of batch sorption of ^{226}Ra onto four fractions of crushed Äspö rock material (drill core sections "a" to "h") are presented in Tables 5-8 below.

Table 5: Results for sorption coefficients R_d (m^3/kg) and the specific surface area normalized R_a (m) in batch sorption of R_a onto crushed and sieved fraction 0.063-0.125mm of Äspö diorite (average of triplicate experiments) from 8 drill core sections, labelled a-h. Sampled after 14 days and 1 month.

	R_d (m^3/kg) $\cdot 10^2$		R_a (m) $\cdot 10^4$ ¹⁾	
	14d	1m	14d	1m
a	3.11±0.92	3.76±0.68	0.79±0.23	0.94±0.17
b	2.38±0.16	3.60±0.35	0.66±0.04	1.00±0.10
c	3.65±0.09	3.37±0.44	1.22±0.03	1.13±0.15
d	2.77±0.43	2.94±0.36	0.92±0.14	0.98±0.12
e	1.93±0.22	2.50±0.64	0.72±0.08	0.93±0.24
f	1.71±0.63	2.52±0.13	0.64±0.24	0.94±0.05
g	2.38±0.50	2.99±0.19	0.76±0.16	0.95±0.06
h	3.28±0.36	5.07±0.27	1.18±0.13	1.83±0.10
average	2.65±0.67(25%)	3.34±0.84(25%)	0.86±0.23(26%)	1.09±0.30(28%)

¹⁾ calculated by using measured specific surface area (Holgerson, 2013).

Table 6: Results for sorption coefficients R_d (m^3/kg) and the specific surface area normalized R_a (m) in batch sorption of R_a onto crushed and sieved fraction 0.125-0.25mm of Äspö diorite (average of triplicate experiments) from 8 drill core sections, labelled a-h. Sampled after 14 days and 1 month.

	R_d (m^3/kg) $\cdot 10^2$		R_a (m) $\cdot 10^4$	
	14d	1m	14d	1m
a	1.67±0.36	2.47±0.52	0.73±0.16	1.08±0.23
b	1.14±0.18	2.01±0.37	0.45±0.07	0.80±0.15
c	1.44±1.20	2.28±0.47	0.66±0.55	1.04±0.22
d	2.04±0.34	1.35±0.18	1.00±0.17	0.66±0.09
e	1.06±0.32	1.32±0.35	0.61±0.18	0.76±0.20
f	0.93±0.28	1.57±0.39	0.48±0.15	0.82±0.20
g	1.08±0.11	2.10±0.71	0.61±0.06	1.18±0.40
h	0.98±0.41	3.95±0.45	0.56±0.23	2.24±0.28
average	1.29±0.39(30%)	2.13±0.85(40%)	0.64±0.17(27%)	1.07±0.51(47%)

Table 7: Results for sorption coefficients R_d (m^3/kg) and the specific surface area normalized R_a (m) in batch sorption of R_a onto crushed and sieved fraction 0.25-0.5mm of Äspö diorite (average of triplicate experiments) from 8 drill core sections, labelled a-h. Sampled after 14 days and 1 month.

	R_d (m^3/kg) $\cdot 10^2$		R_a (m) $\cdot 10^4$	
	14d	1m	14d	1m
a	0.80±0.16	1.16±0.17	0.52±0.10	0.75±0.11
b	0.19±0.31	1.39±0.36	0.22±0.15	0.92±0.23
c	0.59±0.57	1.16±0.21	0.39±0.38	0.77±0.14
d	1.04±0.29	0.68±0.24	0.78±0.22	0.51±0.18
e	0.72±0.22	0.31±0.11	0.56±0.17	0.24±0.09
f	0.23±0.10	0.72±0.24	0.18±0.08	0.58±0.19
g	0.20±0.17	1.40±0.70	0.14±0.12	0.99±0.50
h	0.28±0.25	2.11±1.28	0.26±0.27	1.93±1.17
average	0.51±0.33(64%)	1.12±0.55(50%)	0.38±0.22(58%)	0.84±0.50(60%)

Table 8: Results for sorption coefficients R_d (m^3/kg) and the specific surface area normalized R_a (m) in batch sorption of Ra onto crushed and sieved fraction 0.5-0.5-1mm of Äspö diorite (average of triplicate experiments) from 8 drill core sections, labelled a-h. Sampled after 14 days and 1 month.

	R_d (m^3/kg) $\cdot 10^2$		R_a (m) $\cdot 10^4$	
	14d	1m	14d	1m
a	0.51±0.34	0.75±0.28	0.50±0.33	0.74±0.27
b	n.d.	0.56±0.55	n.d.	0.58±0.50
c	n.d.	0.78±0.28	n.d.	0.92±0.33
d	0.09±0.08	0.30±0.29	0.14±0.12	0.33±0.30
e	0.52±0.32	0.45±0.40	0.64±0.40	0.55±0.50
f	n.d.	0.32±0.30	n.d.	0.41±0.40
g	0.79±0.70	0.61±0.60	0.82±0.60	0.64±0.60
h	n.d.	n.d.	n.d.	n.d.
average	0.48±0.29(61%)	0.54±0.19(36%)	0.52±0.29(55%)	0.60±0.20(33%)

Diffusion experiments

HTO trough-diffusion

The results of HTO through-diffusion are shown in Figure 3 and in Table 9, below.

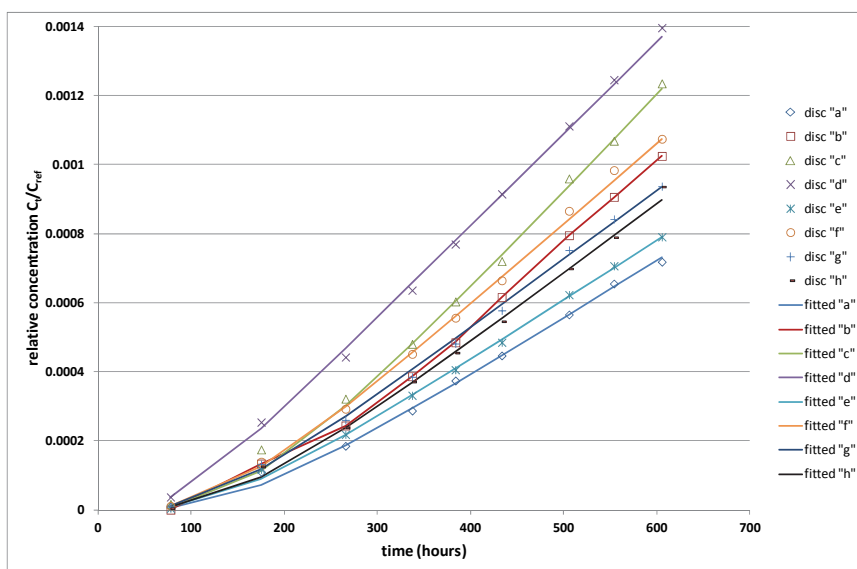


Figure 3: Through diffusion of tritiated water (HTO) in eight samples of Äspö diorite drill-core sections, each of 1.5cm thickness. Lines show Eq.16 fitted to the data.

Table 9: Evaluated parameters for tritium through diffusion: effective diffusivity (D_e), geometrical factor (G), porosity (ϵ_p) and specific pore volume (SPV) . For comparison, porosity and SPV measured with gravimetric method (Holgerrson, 2013) are also shown.

Sample disc	D_e (m^2/s)	$G^{(1)}$	ϵ_p (%) HTO method	SPV ⁽²⁾ (mL/g) HTO method	ϵ_p (%) gravimetric method	SPV (mL/g) gravimetric method
A	$1.27 \cdot 10^{-13}$	$3.45 \cdot 10^{-2}$	$1.73 \cdot 10^{-3}$	$6.42 \cdot 10^{-4}$	$7.48 \cdot 10^{-3}$	$2.78 \cdot 10^{-3}$
B	$1.67 \cdot 10^{-13}$	$2.76 \cdot 10^{-2}$	$2.85 \cdot 10^{-3}$	$1.05 \cdot 10^{-3}$	$9.42 \cdot 10^{-3}$	$3.49 \cdot 10^{-3}$
C	$1.61 \cdot 10^{-13}$	$2.48 \cdot 10^{-2}$	$3.05 \cdot 10^{-3}$	$1.12 \cdot 10^{-3}$	$5.77 \cdot 10^{-3}$	$2.12 \cdot 10^{-3}$
D	$1.35 \cdot 10^{-13}$	$4.33 \cdot 10^{-2}$	$1.46 \cdot 10^{-3}$	$5.32 \cdot 10^{-4}$	$5.84 \cdot 10^{-3}$	$2.13 \cdot 10^{-3}$
E	$9.84 \cdot 10^{-14}$	$2.94 \cdot 10^{-2}$	$1.57 \cdot 10^{-3}$	$5.77 \cdot 10^{-4}$	$5.66 \cdot 10^{-3}$	$2.08 \cdot 10^{-3}$
F	$1.18 \cdot 10^{-13}$	$2.70 \cdot 10^{-2}$	$2.06 \cdot 10^{-3}$	$7.63 \cdot 10^{-4}$	$6.56 \cdot 10^{-3}$	$2.43 \cdot 10^{-3}$
G	$1.13 \cdot 10^{-13}$	$3.23 \cdot 10^{-2}$	$1.65 \cdot 10^{-3}$	$6.16 \cdot 10^{-4}$	$6.73 \cdot 10^{-3}$	$2.52 \cdot 10^{-3}$
H	$1.02 \cdot 10^{-13}$	$2.46 \cdot 10^{-2}$	$1.94 \cdot 10^{-3}$	$7.20 \cdot 10^{-4}$	$7.34 \cdot 10^{-3}$	$2.72 \cdot 10^{-3}$
mean value	1.28 ± 0.26 $\cdot 10^{-13}$	3.04 ± 0.62 $\cdot 10^{-2}$	2.04 ± 0.60 $\cdot 10^{-3}$	7.54 ± 2.21 $\cdot 10^{-4}$	6.85 ± 1.25 $\cdot 10^{-3}$	2.53 ± 0.47 $\cdot 10^{-3}$

1) Calculated using porosity measured with HTO method and $D_{H_2O}(25^\circ C) = 2.13 \cdot 10^{-9} m^2/s$ (Wang, 1951).

2) Calculated using measured densities (Holgerrson, 2013).

Cs-in-diffusion

The results of Cs in-diffusion are shown in Figure 4 and in Table 10, below.

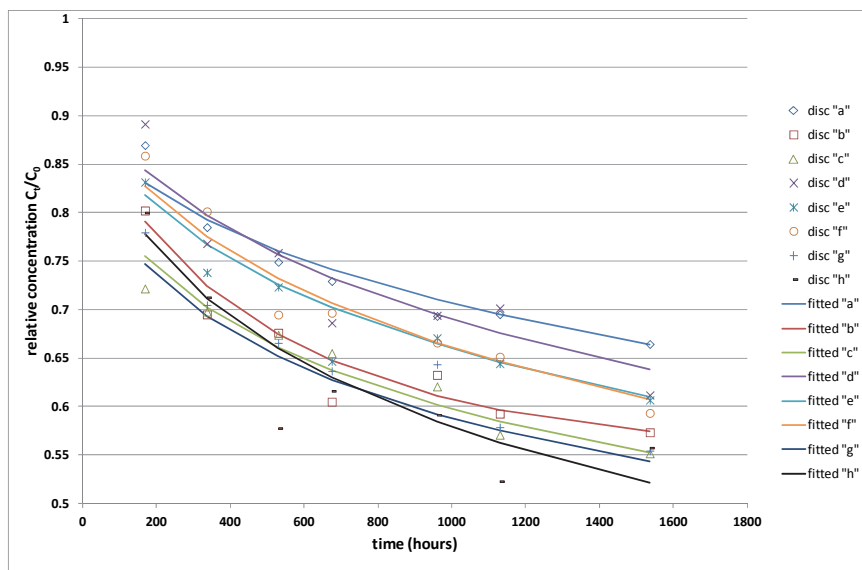


Figure 4: In-diffusion of ^{134}Cs in eight samples of Äspö diorite drill-core sections, each of 1.5cm thickness. Lines show Eq.17 fitted to the data.

Table 10: Evaluated parameters for ¹³⁴Cs in-diffusion: effective diffusivity (D_e), capacity factor (α), formation factor (G_F), sorption constants K_d and K_a . For comparison, G_F from HTO through-diffusion is also shown.

Sample disc	D_e (m ² /s)	α	$G_{F,Cs}^{(1)}$	$G_{F,HTO}^{(2)}$	$K_d^{(3)}$ (m ³ /kg)	$K_a^{(4)}$ (m)
A	$1.13 \cdot 10^{-12}$	2.11	$5.46 \cdot 10^{-4}$	$5.96 \cdot 10^{-5}$	$7.84 \cdot 10^{-4}$	$1.14 \cdot 10^{-4}$
B	$9.10 \cdot 10^{-12}$	1.19	$4.44 \cdot 10^{-3}$	$7.86 \cdot 10^{-5}$	$4.40 \cdot 10^{-4}$	$5.65 \cdot 10^{-5}$
C	$2.99 \cdot 10^{-12}$	1.98	$1.44 \cdot 10^{-3}$	$7.58 \cdot 10^{-5}$	$7.27 \cdot 10^{-4}$	$1.19 \cdot 10^{-4}$
D	$1.13 \cdot 10^{-12}$	4.64	$5.48 \cdot 10^{-4}$	$6.32 \cdot 10^{-5}$	$1.69 \cdot 10^{-3}$	$3.32 \cdot 10^{-4}$
E	$1.93 \cdot 10^{-12}$	2.63	$9.06 \cdot 10^{-4}$	$4.62 \cdot 10^{-5}$	$9.67 \cdot 10^{-4}$	$2.20 \cdot 10^{-4}$
F	$1.30 \cdot 10^{-12}$	4.90	$6.12 \cdot 10^{-4}$	$5.55 \cdot 10^{-5}$	$1.82 \cdot 10^{-3}$	$2.93 \cdot 10^{-4}$
G	$3.12 \cdot 10^{-12}$	1.93	$1.47 \cdot 10^{-3}$	$5.32 \cdot 10^{-5}$	$7.20 \cdot 10^{-4}$	$1.44 \cdot 10^{-4}$
H	$2.26 \cdot 10^{-12}$	5.67	$1.06 \cdot 10^{-3}$	$4.78 \cdot 10^{-5}$	$2.10 \cdot 10^{-3}$	$4.38 \cdot 10^{-4}$
mean value	$1.98 \pm 0.85^{(5)} \cdot 10^{-12}$	3.13 ± 1.68	$9.40 \pm 0.40^{(5)} \cdot 10^{-4}$	$6.00 \pm 1.20 \cdot 10^{-5}$	$1.16 \pm 0.62 \cdot 10^{-3}$	$2.15 \pm 1.31 \cdot 10^{-4}$

- 1) Calculated using $D_{Cs^+}(25^\circ C) = 2.07 \cdot 10^{-9} \text{ m}^2/\text{s}$ (Li and Gregory, 1974).
- 2) Calculated using $D_{H_2O}(25^\circ C) = 2.13 \cdot 10^{-9} \text{ m}^2/\text{s}$ (Wang, 1951).
- 3) Calculated using the measured densities of the rock discs (Holgersson 2013), the porosity is in comparison to rock capacity factor small and neglected.
- 4) Calculated using measures specific surface area of the rock discs (Holgersson 2013).
- 5) sample "B" excluded from mean

Ra-in-diffusion

The results of Ra in-diffusion are shown in Figure 5 and in Table 11, below.

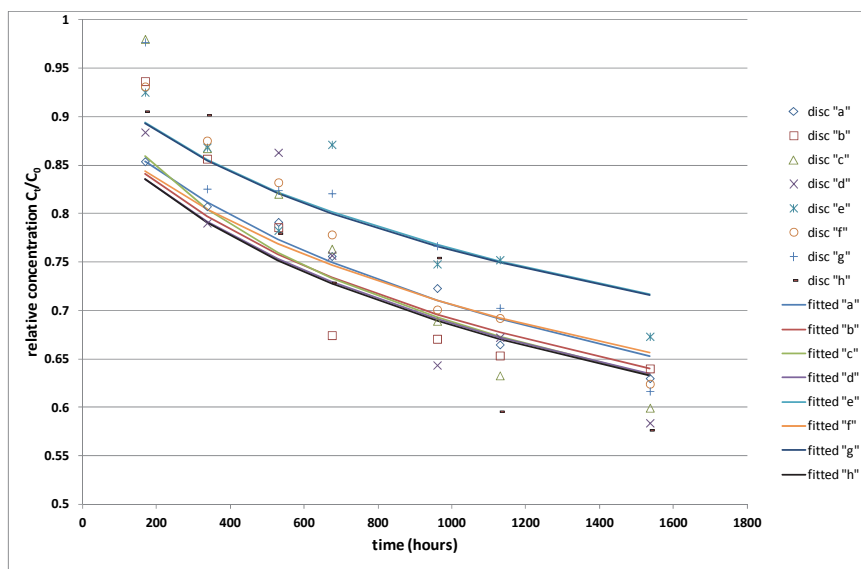


Figure 5: In-diffusion of ²²⁶Ra in eight samples of Äspö diorite drill-core sections, each of 1.5cm thickness. Lines show Eq.17 fitted to the data.

Table 11: Evaluated parameters for ^{226}Ra in-diffusion: effective diffusivity (D_e), capacity factor (α), formation factor (G_F), sorption constants K_d and K_a . For comparison, G_F from HTO through-diffusion is also shown.

Sample disc	D_e (m^2/s)	α	$G_{F,Ra}^{(1)}$	$G_{F,HTO}^{(2)}$	$K_d^{(3)}$ (m^3/kg)	$K_a^{(4)}$ (m)
A	$1.14 \cdot 10^{-12}$	5.87	$1.28 \cdot 10^{-3}$	$5.96 \cdot 10^{-5}$	$2.18 \cdot 10^{-3}$	$3.16 \cdot 10^{-4}$
B	$1.14 \cdot 10^{-12}$	4.31	$1.28 \cdot 10^{-3}$	$7.86 \cdot 10^{-5}$	$1.59 \cdot 10^{-3}$	$2.04 \cdot 10^{-4}$
C	$1.64 \cdot 10^{-12}$	4.63	$1.84 \cdot 10^{-3}$	$7.58 \cdot 10^{-5}$	$1.71 \cdot 10^{-3}$	$2.80 \cdot 10^{-4}$
D	$9.78 \cdot 10^{-13}$	5.50	$1.10 \cdot 10^{-3}$	$6.32 \cdot 10^{-5}$	$2.00 \cdot 10^{-3}$	$3.93 \cdot 10^{-4}$
E	$8.56 \cdot 10^{-13}$	4.05	$9.63 \cdot 10^{-4}$	$4.62 \cdot 10^{-5}$	$1.49 \cdot 10^{-3}$	$3.38 \cdot 10^{-4}$
F	$7.85 \cdot 10^{-13}$	5.53	$8.83 \cdot 10^{-4}$	$5.55 \cdot 10^{-5}$	$2.05 \cdot 10^{-3}$	$3.31 \cdot 10^{-4}$
G	$8.34 \cdot 10^{-13}$	3.98	$9.38 \cdot 10^{-4}$	$5.32 \cdot 10^{-5}$	$1.49 \cdot 10^{-3}$	$2.98 \cdot 10^{-4}$
H	$9.94 \cdot 10^{-13}$	5.55	$1.12 \cdot 10^{-3}$	$4.78 \cdot 10^{-5}$	$2.06 \cdot 10^{-3}$	$4.29 \cdot 10^{-4}$
mean value	$1.05 \pm 0.27 \cdot 10^{-12}$	4.93 ± 0.77	$1.18 \pm 0.31 \cdot 10^{-3}$	$6.00 \pm 1.20 \cdot 10^{-5}$	$1.82 \pm 0.28 \cdot 10^{-3}$	$3.24 \pm 0.69 \cdot 10^{-4}$

1) Calculated using $D_{Ra^{2+}}(25^\circ\text{C})=8.89 \cdot 10^{-10} \text{m}^2/\text{s}$ (Li and Gregory, 1974)

2) Calculated using $D_{H_2O}(25^\circ\text{C})=2.13 \cdot 10^{-9} \text{m}^2/\text{s}$ (Wang, 1951)

3) Calculated using the measured densities of the rock discs (Holgerrson 2013), the porosity is in comparison to rock capacity factor small and neglected.

4) Calculated using measures specific surface area of the rock discs (Holgerrson 2013).

pH measurements

The results for the pH measurements in the separate batch experiment series are shown in Table 12.

Table 12: pH measurements in batch sorption experiments. Single samples and measurements at 14 days and 1 month.

	0.063-0.125mm particles		0.125-0.25mm particles		0.25-0.5mm particles		0.5-1mm particles	
	14d	1m	14d	1m	14d	1m	14d	1m
a	7.28	7.07	7.20	7.07	7.15	6.89	7.07	6.85
b	7.42	7.26	7.46	7.29	7.41	7.32	7.35	7.30
c	7.40	7.54	7.38	7.53	7.41	7.25	7.37	7.24
d	7.42	7.55	7.39	7.57	7.42	7.59	7.40	7.54
e	7.56	7.65	7.44	7.60	7.44	7.62	7.46	7.60
f	7.59	7.76	7.57	7.83	7.56	7.84	7.56	7.74
g	7.61	7.80	7.64	7.78	7.63	7.77	7.58	7.78
h	7.43	7.75	7.47	7.80	7.53	7.75	7.39	7.73

Spatial variations

Some of the results from sections 5.1-5.3 are presented in Figures 6-8 below, showing the spatial variations along the drill core.

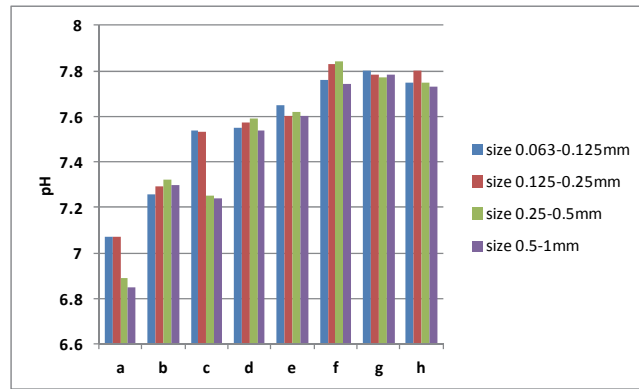


Figure 6: The variation of pH in batch experiments for samples taken along the length of the drill-core. The labels "a-h" refer to the sections shown in Figure 1.

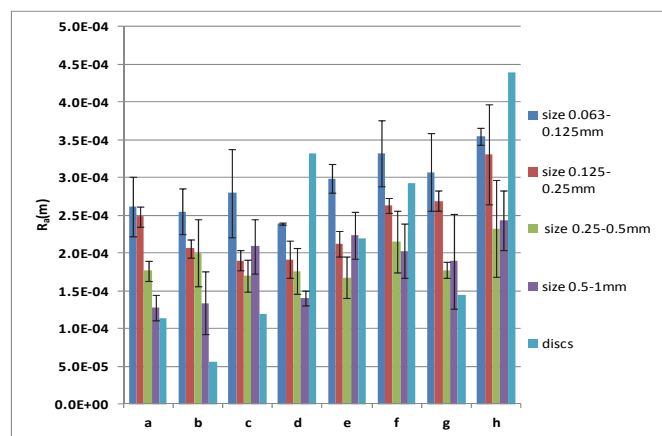


Figure 7: The variation of sorption coefficient R_a (discs: K_a) for C_s for samples taken along the length of the drill-core. The labels "a-h" refer to the sections shown in Figure 1.

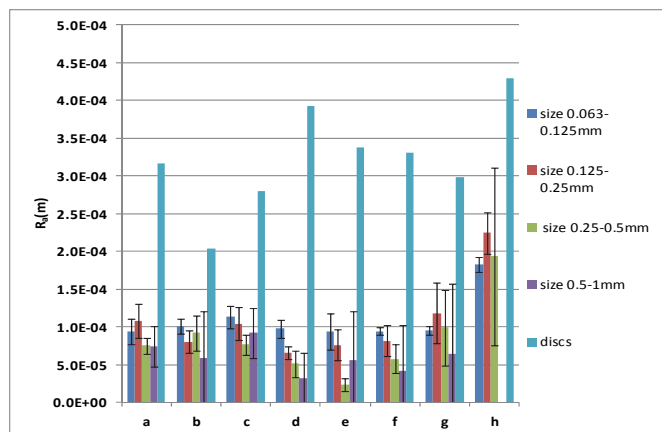


Figure 8: The variation of sorption coefficient R_a (discs: K_a) for R_a for samples taken along the length of the drill-core. The labels a-h refer to the sections shown in Figure 1.

Discussion

Cs batch sorption

The results for R_d values of ^{134}Cs batch sorption on the eight samples taken along the drill-core, each subdivided in four particle-size fractions, show the expected increase in R_d values as the particle-size is reduced (Tables 1 - 4). The values also increase with time, showing the process of on-going in-diffusion in the particles. The reach of an equilibrium R_d can probably be expected within the next few months (data not yet available at this moment). For example, in the batch sorption experiments made to support the site investigation for a Swedish final repository for nuclear waste, sampling was continued up to 6 months (Byegård and Selnert, 2008, Selnert *et al.* 2009). The normalization of R_d values with the measured specific surface areas (SSA) of each fraction (Holgerson 2013), gives R_a values at the 1 month sampling of $2.91 \pm 0.40 \cdot 10^{-4}$, $2.39 \pm 0.48 \cdot 10^{-4}$, $1.89 \pm 0.24 \cdot 10^{-4}$ and $1.84 \pm 0.44 \cdot 10^{-4} \text{m}$ for the size fractions 0.063-0.125, 0.125-0.25, 0.25-0.5 and 0.5-1mm, respectively. Evidently, there is still some difference in sorption between the size fractions, and awaiting an even later sampling occasion (up to 3 months) is recommended, particularly the largest size fractions will be the slowest to equilibrate. Any definitive conclusion can therefore not yet be drawn on the efficiency of SSA normalization for the Cs sorption onto Äspö diorite, but these preliminary results looks promising, already at 1 month giving R_a values almost overlapping when considering the standard deviation errors. The increasing sorption of crushed size fractions with time can be modelled with in-diffusion in a spherical geometry (see for example Byegård *et al.*, 1998), but in the present work far too few points have been collected for this to be a meaningful exercise.

Data for Cs batch sorption onto Äspö-diorite with synthetic groundwater (pH=7.5, $I=0.25\text{M}$) are reported in the literature by Byegård *et al.* (1998), who reports $R_a=8.8 \cdot 10^{-4} \text{m}$ for the 0.5-1mm size fraction (SSA=0.050m²/g) and $R_a=2.2 \cdot 10^{-3} \text{m}$ for the 0.25-0.5mm size fraction (SSA=0.077m²/g), after 36 days contact time. These R_a values are 5 to 12 times larger than what have been measured here and also show size fraction dependency, despite the SSA normalization. The reason behind this, relatively large, difference to our data is not clear. Data for Cs batch sorption experiments with the Swedish granite from the Finnsjön area and synthetic groundwater (pH=8, $I=0.21\text{M}$) are reported by Byegård *et al.* (1995), who reports $R_d=12 \pm 0.3$, 32 ± 3 and $60 \pm 4 \cdot 10^{-3} \text{m}^3/\text{kg}$ for the size fractions 0.5-1, 0.25-0.5 and 0.09-0.25mm, respectively after one week contact time. These values are comparable to those found here: 12.8 ± 1.3 , 21.2 ± 2.5 and $40.3 \pm 4.3 \cdot 10^{-3} \text{m}^3/\text{kg}$ for corresponding size fractions (Tables 5.2-5.4) after 14 days contact time. Data for Cs batch sorption experiments with the also Swedish Ävrö-granodiorite from the Laxemar area and "saline" water is available, which shows $R_d=5.5 \pm 1.1 \cdot 10^{-3} \text{m}^3/\text{kg}$ for 1-2mm size (SSA not reported) after 180 days contact time (Selnert *et al.*, 2009). This size fraction is larger than the largest measured here, but this R_d value is in-line with the decreasing trend of R_d values for increasing particle size: $R_d=1.57 \pm 0.24 \cdot 10^{-2} \text{m}^3/\text{kg}$ is measured here for the largest size fraction 0.5-1mm (Table 4).

Ra batch sorption

The results for R_d values of ^{226}Ra batch sorption on the eight samples taken along the drill-core, each subdivided in four particle-size fractions, show the expected increase in R_d values as the particle-size is reduced (Tables 5 - 8). The values also increase with time, showing the process of on-going in-diffusion in the particles. The reach of an equilibrium R_d can probably be expected within the next few months (data not yet available at this moment). For Ra some values are not detected, due to low sorption in combination with low total radioactivity in the experiments. The tracer loading is limited to 10^{-8}M , since there is a risk of precipitating $\text{RaSO}_4(\text{s})$ (a solubility product of $K_s=3.7\cdot 10^{-11}\text{M}$ is a representative literature value). This detection problem will probably improve for extended sampling times, when sorption is expected to have increased. The low count rate also leads to large relative errors of the average R_d from the triplicate experiments. The normalization of R_d values with the measured specific surface areas (SSA) of each fraction (Holgersson 2013), gives average R_a values at the 1 month sampling of $1.09\pm 0.30\cdot 10^{-4}$, $1.07\pm 0.51\cdot 10^{-4}$, $0.84\pm 0.50\cdot 10^{-4}$ and $0.60\pm 0.20\cdot 10^{-4}\text{m}$ for the size fractions 0.063-0.125, 0.125-0.25, 0.25-0.5 and 0.5-1mm, respectively. Similar to the results for Cs, there are still some differences in sorption strength between the size fractions, and awaiting an even later sampling occasion (up to 3 months) is recommended. Any definitive conclusion can therefore not yet be drawn on the efficiency of SSA normalization for the Ra sorption onto Äspö diorite, but these preliminary results looks promising, already at 1 month giving R_a values that are almost overlapping when considering the standard deviation errors.

For comparison, data for the analogue element Ba batch sorption onto Äspö-diorite with synthetic groundwater (pH7.5, $I=0.25\text{M}$) are reported in the literature by Byegård *et al.* (1998), who reports $R_a=3.8\cdot 10^{-5}\text{m}^3/\text{kg}$ for the 0.5-1mm size fraction (SSA=0.050 m^2/g) and $R_a=3.6\cdot 10^{-5}\text{m}^3/\text{kg}$ for the 0.25-0.5mm size fraction (SSA=0.077 m^2/g), after 36 days contact time. These R_a values are almost inside error limits of what have been measured here for Ra with the corresponding size fractions. Data for Ba batch sorption experiments with the Swedish granite from the Finnsjön area and synthetic groundwater (pH=8, $I=0.21\text{M}$) are reported by Byegård *et al.* (1995), who reports $R_d=1.1\pm 0.4$, 1.6 ± 0.5 and $3.3\pm 0.8\cdot 10^{-3}\text{m}^3/\text{kg}$ for the size fractions 0.5-1, 0.25-0.5 and 0.09-0.25mm, respectively after one week contact time. These values are a bit smaller (a factor of 3-4) to those found here for Ra: 4.8 ± 2.9 , 5.1 ± 3.3 and $12.9\pm 3.9\cdot 10^{-3}\text{m}^3/\text{kg}$ for corresponding size fractions (Tables 6 - 8) after 14 days contact time. There are also data available for Ra batch sorption onto Swedish quartz-monzodiorite from the Laxemar area and "saline" water, which shows $R_d=7.7\pm 1.1\cdot 10^{-3}\text{m}^3/\text{kg}$ for 1-2mm size (SSA not reported) after 180 days contact time (Selnert *et al.*, 2009). The larger particle size should give smaller R_d than what is measured here for the 0.5-1mm fraction: $5.5\pm 1.9\cdot 10^{-3}\text{m}^3/\text{kg}$ after 1 month, which is, however, not the case.

HTO through diffusion

The results for HTO diffusion (Figure 3, Table 9) with the eight samples show some variations for the evaluated parameters effective diffusivity D_e , geometrical factor G , porosity and specific pore-volume (SPV). The data can be compared with those collected by Johansson *et al.* (1997), using a similar method and 1-2cm thick sections of an Äspö diorite drill core, sampled at 220m depth, and a synthetic

groundwater (pH=7.5, $I=0.25M$). A mean value from six 1cm and five 2cm core sections, gives $D_e=1.22\pm0.32\cdot10^{-13}m^2/s$, a value almost exactly the same as the mean value from this work: $D_e=1.28\pm0.26\cdot10^{-13}m^2/s$. Corresponding mean values are for $G= 1.36\pm0.60\cdot10^{-2}$ and for porosity= $4.55\pm2.59\cdot10^{-3}$. This work gave $G= 3.04\pm0.62\cdot10^{-2}$ and for porosity= $2.04\pm0.60\cdot10^{-3}$. The average porosity (which is assumed equal to alpha) measured here is lower (a factor of 2) leading also to a correspondingly larger average geometrical factor. However, the standard deviation for the mean porosity by Johansson *et al.* (1997) is very large and, since G is calculated from the porosity, it is not possible to say if there is a significant difference from the average values measured here. Data for HTO through-diffusion in Japanese granite from the Inada area is available, which give average $D_e=1.2\pm0.2\cdot10^{-12}m^2/s$ (Tsukamoto and Ohe, 1993), that is, one order of magnitude larger values than for Äspö-diorite and, from the same work, $G=6.6\pm1.4\cdot10^{-2}$ and a porosity of $7.78\pm0.46\cdot10^{-3}$, the latter measured with water saturation method. From the Swedish Laxemar-area, a large number of samples (20) of drill-core sections of Ävrö-granodiorite has been measured with HTO through-diffusion for formation factors, giving an average $D_e=3.20\pm3.6\cdot10^{-13}$ (Selnert *et al.*, 2009), which underlines the large variations that can be found in this parameter.

According to a geological characterization of the Äspö site, the porosity of Äspö diorite is generally in the interval $5\pm2\cdot10^{-3}$ (Stanfors *et al.* 1993), a value corresponding well to the average value of $6.85\pm1.25\cdot10^{-3}$ from the gravimetric method (Holgerson, 2013). Johansson *et al.* (1998) reports porosity measurements with the gravimetric method for six 1, 2 and 4cm discs which gave an average of $5.5\pm0.6\cdot10^{-3}$. It is noteworthy that the average porosity measured here in this work with through diffusion is "only" $2.0\pm0.6\cdot10^{-3}$. A more restricted dataset from Johansson *et al.* (1998), using the results from through diffusion of 2cm sections, gives an average porosity of $3.5\pm1.5\cdot10^{-3}$, a value which may support that the through-diffusion porosity is somewhat lower than the porosity measured by the gravimetric method and that there may be a significant part of total porosity that is not available for through-diffusion.

To conclude the HTO experiments, it can be expected that near fracture mineral-altered rock should show some different physical properties than the more pristine material further away from the fracture. The series of samples measured here, does not, however, show any clear trend when going from one fracture (Sample A) to the next (sample H). The total length between the fractures may be too short for this type of differences to appear and therefore, all sections measured here may be considered as affected by the vicinity of the fractures. For all samples, the through-diffusion porosity is lower than what is measured with water-saturation method, which may indicate a water uptake by sheet silicate-type of alteration minerals (chlorite, biotite) with the latter method. This part of water uptake is then not accessible for through-diffusion, at least not during this relatively short experimental period. Non-conducting dead-end pores may also contribute to the discrepancy.

However, even this through-diffusion porosity is still much larger than what was found when extrapolating porosities from the crushed fractions and the presence of macro-porosity have been suggested (Holgerson, 2013). The explanation for the discrepancy between water-saturation porosity (showing largest porosity values) in intact samples and the extrapolated porosity from crushed samples (showing smallest porosity values) can then be two-fold: 1) uptake of water by alteration minerals: this

porosity is not available either for "short-time" through-diffusion, nor Kr gas adsorption, 2) presence of macro-porosity: this part of total porosity is available for through-diffusion and also for Kr gas, but the pores (or perhaps rather micro-fractures) are too wide ($>0.5\mu\text{m}$) for Kr gas to condensate, hence it is not measurable with the latter method but only shows up here with the former method.

Cs in-diffusion

The results for Cs diffusion (Figure 4, Table 10) show that the effective diffusivities are more than one order of magnitude larger (average $D_e=1.98\pm 0.85\cdot 10^{-12}\text{m}^2/\text{s}$, excluding one, possibly outlying, value) than those for HTO through diffusion (average $D_e=1.28\pm 0.26\cdot 10^{-13}\text{m}^2/\text{s}$). This clearly shows that the Cs^+ ion, whose diffusivity in pure water is about the same as for HTO/water itself, is transported in a completely different pore system than the system which is accessible for HTO/water diffusion. This difference can also be illustrated by the widely different average formation factors (G_F) for Cs and HTO diffusion (Table 10). It is here suggested that HTO is diffusing in a macro-porous system, while Cs is diffusing in a meso-porous system, probably consisting of alteration minerals, where it is also sorbed. The meso-pores restrict ion movement more than the macro-pores and a larger constrictivity can be the underlying reason why the effective diffusivity is larger for Cs than for HTO. This gives further evidence for the presence of multiple pathways in Äspö rock. Sorption is indicated by a fairly substantial capacity factor (α) compared with HTO (where $\alpha=\varepsilon_p$), resulting in a mean $K_d = 1.16\pm 0.62\cdot 10^{-3}\text{ kg/m}^3$. Normalization with the measured specific surface area of the discs gives $K_a= 2.15\pm 1.31\cdot 10^{-4}\text{ m}$. Although the relative errors of these values are larger than what is desirable, the K_d measured with in-diffusion falls nicely in row with the diminishing R_d values for larger and larger size fractions (the largest particle size fraction have average $R_d = 1.57\pm 0.24\cdot 10^{-2}\text{ kg/m}^3$). The average R_a values for the particle fractions are in between $1.84\text{-}2.91\cdot 10^{-4}\text{ m}$ at 1 month (Tables 1-4) but these will probably increase somewhat further with time. Even at 1 month they are inside the error margin of the in-diffusion measured R_a value.

In the literature, data for Cs penetration profiles in Äspö-diorite are reported by Johansson *et al.* (1998) and Byegård *et al.* (1998) (same experiments) which gave $D_e=6.5\cdot 10^{-14}\text{m}^2/\text{s}$ for the short penetration path and $D_e=2\cdot 10^{-15}\text{m}^2/\text{s}$ for the long penetration path. Corresponding rock capacity factors were $\alpha=2.2$ and 0.13 , respectively. The reported D_e values are much smaller than those measured here with in-diffusion, but the $K_d=8\cdot 10^{-4}\text{m}^3/\text{kg}$ for the short path is in good agreement with mean $K_d = 1.16\pm 0.62\cdot 10^{-3}\text{ kg/m}^3$ measured in the present work for in-diffusion. Cs penetration profiles in Swedish granitic rocks with synthetic groundwaters (pH=7.3-8.9) are also reported by Allard *et al.* (1985), where effective diffusivities were measured to $0.4\text{-}3\cdot 10^{-10}\text{ m}^2/\text{s}$ and with rock capacity factors in the range 421-3100. Obviously, these values differs (stronger sorption and larger effective diffusivity) from what is measured here in the present work, but it is interesting to note that the non-sorbing Tc tracer, that also was measured, was found to have 1000 times smaller effective diffusivity than Cs, which is supporting the likewise smaller D_e data for non-sorbing HTO versus Cs found in this work, although the difference between the two tracers are not so large here. In a similar work with Swedish granitic rocks by Ittner *et al.* (1989) only apparent diffusivities are reported with $D_a=10^{-13}\text{-}10^{-14}\text{m}^2/\text{s}$ for Cs and Sr, while anionic Tc and I had $D_a=10^{-14}\text{m}^2/\text{s}$, the latter which the authors considered was low due to the fact that the tracers are non-sorbing. Therefore two different pathways for cations and

anions were suggested by the authors. Skagius *et al.* (1982) reports effective diffusivities in the range from $0.29\text{-}37\cdot 10^{-12}\text{m}^2/\text{s}$ from batch experiments with Cs uptake of batches with crushed Swedish granites, values that are clearly comparable with the data obtained here. Cs through-diffusion measurements in granodiorite and 0.1M CsCl solution (pH=5.8) are reported by Sato *et al.* (1997), with $D_e=1.4\cdot 10^{-12}\text{m}^2/\text{s}$ and $\alpha=0.14$ and here the D_e value is also in good agreement with the average value reported here. Another penetration profile study of Cs, this time with granodiorite, is the one made by Jokelainen *et al.* (2013), which gave $D_e=3\cdot 10^{-12}\text{m}^2/\text{s}$ and $K_d=7.6\cdot 10^{-3}\text{m}^3/\text{kg}$, the former value is in good agreement with the average D_e measured in this work for Äspö-diorite. Also, in the cited work, it was found that Cs sorption increased in the borehole disturbed zone, increasing K_d to $4.2\cdot 10^{-2}\text{m}^3/\text{kg}$ and increasing D_e to $6\cdot 10^{-11}\text{m}^2/\text{s}$. Noteworthy is also that the weaker sorbing Na tracer that was also measured, had lower effective diffusivity, both in the matrix and in disturbed zone, thereby confirming the suggestion that different tracers are transported in different pathways. Cs penetration profiles have been measured in cm size samples of Japanese granite from Inada (Tsukamoto and Ohe, 1993), which gave D_e in the range $0.48\text{-}48\cdot 10^{-12}\text{m}^2/\text{s}$, (using dilute CsCl solutions, T=5 or 40°C), also to be compared with their measured value for $D_e=1.2\pm 0.2\cdot 10^{-12}\text{m}^2/\text{s}$ for through-diffusion of HTO. In the latter work, it was noted that up to three different profiles were needed to model the diffusive transport of Cs, which means that Cs can diffuse in multiple pathways.

Ra in-diffusion

The results for Ra diffusion (Table 11) show similar results as for Cs, suggesting that the Ra^{2+} ion uses the same pore system as Cs^+ for diffusive transport. The average effective diffusivity for Ra is slightly less than for Cs: $D_e=1.05\pm 0.27\cdot 10^{-12}\text{m}^2/\text{s}$ for Ra, compared with $D_e=1.98\pm 0.85\cdot 10^{-12}\text{m}^2/\text{s}$ for Cs. From data of ion diffusivities in pure water (Li and Gregory, 1974), the expected difference is a factor of 2.4; here we measure a factor 1.9 larger Cs effective diffusivity. Also from the anticipation that the two ions use the same pore system for diffusive transport, we expect the formation factors for Cs and Ra to be quite similar, which is also what is found: $G_F=9.40\pm 0.40\cdot 10^{-4}$ for Cs and $G_F=1.18\pm 0.31\cdot 10^{-3}$ for Ra. We also expect that K_d for Ra in the disc should be less than what is found for R_d in batch experiments with the coarsest particle; what is found is indeed: $K_d=1.82\pm 0.28\cdot 10^{-3}\text{m}^3/\text{kg}$ for the discs, while $R_d=5.4\pm 1.9\cdot 10^{-3}\text{m}^3/\text{kg}$ (after 1 month, Table 8) is the average value for the 0.5-1.0mm fractions. Normalizing the K_d for discs with specific surface area gives an average $K_a=3.24\pm 0.69\cdot 10^{-4}\text{m}$ to be compared with the batch experimental values $0.60\text{-}1.09\cdot 10^{-4}\text{m}$. The in-diffusion K_a is larger (a factor of about 3) than what is to expect from the batch experimental results. Even if the batch experiments are allowed to equilibrate for longer period of time (say, 3 months), it is doubtful if the equilibrated R_d values will reach as much as $3.24\cdot 10^{-4}\text{m}$. Compared with the measured average Cs $K_a=2.15\pm 1.31\cdot 10^{-4}\text{m}$, the Ra sorption in the discs is also stronger than what can be expected from batch sorption, where Ra sorption always is less than Cs sorption.

Literature data for Ra diffusion is not common and therefore Ba penetration profile data collected by Johansson *et al.* (1998) will be used for comparison. The results gave $D_e=1.6\cdot 10^{-14}\text{m}^2/\text{s}$ for the short penetration path and $D_e=4\cdot 10^{-15}\text{m}^2/\text{s}$ for the long penetration path. Corresponding rock capacity factors were $\alpha=0.65$ and 0.0045, respectively. The reported D_e values are, just as for the case with Cs, much smaller than those measured here with in-diffusion. The $K_d=2\cdot 10^{-4}\text{m}^3/\text{kg}$ for the short penetration path,

is also smaller than the average $K_d=1.82\pm 0.28\cdot 10^{-3}$ m³/kg for in-diffusion, measured here. Skagius *et al.* (1982) measured D_e values for Sr uptake in batch experiments with Swedish granites and got values in the range of $0.011-24\cdot 10^{-12}$ m²/s, a range of values where our data for Ra comfortably fits into. Ittner *et al.* (1990) found that Sr diffusion follows the same pathways as Cs, which corroborates the similarity of Ra and Cs diffusion found in this work.

Conclusions

Cs and Ra sorption in the batch experiments with four different size fractions both show the expected behaviour of increasing sorption R_d with diminishing particle size. This seems to be successfully compensated for by normalizing sorption to specific surface area (SSA) to give R_a sorption coefficients that are essentially the same for all fractions. A final judgment of the success of this normalization has to await data from a later sampling occasion (3-4 months) and, in the case of Ra, also attainment of the mother/daughter secular equilibrium in the samples. Diffusion experiments with HTO in discs of drill core sections show that the porosity is larger than expected from extrapolation of porosity data from crushed fractions (see Holgersson, 2013). This is probably due to a macro-pore system, or a system of small fractures, that is not measurable with the Kr gas adsorption method, due to too wide "pores" for the gas to condensate in them. Results from Cs and Ra in-diffusion also indicate that these ions are transported in an entirely different pore system, where also sorption of these ions takes place. In the case of Cs diffusion, the normalized sorption K_a from diffusion experiments is in the same range as for the R_a from batch experiments, while for Ra the corresponding sorption K_a is a factor 3 larger than what is expected from sorption R_a values. The reason for the latter discrepancy is, at the present, not clear.

The overview in Figures 6-8 of pH variations and sorption R_a and K_a for samples taken along the length of drill-core results, show that there may be some anomalies closest to the fracture at section "a". In the first sections the pH is lower than pH=7.8, the pH expected from synthetic groundwater. This can reflect some on-going ion exchange process, perhaps due to enhanced amounts of secondary mineral phases of the layered silicate types (i.e. chlorite and biotite) in the sections closest to this fracture. It would therefore be of interest to compare this with a geological composition of each of the sections along the drill-core and such data will hopefully be attained in the future, with the results presented in a follow-up reporting on this work, in the form of a scientific paper. This may also be the cause of what seems to be somewhat suppressed Cs sorption in the corresponding drill-core sections. Ra sorption, on the other hand, seems not to be affected by these spatial variations along the drill-core, although the section "h" seems to show somewhat stronger Ra sorption than the other sections (Figure 8). In this figure, the stronger sorption in discs than in crushed material is also evident.

To conclude, there is fairly good agreement in sorption data for Cs between the different experimental techniques that is used. For Ra, there is somewhat stronger sorption in the in-diffusion experiments, than in batch experiments and the underlying reason for this is not yet clear. To attain an agreement between different experimental methods was the primary objective for this work and the Ra results may indicate that there are more parameters than specific surface area (and porosity) to consider, for

example a possible difference in cation exchange capacity of the different size fractions and the rock discs.

By comparison of diffusivity data of the two sorbing type of tracers with the HTO non-sorbing type of tracer it is here suggested that the two types of tracers are transported in different pore systems. The presence of different pore-systems was also suggested from the characterization of the material with gas-adsorption measurements (Holgersson, 2013) and is also supported by literature data (Ittner *et al.* 1990, Johansson *et al.*, 1998). The presence of multi-pathways in rock should not be a surprise, considering the heterogeneity of the material, especially in comparison with the relative homogenous but individually very different character of the pure minerals that constitute the rock.

Acknowledgements

The research leading to these results has received funding from the European Union's European Atomic Energy Community's (Euratom) Seventh Framework Program FP7/2007-2011 under grant agreement n° 269658 (CROCK project) and SKB, the Swedish Nuclear Fuel and Waste Management Company.

References

- Allard, B., Ittner, T. and Torstenfelt, B. (1985) Migration of trace elements into water-exposed natural fissure surfaces of granitic rock. *Chem. Geol.*, **49** 31.
- Andersson, M., Ervanne, H., Glaus, M.A., Holgersson, S., Karttunen, P., Laine, H., Lothenbach, B., Puigdomenech, I., Schwyn, B., Snellman, M., Ueda, H., Vuorio, M., Wieland, E. and Yamamoto, T. (2008) Development of methodology for evaluation of long-term safety aspects of organic cement paste components. POSIVA Working report 2008-28.
- André, M., Malmström, M.E. and Neretnieks, I. (2009) Specific surface area measurements on intact drillcores and evaluation of extrapolation methods for rock matrix surfaces. *J. Cont. Hydr.* **110**, 1.
- Byegård, J., Skarnemark, G. and Skålberg, M. (1995) The use of some ion-exchange sorbing tracers cations in In-Situ experiments in high saline groundwaters. In: *Scientific Basis for Nuclear Waste Management XX. Mat.Res.Soc.Symp. Proc.* **353**, 107.
- Byegård, J., Johansson, H. and Skålberg, M. (1998) The interaction of sorbing and non-sorbing tracers with different Äspö rock types. SKB Technical report TR-98-18.
- Byegård, J. and Selnert, E. (2008) Bedrock transport properties - data evaluation and retardation model. Site descriptive modelling SDM-Site Forsmark. SKB report R-08-98.
- Crank, J. (1975) *The mathematics of diffusion*, 2nd Ed. Oxford Science Publications.

- Holgersson, S. (2013) Characterization of rock samples from Äspö using gas adsorption. Scientific Paper of the 2nd workshop of the EU RECOSEY project.
- Ittner, T., Torstenfelt, B. and Allard, B. (1990) Diffusion of Strontium, Technetium, Iodine and Caesium in Granitic rock. *Radiochim. Acta* **49**, 101.
- Johansson, H., Byegård, J., Skarnemark, G. and Skålberg, M. (1997) Matrix diffusion of some alkali- and alkaline earth metals in granitic rock. In: *Scientific Basis for Nuclear Waste Management XX. Mat.Res.Soc.Symp. Proc.* **465**, 871.
- Johansson, H., Siitari-Kauppi, M., Skålberg, M. and Tullborg, E-L. (1998) Diffusion pathways in crystalline rock - examples from Äspö-diorite and fine-grained granite. *J. Cont. Hydr.* **35**, 41.
- Jokelainen, L., Meski, T., Lindberg, A., Soler, J.M., Siitari-Kauppi, M., Martin, A. and Eikenberg, J. (2013) The determination of ¹³⁴Cs and ²²Na diffusion profiles in granodiorite using gamma spectrometry. *J. Radioanal. Chem.* **295**, 2153.
- KIT-INE (2011) Provision of new fracture bearing drill core samples obtained, handled, transported and stored under anoxic conditions, including first documentation. Deliverable D-N°1-1, published in the EU CROCK Project homepage.
- Li, Y.-H. and Gregory, S. (1974) Diffusion of ions in sea water and in deep sea sediments. *Geochim. Cosmochim. Acta* **38**, 703.
- Sato, H., Shibutani, T. and Yui, M. (1997) Experimental and modelling studies on diffusion of Cs, Ni and Sm in granodiorite, basalt and mudstone. *J. Cont. Hydr.* **26**, 119.
- Selnert, E., Byegård, J., Widestrand, H., Carlsten, S. and Döse, C. (2009) Bedrock transport properties - data evaluation and retardation model. Site descriptive modelling SDM-Site Laxemar. SKB report R-08-100.
- Skagius, K., Svedberg, G. and Neretnieks, I. (1982) A study of strontium and caesium sorption on granite. *Nucl. Techn.* **59**, 302.
- Stanfors, R., Liedholm, M., Munier, R., Olsson, P. and Stille, H. (1993) Geological-structural evaluation of data from section 700-1475m. SKB Progress report 25-93-05.
- Tsukamoto, M. and Ohe, T. (1993) Effects of biotite distribution on caesium diffusion in granite. *Chem. Geol.* **107**, **29**.
- Wang, J.H. (1951) Self-diffusion and structure of liquid water. *J. Am. Chem. Soc.* **73**, 510.

POSTERS



List of posters

J. Crawford

A SIMPLIFIED PA MODEL FOR REACTIVE TRANSPORT FEATURING NON-LINEAR SORPTION PROCESSES

J. Crawford

WHAT MIGHT KD RATIOS BE ABLE TO TELL US ABOUT SURFACE COMPLEXATION SORPTION MECHANISM?

V. Havlová and P. Vecernik

DIFFUSION OF SPECIES THROUGH ASPO DIORITE

S. Holgersson

CROCK AT CHALMERS - EXPERIMENTAL PROGRAM AND RESULTS

K. Schmeide, S. Gürtler, K. Müller, R. Steudtner, C. Joseph, F. Bok and V. Brendler

INTERACTION OF URANIUM(VI) AND NEPTUNIUM(V) WITH ÄSPÖ DIORITE UNDER ANOXIC CONDITIONS

L.M. de Vries, P. Trincherro and J. Molinero

MCPHREEQC: AUTOMATIC STOCHASTIC SIMULATIONS FOR GEOCHEMICAL MODELLING



A simplified PA model for reactive transport featuring non-linear sorption processes



James Crawford

Kemakta Konsult AB, Stockholm, Sweden



INTRODUCTION

- We have developed a simplified PA simulation tool (PATHTRAC) for modelling reactive transport processes involving advective flow coupled with matrix diffusion and non-linear sorptive retention on fracture minerals and rock matrix microsurfaces.
- If the concentration of the migrating nuclide is sufficiently dilute that it does not influence bulk groundwater composition, the non-linear part of the mass balance can be split into a separate **non-linear accumulation term** and a **pseudo-reaction term**. We refer to this as the Decoupled Major Ion Chemistry (DEMIC) approximation.

Mass balance for rock matrix:

C_1 = concentration of nuclide
 C_i = concentration of bulk groundwater component i
 S_1 = sorbed concentration
 ϵ_p = matrix porosity
 ρ_b = bulk density of rock
 D_e = matrix effective diffusivity
 K_d = partitioning coefficient (dynamic)

$$\epsilon_p \frac{\partial C_1}{\partial t} + \rho_b \frac{\partial S_1}{\partial t} = \nabla \cdot (D_e \cdot \nabla C_1)$$

$$K_d = S_1 / C_1 = f(C_1, C_2, \dots, C_k)$$

$$\left(\epsilon_p + K_d \rho_b \left(1 + \frac{\partial \ln K_d}{\partial \ln C_1} \right) \right) \frac{\partial C_1}{\partial t} = \nabla \cdot (D_e \cdot \nabla C_1) - C_1 \rho_b \sum_{i=2}^k \frac{\partial K_d}{\partial C_i} \cdot \frac{\partial C_i}{\partial t}$$

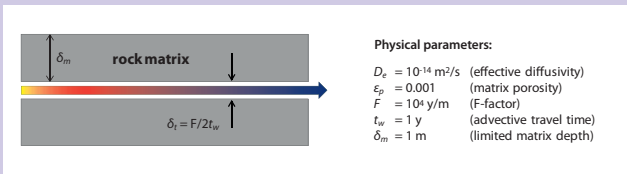
- The sorption of the migrating trace nuclide is simulated using a conditionally constant, although temporally & spatially variable partitioning coefficient ("dynamic K_d ")
- Since groundwater modelling is necessary to demonstrate repository safety functions related to hydrochemical stability, it is not necessary to repeat these simulations for radionuclide migration calculations when using PATHTRAC if such data are already available.
- Decoupling allows independent groundwater modelling (of arbitrary complexity) to establish the background concentrations of solutes as well spatial & temporal trends that influence conditional K_d values. Transport of radionuclides can then be simulated as a separate problem in a streamlined and much more efficient fashion.

OBJECTIVES

To demonstrate the utility of the PATHTRAC program for simulation of a radionuclide migration problem involving strongly non-linear sorption (solute remobilisation) and to compare results with those obtained using a fully coupled reactive transport simulation code.

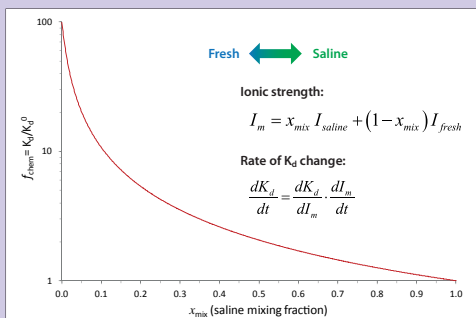
EXAMPLE: RADIONUCLIDE REMOVALISATION

- In a prototype demonstration, a simple scenario is modelled involving migration of a cation-exchanging nuclide (Ra^{2+}) under the influence of alternating pulses of meteoric and saline groundwater intruding into a fracture system initially equilibrated with saline groundwater.
- The simulated hydrodynamic conditions correspond to a flowpath featuring relatively weak transport retardation which might be expected to dominate release from a hypothetical repository:



- Although it is possible to include chemical couplings of arbitrary complexity in PATHTRAC, in the present example the temporally variable K_d is simply correlated with ionic strength using a mixing model for salt transport. The mixing model is based on transport of a non-reactive solute as a proxy for mixing fraction using the analytical solution by (Neretnieks, 1980).
- The parametric K_d is calculated using discrete mixing calculations in PhreeqC (Parkhurst & Appelo, 1999) with a single site cation exchange model based on selectivity coefficients reported for Finnsjón granite (Byegård et al. 1995).

Figure 1: Variation in K_d for Ra^{2+} sorption as a function of mixing fraction (mixing of Forsmark site-specific saline and fresh groundwater types). Data are plotted relative to the K_d estimated for saline conditions. Simulations were made using PhreeqC (Parkhurst & Appelo, 1999) with the SKB-TDB database (Duro et al. 2006). The K_d for Ra^{2+} sorption by cation exchange is found to be roughly 100 times greater for rock in contact with fresh groundwater relative to saline groundwater.



RESULTS

- Simulations have been made of Ra^{2+} migration using PATHTRAC where the simplified parametric K_d model is combined with a mixing approximation to estimate temporal trends in bulk groundwater chemistry.
- Comparative simulations were also made using the fully coupled reactive transport code CrunchFlow (Steefel, 2009) together with the cation exchange selectivities used previously to calculate the parametric K_d model.

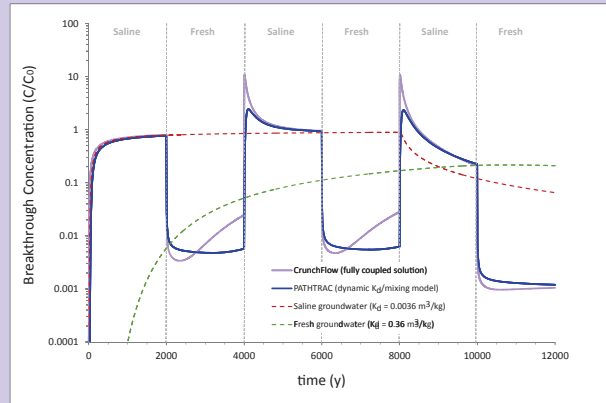


Figure 2: Breakthrough curves for Ra^{2+} migration simulated using PATHTRAC for a series of alternating pulses of saline & fresh groundwater and corresponding results from a fully coupled reactive transport simulation made using CrunchFlow (Steefel, 2009). The Ra^{2+} source term is a constant concentration extended pulse of 8 ka duration. Breakthrough curves are also given for the constant K_d limiting cases for saline and fresh groundwater calculated using the analytical solution described by (Tang et al. 1981).

- The use of a parametric K_d combined with a mixing model description of bulk groundwater chemistry gives a passable approximation of the fully coupled solution although significantly underestimates the remobilised Ra^{2+} concentration peak at 4 ka & 8 ka. Some differences are also noted in the time intervals when the aquifer is flushed with fresh groundwater.
- Differences between the PATHTRAC and CrunchFlow simulation results appear to be due to the inability of a simplified mixing model to adequately capture the chromatographic separation of base cation reaction fronts following switchover between fresh & saline aquifer conditions.

CONCLUSIONS

- The fully coupled solution takes roughly 6 days of CPU time to obtain the breakthrough curves shown in Figure 2. This is too slow to be of routine use in PA, particularly if multiple flowpaths featuring different (usually much larger) F-factors are to be simulated.
- The present version of the PATHTRAC code takes about 10 hours to achieve the same breakthrough time implying a factor 15 increase in speed over the fully coupled model.
- Use of a mixing model approximation for bulk groundwater chemistry may not be appropriate for radionuclide migration simulations involving cation exchange where a more sophisticated groundwater chemistry description is required to properly capture the multicomponent transients.
- Radionuclides sorbing by way of surface complexation may work better in the framework of a mixing model approximation since trends in pH and carbonate concentration are not expected to exhibit significant chromatographic transients. This will need to be investigated further.
- If detailed hydrochemical simulation data are available from independent reactive transport simulations, they can be imported directly into the PATHTRAC program and used to assign K_d values directly from a parametric model of arbitrary complexity thus avoiding problems associated with use of a simplified mixing approximation.

ACKNOWLEDGEMENTS

The research leading to these results has received funding from the European Union's European Atomic Energy Community's (Euratom) Seventh Framework Programme FP7/2007-2011 under grant agreement n° 269658 (CROCK project). Additional funding from the Swedish Nuclear Fuel and Waste Management Co. (SKB) is also gratefully acknowledged.

REFERENCES

Byegård J, Skarnemark G, Skälberg M. (1995). The use of some ion-exchange sorbing tracer cations in in-situ experiments in high saline groundwaters. In: Murakami T, Ewing R C (eds). Scientific basis for nuclear waste management XVIII: symposium held in Kyoto, Japan, 23-27 October 1994. Pittsburgh, PA: Materials Research Society. (Materials Research Society Symposium Proceedings 353), pp 1077-1084.

Duro L, Grivé M, Cera E, Doménech C, Bruno J. (2006). Update of a thermodynamic database for radionuclides to assist solubility limits calculation for performance assessment. SKB TR-06-17, Swedish Nuclear Fuel & Waste Management Company, Stockholm, Sweden.

Neretnieks I. (1980). Diffusion in the rock matrix: An important factor in radionuclide retardation? Journal of Geophysical Research, 85(8), pp. 4379-4397.

Parkhurst D L, Appelo C A J. (1999). User's guide to PHREEQC (version 2): a computer program for speciation, batch-reaction, one-dimensional transport, and inverse geochemical calculations. Water Resources Investigations Report 99-4259. U.S. Geological Survey, Denver CO, USA.

Steefel C. (2009). CrunchFlow. Software for modeling multicomponent reactive flow and transport. User's Manual, Lawrence Berkeley National Laboratory, CA, USA.

Tang D, Frind E, Sudicky E. (1981). Contaminant transport in fractured porous media: Analytical solution for a single fracture. Water Resour. Res., 17(3), pp. 555-564.



What might K_d ratios be able to tell us about surface complexation sorption mechanisms?



James Crawford

Kemakta Konsult AB, Stockholm, Sweden

INTRODUCTION

- Linear Free Energy Relationships (LFER's) are empirical relations commonly applied in aquatic chemistry to describe correlations between paired data sets of closely related phenomena.
- Surface complexation (SC) reactions are analogous to aqueous phase hydrolysis reactions, the main difference being that an immobile surface hydroxyl group takes the place of one of the water molecules in the reaction stoichiometry.
- Since it is not possible to make detailed sorption measurements for all safety relevant nuclides in performance assessment (PA), this is useful for estimating binding constants where no experimental data exist.

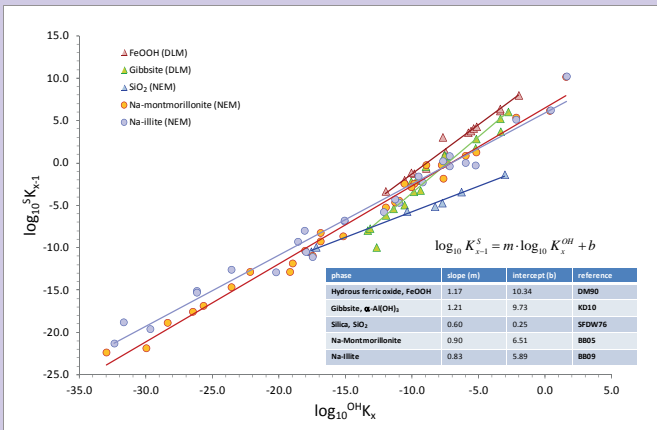


Figure 1: Examples of LFER reported in or interpreted from literature sources for Hydrous ferric oxide (Dzombak & Morel, 1990), Gibbsite (Karamalidis & Dzombak, 2010), Na-Montmorillonite (Bradbury & Baeyens, 2005), and Na-illite (Bradbury & Baeyens, 2009). The LFER for Silica was fitted to binding constants in (Schindler et al. 1976). Intercepts differ slightly from the original sources as they have been renormalised to a common reference site density (2.31 sites/nm²). The LFER is defined in terms of a slope factor (m) and intercept (b) obtained by least squares linear regression.

OBJECTIVES

We seek to find whether the existence of an LFER implies special mathematical properties that might be exploited to uniquely estimate its parameters (i.e. slope & intercept) from limited measurement data.

CONSEQUENCES OF LFER'S IN SC MODELS

The distribution coefficient (K_d) is equal to the sum of contributions of individual surface complexes analogous to successive hydrolysis steps ($n_{H_2O} = 1, 2, 3, \dots$) in the aqueous phase. The assumption of an LFER implies:

- The slope (m) of the LFER alters the relative contribution individual surface species make towards the net sum K_d value for a solute.
- The intercept (b) of the LFER affects each surface species identically and is thus a normalisable parameter (similarly to surface area & site density).
- The K_d ratio of chemically different solutes undergoing sorption on the same binding site type is dependent on the LFER slope (m) and aqueous speciation only. It is independent of reactive surface area, LFER intercept (b), site density, and surface charging behaviour which are the same for all sorbing species and cancel when taking the ratio.

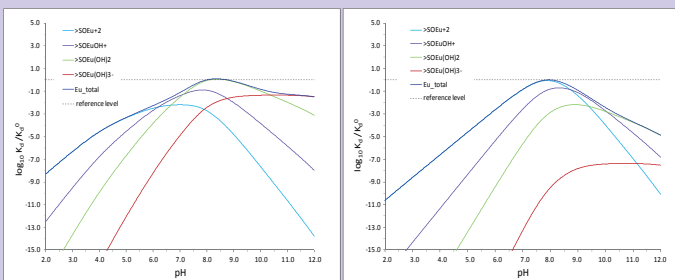


Figure 2a: Sorption of Eu on Na-illite using the LFER ($m=0.83$) described by (Bradbury & Baeyens, 2009). The K_d values are normalised relative to the reference value at pH 8. Relative importance of successive surface species in the LFER analogy is also shown.

Figure 2b: Sorption of Eu on hydrous ferric oxide using the LFER ($m=1.17$) described by (Dzombak & Morel, 1990). The K_d values are normalised relative to the reference value at pH 8. Relative importance of successive surface species in the LFER analogy is also shown.

RESULTS

- Simulated K_d ratios for Am, Eu & Ni as a function of pH have a signature shape that is determined by the slope of the underlying LFER used to parameterise the sorption model.

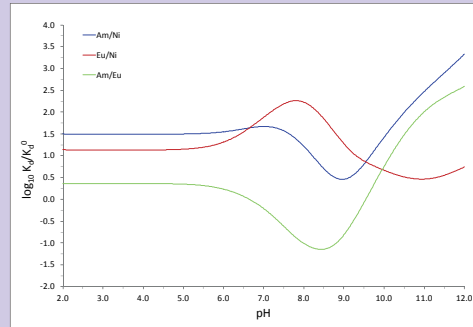
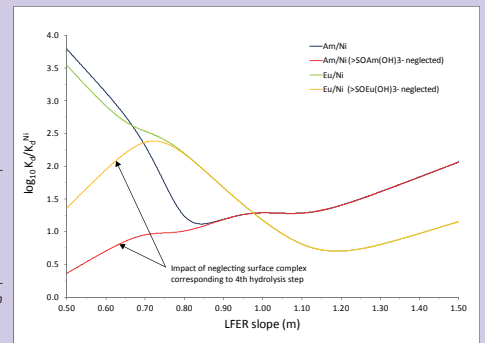


Figure 3: Simulated K_d ratios for Am/Ni, Eu/Ni, and Am/Eu as a function of pH for sorption on Na-illite using the LFER ($m=0.83$) described by (Bradbury & Baeyens, 2009). Simulations were made with PhreeqC (Parkhurst & Appelo, 1999) using the SKB thermodynamic database (Duro et al. 2006). Theoretical differences between Am and Eu are due to the different aqueous hydrolysis reactions recognised in the thermodynamic database and differing equilibrium constants for the reactions.

- If detailed sorption edge data (K_d vs. pH) are not available it may be feasible to use measured K_d ratios for at least 2 (preferably more) solutes in contact with different groundwater types to estimate the LFER slope factor in a least squares sense.
- Hydrolysis constants for higher reaction steps (e.g. $n_{H_2O} \geq 3$) are frequently uncertain and, in some cases, may not even exist although being recognised in thermodynamic databases. This can lead to significant uncertainties for sorption prediction on "low slope" mineral surfaces.

Figure 4: Simulated K_d ratios as a function of LFER slope (m) for Am/Ni, & Eu/Ni. Simulated data are for Forsmark site-specific saline groundwater and include aqueous phase hydrolysis and carbonate speciation (pH 8.43, $P_{CO_2} 10^{-5}$ atm.). Simulations were made with PhreeqC (Parkhurst & Appelo, 1999) using the SKB thermodynamic database (Duro et al. 2006). Theoretical differences between Am and Eu are due to the different aqueous hydrolysis reactions recognised in the thermodynamic database and differing equilibrium constants for the reactions. Neglecting of higher reaction steps has a profound impact on the Eu/Ni & Am/Ni K_d ratio at low slope factors.



CONCLUSIONS

- K_d ratios of 2 or more surface complexing species measured simultaneously or under the same nominal conditions can be used to estimate the slope (m) of an underlying LFER for use in SC modelling. Having fixed the slope of the LFER, the intercept (b) can then be estimated to give a fit to the absolute K_d value.
- K_d ratios measured at a single pH level may be insufficient to give a unique estimate of the slope if thermodynamic data are uncertain. Several solutes and/or measurements at different pH levels might then be necessary to reduce uncertainties.
- The technique simplifies a multivariate optimisation problem to a 2-step sequential procedure to obtain the LFER slope and intercept independently and is well-suited to situations where there are limited measurement data.

ACKNOWLEDGEMENTS

The research leading to these results has received funding from the European Union's European Atomic Energy Community's (Euratom) Seventh Framework Programme FP7/2007-2011 under grant agreement n° 269658 (CROCK project). Additional funding from the Swedish Nuclear Fuel and Waste Management Co. (SKB) is also gratefully acknowledged.

REFERENCES

- Bradbury M H, Baeyens B. (2005). Modelling the sorption of Mn(II), Co(II), Ni(II), Zn(II), Cd(II), Eu(III), Am(III), Sn(IV), Th(IV), Np(V) and U(VI) on montmorillonite: Linear free energy relationships and estimates of surface binding constants for some selected heavy metals and actinides. *Geochimica et Cosmochimica Acta*, 69(4), pp 875-892.
- Bradbury M H, Baeyens B. (2009). Sorption modelling on illite. Part II: Actinide sorption and linear free energy relationships. *Geochimica et Cosmochimica Acta*, 73(4), pp 1004-1013.
- Duro L, Grivé M, Cera E, Doménech C, Bruno J. (2006). Update of a thermodynamic database for radionuclides to assist solubility limits calculation for performance assessment. SKB TR-06-17, Swedish Nuclear Fuel and Waste Management Company, Stockholm, Sweden.
- Dzombak D A, Morel F M M. (1990). Surface complexation modelling. Hydrous ferric oxide. Wiley, New York.
- Karamalidis A K, Dzombak D A. 2010. Surface complexation modelling. Gibbsite. Wiley, New York.
- Parkhurst D L, Appelo C A J. (1999). User's guide to PHREEQC (version 2): a computer program for speciation, batch-reaction, one-dimensional transport, and inverse geochemical calculations. Water Resources Investigations Report 99-4259, U.S. Geological Survey, Denver CO, USA.
- Schindler P, Fuerst B, Dick R, Wolf R. (1976). Ligand properties of surface silanol groups. I. Surface complex formation with Fe³⁺, Cu²⁺, and Pb²⁺. *Journal of Colloid and Interface Science*. 55, pp. 469-475.

INTRODUCTION

Even though the main transport mechanism in the crystalline rock is advection, migration processes from fracture through fracture coating into unaltered rock has to also be studied. The conceptual model is based on the presumption that non-advective migration is driven by diffusion into altered mineral layers and into both undisturbed rock matrix, adjacent to water bearing fissures. This depends on many features: molecule size and charge, sorption on rock components, effective porosity, pore constrictivity, tortuosity, ground water composition.

As it is stated above, the molecule charge can influence the specie diffusion through low porosity rock. As granitic rock mineral surfaces are negatively charged, the anions can be repulsed, namely in most constricted parts of the pores. This is called anion exclusion, as anions are excluded from some parts of the pores.

Aim of the task: to study the influence of exclusion on anion diffusion. ^3H as a conservative tracer and ^{36}Cl were compared, with a reference to I (electromigration experiments).

EXPERIMENTS

POROSITY MEASUREMENT

Water accessible porosity ϵ was measured using water saturation method by [1]. The method was used also for saturation of samples for diffusion experiments.

THROUGH-DIFFUSION (TD) EXPERIMENTS

> The diffusion process is governed by the Fick's first and second law [2, 3, 4, 5];

where C_p is the concentration in the pore water (mol m^{-3}), D_p the pore diffusion coeff. (m^2s^{-1}), R is the retardation factor in the rock matrix (m^3kg^{-1})

> Effective diffusion coefficient D_e (m^2s^{-1}):

$$D_e = \epsilon_r D_p = \epsilon_r D_w \frac{\delta_p}{\tau} = F_f D_w$$

where δ_p is constrictivity, τ^2 tortuosity, D_w the diffusivity in unconfined water, D_p the pore diffusivity in pores, F_f formation factor.

> Through-diffusion methodology is based on emplacement of sample in between spiked reservoir and tracer free reservoir (synthetic Äspo GW). The activities in both input and output reservoirs are measured (Liquid scintillation spectroscopy, HIDEX 300 SL, Hide Oy).

> **Mathematic solution:** compartmental diffusion module, in the environment of GoldSim transport code with the use of the Contaminant Transport Module [6,7].

ELECTROMIGRATION EXPERIMENTS (TEM)

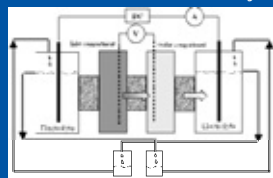
> Through-Electromigration method (TEM) enables speeding up laboratory diffusion experiments, gaining rock migration parameters (F_f , D_e) in relatively short times (minutes to hours)

> Based on [8, 9, 10], etc. Governed by Einstein relation, describing the interrelation between the diffusivity and ionic mobility of ionic solutes:

$$D_e = \frac{\mu_e RT}{z F}$$

> where in inert porous medium is D_e (m^2s^{-1}) the effective diffusivity, μ_e ($\text{m}^2\text{V}^{-1}\text{s}^{-1}$) the effective ionic mobility, z (-) the charge number of the migrating ionic solute, and R ($\text{J}\cdot\text{mol}^{-1}\text{K}^{-1}$), T (K), and F ($\text{C}\cdot\text{mol}^{-1}$) are the gas constant, temperature, and Faraday constant, respectively.

> TEM cell consists of four compartments. The rock sample is placed in a special rubber seal and mounted between two compartments, one filled with electrolyte (0.05M NaCl) with high tracer concentration (in this case I) and one filled with an electrolyte (0.05M NaCl) initially free of the tracer. After resistivity measurement the tracer (NaI, 0.005M) is inserted and measured after migration through the sample (ion selective electrode). Breakthrough curve is then evaluated.



Löfgren M., et al. (2010)

SAMPLES AND SOLUTIONS

Rock samples



AD1 left, AD3 right

Äspo diorite, Borehole KA2368A-01, depth 10,65 m



AD31 left, AD100 right

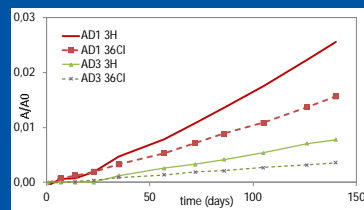
Äspo diorite, Borehole KA2370A-01, depth 11,65m

Äspo synthetic GW

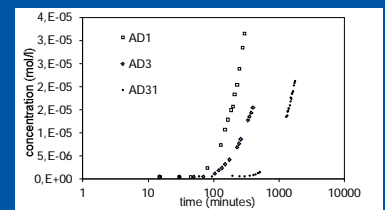
Tracers

Specie	ASGW composition (mg.l ⁻¹ , Heck and Schaffer, 2011)	Synthetic AGW composition, (ICP-AES, ion chromatography)		Solution + Tracers	Activity/ concentration
pH	7,8	7,2	7,3	TD exp.	
Eh (mV)	31	N.A.	N.A.	ASGW +	
I (mol)	0,178	0,181	0,186	^3H	1350 Bq/ml
Na ⁺	1889,9	2000	2100	^{36}Cl	216 Bq/ml
K ⁺	10,5	24,7	25,1		
Mg ²⁺	69,4	89,3	90,5	TEM	
Ca ²⁺	1135	1210	1230	NaCl +	0,18 M
Sr ²⁺	19,9	21,3	22,5	Nal	0,005 M
Cl ⁻	4999	4880	4920		
F ⁻	1,4	1,43	1,42		
Br ⁻	23,2	N.A.	N.A.		
SO ₄ ²⁻	394,4	395,4	396,9		
HCO ₃ ⁻	11,68	N.A.	N.A.		

RESULTS



TD measurement: ^3H and ^{36}Cl breakthrough curves for AD1 and AD3 samples.

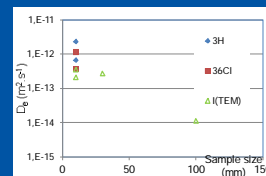


TEM measurement: I breakthrough curves for samples with different length (AD-1, AD-3, AD-31).

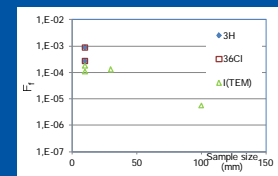
VALUES of MIGRATION PARAMETERS

Sample	Tracer	Porosity (%)	Density ($\text{kg}\cdot\text{m}^{-3}$)	D_e (m^2s^{-1})	F_f
AD-1 (10 mm)	^3H	0.22	2 650	2.3×10^{-12}	8.8×10^{-4}
	^{36}Cl			1.14×10^{-12}	8.8×10^{-4}
	I (TEM)			3.5×10^{-13}	1.75×10^{-4}
AD-3 (10 mm)	^3H	0.21	2 660	6.6×10^{-13}	2.7×10^{-4}
	^{36}Cl			3.6×10^{-13}	2.7×10^{-4}
	I (TEM)			2.1×10^{-13}	1.1×10^{-4}
AD-31 (30 mm)	I (TEM)	0.29	2741	2.7×10^{-13}	1.3×10^{-4}
AD-100 (100 mm)	I (TEM)	presumed 0.29	dtto	1.1×10^{-14}	5.5×10^{-6}

Need to be confirmed



Values of D_e (m^2s^{-1}) for TD and TEM measurement



Values of F_f for TD and TEM measurement

CONCLUSIONS

- diffusion experiments with ^3H and ^{36}Cl and through-electromigration experiments showed that anion exclusion might be the case for Iodine; seemed not to be so important for ^{36}Cl , most probably due to high GW salinity

- sample heterogeneity showed to be important factor for data uncertainty: both TD and TEM experiments revealed different migration values; reasons: sample composition/lineation; sample disturbance due to its preparation. Larger sample set should be measured.

- migration parameters extensively decreased for the longest sample: however the values has to be proved due to test status of the apparatus

References

- [1] Melnyk T.W. and Skeet A.M.M. (1987) Canadian Journal of Earth Sciences, 23, 1068 – 1074.
- [2] Ohlsson Y. and Neretnieks I. (1995) SKB Report, TR 95-12.
- [3] Bradbury M. H. and Green A. (1986) J. of Hydrology, 89, 123 – 139.
- [4] Löfgren I. and Neretnieks I. (2002) SKB Report TR-02-07.
- [5] Vilks P., Miller N.H. and Stanchell F. W. (2004) Rep. AECL No. 06819-REP-01200-10128-R00.
- [6] Vopálka D., Filipská H., Vokál A. (2006): Mat.Res.Soc.Symp.Proc. Vol. 932: 983-990.
- [7] Havlová V. and Vopálka D. (2009): J Radioanal Nucl Chem (2010) 286:785–791.
- [8] Löfgren M. (2004). Diffusive properties of granitic rock as measured by in-situ electrical methods. Doctoral thesis, Royal Institute of Technology Stockholm.
- [9] Löfgren M., Neretnieks I. (2006). J. of Contam. Hydrol. 87, 237-252.
- [9] Löfgren M., Večerník P., Havlová V. (2010). SKB R-09-57.

Acknowledgement: The activities leading to these results has received funding from the European Union's European Atomic Energy Community's (Euratom) Seventh Framework Programme FP7/2007-2011 under grant agreement no. 269658, the CROCK project.

CROCK at Chalmers – Experimental Plans and Results

A Progress Report for CROCK 2nd workshop, Karlsruhe, 14-16th May 2013

Stellan Holgersson

Chalmers University of Technology, Department of Chemical and Biological Engineering- Nuclear Chemistry, Kemivägen 4, SE-41296 Göteborg, Sweden

Overview

In the CROCK project, one task is to measure sorption R_d (m^3/kg) values for some selected radioactive tracers at different laboratories, using the same geological material. The material was sampled in the form of drill-cores at the Äspö laboratory, near Oskarshamn, Sweden [1]. Special care was taken to preserve the reducing conditions for the samples, both at sampling and the subsequent handling and measurements. The overall aim of this task is to try to reduce the experimental uncertainties in R_d values, in order to obtain more exact calculations of radiotracer migration in a performance assessment of a nuclear waste repository in granitic rock.

Chalmers work in the project can be divided into three distinct parts:

- 1) characterization of crushed and intact sections drill-core samples regarding specific surface area and specific pore volume (WP1)
- 2) batch sorption of radiotracers Cs, Ra and U on crushed drill-core samples (WP2)
- 3) diffusion experiments of radiotracers HTO, Cs, Ra and U in intact sections of drill-core samples (WP3)

Batch Sorption Experiments

Batch sorption experiments are underway with eight samples (a-h), crushed into four fractions. The samples are run as triplicates and with separate empty tubes for wall sorption measurements and separate batches for pH measurements. Three radiotracers are used: ^{134}Cs , ^{226}Ra and ^{233}U . Only preliminary results for one pilot experiment is available for the moment, 3 months sampling:

	$R_d(m^3/kg)$				$R_d(m) \cdot 10^{-3}$			
	0.063-0.125	0.125-0.250	0.250-0.500	0.500-1.000	0.063-0.125	0.125-0.250	0.250-0.500	0.500-1.000
Cs	0.43	0.24	0.11	0.046	1.27	1.06	0.745	0.490
Ra	0.015	0.010	0.0079	0.0048	0.044	0.044	0.054	0.051
U	0.0051	0.0030	0.0017	0.00099	0.015	0.013	0.012	0.011

While Ra and U sorption seems to constant when corrected for surface area (R_s values), Cs sorption still show size dependency. This is probably connected with the cation exchange capacity, which seems to increase for the smaller fractions.

Diffusion Experiments

Diffusion experiments are underway with eight drill-core sections samples (A-H). Radiotracers used are HTO for through diffusion and ^{134}Cs , ^{226}Ra and ^{233}U for in-diffusion. Samples are taken on both sides of the diffusion cells. No results are available yet. Evaluation of through-diffusion is made with the equation [8]

$$\frac{C(t)}{C_0} = \frac{A}{V} \cdot \left(\frac{D_e \cdot t}{l} - \frac{\alpha \cdot l}{6} - \frac{2 \cdot \alpha \cdot l}{\pi^2} \cdot \sum_{n=1}^{\infty} \frac{(-1)^n}{n^2} \cdot \exp\left(-\frac{D_e \cdot n^2 \cdot \pi^2 \cdot t}{\alpha \cdot l^2}\right) \right)$$

Where A and l are sample area and length, respectively, V solution volume (38ml), D_e is the effective diffusivity and α ($=\epsilon + K_d \cdot \rho$) the capacity factor. For HTO K_d is assumed to be zero.

Evaluation of in-diffusion is made with equations

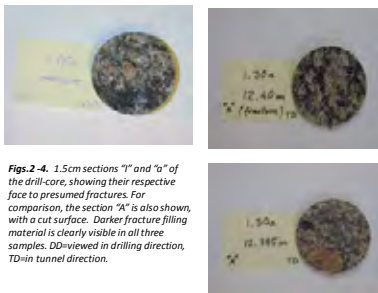
$$\frac{C(t)}{C(0)} = 1 - \frac{C(0) - C_{\infty}}{C(0)} \cdot \left(1 - \sum_{n=1}^{\infty} \frac{(2z + 2z^2) \cdot \exp\left(-\frac{D_e \cdot q_n^2 \cdot t}{l^2 \cdot \alpha}\right)}{1 + z + (q_n \cdot z)^2} \right)$$

$$z = \frac{C_{\infty}}{C(0) - C_{\infty}}$$

$$\tan q_n = -z \cdot q_n$$



Fig. 1. Section of drill-core, used in subsequent experiments. The core was cut into smaller 1.5cm sections (a-h) for batch sorption and (A-H) for diffusion experiments



Figs. 2-4. 1.5cm sections "a" and "o" of the drill-core, showing their respective face to presumed fractures. For comparison, the section "h" is also shown, with a cut surface. Darker fracture filling material is clearly visible in all three samples. DD-viewed in drilling direction, TD=in tunnel direction.

Characterization of rock samples from Äspö (for WP 1)

The specific surface area has been identified as a key parameter for extrapolating the results from laboratory experiments to the field-scale [2,3], in order to obtain surface area normalized R_s (m) values. Also, the available porosity may not be constant between different size fractions up to the intact rock. It is also an essential parameter in the interpretation of sorption K_d values obtained from diffusion experiments. The porosity may therefore also be a key parameter to understand how sorption should be extrapolated from laboratory to field-scale. The interdependency of specific surface area and porosity for pure minerals have been the object of separate investigations [4,5] and in this work, the rock is now investigated for similar interdependency.

Cutting of drill-core

One section of drill-core from borehole KA2368A-01 was selected. This section from 12.11-12.4m is about 29cm long, with at least one natural fracture in one end and possibly another fracture (or part of) in the other end (See Figures 1-4 below). The core was cut into eight sections (labeled A-H) for diffusion and eight sections (a-h) for batch sorption experiments. The sections a-h were then crushed and sieved into four size fractions: 0.5-1, 0.25-0.5, 0.125-0.25 and 0.063-0.125mm.

Specific Surface Area (SSA) Measurements

The crushed samples were measured using a 10 point Kr sorption isotherm with p/p_0 from 0.05 to 0.2. For intact 1.5cm drill cores, only the first points of the isotherm were used. The results were interpreted with the instrument software using the BET model [6].

Sample	Core section (m)	1-0.5mm		0.5-0.25mm		0.25-0.125mm		0.125-0.063mm	
		SSA (m ² /g)							
a	12.385-12.4	0.102110.0008	0.154440.0010	0.229510.0014	0.399940.0015				
b	12.355-12.37	0.095360.0008	0.135160.0010	0.25070.0011	0.358540.0015				
c	12.325-12.34	0.080500.0006	0.115160.0008	0.21880.0009	0.298040.0017				
d	12.295-12.31	0.09280.0005	0.13580.0005	0.20480.0005	0.300840.0005				
e	12.265-12.28								
f	12.235-12.25								
g	12.205-12.22								
h	12.175-12.19								
average		0.09380.00071	0.14760.0100	0.22570.0193	0.339340.0491				

Specific Pore Volume (SPV) measurements

The crushed samples were measured using N_2 adsorption up to saturation pressure and then desorption with, in total about 90 pressure points (the number varies from different measurements). The results were interpreted as mesoporosity (pore width from 20 to 500Å) with the instrument software using the BJH model [7]. The porosity of the intact 1.5cm section samples were measured using the dry/wet weighing method, since it is impossible to measure any porosity with gas adsorption.

Sample	Core section (m)	1-0.5mm		0.5-0.25mm		0.25-0.125mm		0.125-0.063mm	
		SPV (ml/g)	SPV (ml/g)	SPV (ml/g)	SPV (ml/g)	SPV (ml/g)	SPV (ml/g)	SPV (ml/g)	SPV (ml/g)
a	12.385-12.4	2.29*10 ⁻⁴	5.22*10 ⁻⁴	7.29*10 ⁻⁴	1.61*10 ⁻³				
b	12.355-12.37	3.42*10 ⁻⁴	7.19*10 ⁻⁴	9.72*10 ⁻⁴	1.30*10 ⁻³				
c	12.325-12.34	5.60*10 ⁻⁴	5.48*10 ⁻⁴	8.22*10 ⁻⁴	1.11*10 ⁻³				
d	12.295-12.31	6.12*10 ⁻⁴	5.40*10 ⁻⁴	7.98*10 ⁻⁴	1.13*10 ⁻³				
e	12.265-12.28								
f	12.235-12.25								
g	12.205-12.22								
h	12.175-12.19								
average		4.581140*10 ⁻⁴	5.850500*10 ⁻⁴	8.241106*10 ⁻⁴	1.290123*10 ⁻³				

Conclusions

The results shown in a diagram as SSA versus SPV gives a linear relationship for the crushed fractions (Fig. 5). This is consistent with a model where the particles have a two-zone porosity: one outer layer of large porosity and one inner core of much less porosity [5].

When comparing the linear trend with the data of intact 1.5cm section samples, it shows that the measured SPV for the latter is much larger than what to expect from the trend for crushed samples. This is interpreted that there is a macroporous system in the rock that cannot be measured by the gas adsorption method because the pores (or rather microfractures) are too large for the gas to condensate in them. The upper detection limit of gas adsorption is 0.5µm. The macroporous system is expected to contribute very little to SSA.

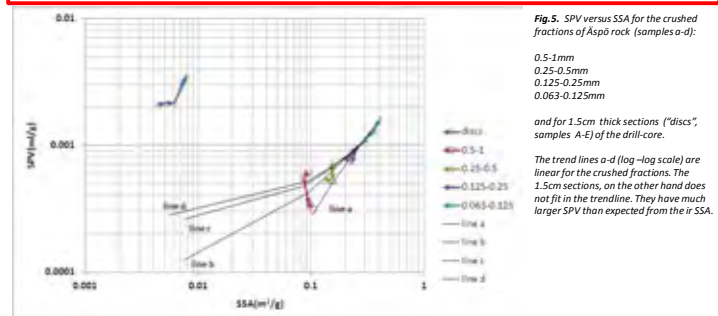


Fig. 5. SPV versus SSA for the crushed fractions of Äspö rock (samples a-d):

0.5-1mm
0.25-0.5mm
0.125-0.25mm
0.063-0.125mm

The trend lines a-d (log-log scale) are linear for the crushed fractions. The 1.5cm sections, on the other hand does not fit in the trendline. They have much larger SPV than expected from the trend.

References

- [1] KIT-INE: Provision of new fracture bearing drill core samples obtained, handled, transported and stored under anoxic conditions, including first documentation. Deliverable D-N*1-1, published in the EU CROCK Project homepage (2011).
- [2] André, M., Malmström, M.E. and Neretnieks, I.: Specific surface area measurements on intact drillcores and evaluation of extrapolation methods for rock matrix surfaces. Journal of Contaminant Hydrology **110**, 1-8. (2009).
- [3] Dubois, I.E., Holgersson, S., Allard, S. and Malmström, M.E.: Dependency of BET surface area on particle size for some granitic minerals. Proc. Radiochim. Acta **1**, 75-82 (2011).
- [4] Brantley, S.L. and Mellott, N.P.: Surface area and porosity of primary silicate minerals. American Mineralogist, **85**, 1767 (2000).
- [5] Dubois, I.E., Holgersson, S., Allard, S. and Malmström, M.: Interdependency of specific surface area and specific volume for some granitic minerals (Manuscript to be submitted 2012).
- [6] Brunauer, S., Emmet, P.H. and Teller, E.: Adsorption of gases in multimolecular layers. J. Am. Chem. Soc. **60** (2), 309-319 (1938).
- [7] Barrett, E.P., Joyner, L.G. and Halenda, P.P.: The determination of pore volume and area distributions in porous substances. I. Computations from nitrogen isotherms. J. Am. Chem. Soc. **73** (1), 373-380 (1951).
- [8] Crank, J.: The Mathematics of Diffusion. Oxford Science Publications (1975).

The research leading to these results has received funding from the European Union's European Atomic Energy Community's (Euratom) Seventh Framework Programme FP7/2007-2011 under grant agreement n° 269658 (CROCK project) and SKB, the Swedish Nuclear Fuel and Waste Management Company.



CHALMERS



Interaction of uranium(VI) and neptunium(V) with Äspö diorite under anoxic conditions



K. Schmeide, S. Görtler, K. Müller, R. Steudtner,
C. Joseph, F. Bok, V. Brendler



Introduction

- Crystalline rock is considered as potential host rock for nuclear waste repositories in deep geological formations [1].
- We studied the sorption of redox-sensitive actinides U and Np onto Äspö diorite (HRL, Sweden) by batch sorption experiments and by in situ ATR FT-IR spectroscopy.
- The influence of various parameters on the actinide sorption was studied: grain size, temperature, atmosphere, sorption time, actinide concentration.

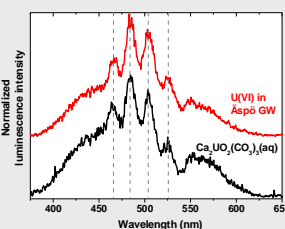
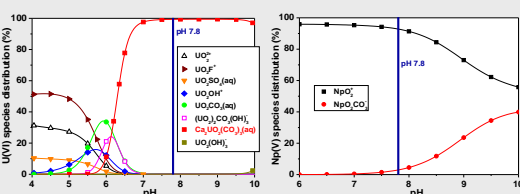
Diorite (Äspö HRL, Sweden):

Grain size fraction (mm)	Specific surface area (m ² /g)
1 - 2	0.125 ± 0.012
0.5 - 1	0.147 ± 0.007
0.063 - 0.2	0.367 ± 0.011
< 0.063	1.583 ± 0.031

Synthetic Äspö groundwater:

Element/ion	mol/L
Li	7.4·10 ⁻⁵
Na	8.2·10 ⁻²
K	2.7·10 ⁻⁴
Mg	4.1·10 ⁻³
Ca	2.8·10 ⁻²
Sr	2.3·10 ⁻⁴
B	4.0·10 ⁻⁵
F	7.4·10 ⁻⁵
Cl	1.4·10 ⁻¹
Br	2.7·10 ⁻⁴
SO ₄ ²⁻	4.1·10 ⁻³
CO ₃ ²⁻ /HCO ₃ ⁻	1.9·10 ⁻⁴
I	0.178
pH	7.8

U(VI) and Np(V) speciation in Äspö GW:

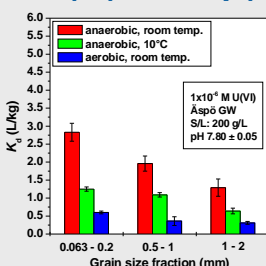


Formation of Ca₂UO₂(CO₃)₃(aq) (log β²¹³ = 30.45 ± 0.35 [2]) could be verified by time-resolved laser-induced fluorescence spectroscopy.

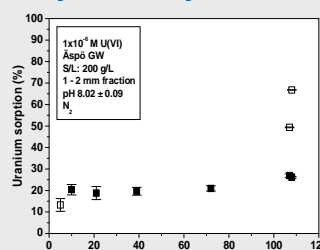
Conditions of batch sorption experiments:

- [²³³U(VI)] or [²³⁷Np(V)]: 1·10⁻⁶ M
- Isotherm: [²³³U(VI)]/U(VI)_{total}: 3·10⁻⁹ to 2·10⁻⁵ M
- Electrolyte: Synthetic Äspö groundwater
- S/L: 200 g/L
- N₂ atmosphere or pCO₂ = 10^{-3.5} atm
- Temperature: 25°C and also 10°C

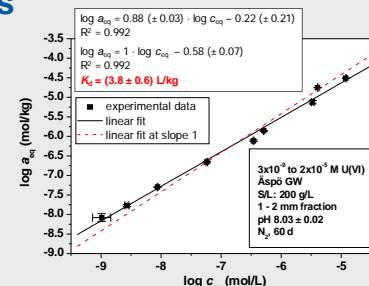
U(VI) and Np(V) sorption experiments



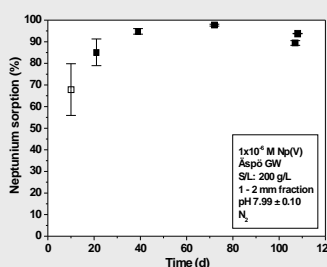
U(VI) sorption onto diorite as a function of grain size, temperature and atmosphere.



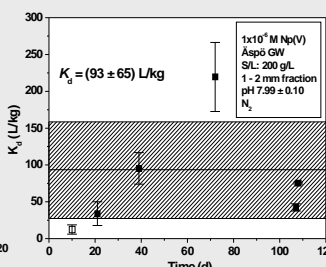
U(VI) sorption onto diorite as a function of sorption time.



Freundlich isotherm of U(VI) sorption onto diorite as a function of U(VI) concentration.



Np(V) sorption onto diorite as a function of sorption time.

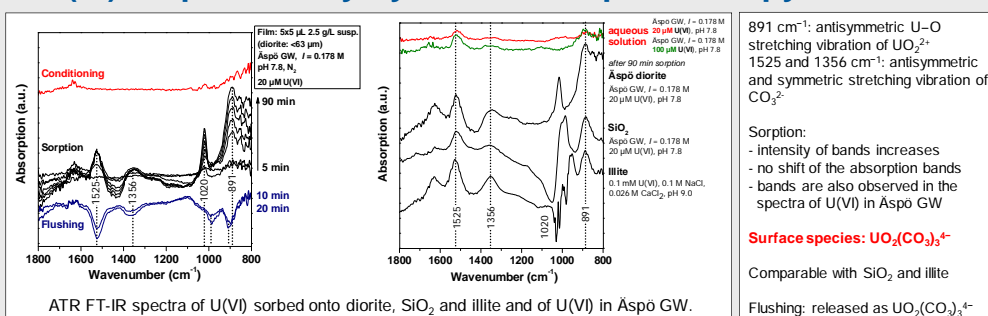


Np(V) sorption onto diorite as a function of sorption time.

Desorption / Redox speciation:

- 45-50% of the sorbed U can be desorbed with Äspö GW. This is mainly U(VI) (94%) as shown by TTA extraction.
- Only 5-6% of the sorbed Np can be desorbed with Äspö GW. This small amount was identified as Np(V) by TTA extraction.

U(VI) sorption study by ATR FT-IR spectroscopy



891 cm⁻¹: antisymmetric U-O stretching vibration of UO₂²⁺
1525 and 1356 cm⁻¹: antisymmetric and symmetric stretching vibration of CO₃²⁻

Sorption:
- intensity of bands increases
- no shift of the absorption bands
- bands are also observed in the spectra of U(VI) in Äspö GW

Surface species: UO₂(CO₃)₃⁺

Comparable with SiO₂ and illite

Flushing: released as UO₂(CO₃)₃⁴⁻

Conclusion

Uranium / Diorite / Äspö groundwater

- Speciation of U(VI) in solution and thus, its sorption onto diorite is strongly influenced by the groundwater composition (esp. Ca²⁺ and CO₃²⁻). → The weakly sorbing Ca₂UO₂(CO₃)₃(aq) complex is predominating at pH > 6.5.
- UO₂(CO₃)₃⁴⁻ was identified as surface species on diorite by in situ time-resolved ATR FT-IR spectroscopy.
- K_d values decrease with decreasing temperature. The K_d values determined under oxic conditions are lower than those determined under anoxic conditions.

Neptunium / Diorite / Äspö groundwater

- Effect of groundwater composition on Np solution speciation and sorption behavior is weak.
- Np interaction with diorite is mainly determined by Fe(II) at the diorite since Np(V) is reduced to the sparingly soluble Np(IV) under anoxic conditions. → XPS measurements



Under anoxic conditions, the retention capacity of anoxic diorite towards neptunium is much higher than towards uranium.

References

- [1] Backblom, G., Tunn. Undergr. Space Technol. 4, 463 (1991). [3] Müller, K. et al., Geochim. Cosmochim. Acta 76, 191 (2012).
[2] Bernhard, G. et al., Radiochim. Acta 89, 511 (2001).

Acknowledgement

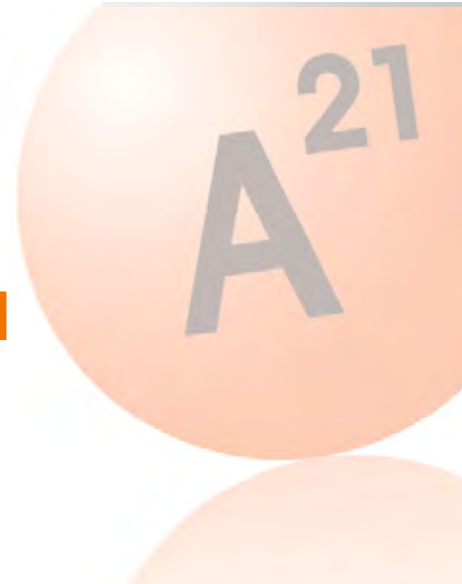
The research leading to these results has received funding from the European Union's European Atomic Energy Community's (Euratom) Seventh Framework Programme FP7/2007-2011 under grant agreement n° 269658 (CROCK project). We also thank KIT-INE for providing the diorite, Ch. Müller for technical support, A. Ritter and C. Eckardt for cation and anion analyses and BET determinations.



MCPHREEQC: AUTOMATIC STOCHASTIC SIMULATIONS FOR GEOCHEMICAL MODELLING

L.M. de Vries, P. Trinchero, J. Molinero

AMPHOS 21 Consulting S.L., Passeig de Garcia i Fària, 49-51, 1-1, 08019 Barcelona, Spain (Luis.de.Vries@Amphos21.com)



Introduction

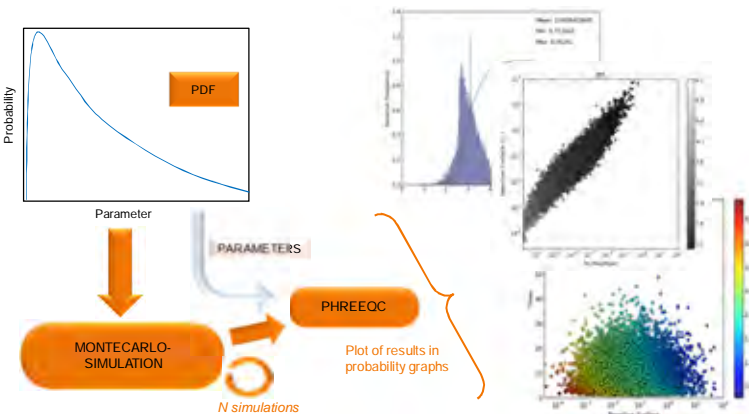
Geochemical processes can be modelled with many different types of software. These processes all have in common the uncertainty about the exact value of the used parameters. The classical approach is to do direct modelling combined with calibration to find the “correct” parameter values. A limited trial-and-error sensitivity analysis is often applied afterwards. In this work we present a **framework**, called **MCPHreeqc**, to apply **Monte-Carlo simulations** automatically to the PHREEQC geochemical models. The tool has been used to infer statistical distributions of cesium K_d values in a typical Fennoscandian crystalline medium.

Objectives

The objective of this work is to apply **stochastic modelling** to PHREEQC models using an automated approach. To this end a framework is developed that consists of an engine, which takes care of all functionality, and a **graphical user interface** to provide the Monte-Carlo configuration. In addition it can **automatically generate histograms and scatter plots** from the results. The software is multi-threaded and it takes advantage of modern multi-core and multi-processor systems.

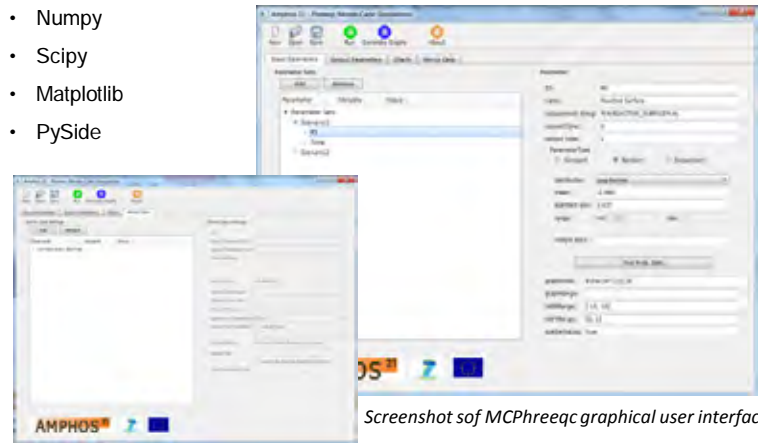
Stochastic Simulations

A probability distribution is chosen for each parameter. Combinations of random values are generated from these distributions and the modelling software is run taking each of these combinations as input.



The cross-platform framework is written in Python, following the object orientated method and includes the following libraries:

- Numpy
- Scipy
- Matplotlib
- PySide



Screenshot of MCPHreeqc graphical user interface

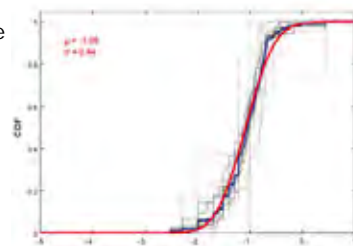
Application – Stochastic Analysis of Cesium Sorption

Motivation

- Radionuclide transport models usually rely on **lumped parameters** (i.e. K_d) that provide aggregated information on sorption and other processes.
- In these approaches, **uncertainties and nonlinearities** are usually neglected.
- Here, MCPHreeqc is applied for the **stochastic analysis** of “effective” K_d values.

Conceptual model

- We evaluate “effective” distribution coefficients related to cesium sorption in a typical Fennoscandian crystalline medium.
- The **statistical distribution** of clay minerals (and the related Cation Exchange Sites, CES) is borrowed from the mineralogical data of Forsmark (Sweden).
- The model of cation exchange proposed by Bradbury and Baeyens (2000) has been used. It consists of three types of exchange sites.

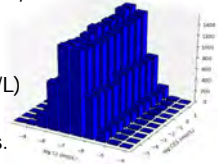


CDF of clay minerals thickness (Löfgren and Sidborn, 2010)

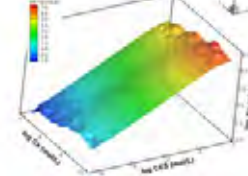
Numerical model

- The **CES** (lognormal distribution, $\mu = -2.03$ mol/L and $\sigma = 0.95$ mol/L) and the aqueous **concentration of cesium** (log-uniform distribution, from 10^{-14} to 10^{-4} mol/L) are the **random variables**.
- Monte Carlo simulation is run with **50,000 realizations**.

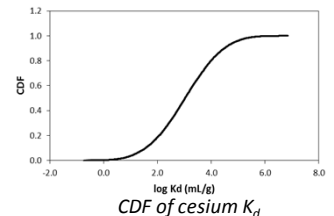
Bivariate histogram of the input random variables



Results



cesium K_d vs cesium concentration and the number of exchange sites (CES).



Conclusions

- MCPHreeqc provides the user a way to **couple PHREEQC with stochastic modelling**.
- The results, are **processed automatically**.
- The tool has been used to infer effective K_d distributions of cesium in a Fennoscandian medium.
- The resulting CDF spans several orders of magnitudes suggesting that **uncertainties and nonlinearities** should be explicitly recognized and properly accounted for.

References

- Bradbury, M.H., Baeyens, B. (2009). Sorption modelling on illite Part I: Titration measurements and the sorption of Ni, Co, Eu and Sn. *Geochimica et Cosmochimica Acta*, 73, 990–1003.
- Löfgren, M., Sidborn, M., (2010) Statistical analysis of results from the quantitative mapping of fracture minerals in Forsmark Site descriptive modelling – compl. studies SKB R-09-30
- Parkhurst, D.L. and Appelo, C.A.J., 1999, User's guide to PHREEQC (Version 2), U.S.G.S Water-Res. Inv. Report 99-4259, 310 p.
- MCPHreeqc (Amphos 21, 2012). <http://www.amphos21.com/downloads>

The development of this tool has received funding from the European Union's European Atomic Energy Community's (Euratom) Seventh Framework Programme FP7/2007-2011 under grant agreement n° 269658 (CROCK project).





ISSN 1869-9669
ISBN 978-3-7315-0145-9

